

# Renormalization of Wilson Lines and Applications to Scattering Processes

## Dissertation

zur Erlangung des Grades „Doktor der Naturwissenschaften“  
am Fachbereich Physik, Mathematik und Informatik  
der Johannes Gutenberg-Universität in Mainz

Robin Brüser

geb. in Freudenberg

Mainz, den 11. Oktober 2019

Erster Berichterstatter: Prof. Dr. Johannes M. Henn  
Zweiter Berichterstatter: Prof. Dr. Stefan Weinzierl

## Abstract

Wilson lines are fundamental objects in gauge theories like quantum chromodynamics (QCD) and supersymmetric Yang-Mills theories. They play for instance a crucial role in low energy effective field theories such as heavy quark effective theory (HQET) and soft collinear effective theory (SCET). For this reason Wilson lines are ubiquitous in modern high precision computations. In this thesis we study three important quantities involving Wilson lines to high order in perturbation theory: the cusp anomalous dimension, massive scattering amplitudes in  $\mathcal{N} = 4$  super Yang-Mills theory (sYM) and the massless quark jet function.

The cusp anomalous dimension is defined by the ultraviolet divergences that arise due to a cusp in a Wilson loop. It is an important quantity, appearing in many physical applications. For instance it governs the infrared behavior of scattering amplitudes and is an universal ingredient in HQET and SCET. In particular it appears in the Regge limit of the massive scattering amplitudes in  $\mathcal{N} = 4$  sYM and the renormalization group equation of the massless quark jet function. In this thesis we consider the angle-dependent cusp anomalous dimension in QCD and compute its small angle expansion at four loops. We test and partially confirm a conjecture based on the observations made at lower loops. That is, the angle-dependent cusp anomalous dimension expanded in terms of the light-like cusp anomalous dimension as coupling constant is conjecturally universal and thus the same in QCD, pure Yang-Mills theory and  $\mathcal{N} = 4$  sYM.

We also study massive scattering amplitudes in  $\mathcal{N} = 4$  sYM in the planar limit, where the mass is generated through a Higgs mechanism. The scattering amplitudes we consider are those of massless particles interacting through loops of massive  $W$ -bosons. In such a model it is known that at leading power, both the Regge limit, as well as the soft divergences are controlled by the angle-dependent cusp anomalous dimension. We show that in the Regge limit the first power suppressed term is governed by a single power law. Furthermore we provide perturbative evidence at two-loop accuracy that the exponent of this power law is given by the anomalous dimension of a cusped Wilson loop with a scalar operator inserted at the cusp.

The massless quark jet function is a universal building block in SCET factorization for many collider and decay processes. It is for instance needed for resummed predictions of the event shapes thrust,  $C$ -parameter, heavy jet mass as well as for deep inelastic scattering and the  $\bar{B} \rightarrow X_s \gamma$  decay rate. The resummation is achieved by solving the renormalization group equation of the massless quark jet function and is crucial to obtain precise theoretical results for these observables. We compute the massless quark jet function up to and including three loops.



---

# Contents

---

<b>1</b>	<b>Introduction</b>	<b>1</b>
<b>2</b>	<b>Review of advanced topics in quantum field theory</b>	<b>5</b>
2.1	Gauge Theories . . . . .	5
2.2	Wilson lines . . . . .	15
2.3	Heavy quark effective theory . . . . .	22
2.4	Factorization in soft collinear effective theory . . . . .	29
2.5	Maximally supersymmetric Yang Mills theory . . . . .	40
<b>3</b>	<b>Multiloop techniques</b>	<b>47</b>
3.1	Workflow of a loop calculation . . . . .	47
3.2	Integration-by-parts reductions of Feynman integrals . . . . .	54
3.3	Feynman parameter integrals . . . . .	59
3.4	Harmonic polylogarithms . . . . .	65
3.5	Differential equation method . . . . .	69
<b>4</b>	<b>Subleading Regge limit from a soft anomalous dimension</b>	<b>81</b>
4.1	Introduction . . . . .	81
4.2	Massive scattering amplitudes in $\mathcal{N} = 4$ super Yang-Mills . . . . .	83
4.3	Regge expansion using dual conformal partial waves . . . . .	90
4.4	Renormalization of Wilson lines with operator insertions . . . . .	94
4.5	Conclusion and outlook . . . . .	99
4.6	Appendix I: The total cross section to three loops . . . . .	101
4.7	Appendix II: Regge expansion using dual conformal partial waves . . . . .	103
4.8	Appendix III: Method for expanding the three-loop amplitude . . . . .	106
4.9	Appendix IV: Soft current computation . . . . .	112
<b>5</b>	<b>Massless quark jet function</b>	<b>119</b>
5.1	Introduction . . . . .	119
5.2	Calculation . . . . .	121
5.3	Result . . . . .	124
5.4	Summary . . . . .	127

<b>6</b>	<b>Matter dependence of the four-loop QCD cusp anomalous dimension</b>	<b>129</b>
6.1	Introduction . . . . .	129
6.2	Definitions and ultraviolet properties of Wilson line operators . . . . .	132
6.3	Four-loop calculation of matter-dependent terms at small angle . . . . .	135
6.4	Results . . . . .	140
6.5	Conjecture on full angle dependence . . . . .	142
6.6	Anti-parallel lines limit . . . . .	146
6.7	Conclusion . . . . .	148
6.8	Appendix I: Lower-loop and conjectured four-loop $\Gamma_{\text{cusp}}(\phi)$ . . . . .	148
6.9	Appendix II: Master integrals . . . . .	152
<b>7</b>	<b>Summary</b>	<b>155</b>
	<b>Overview of publications</b>	<b>157</b>
	<b>Bibliography</b>	<b>159</b>
	<b>Acknowledgements</b>	<b>185</b>

## Introduction

---

The standard model of particle physics (SM) is a gauge theory describing within the context of quantum field theory (QFT) the strong and weak interactions as well as electromagnetism. It is experimentally well established and has immense predictive power. With the discovery of the Higgs boson at the LHC [1, 2] the entire particle content of the SM is experimentally confirmed. This spectacular discovery again showed that the SM is an extremely successful theory, describing a wide variety of phenomena. However, several open questions and problems cannot be explained by the SM, like for instance: What is dark matter? Why are there three generations of fermions in the SM? Why is the observed matter antimatter asymmetry much bigger than the SM prediction? For this reason the search for physics beyond the SM is almost as old as the SM itself. So far, however, no experimental evidence contradicting the SM at the current accessible energy scales has been found, therefore the SM should be viewed as a low energy effective field theory (EFT) of a more fundamental theory.

Precise theoretical predictions in particle physics are important in order to compete with the accuracy of the experimental results from current particle colliders like the LHC and SuperKEKB as well as future colliders. By comparing theory to experiment we can test the SM and indirectly search for new physics beyond the SM. There is also the possibility for direct searches, where new (heavy) elementary particles are produced in collider experiments and lead to e.g. a resonance in the total cross section. For the production of a new heavy elementary particle the collision energy of the collider has to be sufficiently high. Therefore direct collider searches are limited by the available collision energy, whereas indirect searches allow to probe energy scales, which are not accessible by current particle colliders. In indirect searches particles beyond the SM can contribute to observables due to quantum effects and do not necessarily have to be produced. Often the predicted contribution from new physics models are small compared to the one from the SM. Hence indirect searches require precise experimental results as well as precise theoretical prediction of the collider observables in the SM.

In this thesis we are interested in the strong interaction. It is described by quantum chromodynamics (QCD) with the gauge group  $SU(3)$ . We focus on precision calculations in QCD and its maximally supersymmetric version:  $\mathcal{N} = 4$  super Yang-Mills theory (sYM). QCD describes the interaction of quarks and gluons, where the former are the matter and the latter are the force carriers. QCD is an asymptotic free theory [3, 4]. At large energies (short distances) the coupling constant becomes small and at low energies (long distances) large. Asymptotic freedom allows us to study QCD scattering amplitudes and correlation functions at high energies in a perturbative expansion in the small coupling constant. Perturbation theory however breaks down for long distance effects. Furthermore, the long distance behavior leads to confinement. We do not observe free quarks or gluons, but only hadrons which are color singlet bound states.

In QCD a scattering process, starting from the collision up to the detection of the final state particles, involves not only one, but several energy scales. Short and long distance effects have to be taken into account. Often factorization theorems can be derived, which disentangle the short and long distance effects from one another. The non-perturbative long distance effects are then described by universal (process-independent) functions such as the parton distribution functions. These functions can often not be deduced from first principles. They are modeled and fitted to experimental data. The short distance effects on the other hand can be computed from first principles using perturbation theory. Due to the factorization theorems, perturbation theory has predictive power and is an invaluable tool in QCD. Note that the factorization theorems in general only hold in certain limits and receive (small) power corrections. For example in deep inelastic scattering, which was crucial in the development of the parton model of hadrons, the power correction are of order  $\mathcal{O}(\Lambda_{\text{QCD}}/\sqrt{s})$ , where  $\sqrt{s}$  is the center of mass energy and  $\Lambda_{\text{QCD}}$  the hadronization scale.

Factorization theorems can conveniently be derived with the help of (low energy) EFT of QCD, like for instance heavy quark effective theory (HQET) [5–13] and soft collinear effective theory (SCET) [14–19]. The EFT description also allows the systematic resummation of large logarithms, which are often present in fixed order perturbative calculations. The Sudakov double logarithm is a famous example for such logarithms. The large logarithms spoil perturbation theory and their resummation is crucial to obtain precise theoretical results. In order to resum the large logarithms one solves the renormalization group equations (RGEs) of the different ingredients in the factorization theorems. We compute in this thesis the **massless quark jet function** in SCET up to three loops. It is a universal ingredient in factorization theorems for many QCD processes with quark initiated final state jets. In particular the jet function is needed for the event shape observables thrust and  $C$ -parameter, which are used for a precise determination of the strong coupling constant  $\alpha_s$ , see e.g. [20–22].

RGEs in HQET and SCET needed for the resummation of Sudakov (double) logarithms involve a universal ingredient: the **cusp anomalous dimension**. We distinguish between the angle-dependent ( $\Gamma_{\text{cusp}}(\phi, \alpha_s)$ ) and the light-like cusp anomalous dimension ( $K(\alpha_s)$ ). The former is defined by the ultraviolet (UV) divergences arising from a



cusp with Euclidean angle  $\phi$  in a time-like Wilson loop [23–25], whereas the latter arises due to a cusp in a light-like Wilson loop [26]. We can also compute the light-like cusp anomalous dimension  $K(\alpha_s)$  in the limit  $\phi \rightarrow i\infty$  from  $\Gamma_{\text{cusp}}(\phi, \alpha_s)$  [27, 28]. The infrared (IR) divergences of scattering amplitudes with massless external partons are governed by  $K(\alpha_s)$ , independent of the type and properties of the involved partons [27, 29–37]. If the scattering amplitude involves massive external partons, we instead need  $\Gamma_{\text{cusp}}(\phi, \alpha_s)$  [38]. Therefore the cusp anomalous dimension is a truly universal object in QCD (and also supersymmetric theories).

In this thesis we compute the fermionic contributions to  $\Gamma_{\text{cusp}}(\phi)$  in QCD in an expansion for small cusp angles  $\phi$  at four loops. These are the contribution depending on the active number of quark flavours  $n_f$ . Our results are for instance relevant for the extraction of the CKM matrix element  $V_{cb}$  from semileptonic  $B \rightarrow D^{(*)}$  decays, see e.g. [39]. Our main motivation, however, lies in a stringent test of a conjecture based on the observation made at lower loop order. It was observed up to three loops that when  $\Gamma_{\text{cusp}}(\phi)$  is expanded in  $K(\alpha_s)$  instead of  $\alpha_s$ , the expansion coefficients of  $K^n(\alpha_s)$  are universal [40, 41]. They are in particular identical in QCD, pure Yang-Mills theory and  $\mathcal{N} = 4$  sYM. Hence all the information about the matter content of the theory is encoded in the expansion parameter, i.e. in  $K(\alpha_s)$ . The authors of [40, 41] conjectured that this intriguing observation holds to all orders in perturbation theory. The conjecture then allows for the prediction of the full angle dependence of the fermionic contributions to  $\Gamma_{\text{cusp}}(\phi, \alpha_s)$  in QCD at four loops using the known three-loop results. We test the conjecture with our results in the small angle limit. The conjectured expressions for five of the seven fermionic color structures contributing to  $\Gamma_{\text{cusp}}(\phi, \alpha_s)$  at four loops pass several non-trivial tests. In this way we obtain novel analytic results for  $\Gamma_{\text{cusp}}(\phi, \alpha_s)$  and  $K(\alpha_s)$ .

As previously mentioned, factorization theorems for observables hold in certain limits and receive power corrections. For precise theoretical predictions these power corrections become more and more important and are currently intensively studied, see e.g. [42–50]. There also exists observables, where it is not possible to establish a factorization theorem, but one still is interested in an expansion in various kinematic limits of these observables. Another frontier of precision physics are multi-scale problems such as mixed QCD and electroweak processes, processes involving the top quark or the Higgs-boson as well as five point amplitudes in QCD, see for instance [51–71]. We investigate power corrections and multi-scale problems in this thesis in the example of **massive scattering amplitudes in  $\mathcal{N} = 4$  sYM**, where the mass is generated through a Higgs mechanism [72]. We consider  $\mathcal{N} = 4$  sYM as a particular nice toy model of QCD to test and develop new ideas. We study four point scattering amplitudes of massless particles with interaction mediated by massive  $W$ -bosons up to three loops. These amplitudes are UV and IR finite. Furthermore, they exhibit dual conformal symmetry and are natural from the standpoint of the AdS/CFT correspondence. The amplitudes depend on two Mandelstam variables and the mass of the  $W$ -boson, allowing us to study it in various kinematic limits. In particular we focus on the Regge limit, where it is known that the leading term

exponentiate and the exponent equals the angle-dependent cusp anomalous dimension [73, 74]. Going beyond the leading term, we show that also the subleading term can be written as a single power law. We conjecture that the corresponding exponent is given by an anomalous dimension of a cusped Wilson line with a scalar insertion at the cusp. To provide evidence for the conjecture we directly compute this anomalous dimension in a soft current calculation up to two loops and find perfect agreement. Furthermore, using the leading term in the Regge limit and the optical theorem we conjecture an all order result for the total cross section in the high energy limit and verify our finding up to three loops.

From the example of the cusp anomalous dimension and the massive  $\mathcal{N} = 4$  sYM scattering amplitudes we see that Wilson lines are necessary for scattering processes and EFT descriptions. Therefore Wilson lines are important objects in precision calculations. Looking at the definition of Wilson lines, their universality seems at first surprising. In gauge theories they are introduced as gauge links and given by the path-ordered exponential of the gauge field integrated along a contour. Their property under gauge transformations, however, allows for the construction of gauge invariant non-local operators. This is for instance relevant in SCET and is used in the quark jet function to ensure gauge invariance. In addition another property makes them crucial for many low energy EFTs. The soft radiation off a heavy quark or a massless highly energetic quark is captured by a Wilson line with a contour given by the trajectory of the quark. In this thesis we study the renormalization of physical quantities involving Wilson lines, to high order in perturbation theory.

This thesis is organized as follows: In chapter 2 we review selected advanced topics in QFT, needed for the theoretical background of our research results. We proceed in chapter 3 with an introduction to multi-loop techniques. The presented techniques were extensively used in our calculations. In the following three chapters we present our research results. These chapters are except for minor modification identical to the refs. [75–77]. The massive scattering amplitudes are studied in chapter 4. Here we investigate various kinematic limits of the scattering amplitudes and in particular focus on the Regge limit. Next we present in chapter 5 the computation of the three-loop massless quark jet function. In chapter 6 we calculate the fermionic contributions to the four-loop cusp anomalous dimension in QCD in an expansion in for small cusp angles. With these results we test a conjecture, which predicts the full angle dependence of the fermionic contribution at four loops from known lower loop results. Finally, we summarize in chapter 7.

# Review of advanced topics in quantum field theory

---

This chapter serves as an introduction to the theoretical background of the research results. We begin with a short review on gauge theories, where we concentrate on the UV renormalization and the IR divergences of scattering amplitudes. Then we discuss Wilson lines and HQET with the main focus on the cusp anomalous dimension. Next we illustrate how the quark jet function enters physical observables on the example of the event shape observable thrust. For this we motivate a factorization formula for thrust within the framework of SCET. We conclude this chapter with an overview of the maximally supersymmetric Yang-Mills theory.

## 2.1 Gauge Theories

In this section we briefly review gauge theories. As an example we consider QCD. First we explain the QCD Lagrangian and discuss its symmetries. Then we discuss the divergences of loop integrals, the UV renormalization and finally the IR structure of scattering amplitudes. Most of the topics covered in this section is textbook knowledge and we refer to [78–81] for further information.

### 2.1.1 QCD Lagrangian and gauge transformations

QCD is described by a Lagrangian  $\mathcal{L}_{\text{QCD}}$ , built from the field operators of the particles in the theory: the quarks  $\psi_j(x)$  and the gluons  $A^\mu(x)$ . The former represent the matter content of the theory, whereas the latter are gauge bosons. The operators allowed in the QCD Lagrangian are restricted by symmetry considerations. A transformation leaving the equation of motions invariant is a symmetry. The equation of motions are derived

form the condition that the variation of the action vanishes  $\delta S = 0$ , where the action is given by

$$S = \int d^4x \mathcal{L}(x). \quad (2.1)$$

If the Lagrangian is invariant under the symmetry transformation, then the condition  $\delta S = 0$  is trivially fulfilled. It is however also satisfied if the Lagrangian changes at most by an additional term given by a total derivative.

QCD is invariant under transformations of the Poincaré group, which are transformations relating different inertial systems to each other. Translation invariance in time and space as well as rotational invariance imply due to Noether's theorem the conservation of energy, three momentum and angular momentum, respectively. Furthermore, the Poincaré group allows for the classification of the particles in the theory. The one-particle states are eigenstates of the Casimir operators  $P^2 = P_\mu P^\mu$  and  $W^2 = W_\mu W^\mu$  of the Poincaré group. Here  $P^\mu$  is the momentum operator and  $W^\mu$  the Pauli-Lubanski vector. The eigenvalues of  $P^2$  and  $W^2$  correspond to the mass and the spin of the particle. The quarks are massive spin- $\frac{1}{2}$  Dirac fermions and the gluons are massless spin-1 vector bosons.

In addition to space-time symmetries QCD has also an internal symmetry called gauge symmetry. The QCD Lagrangian is invariant under local  $SU(N_c)$  gauge transformations. From the experiments we know that there are three *colors*  $N_c = 3$ . Before we discuss the transformation laws for the fields, we state some useful properties of  $SU(N_c)$ . It is a Lie group with Lie algebra

$$[T_R^a, T_R^b] = i f^{abc} T_R^c, \quad (2.2)$$

where  $f^{abc}$  are the structure constants and we consider the generators  $T_R$  to be in some representation  $R$  of the gauge group. An element  $U$  of  $SU(N_c)$  in the representation  $R$  can be expressed using the exponential  $U_R(\theta) = \exp(\theta^a T_R^a)$ , where  $\theta^a$  are the parameters of the transformation. In practical calculation it is convenient in the final result as well as in intermediate steps to collect the terms with the same color factor. A color factor is essentially a monomial in the Casimir operators<sup>1</sup>  $T_R^a T_R^a = C_R \mathbb{1}_R$  of  $SU(N_c)$  with  $\text{Tr}[\mathbb{1}_R] = N_R$  and  $\text{Tr}[T_R^a T_R^b] = T_R \delta^{ab}$ . Here  $N_R$  is the dimension of the representation  $R$ . Note that closed fermion loops in Feynman diagrams give rise to factors  $T_F n_f$  with  $T_F = 1/2$  and  $n_f$  being the number of quark flavours. For QCD we only need the fundamental ( $R = F$ ) and the adjoint ( $R = A$ ) representation.

We consider local gauge transformations, meaning that the transformation depends on the space-time point, and we introduce the short-hand notation  $U(x) \equiv U_F(\theta(x))$ . The quarks transform under the fundamental representation as matter fields, while the gluons transform under the adjoint representation as gauge fields

$$\psi(x) \rightarrow U(x)\psi(x), \quad A^\mu(x) \rightarrow U^\dagger(x)A^\mu(x)U(x) + \frac{i}{g}U^\dagger(x)(\partial^\mu U(x)). \quad (2.3)$$

---

<sup>1</sup>Starting at four loops also quartic Casimir operators appear, see chapter 6 and [82]

This means that the quarks are vectors and the gluons are matrices  $A_\mu(X) = A_\mu^a(x)T^a$  in color space.

The quantization of gauge fields, especially in the case of a non-abelian gauge group, is more subtle compared to e.g. the quantization of spin- $\frac{1}{2}$  Dirac fermions. The reason becomes particularly transparent in the path integral formalism, where one integrates over all field configurations. The integral over  $A^\mu(x)$  includes physically equivalent configurations that are related by gauge transformations. The procedure of Faddeev-Popov introduces ghost fields  $c(x)$  to remove the redundancy. The ghosts are unphysical auxiliary fields. They violate the spin-statistics theorem, since they obey Fermi-Dirac statistics, but satisfy the equation of motion for scalars. Under gauge transformations they transform as matter fields in the adjoint representation  $c(x) \rightarrow U(x)^\dagger c(x) U(x)$ , i.e. they are matrices in color space  $c(x) = c^a(x)T^a$ . A mathematically rigorous approach to quantize non-abelian gauge theories such as QCD is the BRST formalism (after Becchi, Rouet, Stora and Tyutin). In this formalism a global symmetry is imposed. A BRST transformation mixes the field operators having different statistics, including the ghosts. Under gauge transformation the fields do not mix.

The QCD Lagrangian is constructed from all operators with mass dimension four or less which allow for  $\delta S = 0$  under Poincaré and BRST transformations:

$$\mathcal{L}_{\text{QCD}} = \sum_{j=1}^{n_f} \bar{\psi}_j(i\not{D} + m_j)\psi_j - \frac{1}{4}(F_{\mu\nu}^a)^2 - \frac{1}{2(1-\xi)}(\partial^\mu A_\mu^a)^2 + \bar{c}^a(-\partial^\mu D_\mu^{ab})c^b, \quad (2.4)$$

where we assume that there are  $n_f$  quark flavours  $\psi_j$  with masses  $m_j$ . The gluon field strength tensor is given by  $F_{\mu\nu}^a = \partial_\mu A_\nu^a - \partial_\nu A_\mu^a + g_{\text{YM}} f^{abc} A_\mu^b A_\nu^c$  with the Yang-Mills coupling  $g_{\text{YM}}$ . We use the slash notation  $\not{D} = \gamma_\mu D^\mu$ , where  $\gamma^\mu$  are the gamma matrices. Furthermore,  $D_\mu = \partial - ig_{\text{YM}} A_\mu$  and  $D_\mu^{ab} = \partial_\mu \delta^{ab} + g_{\text{YM}} f^{abc} A_\mu^c$  are the covariant derivatives in the fundamental and the adjoint representation. A mass term for the gluon, which would have the form  $m^2(A_\mu^a)^2$ , is forbidden by BRST and gauge invariance.

The Lagrangian above gives rise to the interaction vertices presented in figure 2.1. Note that  $\mathcal{L}_{\text{QCD}}$  is gauge invariant except for the third term. This gauge fixing term is also present in quantum electrodynamics (QED). The gluon propagator in momentum space then reads

$$D_{\mu\nu}^{ab}(p) = \frac{-i\delta^{ab}}{p^2 + i0^+} \left( g_{\mu\nu} + \xi \frac{p_\mu p_\nu}{p^2 + i0^+} \right). \quad (2.5)$$

In a physical observable the dependence on  $\xi$  has to drop out, which can be used as a strong-cross check in a calculation.

Gauge invariance implies in QED the conservation of the electrical charge. In QCD the Noether charges associated to gauge invariance are gauge dependent. Hence they are unphysical. The difference between QCD and QED is that QED has an abelian  $U(1)$  gauge group, whereas the  $SU(N_c)$  gauge group of QCD is non-abelian. Gauge as well as

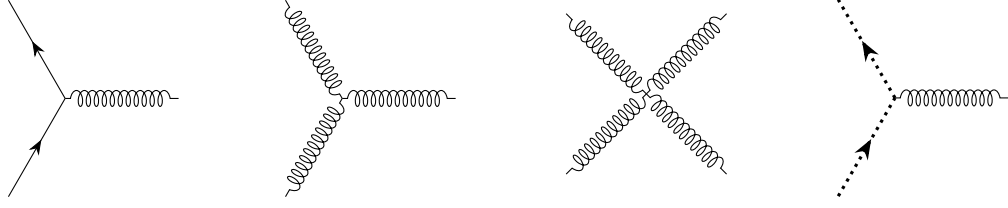


**Figure 2.1:** Vertices in QCD. Quarks, gluons and ghosts are represented by solid, curly and dotted lines, respectively. The fermion and ghost flow is indicated by the arrows.

BRST symmetry are necessary for the quantization and the renormalization of the QCD Lagrangian.

In the following we discuss the divergences that appear in perturbative calculations, where we compute correlation functions or scattering amplitudes in an expansion for small  $g_{\text{YM}}$ . Then we address the renormalization of these divergences.

### 2.1.2 Infrared and ultraviolet divergences

If we go beyond tree level and compute correlation functions and scattering amplitudes at higher order in perturbation theory, we encounter loop integrals. Often these loop integrals are also called Feynman integrals and we use both terms interchangeably. The loop integrals can be infrared (IR) or ultraviolet (UV) divergent. IR divergences are spurious in the sense that they appear only in intermediate (non-physical) results like for instance a scattering amplitude. We discuss the structure of IR divergences in subsection 2.1.4. In observables like a total cross section or a decay rate the IR divergences cancel out. UV divergences on the other hand are removed by means of renormalization, which is explained in subsection 2.1.3. They give rise to interesting features in quantum field theory. The most prominent example is the running of the coupling constant.

The first step in order to compute loop integrals is to regulate the IR and UV divergences, such that the integrals are well defined. There are many regulation schemes available. Throughout this thesis we use dimension regularization [83, 84], which is most commonly used. In dimensional regularization we compute the loop integrals in  $d = 4 - 2\epsilon$  dimensions. Then the divergences manifest themselves as  $1/\epsilon^n$  poles, with  $n \in \mathbb{N}$ . Dimensional regularization has the advantage that it can deal with IR and UV divergences simultaneously and preserves Lorentz invariance. In dimensional regularization there is a subtlety with the gamma matrix  $\gamma_5 = i\gamma_0\gamma_1\gamma_2\gamma_3$ , since it is a four-dimensional object. For the scope of this thesis we do not have to worry about this problem and refer the interested reader for instance to [85, 86].

To illustrate both types of divergences let us consider the massless bubble and the

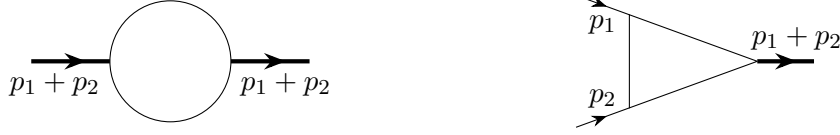


**Figure 2.2:** Bubble and triangle integral defined in eq. (2.6). Massless quadratic propagators and on-shell legs are represented by thin lines, whereas for off-shell legs thick lines are used.

massless triangle integral

$$I_{\text{bub}}(s, \epsilon) = \int \frac{d^d k}{i\pi^{d/2}} \frac{1}{k^2(k+p_1+p_2)^2}, \quad I_{\text{tri}}(s, \epsilon) = \int \frac{d^d k}{i\pi^{d/2}} \frac{1}{k^2(k+p_1)^2(k-p_2)^2}, \quad (2.6)$$

with  $p_1^2 = p_2^2 = 0$  and  $s = (p_1 + p_2)^2$ . A graphical representation of the integrals is shown in figure 2.2. Both integrals often appear in one loop calculations or as subintegrals in a multi-loop integral. Due to Lorentz invariance the integrals can only depend on  $s$  and the space-time dimension  $d = 4 - 2\epsilon$ . Note that for  $s = 0$  both integrals become scaleless. Scaleless integrals evaluate to zero due to the axioms underlying dimensional regularization, see e.g [85].

The bubble integral is IR finite, but UV divergent. The UV divergence appears in the integration region for large loop momentum  $k^\mu$ . In this region the integrand scales like

$$\frac{d^d k}{k^2(k+p_1+p_2)^2} \sim \frac{d|k| |k|^{d-1}}{|k|^4} = \frac{d|k|}{|k|^{1+2\epsilon}} \quad \text{for } k^\mu \rightarrow \infty, \quad (2.7)$$

where we assume  $\epsilon > 0$  such that the integral is well defined. Hence we have a logarithmic divergence, which translates to a  $1/\epsilon$  pole in the end result. IR divergences can only appear in the integration region where the internal propagator become on-shell. Let us consider the region where the loop momentum is soft, i.e. all components of  $k^\mu$  approach zero. We have

$$\frac{d^d k}{k^2(k+p_1+p_2)^2} \sim \frac{d|k| |k|^{d-1}}{|k|^2(p_1+p_2)^2} = \frac{d|k| |k|^{1-2\epsilon}}{s} \quad \text{for } k^\mu \rightarrow 0. \quad (2.8)$$

Due to the scaling behavior of the integration measure this region does not give rise to IR divergences, although the propagator  $1/k^2$  becomes on-shell. To have an IR divergence we need a region where both propagators become on-shell sufficiently fast. However, there exists no such region and we conclude that the bubble integral is IR finite. The bubble integral can be expressed in terms of Gamma functions, where the dependence on  $s$  is fixed by dimensional analysis

$$I_{\text{bub}}(s, \epsilon) = \frac{\Gamma(\epsilon)\Gamma^2(1-\epsilon)}{\Gamma(2-2\epsilon)} (-s)^{-\epsilon}. \quad (2.9)$$

In section 3.3 we compute it using Feynman parameters. From this example we see that we can assess if an integral is UV finite or not by a simple power counting argument.

Next we study the triangle integral. Due to Lorentz invariance and dimension analysis  $I_{\text{tri}}$  is proportional to  $s^{-1-\epsilon}$ . Going through the same steps as in the bubble integral we see that the triangle integral is UV finite. Here we have however IR divergences. Again we have to study the regions where the propagators become on-shell. In the soft region all three propagators become on-shell. The singular behavior of the denominator cannot be compensated by the scaling behavior of the integration measure and the soft region gives rise to an IR divergence in the triangle integral. Furthermore, we have the regions where the loop momentum is collinear to  $p_1$  or  $p_2$ . In the former region the propagators  $1/k^2$  and  $1/(k+p_1)^2$  become on-shell and analogously for the latter region. Both collinear regions give rise to IR divergences. Since the soft region has an overlap with the collinear regions, the triangle integral has not only a  $1/\epsilon$  but also a  $1/\epsilon^2$  pole. It turns out that the triangle integral can be related to the bubble integral as

$$I_{\text{tri}}(s, \epsilon) = \frac{2\epsilon - 1}{\epsilon s} I_{\text{bub}}(s, \epsilon). \quad (2.10)$$

This relation follows from the integration-by-parts identities (IBP), which are discussed in chapter 3.2.

In both examples the integral is either IR or UV divergent. A one-loop integral has at most a  $1/\epsilon^2$  pole. This generalizes to higher loops: a  $L$  loop integral has at most a  $1/\epsilon^{2L}$  pole. The UV and especially the IR analysis becomes more involved beyond one loop. To search for UV divergences we not only have to use the power counting argument on the whole integral, but also on each subintegral separately. In the IR analysis we have to test all possible integration regions, where the loop momenta are soft or collinear to the external momenta. For instance at two loops both loop momenta can be soft or one loop momentum is soft and the other is collinear to an external momentum and so on.

### 2.1.3 Ultraviolet renormalization of the QCD Lagrangian

In the example of the bubble and triangle integrals we encountered IR and UV divergences. These divergences are in general also present in correlation functions and scattering amplitudes. In this subsection we are only interested in the UV divergences. They are removed by renormalization of each operator in the QCD Lagrangian with separate renormalization factors  $Z_i$ . Also the quark masses and the gauge fixing parameter are renormalized. For simplicity we consider at first QCD with only one quark flavour  $n_f = 1$  and later generalize to an arbitrary number  $n_f$ . Due to gauge invariance the renormalization factors are not all independent. They are related to each other by the Slavnov-Taylor identities, and only five are independent. Three of them are given by the field renormalization

$$\psi^b(x) = \sqrt{Z_2} \psi^r(x), \quad A_\mu^b(x) = \sqrt{Z_3} A_\mu^r(x), \quad c^b(x) = \sqrt{Z_3^c} c^r(x), \quad (2.11)$$



where the bare and the renormalized quantities have the superscripts b and r, respectively. The fourth is the mass renormalization factor defined by  $m^b = Z_m m^r$ . Note that the bare mass is unphysical. The same is true for the bare coupling constant. We can introduce a new factor  $Z_g$  which renormalizes the coupling constant, such that all renormalization factors of the vertices are expressed through the field renormalization factors and  $Z_g$  with the help of the Slavnov-Taylor identities [87–89]. Therefore  $Z_g$  is the last independent renormalization factor. The coupling constant then renormalizes according to  $g_{\text{YM}}^b = \mu^\epsilon Z_g g_{\text{YM}}^r$ , where we introduce a scale  $\mu$  with mass dimension one such that  $g_{\text{YM}}^r$  is dimensionless<sup>2</sup>.

In multi-loop calculations  $g_{\text{YM}}$  usually appears in even powers. Therefore it is more convenient to use the strong coupling constant  $\alpha_s = g_{\text{YM}}^2/(4\pi)$ . Its renormalization properties are directly inherited from  $g_{\text{YM}}$  and given by

$$\alpha_s^b = \mu^{2\epsilon} Z_\alpha \alpha_s^r, \quad Z_\alpha = Z_g^2. \quad (2.12)$$

Finally we comment on the gauge parameter. When computing a gauge invariant object, the gauge parameter has to drop out and one usually does not have to worry about its renormalization. If the object is however gauge dependent, then the gauge parameter does not drop out and it has to be renormalized according to  $1 - \xi^b = Z_3(1 - \xi^r)$ , where we use the same renormalization factor as the one for the gauge field in eq. (2.11).

The renormalization factors are determined by renormalization conditions. Assuming that all IR divergences are taken care of in a suitable way, the renormalization conditions are that renormalized correlation functions are finite. See for example subsection 2.2.4, where we discuss the renormalization of a cusped Wilson loop. Note that handling the possible IR divergences can be non-trivial. We refer the interested reader e.g. to [90–95] and the refs. [96, 97] where the QCD renormalization factors were computed up to five loops. With the renormalization conditions the renormalization factors are not uniquely determined. They are in fact scheme dependent.

Throughout this thesis we use the  $\overline{\text{MS}}$  scheme [98, 99], where only the divergences in the renormalized correlation functions are removed. The renormalization factors have then the following form

$$Z(\alpha_s^r, \xi^r) = 1 + \alpha_s^r \frac{Z^{(1,1)}(\xi^r)}{\epsilon} + (\alpha_s^r)^2 \left( \frac{Z^{(2,2)}(\xi^r)}{\epsilon^2} + \frac{Z^{(2,1)}(\xi^r)}{\epsilon} \right) + \mathcal{O}\left((\alpha_s^r)^3\right). \quad (2.13)$$

In general the renormalization factors have a polynomial dependence on the gauge parameter  $\xi^r$ . This is for instance the case for the field renormalization, because it is

---

<sup>2</sup>This is necessary, because in dimensional regularization the integral in the action  $S$  in eq. (2.1) is not four- but  $d$ -dimensional. The action is dimensionless, hence all operators in the Lagrangian have to have mass dimension  $d$ . The mass dimensions of the fields are completely fixed by their respective kinetic terms in a free theory. This has implications on the interaction terms and motivates the factor of  $\mu^\epsilon$ .

unphysical. The renormalization factors of observables, like the strong coupling constant, are independent of  $\xi^r$ , because observables are gauge invariant. In the  $\overline{\text{MS}}$  scheme the renormalization factors for the fields, the quark mass and the coupling constant do not depend on the quark mass (or any momenta). Hence the generalization to a theory with an arbitrary number of quark flavours  $n_f$  is straightforward. Each quark field  $\psi_j$  simply renormalizes with the same factor  $Z_2$ . Also for the renormalization of the quark masses  $m_j$  only one factor  $Z_m$  is needed.

The bare quantities like the fields, the mass and the strong coupling constant do not depend on the renormalization scale  $\mu$ . This is however no longer true for the renormalized counterparts. Their dependence on  $\mu$  is characterized by their respective anomalous dimension. In the case of the strong coupling constant the anomalous dimension is called beta function. It is defined through the equation

$$\frac{d \log \alpha_s^r(\mu)}{d \log \mu} = -2\epsilon - 2\beta(\alpha_s^r(\mu)), \quad (2.14)$$

where the  $2\epsilon$  term is introduced to account for the factor  $\mu^{2\epsilon}$  in eq. (2.12), i.e. the beta function captures only the non-trivial  $\mu$  dependence. The above equation is called renormalization group equation (RGE). The beta function can be computed from the renormalization factor  $Z_\alpha$  using that  $\alpha_s^b$  is independent of  $\mu$ . Taking the logarithmic derivative w.r.t.  $\log \mu$  of eq. (2.12) we obtain

$$\beta(\alpha_s^r(\mu)) = \frac{d \log Z_\alpha(\alpha_s^r(\mu))}{d \log \mu} = \sum_{k \geq 0} \left( \frac{\alpha_s^r(\mu)}{4\pi} \right)^k \beta_k. \quad (2.15)$$

The beta function is computed in a perturbative expansion as indicated above. Currently it is known up to and including five loops, see [96, 97, 100] and references therein. At one loop we have  $\beta_0 = 11C_A/3 - 4T_F n_f/3$ . In the following we will drop the superscript “r” whenever the dependence on the renormalization scale  $\mu$  is indicated.

To illustrate the running of the strong coupling constant we solve the RGE (2.14) up to one loop. Since after renormalization the UV divergences are removed, we can set  $\epsilon = 0$  and get the well known one loop formula

$$\alpha_s(\mu) = \frac{2\pi}{\beta_0 \log \left( \frac{\mu}{\Lambda_{\text{QCD}}} \right)}, \quad (2.16)$$

where  $\Lambda_{\text{QCD}}$  is the scale where  $\alpha_s(\mu)$  diverges. In QCD we have three colors  $N_c = 3$  and six quark flavours  $n_f = 6$ , leading to  $\beta_0 > 0$ . Note that the number of active quarks can be smaller and depends on the typical energy of process: only the quarks with masses smaller than the typical energy of the process are counted. We finish this subsection with a few remarks:

- In the limit of massless quarks the QCD Lagrangian does not have any scale, and is thus conformal. This is however only a classical symmetry. Due to quantum

effects, this symmetry is broken, as it becomes evident from eq. (2.16), where the scale  $\Lambda_{\text{QCD}}$  appears. We discuss in section 2.5 the maximally supersymmetric Yang-Mills theory, which is a conformal theory, even at the quantum level.

- For increasing energy  $\mu > \Lambda_{\text{QCD}}$  or equivalently at short distances the strong coupling constant  $\alpha_s(\mu)$  becomes smaller. This is known as asymptotic freedom. At long distances  $\alpha_s(\mu)$  becomes large and perturbation theory is no longer applicable.
- The scale  $\Lambda_{\text{QCD}}$  is renormalization scheme dependent. In the  $\overline{\text{MS}}$  scheme the world average for  $n_f = 3$  reads  $\Lambda_{\text{QCD}} = 332 \pm 17 \text{ MeV}$  [101]. In the literature most commonly the value for  $\alpha_s$  is given at the mass  $m_Z$  of the  $Z$ -boson. The world average is  $\alpha_s(m_Z) = 0.1181 \pm 0.0011$  MeV [101]. Starting from this point  $\alpha_s$  can then be evolved to the desired scale  $\mu$  by solving the RGE (2.16).
- In nature we do not observe free quarks or gluons (in contrast to electrons and photons). Quarks and gluons hadronize and form color singlet bound states (mesons and baryons). The typical timescale of the hadronization is of order  $\mathcal{O}(1/\Lambda_{\text{QCD}})$ . Therefore  $\Lambda_{\text{QCD}}$  is also often called hadronization scale.

#### 2.1.4 Infrared divergences of scattering amplitudes

After UV renormalization scattering amplitudes (or correlation functions) can still suffer from IR divergences. In physical observables, like for instance the total cross section of a scattering process or the decay rate of an unstable particle, the IR divergences from loop integrals cancel out with the IR divergences that arise in the phase space integration due to the real radiation of soft or collinear gluons [102–104]. The IR structure of scattering amplitudes is even further constrained beyond the IR cancellation. It is universal and only depends on the external particles [27, 29–38]. There are two important observations:

- First, the IR divergences factorize. Having a UV renormalized QCD amplitude  $\mathcal{A}$ , which is a matrix in color space, we can define a finite remainder  $\mathcal{A}_f$  by

$$\mathcal{A}_f = \mathbf{Z}^{-1} \mathcal{A}, \quad (2.17)$$

where  $\mathbf{Z}^{-1}$  is a matrix in color space that removes the IR divergences.

- Second, the IR divergences are related to UV divergences of operators in SCET and HQET <sup>3</sup> [34–36, 38]. For this reason  $\mathbf{Z}$  satisfies a RGE

$$\mathbf{Z}^{-1} \frac{d\mathbf{Z}}{d \log \mu} = -\mathbf{\Gamma}, \quad (2.18)$$

where the soft anomalous dimension matrix  $\mathbf{\Gamma}$  is constructed from the anomalous dimension of the EFT operators. Hence  $\mathbf{Z}$  can be interpreted as a renormalization factor just like the beta function, albeit with a more complicated structure.

---

<sup>3</sup>Both effective theories describe the low energy behavior of QCD in certain limits. We briefly discuss these theories in subsections 2.3 and 2.4.

In the following we focus on the IR divergences that arise due to the correlations between two partons (external particles). Three parton correlations are beyond the scope of this thesis and for more details we refer the interested reader to [34–38]. We consider in the following photon-quark-antiquark form factors to discuss the two parton correlations. These form factors are proportional to the unit matrix in color space, thus allowing us to treat them as scalars in therein.

We begin our discussion with the light-to-light quark form factor  $\mathcal{F}_{ll}$ . Using the vertex function  $\Gamma^\mu$ , which describes the coupling of a quark (anti-)quark pair to a photon to all orders in  $\alpha_s$ , we have

$$\mathcal{F}_{ll} = -\frac{1}{4(1-\epsilon) \times 2p_1 \cdot p_2} \text{Tr}[\not{p}_2 \Gamma^\mu \not{p}_1 \gamma_\mu], \quad (2.19)$$

where  $p_1$  and  $p_2$  are the incoming momenta of the massless quarks.  $\mathcal{F}_{ll}$  can be interpreted as a three particle amplitude with two on-shell quarks and an off-shell photon, see also figure 2.3. Only the on-shell particles give rise to IR divergences. The off-shellness of the photon naturally regulates any IR divergence that can be associated with it. The UV renormalized one loop result is given by (see e.g. [105])

$$\mathcal{F}_{ll} = 1 + \frac{\alpha_s}{\pi} C_F \left[ -\frac{1}{2\epsilon^2} \left( 1 + \epsilon \log \left( \frac{\mu^2}{-2p_1 \cdot p_2} \right) \right) - \frac{3}{4\epsilon} + \mathcal{O}(\epsilon^0) \right] + \mathcal{O}(\alpha_s^2). \quad (2.20)$$

The corresponding soft anomalous dimension reads

$$\Gamma_{ll} = -K(\alpha_s) \log \left( \frac{\mu^2}{-2p_1 \cdot p_2} \right) + 2\gamma_q(\alpha_s), \quad (2.21)$$

where  $K(\alpha_s) = \alpha_s K^{(1)}/\pi + \mathcal{O}(\alpha_s^2)$  is the light-like cusp anomalous dimension and  $\gamma_q(\alpha_s) = \alpha_s \gamma_q^{(1)}/\pi + \mathcal{O}(\alpha_s^2)$  is the collinear anomalous dimension of a massless quark. The logarithmic term is due to the interplay between the two quarks. The specific form of the soft anomalous dimension in eq. (2.21) is known as dipole formula.

In order to show that  $\Gamma_{ll}$  indeed governs the IR divergences of  $\mathcal{F}_{ll}$ , we compute the  $Z$ -factor by solving the RGE (2.18) in a perturbative expansion:

$$Z^{-1} = 1 + \frac{\alpha_s}{\pi} \left[ \frac{K^{(1)}}{2\epsilon^2} \left( 1 + \epsilon \log \left( \frac{\mu^2}{-2p_1 \cdot p_2} \right) \right) - \frac{\gamma_q^{(1)}}{\epsilon} \right] + \mathcal{O}(\alpha_s^2). \quad (2.22)$$

With the condition  $Z^{-1} \mathcal{F}_{ll} = \mathcal{O}(\epsilon^0)$  we get  $K^{(1)} = C_F$  and  $\gamma_q^{(1)} = -3/4 C_F$ , which is in perfect agreement with the known results.

Similarly to before we can also consider heavy-to-light ( $\mathcal{F}_{hl}$ ) or heavy-to-heavy form factors ( $\mathcal{F}_{hh}$ ), where one or both quarks are massive. The soft anomalous dimension governing the IR divergences of  $\mathcal{F}_{hl}$  is given by

$$\Gamma_{hl} = -K(\alpha_s) \log \left( \frac{\mu m_1}{2p_1 \cdot p_2} \right) + \gamma_q(\alpha_s) + \gamma_Q(\alpha_s), \quad (2.23)$$

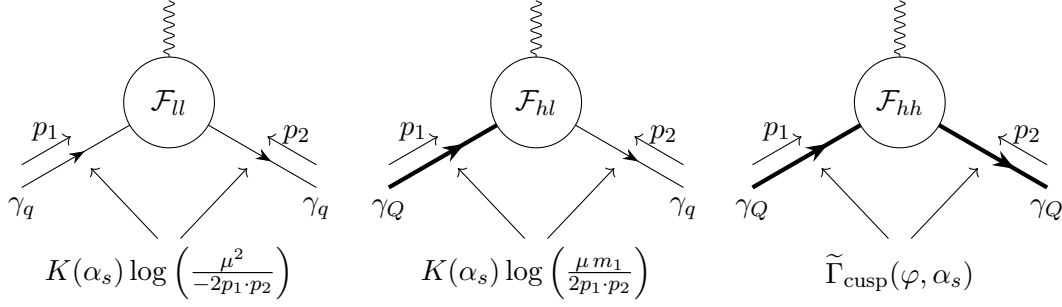


**Figure 2.3:** Building blocks for the dipole part in the anomalous dimension matrix in eq. (2.18) illustrated for the example of form factors, c.f. eqs. (2.21)–(2.24). The thin and thick lines represent massless and massive quarks, respectively.

with  $p_1^2 = m^2$  and  $p_2^2 = 0$  for the momenta of the quarks.  $\gamma_Q(\alpha_s)$  is the collinear anomalous dimension of a massive quark.

The soft anomalous dimension for the heavy-to-heavy form factors

$$\Gamma_{hh} = \tilde{\Gamma}_{\text{cusp}}(\varphi, \alpha_s) + 2\gamma_Q(\alpha_s) \quad (2.24)$$

is more complicated due to the non-trivial dependence on the Minkowskian angle  $\varphi$  defined by  $\cosh \varphi = (p_1 \cdot p_2)/(m_1 m_2)$  with  $p_i^2 = m_i^2$ . Traditionally and throughout this thesis we refer to  $\Gamma_{hh}$  as the angle-dependent cusp anomalous dimension, whereas in [38] only the term  $\tilde{\Gamma}_{\text{cusp}}(\varphi, \alpha_s)$  is called this way. In the following we use the symbol  $\Gamma_{hh} \equiv \tilde{\Gamma}_{\text{cusp}}(\varphi, \alpha_s)$ .

In figure 2.3 we illustrate the dipole structure of the soft anomalous dimension for the form factors. For the general form of the two parton correlations in the soft anomalous dimension matrix for an arbitrary scattering amplitude we refer to [34–38]. Note that in the general formula there are no new “building blocks” and only the collinear anomalous dimensions of the external particles and the cusp anomalous dimension appear. The cusp anomalous dimension can for example be computed with the help of Wilson lines or HQET, as we discuss in sections 2.2 and 2.3.

The soft anomalous dimension matrix receives also non-dipole like corrections when there are more than two legs. These corrections are needed at three loops [37, 106] or already at two loops if two or more legs are massive [38].

## 2.2 Wilson lines

Wilson lines are universal objects in gauge theories and often appear in the context of EFTs as well. In a non-abelian gauge theory like QCD, they are defined by the path

ordered exponential of the gauge field  $A^\mu(x)$  integrated along some path or contour  $C$  with start point  $y$  and endpoint  $z$

$$W[C(z, y)] = \text{P exp} \left[ ig_{\text{YM}} \int_C dx_\mu A^\mu(x) \right]. \quad (2.25)$$

Here  $\text{P}$  is the path ordering operator. Its definition is analogous to the time ordering operator  $\text{T}$ . To make the path ordering more apparent we introduce a parametrization for the contour  $C = \{x^\mu(s) | s \in [0, \tilde{s}]\}$  with  $y = x(0)$ ,  $z = x(\tilde{s})$  and  $\tilde{s} > 0$  (e.g.  $\tilde{s} = 1$ ). Then we can rewrite the Wilson line as

$$W[C(z, y)] = \text{P exp} \left[ ig_{\text{YM}} \int_0^{\tilde{s}} ds \dot{x}_\mu(s) A^\mu(x(s)) \right], \quad \dot{x}^\mu(s) = \frac{dx^\mu(s)}{ds}. \quad (2.26)$$

Note that we can consider the Wilson line above in different representations  $R$  of the gauge group using  $A_\mu(x) = A_\mu^a(x) T_R^a$ .

Wilson lines have several interesting properties and features. An important property is their behavior under gauge transformations that we address in the following subsection. After this we discuss the UV divergences of Wilson lines. Here we focus especially on Wilson lines which have a closed and smooth contour except for one cusp point. Such Wilson lines have UV divergences that renormalize multiplicatively [24, 25] and the corresponding anomalous dimension is precisely the cusp anomalous dimension we already encountered when we discussed the dipole formula for IR divergences of scattering amplitudes. In the subsections 2.3 and 2.4 about HQET and SCET we discuss the relevance of Wilson lines for low energy EFTs.

### 2.2.1 Gauge transformation of Wilson lines

In order to show the behavior of Wilson lines under gauge transformations, it is convenient to first discuss a first order differential equation that Wilson lines fulfill. The differential equation is similar to the Schrödinger equation

$$\frac{d}{d\tilde{s}} W[C(z, y)] = ig_{\text{YM}} \dot{x}_\mu A^\mu(z) W[C(z, y)], \quad z = x(\tilde{s}). \quad (2.27)$$

This is not surprising, because the Wilson line given in eq. (2.26) closely resembles the time evolution operator in quantum mechanics or quantum field theory. To show that eq. (2.27) holds, we first expand the exponential in the Wilson line in its Taylor series and then we rewrite the tower of independent parameter integrals in terms of iterated integrals, such that the path ordering becomes manifest. By taking the derivative w.r.t.  $\tilde{s}$

of this expression we directly obtain the right-hand side of eq. (2.27). Using the covariant derivative, eq. (2.27) can be written in a more compact form

$$(\dot{z} \cdot D) W[C(z, y)] = 0, \quad D^\mu = \frac{\partial}{\partial z_\mu} - ig_{\text{YM}} A^\mu(z). \quad (2.28)$$

Under a gauge transformation  $U$  Wilson lines transform as gauge links

$$W[C(z, y)] \rightarrow W'[C(z, y)] = U(z)W[C(z, y)]U^\dagger(y). \quad (2.29)$$

They connect two space time points through the gauge group. To prove this transformation law we use the differential eq. (2.28) and the fact that a first order differential equation has a unique solution, provided a initial (or boundary) condition. Therefore we have to show that the right-hand side of eq. (2.29) fulfills the gauge transformed version of eq. (2.28). Using the transformation law of the covariant derivative and the unitarity of  $U(z)$  we indeed find

$$(\dot{z} \cdot D') [U(z)W[C(z, y)]U^\dagger(y)] = U(z)(\dot{z} \cdot D)W[C(z, y)]U^\dagger(y) = 0. \quad (2.30)$$

For the initial condition we have  $W[C(z, y)]|_{\tilde{s}=0} = \mathbb{1}_R$  and for the right-hand side of eq. (2.29) we get the same  $U(z)W[C(z, y)]U^\dagger(y)|_{\tilde{s}=0} = \mathbb{1}_R$ , which completes the proof. Note that  $y = z$  for  $\tilde{s} = 0$ . The transformation law of Wilson lines is for instance utilized in SCET to build non-local gauge invariant operators. It is also possible to construct non-local gauge invariant operators only involving Wilson lines. For this we simply have to consider a Wilson loop, that is a Wilson line with a closed contour. By taking the trace in color space of a Wilson loop we ensure gauge invariance. Before we discuss Wilson loops in more detail in the next section, we briefly study a Wilson line with a finite and straight contour in perturbation theory.

### 2.2.2 Straight Wilson lines

In the weak coupling regime we can use perturbation theory to study Wilson lines or Wilson loops. Here we consider the vacuum expectation value of a Wilson line with a time-like and straight integration contour

$$\langle 0 | T W[C(Lv, 0)] | 0 \rangle, \quad C = \{v^\mu s | s \in [0, L], v^2 = 1\}, \quad (2.31)$$

where  $T$  denotes time ordering. The perturbative expansion starts with  $\mathbb{1}_R$  and at one-loop we have the gluon propagator, whose start and endpoints are integrated along the contour. We restrict the parameter integrals at one loop according to  $0 \leq s_1 \leq s_2 \leq L$  to make the path ordering manifest and multiply by a factor of 2 to compensate for the missing integration region where  $s_1$  and  $s_2$  are interchanged. We obtain

$$\mathbb{1}_R + 2 \frac{(ig_{\text{YM}})^2}{2} T_R^a T_R^b \int_0^L ds_2 \int_0^{s_2} ds_1 v^\mu v^\nu \langle 0 | T A_\mu^a(x(s_2)) A_\nu^b(x(s_1)) | 0 \rangle + \mathcal{O}(g^4). \quad (2.32)$$

To continue the computation we need the gluon propagator in position space

$$\tilde{D}_{\mu\nu}^{ab}(x-y) = \int \frac{d^d p}{(2\pi)^d} e^{-ip \cdot (x-y)} D_{\mu\nu}^{ab}(p) = \frac{g_{\mu\nu} \delta^{ab} \Gamma(1-\epsilon)}{4\pi^{2-\epsilon} [- (x-y)^2 + i0^+]^{1-\epsilon}}. \quad (2.33)$$

To keep the expressions short we work in Feynman gauge  $\xi = 0$ . Performing the parameter integrals and the UV renormalization of the coupling constant we have up to one loop

$$\langle 0 | T W[C(Lv, 0)] | 0 \rangle = \mathbb{1}_R + \mathbb{1}_R C_R (-L\mu)^{2\epsilon} \frac{\alpha_s(\mu)}{\pi} \left( \frac{1}{2\epsilon} + 1 + \mathcal{O}(\epsilon) \right) + \mathcal{O}(\alpha_s^2). \quad (2.34)$$

We see that the Wilson line considered here is divergent. The divergence is of UV origin. There are no IR divergences, since the finite length  $L$  of the contour serves as an IR regulator. The only possible source for UV divergences are the configurations where the two endpoints of the gluon become close to each other. In fact, in the next subsection we show that a smooth and closed contour without intersections does not give rise to UV divergences in dimensional regularization. Therefore the UV divergences present in this example arise at the start and endpoint of the finite contour.

### 2.2.3 Wilson loops

In this section we study Wilson loops, i.e. Wilson lines with closed contours. Due to the transformation law in eq. (2.29) we can construct a non-local gauge invariant operator by taking the trace in color space of a Wilson loop. Since we study the Wilson loops in perturbation theory we introduce the following short hand notation

$$\langle W[C] \rangle = \frac{1}{N_R} \text{Tr}_R \langle 0 | T P \exp \left( ig \oint_C dx_\mu A^\mu(x) \right) | 0 \rangle. \quad (2.35)$$

The normalization is chosen such that the perturbative expansion starts with one. Proceeding in the same way as for the straight Wilson line we get at one loop

$$\langle W[C] \rangle = 1 + \frac{(ig_{\text{YM}})^2 C_R \Gamma(1-\epsilon)}{8\pi^{2-\epsilon}} \oint_C dx_\mu \oint_C dy^\mu \frac{1}{[- (x-y)^2 + i0^+]^{1-\epsilon}} + \mathcal{O}(g^4). \quad (2.36)$$

IR divergences in the integrals above are regulated by the finite size of the Wilson loop. Potential UV divergences can arise only from the integration region where  $x \approx y$ , i.e. where the endpoints of the gluon are close to each other. The presence of UV divergences depends on the form of the contour  $C$ . We distinguish the three cases shown in figure 2.4 for the contour:

- A Wilson loop with a smooth contour without intersections is finite in dimensional regularization. Using a cut-off regularization the Wilson loop has a power-like divergence proportional to the length of the loop [23].





**Figure 2.4:** The UV divergences of Wilson loops depend on the contour. We discuss in the text the cases of a smooth contour (left), a contour with one cusp (middle), and a contour with one intersection (right).

- If we lift the restriction of smoothness and allow for one cusp in the contour, then the Wilson loop is UV divergent, where the divergence arises from the cusp point [23]. This divergence renormalizes multiplicatively and gives rise to the so called cusp anomalous dimension [24, 25]. For a time-like contour the cusp anomalous dimension  $\Gamma_{\text{cusp}}(\phi, \alpha_s)$  depends on the cusp angle  $\phi$ . In the case of a light-like contour the light-like cusp anomalous dimension  $K(\alpha_s)$  is a constant. The extension to a contour with several cusp points is straightforward. For each cusp a separate renormalization factor is needed.
- Finally, a smooth contour with one intersection gives also rise to UV divergences. The renormalization is however more complicated, because operator mixing is involved [24].

We address the first point below and the second point in the next subsection in some detail. The third point is beyond the scope of this thesis.

We show that a smooth Wilson loop without intersections is finite in dimensional regularization. For this we do not need the exact form of the contour. We choose a parametrization for  $x^\mu(s_1)$  and  $y^\mu(s_2)$  in eq. (2.36) with  $\dot{x}^2(s_1) = \dot{y}^2(s_2) = 1$ . This can always be achieved by means of reparametrization. Then we have  $s_1 \in [0, L]$ , where  $L$  is the length of the Wilson line and we use the other integration over  $s_2$  to make the possible divergences manifest. We only need to consider the integration region where  $x \approx y$  and parametrize this region by  $y(s_2) = x(s_1) + \dot{x}(s_1)s_2 + \mathcal{O}(s_2^2)$  with  $s_2 \in [-\ell, \ell]$ . For  $\ell \ll L$  we can truncate the expansion after the linear term and get for the integral in eq. (2.36) the expression

$$\oint_C dx_\mu \oint_C dy^\mu \frac{1}{[-(x-y)^2 + i0^+]^{1-\epsilon}} = \int_0^L ds_1 \int_{-\ell}^{\ell} ds_2 \frac{1}{[-s_2^2]^{1-\epsilon}} + \mathcal{O}(\epsilon^0) = \mathcal{O}(\epsilon^0). \quad (2.37)$$

We see that the divergence is power-like, hence in dimension regularization a Wilson loop with a smooth contour without intersection is finite. In order to compute the finite term the specific information on the contour is required.

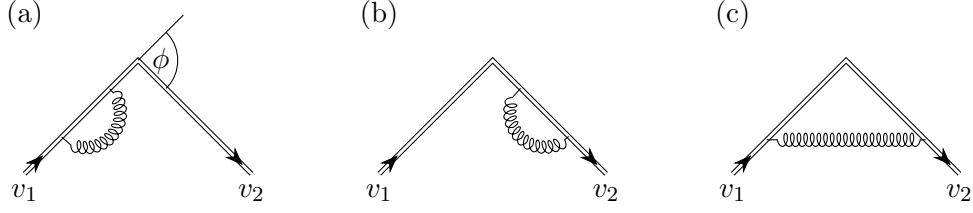


**Figure 2.5:** Integration regions that give rise to UV divergences in a Wilson loop with a cusp. We only show the part of the Wilson loop near the cusp point, where we can approximate the contour by two straight line segments with directions  $v_1$  and  $v_2$ .

### 2.2.4 Cusp anomalous dimension

In the following we show that if we allow for one cusp in an otherwise smooth contour  $C$  without intersections, the Wilson loop is UV divergent. From our previous analysis it is clear that the UV divergence can only arise from the cusp point. Since we are not interested in the finite piece of the Wilson loop, we consider only the integration regions in the integral in eq. (2.36) which give rise to the divergence. This is the region where the endpoints of the gluon are both close to the cusp point. For convenience we split this region further in three distinct regions, which are illustrated in figure 2.5. For the integral we then have

$$\oint_C dx_\mu \oint_C dy^\mu \frac{1}{[-(x-y)^2 + i0^+]^{1-\epsilon}} = I_{(a)} + I_{(b)} + I_{(c)} + \mathcal{O}(\epsilon^0). \quad (2.38)$$

In the regions (a) and (b) the endpoints of the gluon are both either to the left or to the right of the cusp point. They are not allowed to pass over the cusp point. The resulting divergence was already computed in the straight line example in eq. (2.34), because the divergence of a smooth, non-closed and non-intersecting contour arises only from the endpoints of the contour. We can deform the straight line to match the contour with the cusp without introducing any new divergences as long we do not allow the gluon to pass over the cusp point. Therefore we have

$$I_{(a)} + I_{(b)} = -\frac{1}{\epsilon} + \mathcal{O}(\epsilon^0). \quad (2.39)$$

The third integral  $I_{(c)}$  is more complicated and depends non-trivially on the cusp angle. Near the cusp point we can approximate the contour by two straight line segments with directions  $v_1$  and  $v_2$  ( $v_1^2 = v_2^2 = 1$ )

$$C_1 = \{x^\mu(s_1) = -v_1^\mu s_1 | s_1 \in [0, \ell]\}, \quad C_2 = \{x^\mu(s_2) = v_2^\mu s_2 | s_2 \in [0, \ell]\}, \quad (2.40)$$

c.f. figure 2.5. The Euclidean cusp angle  $\phi$  is then defined by  $\cos \phi = v_1 \cdot v_2$ . Using this parametrization we arrive at the following integral

$$I_{(c)} = 2 \int_0^\ell ds_1 \int_0^\ell ds_2 \frac{-\cos(\phi)}{[-(s_1^2 + s_2^2 + 2\cos(\phi)s_1s_2)]^{1-\epsilon}}, \quad (2.41)$$

where the factor of two reflects that in eq. (2.38) either  $x$  or  $y$  can be on the left or right side of the cusp in figure 2.5 (c). We introduce a parametrization which makes the UV divergence manifest by rewriting  $s_1 = \rho t$  and  $s_2 = \rho(1-t)$  with  $\rho \in [0, \ell]$  and  $t \in [0, 1]$ . Note that with these restrictions on  $\rho$  and  $t$  we are missing half of the original integration region, but the missing integration region does not give rise to any divergences. Substituting the new parametrization we obtain

$$\begin{aligned} I_{(c)} &= -2 \int_0^\ell d\rho \frac{\rho}{[-\rho^2]^{1-\epsilon}} \int_0^1 dt \frac{\cos(\phi)}{t^2 + (1-t)^2 + 2t(1-t)\cos(\phi)} + \mathcal{O}(\epsilon^0). \\ &= \frac{1}{\epsilon} \phi \cot(\phi) + \mathcal{O}(\epsilon^0) \end{aligned} \quad (2.42)$$

We combine all pieces to get the bare result for the Wilson loop with a cusp

$$W_{\text{cusp}}^b(\alpha_s^b) = 1 - \frac{\alpha_s^b}{\pi} \left( \frac{C_R}{2\epsilon} [\phi \cot(\phi) - 1] + \mathcal{O}(\epsilon^0) \right) + \mathcal{O}(\alpha_s^2). \quad (2.43)$$

The next step in the calculation is the renormalization as well as the computation of the anomalous dimension. In [24, 25] it was shown that the cusp divergence renormalizes multiplicatively. We introduce a renormalization factor

$$W_{\text{cusp}}^b(\alpha_s^b) = Z_{\text{cusp}}(\phi, \alpha_s(\mu)) W_{\text{cusp}}^r(\alpha_s(\mu)), \quad (2.44)$$

such that  $W_{\text{cusp}}^r(\alpha_s(\mu))$  is finite, i.e. it has no pole in  $\epsilon$ . Note that on the right-hand side the renormalized coupling appears. After replacing the bare coupling with the renormalized one in  $W_{\text{cusp}}^b$ , the only divergences left are those from the cusp point. Hence the renormalization factor does not depend on the specific contour of the Wilson loop. In the  $\overline{\text{MS}}$  scheme the renormalization factor has the form

$$Z_{\text{cusp}}(\phi, \alpha_s(\mu)) = 1 + \frac{\alpha_s(\mu)}{\pi} \frac{Z^{(1,1)}(\phi)}{\epsilon} + \mathcal{O}(\alpha_s^2(\mu)). \quad (2.45)$$

From eqs. (2.43) and (2.44) we find  $Z^{(1,1)}(\phi) = -C_R[\phi \cot(\phi) - 1]/2$ .

The anomalous dimension  $\Gamma_{\text{cusp}}(\alpha_s(\mu))$  of the Wilson loop is defined by the RGE

$$\frac{d \log W_{\text{cusp}}^r(\alpha_s(\mu))}{d \log \mu} + \Gamma_{\text{cusp}}(\alpha_s(\mu)) = 0. \quad (2.46)$$

In order to compute it, it is sufficient to know the renormalization factor. We use that the bare result for the Wilson loop is independent of the renormalization scale to obtain the well known result

$$\Gamma_{\text{cusp}}(\phi, \alpha_s(\mu)) = \frac{d \log Z_{\text{cusp}}(\phi, \alpha_s(\mu))}{d \log \mu}. \quad (2.47)$$

Since the renormalization factor is independent of the specific form of the contour of the Wilson loop, except for the cusp angle, the same applies to the anomalous dimension. Therefore  $\Gamma_{\text{cusp}}(\phi, \alpha_s)$  is universal and only depends on the cusp angle. For this reason it is called (angle-dependent) cusp anomalous dimension. With the one-loop result for the renormalization factor we get

$$\Gamma_{\text{cusp}}(\phi, \alpha_s) = \frac{\alpha_s C_R}{\pi} [\phi \cot(\phi) - 1] + \mathcal{O}(\alpha_s^2). \quad (2.48)$$

So far we have discussed Wilson lines with time-like contours. A light-like contour with a cusp is more subtle. In addition to the divergence from the cusp point it also has a divergence due to the light-like direction. Here we are only interested in the cusp divergence and the corresponding light-like cusp anomalous dimension  $K(\alpha_s)$ . We refer to [26] for a detailed discussion on this subject. For the scope of this thesis we can define it as a limiting case for large imaginary Euclidean angles of  $\Gamma_{\text{cusp}}(\phi, \alpha_s)$ . In this limit we have [27, 28]

$$\Gamma_{\text{cusp}}(\phi, \alpha_s) = -i\phi K(\alpha_s) \quad \text{for } \phi \rightarrow i\infty. \quad (2.49)$$

The two- and three-loop results for  $\Gamma_{\text{cusp}}(\phi, \alpha_s)$  in QCD were computed in [25] and [40, 41], respectively. In both calculations the anomalous dimension was obtained from the UV divergences of a cusped Wilson loop. Due to its universality,  $\Gamma_{\text{cusp}}(\phi, \alpha_s)$  can also be extracted from other calculations, like for instance, from a form factor with massive quarks (see subsection 2.1.4). The three-loop result for  $K(\alpha_s)$  was obtained from splitting functions [107, 108]. For the status of the four-loop calculation of both objects see chapter 6.

In the following subsection we discuss how to compute the angle-dependent cusp anomalous dimension with the help of HQET, a low energy EFT of QCD.

## 2.3 Heavy quark effective theory

Heavy quark effective theory (HQET) is a low energy EFT of QCD. It was developed to describe processes involving heavy quarks where the energy of the process is considerably smaller than the mass of the heavy quarks. A typical process is for instance the decay of a B-meson. For early works on systems with heavy quarks see for example [5–11].

The leading order HQET Lagrangian was first derived in [12, 13]. We are in particular interested in the close relation between Wilson lines and HQET [109–111]. This relation eventually allows us to compute the cusp anomalous dimension using HQET Feynman rules.

### 2.3.1 HQET Lagrangian

In order to derive the HQET Lagrangian we consider the QCD Lagrangian with one massive and otherwise massless quarks. In the following we are only interested in the kinetic term of the heavy quark  $Q(x)$  with mass  $m$ , which is given by

$$\mathcal{L}_Q = \bar{Q}(x)(i\not{D} - m)Q(x). \quad (2.50)$$

The other parts in the Lagrangian are not affected in the large mass limit. In the form presented above,  $\mathcal{L}_Q$  cannot be naively expanded in a power series in  $1/m$ . Therefore we have to rewrite it into a more suitable form. For this we follow in most parts the ref. [39, 112].

The momentum  $P^\mu$  of a heavy quark in the large mass limit can conveniently be parametrized by  $P^\mu = mv^\mu + p^\mu$ , where  $v$  is the velocity of the heavy quark with  $v^2 = 1$  and  $p$  its residual momentum such that  $p^\mu \ll m$  (for all  $\mu = 0, \dots, 4$ ). We decompose the quark field  $Q(x)$  into a so-called large component  $h_v(x)$  and a small component  $H_v(x)$  leading to

$$Q(x) = e^{-imv \cdot x}(h_v(x) + H_v(x)). \quad (2.51)$$

We explicitly pull out the factor  $e^{-imv \cdot x}$  to ensure that  $h_v(x)$  and  $H_v(x)$  vary slowly with  $x$  and that their respective Fourier transforms have support only for small momenta  $k^\mu \ll m$ . In the rest frame with  $v = (1, \vec{0})$  and using the Dirac representation for the gamma matrices,  $h_v(x)$  describes the upper two components and  $H_v(x)$  the lower two components of  $Q(x)$ . Therefore  $h_v(x)$  annihilates a heavy quark with velocity  $v$  and  $H_v(x)$  creates a heavy antiquark with velocity  $v$ . By introducing the projection operators  $P_\pm = (\mathbb{1} \pm \not{v})/2$  we have

$$h_v(x) = e^{+imv \cdot x} P_+ Q(x), \quad H_v(x) = e^{+imv \cdot x} P_- Q(x). \quad (2.52)$$

Below we show that  $H_v$  is power suppressed w.r.t.  $h_v$ , i.e. we have the scaling  $H_v \sim h_v/m$ , which justifies the names large and small components. Expressed in terms of  $h_v(x)$  and  $H_v(x)$  the Lagrangian of the heavy quark reads

$$\begin{aligned} \mathcal{L}_Q = & \bar{h}_v(x) i v \cdot D h_v(x) - \bar{H}_v(x) (i v \cdot D + 2m) H_v(x) \\ & + \bar{h}_v(x) i v \cdot \not{D}_\perp H_v(x) + \bar{H}_v(x) i v \cdot \not{D}_\perp h_v(x). \end{aligned} \quad (2.53)$$

The perpendicular part of the covariant derivative is defined by  $D_\perp^\mu = g_\perp^{\mu\nu} D_\nu$  with  $g_\perp^{\mu\nu} = g^{\mu\nu} - v^\mu v^\nu$ .

As argued above the momenta of  $h_v(x)$  and  $H_v(x)$  are small compared to the mass  $m$  of the heavy quark. Hence we see from eq. (2.53) that  $h_v(x)$  describes the light on-shell degrees of freedom and that  $H_v(x)$  describes the heavy off-shell degrees of freedom. The next step in order to derive an effective Lagrangian is to integrate out the heavy off-shell degrees of freedom in the path integral formalism. There exists also a short cut and the effective Lagrangian can also be obtained by classical means. For this we need the equation of motion for  $H_v(x)$ , which is given by

$$(iv \cdot D + 2m)H_v(x) = iv \cdot \not{D}_\perp h_v(x). \quad (2.54)$$

Then we solve for  $H_v(x)$  and use the result in  $\mathcal{L}_Q$ . In order to solve for  $H_v(x)$  we need the Green's function  $G(x)$ , defined by

$$(iv \cdot D + 2m - i0^+)G(x) = \delta^{(D)}(x). \quad (2.55)$$

The Green's function is the inverse of the differential operator in the distributional sense. Therefore we have

$$H_v(x) = \int d^d y G(x-y) i \not{D}_\perp h_v(y). \quad (2.56)$$

This notation is inconvenient for several reasons and we introduce a more intuitive notation

$$H_v(x) = \frac{1}{iv \cdot D + 2m - i0^+} i \not{D}_\perp h_v(x), \quad (2.57)$$

which however disguises the convolution integral. The  $1/m$  expansion in terms of local operators is especially straightforward with the second notation, whereas in the first notation the feature of non-locality is apparent.

Substituting the result in the full theory Lagrangian in eq. (2.53) we get the non-local EFT Lagrangian

$$\mathcal{L}_{\text{EFT}} = \bar{h}_v(x) iv \cdot D h_v(x) + \bar{h}_v(x) i \not{D}_\perp \frac{1}{iv \cdot D + 2m - i0^+} i \not{D}_\perp h_v(x). \quad (2.58)$$

Note that when we do not follow the classical approach, but use the path integral to integrate out the off-shell degrees of freedom we get an additional term in the Lagrangian. However, one can show that this term is an irrelevant constant [113]. To obtain a local Lagrangian we expand the second term in  $1/m$  and use the geometric series

$$\mathcal{L}_{\text{EFT}} = \bar{h}_v(x) iv \cdot D h_v(x) + \frac{1}{2m} \sum_{k \geq 0} \bar{h}_v(x) i \not{D}_\perp \left( \frac{-iv \cdot D}{2m} \right)^k i \not{D}_\perp h_v(x). \quad (2.59)$$

The EFT is constructed to describe the long distance physics at energies below the mass of the heavy quark. In the form above the Lagrangian does not account for short

distance effects at energies greater than the quark mass. To take care of the short distance effects, the operators in the Lagrangian are multiplied by Wilson coefficients depending on the heavy quark mass and the renormalization scale. The Wilson coefficients can be computed from a matching calculation and at tree level they are simply one. Due to quantum effects, even additional operators can appear.

In order to understand the close relation between Wilson lines and HQET we only need the leading order term of the EFT Lagrangian

$$\mathcal{L}_{\text{HQET}} = \bar{h}_v(x) i v \cdot D h_v(x). \quad (2.60)$$

This Lagrangian was derived in [12, 13]. At leading order in HQET we are not sensitive to the spin of the heavy quark, because of the absence of gamma matrices in  $\mathcal{L}_{\text{HQET}}$ . This leads to a  $SU(2)$  spin symmetry [13]. We will not go into more detail about the symmetries, power corrections or the phenomenological applications of HQET, and refer the interested reader to [39, 114, 115].

The HQET Feynman rules read [116]

$$\begin{aligned} \text{double line with } v \text{ and } p \rightarrow &= \frac{i}{v \cdot p + \delta}, & \text{double line with } v \text{ and a wavy line} &= i g_{\text{YM}} v^\mu T_R^a, \end{aligned} \quad (2.61)$$

where the double line represents the heavy quark line in the  $SU(N_c)$  representation  $R$ . We allow the heavy quark to be slightly off-shell  $\delta \neq 0$ . The off-shellness serves as an IR regulator. However, it breaks gauge invariance. The Feynman rule for the propagator for example can also easily be deduced from the full theory. We parametrize the momentum of the heavy quark by  $P^\mu = m v^\mu + p^\mu$ , where the residual momentum  $p$  is much smaller than the mass of the quark. Then we can expand the full theory quark propagator in  $1/m$ , and at leading order we get

$$i \frac{(\not{P} + m)}{P^2 - m^2} = i \frac{(1 + \not{p})m + \not{p}}{2m v \cdot p + p^2} = \frac{1 + \not{p}}{2} \frac{i}{v \cdot p} + \mathcal{O}(1/m). \quad (2.62)$$

The first factor is just the projection operator  $P_+$  and can be ignored at leading order in  $1/m$ .

### 2.3.2 Decoupling transformation and relation to Wilson lines

Even before the formal development of HQET as a low energy EFT of QCD it was shown that Wilson lines can be represented as infinitively heavy quarks [109–111]. This relation can also be understood at the level of the HQET Lagrangian, see e.g. [117]. We rescale the HQET field  $h_v(x)$  with a straight Wilson line with direction  $v$ , which starts at infinity and ends at  $x$

$$h_v(x) = W_v(x, \infty) h_v^0(x). \quad (2.63)$$

Here we assume that the gauge field approaches zero at infinity sufficiently fast. Using the basic property of a Wilson line  $v \cdot DW_v(x, \infty) = 0$ , we see that the new field  $h_v^0(x)$  is described by a free theory Lagrangian

$$\mathcal{L}_{\text{HQET}}^0(x) = \bar{h}_v^0(x) i v \cdot \partial h_v^0(x). \quad (2.64)$$

For this reason eq. (2.63) is called decoupling transformation. All interactions are now encoded in the Wilson line and we see that, up to a trivial overall factor, correlation functions involving heavy quark fields  $h_v(x)$  can equivalently be described by correlation functions of Wilson line operators. The free field does not transform under gauge transformations.

Let us consider the full HQET propagator  $\tilde{S}_v(x) = \langle 0 | T h_v(x) \bar{h}_v(0) | 0 \rangle$  as an example. Using the decoupling transformation we can write

$$\tilde{S}_v(x) = \langle 0 | T W_v(x, 0) | 0 \rangle \times \frac{1}{N_R} \text{Tr} \langle 0 | T h_v^0(x) \bar{h}_v^0(y) | 0 \rangle. \quad (2.65)$$

Here we used  $W_v(x, \infty) W_v^\dagger(0, \infty) = W_v(x, 0)$  and that the two-point function in the trace is just the free HQET propagator, which is diagonal in color space. In position space the free propagator evaluates to  $\delta^{(d-1)}(x_\perp) \theta(v \cdot x) \mathbb{1}_R$ , with  $x_\perp^\mu = g_\perp^{\mu\nu} x_\nu$ . This is simply the trajectory of a classical particle moving in direction  $v$ . Combining the results we get

$$\tilde{S}_v(x) = \delta^{(d-1)}(x_\perp) \theta(v \cdot x) \langle 0 | T W_v(x, 0) | 0 \rangle. \quad (2.66)$$

Switching to momentum space via Fourier transformation we have

$$S_v(\delta) = \int d^d x e^{iq \cdot x} \tilde{S}_v(x) = \int_0^\infty ds e^{is\delta} \langle 0 | T W_v(sv, 0) | 0 \rangle = \frac{i \mathbb{1}_R}{\delta} + \mathcal{O}(\alpha_s), \quad (2.67)$$

where  $\delta = v \cdot q$  and  $\mathbb{1}_R$  is the identity matrix in the representation  $R$  of the  $SU(N_c)$  gauge group. As indicated above we can compute  $S_v(\delta)$  in perturbation theory. In loop integrals  $\delta$  will appear as the off-shellness of the HQET propagators, c.f. eq. (2.61).

The Wilson line picture does not rely on an EFT approach and is quite instructive at one-loop in position space. Beyond one-loop, however, one wants to perform the computation in momentum space using all the available multi-loop techniques, like for instance IBP reduction and the differential equation method to compute the necessary Feynman integrals. In momentum space we naturally end up in the HQET picture. Furthermore, renormalization is more easily understood in HQET compared to the non-local Wilson loop operators. Like QCD, also HQET is renormalizable, albeit order by order in the  $1/m$  expansion. Since we are interested in the  $m \rightarrow \infty$  limit, we only need to consider the Lagrangian in eq. (2.60).



### 2.3.3 HQET field anomalous dimension

At loop level the HQET field  $h_v(x)$  in the Lagrangian has to be renormalized  $h_v^b(x) = Z_h^{1/2} h_v^r(x)$ , just as in the QCD case. In the  $\overline{\text{MS}}$  scheme only the divergences are subtracted, hence the renormalization factor  $Z_h$  has the form

$$Z_h = 1 + \frac{\alpha_s(\mu)}{\pi} \frac{Z_h^{(1)}}{\epsilon} + \mathcal{O}(\alpha_s^2). \quad (2.68)$$

The renormalization factor can be for instance obtained from the computation of the full HQET propagator with the condition

$$\langle 0 | T h_v^r(x) \bar{h}_v^r(0) | 0 \rangle = \frac{1}{Z_h} \langle 0 | T h_v^b(x) \bar{h}_v^b(0) | 0 \rangle = \mathcal{O}(\epsilon^0). \quad (2.69)$$

We already computed the UV divergences of a straight Wilson line in Feynman gauge in eq. (2.34). With eq. (2.65) we get  $Z_h^{(1)} = C_R(1/2 + \xi(\mu)/4)$ , where we added the  $\xi$ -dependent term that arises in a covariant gauge. The HQET field anomalous dimension then evaluates to

$$\gamma_h = \frac{d \log Z_h}{d \log \mu} = \frac{\alpha_s(\mu)}{\pi} C_R \left( -1 - \frac{\xi(\mu)}{2} \right) + \mathcal{O}(\alpha_s^2), \quad (2.70)$$

When computing the derivative above one has to take the dependence of the renormalized gauge parameter on the renormalization scale  $\mu$  into account. Since  $\gamma_h(\alpha_s)$  is unphysical it is no problem that it depends on the gauge parameter.

The HQET field anomalous dimension was computed at two and three loops in [118] and [119, 120], respectively. For an overview of the status at four loops see chapter 6.

### 2.3.4 Cusp anomalous dimension in HQET

The cusp anomalous dimension describes UV divergences originating from a cusp point in a Wilson line. We already argued that we can choose any non-intersecting contour with a cusp to compute  $\Gamma_{\text{cusp}}(\phi, \alpha_s)$ . We can translate the problem into the HQET language by choosing a contour consisting of two straight line segments with directions  $v_1$  and  $v_2$ , which form a cusp in the origin. In HQET such a Wilson line corresponds to an infinitely heavy quark moving with velocity  $v_1$ , which scatters at an external electromagnetic field to instantaneously change its direction to  $v_2$ . The process is described by the heavy-to-heavy current  $\bar{h}_{v_2}(x) \gamma^\mu h_{v_1}(x)$ , which couples to the external electromagnetic field. At leading power the HQET Feynman rules do not contain any gamma matrices, hence the the gamma matrix in the current can be omitted, leading to

$$J_{\text{cusp}}(x) = \bar{h}_{v_2}(x) h_{v_1}(x). \quad (2.71)$$

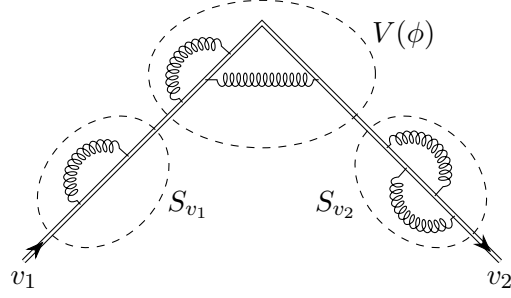


**Figure 2.6:** Sample Feynman diagram contributing to the correlation function in eq. (2.72). In momentum space all the diagrams can be disassembled into three pieces contributing to either  $S_{v_1}$ ,  $S_{v_2}$  or  $V(\phi)$ . This leads to the factorization in eq. (2.73).

From the Wilson line description we know that this operator gives rise to UV divergences, which are governed by the cusp anomalous dimension<sup>4</sup>  $\Gamma_{\text{cusp}}(\phi, \alpha_s)$  [28]. Hence this operator renormalizes according to  $J_{\text{cusp}}^b = Z_{\text{cusp}}(\phi) J_{\text{cusp}}^r$ , where the Euclidean cusp angle is given by  $\cos \phi = v_1 \cdot v_2$ .

To understand the renormalization of a cusped Wilson loop in HQET we consider the following correlation function

$$C(x, y) = \langle h_{v_2}(x) J_{\text{cusp}}(0) \bar{h}_{v_1}(y) \rangle = \langle h_{v_2}(x) \bar{h}_{v_2}(0) h_{v_1}(0) \bar{h}_{v_1}(y) \rangle. \quad (2.72)$$

We study the correlation function in perturbation theory and from figure 2.6 we see that the Feynman diagrams arrange themselves in such a way that  $C$  factorizes in momentum space into three contributions. There are two full HQET propagators with directions  $v_1$  and  $v_2$ , respectively. The third factor is the one-particle irreducible vertex function  $V(\phi)$ . Therefore we have

$$\int d^d x \int d^d y e^{i(p \cdot x + q \cdot y)} C(x, y) = S_{v_1}(\delta_1) S_{v_2}(\delta_2) V(\phi, \delta_1, \delta_2) \Big|_{\substack{\delta_1 = v_1 \cdot q \\ \delta_2 = v_2 \cdot p}}, \quad (2.73)$$

see e.g. [41]. Here  $\delta_1$  and  $\delta_2$  serve as IR regulators. In the calculation of the vertex function we can choose  $\delta_1 = \delta_2 = \delta$ . Then the dependence on  $\delta$  is fixed by dimensional analysis. Hence we can assign it some value and restore the full dependence at the end of the calculation. In practice we find it convenient to use  $\delta = -1/2$ .

Now we address the renormalization. Our aim is to relate the renormalization factor  $Z_{\text{cusp}}(\phi)$  solely to the vertex function. On the one hand we have  $S_v^b = Z_h S_v^r$  for the full HQET propagator, and on the other hand the renormalized and therefore finite version of eq. (2.72) reads  $C^r = Z_h^{-1} Z_{\text{cusp}}^{-1} C^b$ . In combination with eq. (2.73) we therefore get

$$\log V(\phi) + \log Z_h = \log Z_{\text{cusp}}(\phi) + \mathcal{O}(\epsilon^0), \quad (2.74)$$

<sup>4</sup>The anomalous dimension of  $J_{\text{cusp}}$  was computed at one-loop in [116] within the HQET framework. At that time  $\Gamma_{\text{cusp}}(\phi, \alpha_s)$  was already known at two loops from a Wilson line calculation [25]. In [28] the equivalence of both anomalous dimensions was shown.

where we neglect the finite terms  $\log S_{v_i}^r$ . To get rid of  $Z_h$  we evaluate the equation at zero cusp angle and use that  $Z_{\text{cusp}}(0) \equiv 1$ , since only a cusp in a non-intersecting Wilson loop can give rise to UV divergences. We then have

$$\log V(0) = \log Z_h + \mathcal{O}(\epsilon^0) \quad (2.75)$$

As a byproduct we therefore also obtain the HQET field anomalous dimension. Note that this equation can also be derived from a HQET off-shell Ward identity, which relates the HQET self energy to the vertex function. Using eq. (2.75) we finally obtain the desired result [25]

$$\log V(\phi) - \log V(0) = \log Z_{\text{cusp}}(\phi) + \mathcal{O}(\epsilon^0). \quad (2.76)$$

The cusp anomalous dimension  $\Gamma_{\text{cusp}}(\phi, \alpha_s)$  is then computed in the usual way. The vertex function is gauge dependent, but after the UV renormalization of the left-hand side of eq. (2.76) the gauge parameter drops out in the divergent terms. The renormalization factor  $Z_{\text{cusp}}(\phi)$  and thus  $\Gamma_{\text{cusp}}(\phi, \alpha_s)$  are gauge invariant objects, which can be directly understood from the Wilson loop picture.

The main goal of this section about HQET was to reveal the connection between Wilson lines and infinitely heavy quarks as well as to establish eq. (2.76). This allows one to compute the cusp anomalous dimension using HQET momentum space Feynman rules. Furthermore, we sketched how to derive an EFT from the known full theory. In the following section we briefly discuss some aspects of SCET with the focus on deriving a factorization formula for thrust.

## 2.4 Factorization in soft collinear effective theory

We discuss in this section the event shape observable thrust  $T$  [121] and motivate a factorization formula for the differential cross section, which is valid for  $T \rightarrow 1$ . The arguments presented in this section follow in most parts the lines of [81, 122], where also a rigorous derivation of the factorization formula can be found. Thrust can for instance be used for a precise determination of the strong coupling constant [20, 21, 123]. The main goal of this section is to motivate the definition of the quark jet function [17], which is a building block in the factorization formula. In chapter 5 we compute the jet function for jets initiated by a quark up to including three loops. Note that the quark jet function is an universal building block in factorization formulas not only for thrust, but for a large class of observables like for instance deep inelastic scattering near the threshold [124], C-parameter [22, 125], heavy jet mass [126] and also the decay  $b \rightarrow s\gamma$  in the endpoint region [127]. In the following we use thrust as a prototype to illustrate the factorization for these observables in soft collinear effective theory (SCET).

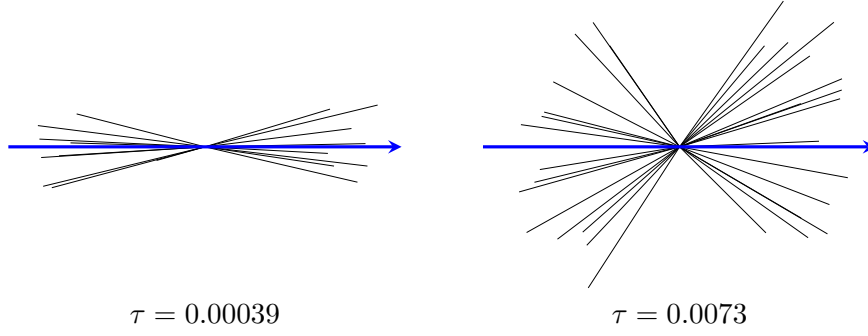


**Figure 2.7:** The direction of the thrust axis  $\vec{n}_T$  is indicated by the thick blue arrow. For low values of  $\tau = 1 - T$  we have two highly collimated jets (left) and with increasing values for  $\tau$  the shape of the event becomes more spherical symmetric (right).

### 2.4.1 Definition of thrust

Thrust is an inclusive observable that quantifies the shape of an event in a lepton collider. We are interested in events with large center of mass energy  $Q$ , such that we can work in the limit of massless particles. Then thrust is defined by [121]

$$T = \frac{1}{Q} \max_{\vec{n}_T} \sum_j |\vec{n}_T \cdot \vec{p}_j|, \quad (2.77)$$

where the sum is over the three-momenta  $\vec{p}_j$  of all particles in the final state. The thrust axis  $\vec{n}_T$  has unit length and is defined by maximizing  $T$ . In the massless limit we have for the center of mass energy

$$Q = \sum_j |\vec{p}_j|. \quad (2.78)$$

It is easy to show that  $T \in [1/2, 1]$ , where the lower bound is reached for a spherical symmetric event. In the limit  $T \rightarrow 1$  we have an event with two highly collimated jets. Then  $\vec{n}_T$  coincides with the jet axis. In figure 2.7 we present two events and their respective values for thrust. In the following we are mostly interested in the limit  $T \rightarrow 1$  and introduce for this reason the new variable  $\tau = 1 - T$ .

In a collider experiment one can measure the differential cross section  $d\sigma/d\tau$  and by fitting the theoretical prediction to the experimental data the strong coupling constant  $\alpha_s$  can be determined to very high precision [20, 21, 123]. On the theoretical side we have [122]

$$\frac{d\sigma}{d\tau} = \frac{1}{2Q^2} \int d\Pi_X |\mathcal{M}(e^+e^- \rightarrow \gamma^* \rightarrow X)|^2 (2\pi)^d \delta^d(q_1 + q_2 + p_X) \delta(\tau - \tau(X)), \quad (2.79)$$

where  $X$  is the final state consisting of hadrons,  $p_X$  the total momentum of the final state particles,  $q_1$  and  $q_2$  are the momenta of the electron and positron and we integrate over the phase space of the particles in the final state  $X$ . Here  $\tau$  is the value we assign and  $\tau(X)$  is computed from the momenta of the final state particles according to eq. (2.77). Here and in the following we assume that we only have hadrons in the final state. We work to lowest order in QED, where the electron and positron annihilate to a virtual photon which then creates a quark and antiquark. For simplicity we do not include the equivalent process where the photon is replaced by a  $Z$ -boson. In the region of small  $\tau$  the quark and antiquark initiate each a jet that are eventually measured in the detector. To describe the physics after the pair creation we solely use QCD or rather an EFT of QCD. We neglect any higher order correction due to the electroweak interaction.

To compute thrust for a given event we only need the three-momenta of the particles in the final state that we measure in a detector. Hence thrust is not sensitive to the particle content of the final state. In this sense it is an inclusive observable just like the total cross section. Sufficiently inclusive observables are IR safe and we can compute them in perturbation theory if the energy scale is much greater than  $\Lambda_{\text{QCD}}$  [102–104]. In these observables the IR divergences from virtual diagrams cancel with the IR divergences that arise in the phase space integral due to real radiation of soft or collinear partons. Thrust is such an IR safe observable.

The final state particles in the detector are hadrons and not quarks or gluons. However, due to the quark hadron duality [128, 129] we can simply work with quarks and gluons and do not have to worry to good approximation about the hadronization when computing the differential cross section in perturbation theory. At leading order in  $\alpha_{\text{em}}$  and at order  $\mathcal{O}(\alpha_s^0)$  we have to consider the process  $e^+e^- \rightarrow \gamma^* \rightarrow q\bar{q}$ . Working in the center of mass system the outgoing quarks move back to back and therefore the phase space integral in eq. (2.79) is trivial and we have  $\tau(q\bar{q}) = 0$ . Putting all pieces together we get  $\sigma_0 \times \delta(\tau)$ , where  $\sigma_0$  is the total cross section. Going to next-to-leading order and keeping only the terms that are singular in the limit of small  $\tau$  we have (see e.g. [81, 130])

$$\frac{1}{\sigma_0} \frac{d\sigma}{d\tau} = \delta(\tau) + C_F \frac{\alpha_s}{2\pi} \left[ \left( \frac{\pi^2}{3} - 1 \right) \delta(\tau) - 3\mathcal{L}_0(\tau) - 4\mathcal{L}_1(\tau) + \mathcal{O}(\tau^0) \right] + \mathcal{O}(\alpha_s^2). \quad (2.80)$$

Here we introduced the plus distribution  $\mathcal{L}_n$ , which is defined by

$$\mathcal{L}_n(\tau) = \left[ \frac{\theta(\tau) \log^n(\tau)}{\tau} \right]_+ = \lim_{\eta \rightarrow 0} \frac{d}{d\tau} \left[ \theta(\tau - \eta) \frac{\log^{n+1}(\tau)}{n+1} \right]. \quad (2.81)$$

The differential cross section suffers in the small  $\tau$  region from large logarithms  $\log^n(\tau)$ . Due to these large logarithms fixed order perturbation theory breaks down in this limit. However, it is possible to resum these large logarithms. In figure 2.8 we see that the fixed order result, i.e. the result where the large logarithms are not resummed, does not match the experimental data in the region for small  $\tau$ . The agreement

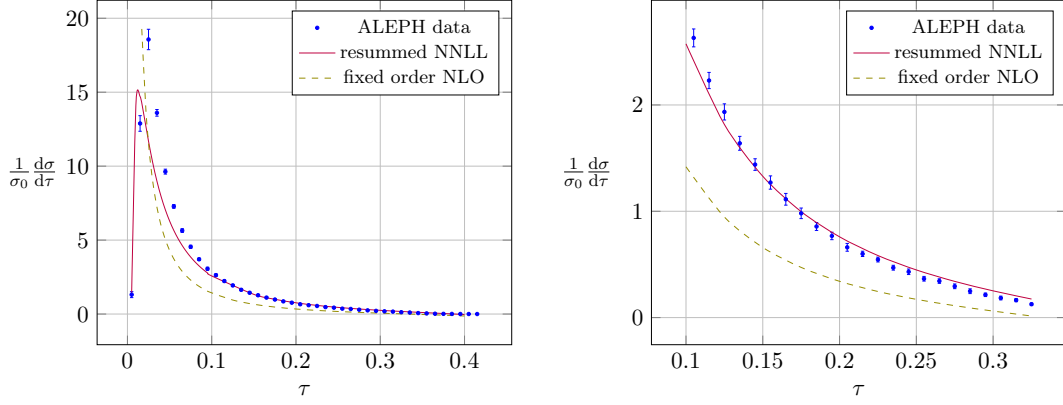


**Figure 2.8:** Differential cross section for the event shape observable thrust  $\tau$  at a center of mass energy  $m_Z = 91.2$  GeV. The blue data points are from ALEPH [131] and the fixed order prediction at one-loop is represented by the dashed line, see e.g. [81, 130]. In eq. (2.80) its singular terms are given. The solid line is the resummed prediction at next-to-next-to-leading-logarithmic accuracy. The analytic expression was provided by the courtesy of Thomas Becher, see also [20].

of the resummed result is considerably better. We proceed in the next subsections with discussing a factorization formula for the differential cross section that is valid for small  $\tau$  and allows to compute the singular terms. In particular it provides the means to resum the large logarithms to all orders in perturbation theory. The factorization formula can conveniently be derived within SCET. For this we study in the next subsection the SCET vector current which couples to a photon.

### 2.4.2 Vector current in SCET

We are interested in the region of small  $\tau$ , where we have two highly collimated jets. One is collinear and the other is anticollinear to the thrust axis  $\vec{n}_T$ . To describe this kinematics we introduce light-cone coordinates  $n^\mu = (1, \vec{n}_T)$  and  $\bar{n}^\mu = (1, -\vec{n}_T)$ . Then we have  $n^2 = \bar{n}^2 = 0$  and  $n \cdot \bar{n} = 2$ . We can decompose a momentum  $p$  (or any other four-vector) as

$$p^\mu = (\bar{n} \cdot p) \frac{n^\mu}{2} + (n \cdot p) \frac{\bar{n}^\mu}{2} + p_\perp^\mu = p_-^\mu + p_+^\mu + p_\perp^\mu \quad (2.82)$$

with  $n \cdot p_\perp = \bar{n} \cdot p_\perp = 0$ . For simplicity we often use the shorthand notation  $p = (\bar{n} \cdot p, n \cdot p, p_\perp)$ .

We introduce a small scaling parameter  $\lambda \ll 1$  to establish a power counting argument in the region for small  $\tau$  to identify the relevant contributions. In the small  $\tau$  region we have collinear and anticollinear particles (modes) with momentum scaling  $p_c \sim Q(1, \lambda^2, \lambda)$  and  $p_{\bar{c}} \sim Q(\lambda^2, 1, \lambda)$ . The on-shell condition for these modes is then given by

$p_c^2, p_{\bar{c}}^2 \sim \lambda^2$ . Expressing  $\tau$  in terms of the light-cone variables:  $Q\tau = \sum_i \min(n \cdot p_i, \bar{n} \cdot p_i)$ , we directly see that  $\tau \sim \lambda^2$ . Additionally we have to allow for ultra-soft (usoft) particles with  $p_{us} \sim Q(\lambda^2, \lambda^2, \lambda^2)$  and  $p_{us}^2 \sim \lambda^4$ . They contribute also at order  $\mathcal{O}(\lambda^2)$  to  $\tau$ . The hard or soft modes with the momentum scaling  $p_h \sim Q(1, 1, 1)$  and  $p_s \sim Q(\lambda, \lambda, \lambda)$  in the final state give rise to  $\mathcal{O}(1)$  and  $\mathcal{O}(\lambda)$  contribution to  $\tau$ . Since we are only interested in the region for  $\tau \sim \lambda^2$ , these modes will eventually be integrated out in the EFT approach to describe the kinematics. Based on this analysis we can identify three scales in our problem that are separated by  $\tau \ll 1$  (or equivalently by  $\lambda^2$ ) in the following way

$$\begin{array}{ccccc} \text{hard} & & \text{collinear} & & \text{usoft} \\ & & \text{anticollinear} & & \\ p_h^2 \sim Q^2 & \gg & p_c^2 \sim p_{\bar{c}}^2 \sim Q^2 \tau & \gg & p_{us}^2 \sim Q^2 \tau^2 \end{array} . \quad (2.83)$$

Note that soft particles decouple and are not relevant for this problem, while the hard modes contribute (in the matching of the EFT operators) via virtual diagrams.

The large separation of scales allows us to describe the problem with an EFT approach. The appropriate EFT in our case is soft collinear effective theory (SCET)<sup>5</sup> [14–19]. As the name suggest, SCET is tailored to deal with problems with collinear and soft (or usoft) particles which is for instance the case in jet- and  $B$ -physics. The usual ansatz to derive the EFT Lagrangian  $\mathcal{L}_{\text{SCET}}$  from the full theory Lagrangian  $\mathcal{L}_{\text{QCD}}$  is to split the full theory fields into collinear, anticollinear and usoft fields

$$\psi \rightarrow \psi_c + \psi_{\bar{c}} + \psi_{us}, \quad A^\mu \rightarrow A_c^\mu + A_{\bar{c}}^\mu + A_{us}^\mu \quad (2.84)$$

and then collect the terms with the same power counting in  $\lambda$  using the scaling behavior in table 2.1. Similar to HQET the collinear quark field  $\psi_c(x)$  has a leading component  $\xi_c(x)$  and a subleading component  $\eta_c(x)$  that can be projected out

$$\xi_c(x) = \frac{\not{n} \not{\bar{n}}}{4} \psi_c(x) \quad \eta_c(x) = \frac{\not{\bar{n}} \not{n}}{4} \psi_c(x). \quad (2.85)$$

The subleading component can be integrated out using for example the path integral formalism and we are left with only the leading component  $\xi_c(x)$ . The particle content of  $\mathcal{L}_{\text{SCET}}$  is summarized in table 2.1. In principle each operator in the EFT Lagrangian  $\mathcal{L}_{\text{SCET}}$  has to be multiplied by a Wilson coefficient to account for the physics at the hard scale. The Wilson coefficient are determined perturbatively by a matching calculation to the full theory. However, at leading power in  $\lambda$  it turns out that all Wilson coefficients are exactly one to all orders in  $\alpha_s$ , except for operators involving collinear and anticollinear fields [19]. Further below we discuss the vector current in SCET, which is such an operator and is the proper operator to describe the pair creation of the quark and antiquark in the limit of small  $\tau$ .

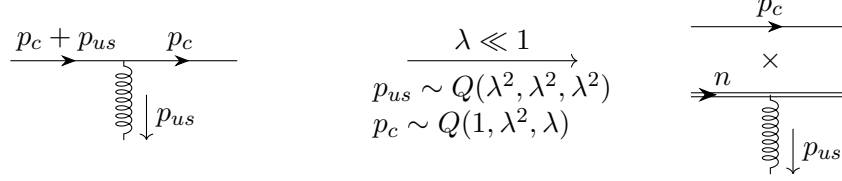
Within the SCET framework we can derive a factorization formula describing the singular terms in the differential cross section in eq. (2.80) and thus conveniently resum

<sup>5</sup>To be more precise in our example we use SCET<sub>I</sub> due to the presence usoft modes. In SCET<sub>II</sub> there are no usoft but soft modes.

mode	momentum scaling	scaling of fields
usoft	$p_{us} \sim Q(\lambda^2, \lambda^2 \lambda^2, )$	$A_{us}^\mu \sim Q(\lambda^2, \lambda^2, \lambda^2), \psi_{us} \sim Q\lambda^6$
collinear	$p_c \sim Q(1, \lambda^2, \lambda, )$	$A_c^\mu \sim Q(1, \lambda^2, \lambda), \xi_c \sim Q\lambda^2$
anticollinear	$p_{\bar{c}} \sim Q(\lambda^2, 1, \lambda, )$	$A_{\bar{c}}^\mu \sim Q(\lambda^2, 1, \lambda), \xi_{\bar{c}} \sim Q\lambda^2$

**Table 2.1:** Particle in SCET and the scaling behavior of their field operators [17]. The scaling of the field operators can be derived from the full theory propagators using the respective momentum scaling of the fields [81].

usoft factorization:



electrostatics:

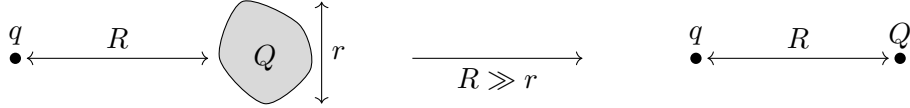


**Figure 2.9:** The radiation of usoft gluon from a highly energetic quark factorizes. In the factorized form the usoft emission is described by a Wilson line. Hence the usoft gluon cannot resolve the spin structure of the collinear quark. This is analogous to the multipole expansion in electrostatics.

large logarithm by solving RGEs. Since our further discussion is mostly based on physical arguments we do not need  $\mathcal{L}_{\text{SCET}}$  explicitly. For further information on SCET we refer to the original works where SCET was introduced [14–19] and for pedagogical introductions to [81, 132, 133]. Note that the gauge structure of SCET is much richer than the one of QCD, because each sector has its own gauge transformation [17].

To motivate the factorization formula we first discuss the vector current in SCET. Following the guideline from above, we naively have  $\bar{\psi}(x)\gamma^\mu\psi(x) \rightarrow \bar{\xi}_c(x)\gamma^\mu\xi_{\bar{c}}(x)$ . However, this is not completely correct. One obvious reason is that the vector current is not gauge invariant. The collinear quark fields  $\xi_c(x)$  and the anticollinear quark fields  $\xi_{\bar{c}}(x)$  transform under different gauge transformation. In the following we deduce the correct vector current using mostly physical arguments based on the kinematics of a two jet event in the small  $\tau$  region. We have to take the emission of usoft radiation, gauge invariance and non-local operators with derivatives into account.

- Usoft radiation: A collinear or anticollinear particle can emit an usoft gluon without changing its momentum scaling. The Feynman diagram for usoft gluon emission



from a collinear quark is shown on the top left in figure 2.9. Using the full theory Feynman rules and the decomposition in light cone coordinates in eq. (2.82) we can easily expand in  $\lambda$ . Keeping only the leading term we have

$$\frac{i\not{p}_c}{p_c^2} ig_{\text{YM}} \gamma^\mu \frac{i(\not{p}_c + \not{p}_{us})}{(p_c + p_{us})^2} \rightarrow \frac{i\not{p}_c}{p_c^2} \times ig_{\text{YM}} n^\mu \frac{i}{n \cdot p_{us}}. \quad (2.86)$$

The usoft gluon emission factorizes in the propagator for the collinear quark with momentum  $p_c$  and an eikonal factor. This factorization is graphically shown in figure 2.9. The emission of a usoft gluon can be arbitrarily often iterated and can be accounted for in SCET by a field redefinition of the collinear quark using a usoft Wilson line

$$S_n(x) = \text{P exp} \left[ ig_{\text{YM}} \int_{-\infty}^0 ds n \cdot A_{us}(x + sn) \right]. \quad (2.87)$$

The field redefinition reads  $\xi_c(x) \rightarrow S_n(x_-) \xi_c(x)$  with  $x_- = (\bar{n} \cdot x) n^\mu / 2$ . The other components of  $x$  are dropped, because they lead to power suppressed terms<sup>6</sup>. This expansion is called due to its similarity to electrostatics multipole expansion [19, 134]. By expanding the usoft Wilson line in  $g_{\text{YM}}$  and switching to momentum space we recover the eikonal factors in eq. (2.86). The field redefinition completely decouples the usoft sector from the collinear sector in the SCET Lagrangian at leading power in  $\lambda$  [17]. This is similar to the decoupling transformation in HQET. With  $\xi_{\bar{c}}(x) \rightarrow S_{\bar{n}}(x_+) \xi_{\bar{c}}(x)$  also the interactions between the anticollinear and usoft particle decouple and we have [17]

$$\mathcal{L}_{\text{SCET}} = \mathcal{L}_c + \mathcal{L}_{\bar{c}} + \mathcal{L}_{us} + \dots, \quad (2.88)$$

where the ellipses denote power corrections and  $\mathcal{L}_c$ ,  $\mathcal{L}_{\bar{c}}$  and  $\mathcal{L}_{us}$  are the Lagrangian of the collinear, anticollinear and usoft sector, respectively. These Lagrangian are each formally equivalent (boosted) copies of the QCD Lagrangian at leading order in  $\lambda$  [14, 15]. The relevant interactions among the different sectors are only due to external current operators in SCET, see e.g. eq. (2.93) below.

- Gauge invariance: To render the proposed vector current gauge invariant we introduce a collinear Wilson line

$$W_c(x) = \text{P exp} \left[ ig_{\text{YM}} \int_{-\infty}^0 ds \bar{n} \cdot A_c(x + sn) \right] \quad (2.89)$$

---

<sup>6</sup>The position vector in the collinear field has the scaling  $x \sim (1/\lambda^2, 1, 1/\lambda)/Q$ , such that  $x \cdot p_c \sim 1$ . Next we expand the usoft gluon field for small distances keeping only the leading term

$$\begin{aligned} A_{us}^\mu(x) &= A_{us}^\mu(0) + (x \cdot \partial) A_{us}^\mu(0) + \mathcal{O}(x^2) \\ &= A_{us}^\mu(0) + [(x_- \cdot \partial) A_{us}^\mu(0) + \mathcal{O}(\lambda^3)] + \mathcal{O}(x^2) = A_{us}^\mu(x_-) + \mathcal{O}(\lambda^3). \end{aligned}$$

and use  $W_c^\dagger(x)\xi_c(x)$  as gauge invariant building block [16]. Here we assume that the gauge transformation at infinity is trivial. In principle we can choose any path starting at infinity and ending at  $x$  to achieve gauge invariance. However, the collinear Wilson line has also a physical interpretation beyond the need for gauge invariance and for the reasons discussed below the path has the direction  $\bar{n}^\mu$ . In the final state we not only have collinear particles which arise from collinear splitting. For instance in the full theory a collinear gluon can also be emitted from a anticollinear quark or a usoft gluon. To analyze these processes we conveniently work in the frame where the collinear particles become usoft. In this frame the originally usoft particles are highly energetic and the anticollinear particle are even more boosted, see figure 2.10. Hence in the boosted frame we have to deal with the emission of usoft (formerly collinear) gluons from highly energetic anticollinear particles which is accounted for by the Wilson line in eq. (2.89).

- Non-local operators: In HQET operators with derivatives are power suppressed. This is no longer the case in SCET due to the particular momentum scaling of the collinear (and anticollinear) particles

$$(\bar{n} \cdot \partial)\xi_c(x) \sim (\bar{n} \cdot p_c)\xi_c(x) \sim \lambda^0 \xi_c. \quad (2.90)$$

Therefore we have to include an infinite tower of derivatives

$$\sum_{k \geq 0} \frac{C_k}{k!} (\bar{n} \cdot \partial)^k \xi_c(x) \quad (2.91)$$

in the vector current, where  $C_k$  is a Wilson coefficient. Note that for  $C_k = s$  the expression above simply evaluates to  $\xi_c(x + \bar{n}s)$ . Hence the infinite tower of derivatives effectively smears the collinear quark field along the light-like direction  $\bar{n}^\mu$  and we can replace it by

$$\int ds C(s) \xi_c(x + \bar{n}s). \quad (2.92)$$

In this way we get rid of the derivatives, but we have a non-local operator due to the convolution integral. Note that the coefficient  $C_k$  is the  $k$ -th moment of the function  $C(s)$ .

Putting all pieces together the most general vector current in SCET reads (see e.g. [122, 132])

$$j^\mu(x) = \int ds_1 \int ds_2 C(s_1, s_2) \bar{\xi}_c(x_1) W_c(x_1) S_n^\dagger(0) \gamma^\mu S_{\bar{n}}(0) W_c^\dagger(x_2) \xi_{\bar{c}}(x_2) \Big|_{\substack{x_1=x+\bar{n}s_1 \\ x_2=x+\bar{n}s_2}}. \quad (2.93)$$

Here we evaluate the usoft Wilson lines at the origin, because we again perform a multipole expansion keeping only the leading term. Note that the position vector scales like  $x \sim (1, 1, 1/\lambda)/Q$ , since the current has collinear and anticollinear fields  $p_c + p_{\bar{c}} \sim Q(1, 1, \lambda)$ . The Wilson coefficient  $C(s_1, s_2)$  can be computed from a matching calculation to full QCD and encodes the information on the physics at the hard scale. At leading order we have  $C(s_1, s_2) = \delta(s_1)\delta(s_2) + \mathcal{O}(\alpha_s)$ .

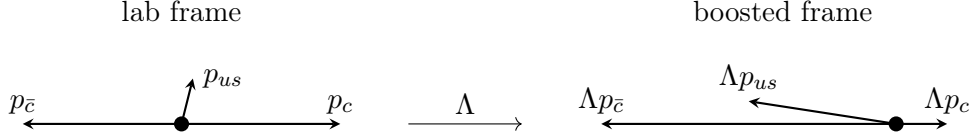


**Figure 2.10:** In the lab frame the collinear and anticollinear particles move back to back and we have wide angle usoft radiation. The boosted frame is related to the lab frame via the Lorentz transformation  $\Lambda$ . In the boosted frame the collinear particles become usoft and the usoft particles highly energetic. The length of the arrows indicates the energy of the particles.

### 2.4.3 Factorization formula for thrust and the jet function

After deriving the general form of the external vector current in SCET we can now study the matrix element in eq. (2.79) at leading order in  $\alpha_{\text{em}}$

$$i\mathcal{M}(e^+e^- \rightarrow \gamma^* \rightarrow X)(2\pi)^d \delta^d(q_1 + q_2 - p_X) \quad (2.94)$$

$$= -\alpha_{\text{em}} \int d^d x \int d^d y \langle X | j_\mu(x) A_{\text{em}}^\mu(x) A_{\text{em}}^\nu(y) \bar{\psi}(y) \gamma_\nu \psi(y) | e^-(q_1) e^+(q_2) \rangle \quad (2.95)$$

In order to perform the space-time integrals we compute the leptonic part including the photon propagator and we use the translation operator  $\hat{P}$  to move the vector current to the origin  $j^\mu(x) = e^{i\hat{P} \cdot x} j^\mu(0) e^{-i\hat{P} \cdot x}$ . The integrals evaluate to the momentum conserving  $\delta$ -distribution on the left-hand side in the equation above.

To get rid of the parameter integrals in the vector current in eq. (2.93) we again use the translation operator in the same fashion as before. We expand away all the power suppressed terms in  $\lambda$  and use that the total momentum  $p_X$  is in first approximation given by the sum of the collinear and anticollinear momenta. Eventually we end up with the Fourier transform of the Wilson coefficient

$$\tilde{C}(Q) = \int ds_1 \int ds_2 C(s_1, s_2) e^{i\bar{n} \cdot p_c s_1} e^{-in \cdot p_{\bar{c}} s_2}, \quad (2.96)$$

Due to symmetry considerations  $\tilde{C}$  can only depend on the product  $Q^2 = (\bar{n} \cdot p_c)(n \cdot p_{\bar{c}})$ . This is also intuitive, since the Fourier transformed Wilson coefficient  $\tilde{C}$  encodes the physics at the hard scale  $Q^2$ .

Combining all pieces and abbreviating the leptonic part with  $L_\mu(q_1, q_2)$  we have

$$i\mathcal{M}(e^+e^- \rightarrow \gamma^* \rightarrow X) = \alpha_{\text{em}} \tilde{C}(Q) L_\mu(q_1, q_2) \langle X | \bar{\xi}_c(0) W_c(0) S_n^\dagger(0) \gamma^\mu S_{\bar{n}}(0) W_{\bar{c}}^\dagger(0) \xi_{\bar{c}}(0) | 0 \rangle \quad (2.97)$$

When deriving the vector current we already argued that the soft, collinear and anticollinear sectors decouple at leading order, cf. eq. (2.88). Hence we have  $|X\rangle = |X_c\rangle \otimes |X_{\bar{c}}\rangle \otimes |X_{us}\rangle$  and see that already the matrix element factorizes

$$\langle X | \bar{\xi}_c(0) W_c(0) S_n^\dagger(0) \gamma^\mu S_{\bar{n}}(0) W_{\bar{c}}^\dagger(0) \xi_{\bar{c}}(0) | 0 \rangle \quad (2.98)$$

$$= \langle X_c | \bar{\xi}_c(0) W_c(0) | 0 \rangle \times \langle X_{us} | S_n^\dagger(0) \gamma^\mu S_{\bar{n}}(0) | 0 \rangle \times \langle X_{\bar{e}} | W_{\bar{e}}^\dagger(0) \xi_{\bar{e}}(0) | 0 \rangle.$$

Substituting the result in eq. (2.79) we get after some straightforward calculations the desired factorization formula for the differential cross section (see e.g. [20, 130] and references therein)

$$\begin{aligned} \frac{1}{\sigma_0} \frac{d\sigma}{d\tau} = & H(Q^2, \mu) \int dp^2 \int dq^2 \int d\omega J_c(p^2, \mu) J_{\bar{e}}(q^2, \mu) S_T(\omega, \mu) \delta \left( \tau - \frac{p^2 + q^2 + Q\omega}{Q^2} \right) \\ & + \mathcal{O}(\tau^0), \end{aligned} \quad (2.99)$$

where  $\mu$  is the renormalization scale, which we have for readability suppressed so far. The formula is valid to all orders in the strong coupling constant  $\alpha_s$  and at leading order in  $\tau$ , i.e. it gives the singular part of the differential cross section.

The hard function is given by  $H(Q^2, \mu) = |\tilde{C}(Q^2, \mu)|^2$ . Hence it is computed from a matching calculation to QCD and it is universal. The quark jet function  $J(p^2, \mu)$  is essentially given by the phase space integral over the squared absolute value of the collinear factor in eq. (2.98) (see eq. (2.100) below) and similar for the soft function  $S_T(\omega, \mu)$ . Also the quark jet function is universal in the sense that it is present in factorization formulas for many observables probing the invariant mass of the jets. It was introduced in [17] in the context of inclusive  $B$  decays. The soft function  $S_T(\omega, \mu)$  on the other hand is specific to the observable and encodes the information on the measurement. Note that the hard, jet and soft functions describe the physics at the scale  $Q^2$ ,  $Q^2\tau$  and  $Q^2\tau^2$ , respectively.

In this example the jets are initiated by a quark or antiquark, whereas there are also cases where a jet can be initiated by a gluon. For this reason we have to distinguish between a quark and gluon jet function. The gluon jet function was computed at one, two and three loops in [135], [136] and [137], respectively. The one loop result for the quark jet function was obtained in [138, 139] and the two-loop result in [140]. In chapter 5 we compute the quark jet function up to and including three loops. Going through the derivation of eq. (2.99) one finds

$$\begin{aligned} J(p^2) = & \frac{1}{2N_c} \oint d\Pi_{X_c} \text{Tr} \left[ \not{n} \langle 0 | W_c^\dagger(0) \xi_c(0) | X_c \rangle \langle X_c | \bar{\xi}_c(0) W_c(0) | 0 \rangle \right] \\ & \times (2\pi)^{d-2} \delta^{(d-2)}(p_{X_c}^\perp) (2\pi) \delta(Q - \bar{n} \cdot p_{X_c}) \delta(p^2 - p_{X_c}^2), \end{aligned} \quad (2.100)$$

where the trace is over color and spinor indices. The first  $\delta$ -distribution sets the total transverse momentum w.r.t. the jet direction to zero and the second sets the jet energy to  $Q/2$ . This is exactly what we expect when working in the lab frame. The last  $\delta$ -distribution fixes the invariant mass  $p^2$  of the jet. If all particles in the jet are perfectly collinear to the thrust axis, then the invariant mass vanishes. From eq. (2.100) we see that the jet function  $J(p^2)$  is related to the probability to find a jet with invariant mass  $p^2$ , where we however neglect any soft radiation. At leading order we simply have  $J(p^2) = \delta(p^2)$ . Using the (generalized) optical theorem we can rewrite the function as the

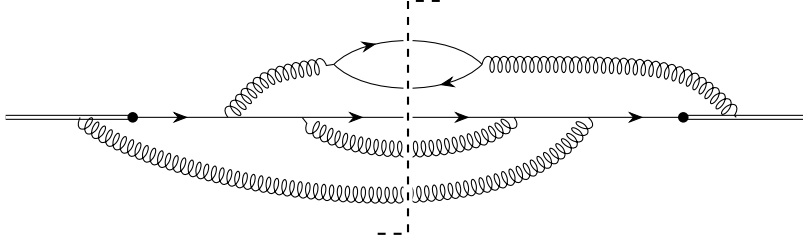


**Figure 2.11:** Graphical representation of the jet function given in eq. (2.100). The cut lines are on-shell, where the cut is indicated by the dashed line. Gluon, quarks and Wilson lines are represented by curly, solid and double lines, respectively.

imaginary part of a two point function, which is illustrated in figure 2.11. Furthermore, we can use that the collinear sector at leading order is equivalent to QCD and rewrite the two point function in terms of ordinary QCD fields [140]:

$$J(p^2) = \frac{1}{\pi N_c} \text{Im} \left[ \frac{i}{\bar{n} \cdot p} \int d^d x e^{-ip \cdot x} \langle 0 | \text{Tr} \left[ \frac{\not{\bar{n}}}{4} W^\dagger(0) \psi(0) \bar{\psi}(x) W(x) \right] | 0 \rangle \right], \quad (2.101)$$

Here the QCD Wilson line is given by

$$W(x) = \text{P exp} \left[ ig \int_{-\infty}^0 ds \bar{n} \cdot A(x + \bar{n}s) \right]. \quad (2.102)$$

To compute the jet function to high order in perturbation theory the representation in eq. (2.101) is more convenient, since it does not involve any phase space integrals. Note that in light-cone gauge with  $\bar{n} \cdot A(x) = 0$  the Wilson lines are trivial and the jet function equals the imaginary part of the quark propagator in this particular gauge. For practical calculations we find Feynman or covariant gauge more convenient, because the eikonal propagators arise from the Wilson lines and therefore have a graphical representation. In light cone gauge the eikonal factors are part of the gluon propagator and the Wilson lines are absent. Therefore in light cone gauge one has fewer Feynman diagrams, but the diagrams are more complicated than in covariant gauge.

#### 2.4.4 Resummation of the large logarithms

Finally we want to comment on the resummation of the large logarithms in the differential cross sections in eq. (2.79). The large logarithms are present due to the fact that in eq. (2.99) the hard, jet and soft functions are evaluated at the same renormalization scale, but each function describe the physics at a different scale. Therefore in order to resum the large logarithms we compute these functions at their natural scale where the logarithm are of order one and then evolve the result to the common scale using their respective RGE.

Let us consider the hard function  $H(Q^2, \mu)$  as an example. It has logarithms of the form  $\log(Q^2/\mu^2)$ , which become large when  $Q$  and  $\mu$  are not of the same order of magnitude. The RGE reads (see e.g. [141])

$$\frac{dH(Q^2, \mu)}{d \log \mu} = \left[ 2K(\alpha_s) \log \left( \frac{Q^2}{\mu^2} \right) + \gamma_H(\alpha_s) \right] H(Q^2, \mu) \equiv \gamma_H(\alpha_s, \mu) H(Q^2, \mu), \quad (2.103)$$

where  $K(\alpha_s)$  is the light-like cusp anomalous dimension and  $\gamma_H(\alpha_s)$  the non-cusp anomalous dimension of the hard function. The solution is given by

$$H(Q^2, \mu) = \exp \left[ \int_{\mu_h}^{\mu} \frac{d\tilde{\mu}}{\tilde{\mu}} \gamma_h(\alpha_s, \tilde{\mu}) \right] H(Q^2, \mu_h). \quad (2.104)$$

By choosing  $\mu_h \sim Q$  the logarithms in  $H(Q^2, \mu_h)$  are of order one. With the exponential factor we evolve the hard function from the scale  $\mu_h$  to any scale  $\mu$ , for instance the usoft scale  $\mu_{us}$  and resum in this way the large logarithms.

The RGEs for the jet function  $J(p^2, \mu)$  [140] and the soft function  $S_T(\omega, \mu)$  [20, 130] are nonlocal in  $p^2$  and  $\omega$ , because they involve a convolution integral. Using the plus distribution defined in eq. (2.81) we can write the RGE for the jet function in a very compact form

$$\frac{dJ(p^2, \mu)}{d \log \mu} = \left[ -2K(\alpha_s) \frac{1}{\mu^2} \mathcal{L}_0 \left( \frac{p^2}{\mu^2} \right) + \gamma_J(\alpha_s) \delta(p^2) \right] \otimes J(p^2, \mu), \quad (2.105)$$

where  $\gamma_J(\alpha_s)$  is the anomalous dimension of the jet function and the symbol  $\otimes$  denotes a convolution integral. This RGE can be solved in Laplace space. The RGE for the soft function looks similar.

## 2.5 Maximally supersymmetric Yang Mills theory

This chapter concludes with a brief overview of the maximally supersymmetric Yang-Mills theory [142, 143]. First we discuss the particle content and the Lagrangian of the theory, then conformal and dual conformal symmetry and finally a supersymmetric Wilson line operator. For a general introduction on supersymmetry see for example [144].

### 2.5.1 Lagrangian

We consider a gauge theory with  $\mathcal{N} = 4$  supersymmetries. This is the maximum number of supersymmetries for a supermultiplet of particles with spin  $s \leq 1$  allowing for a renormalizable Lagrangian. The supermultiplet consists of gluons  $A^\mu(x)$ , six scalars  $\phi^I(x)$  with  $I = 1, \dots, 6$  and four Majorana fermions  $\lambda_A$  with  $A = 1, \dots, 4$ . All particles

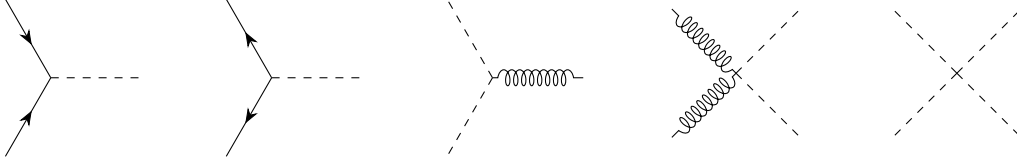


**Figure 2.12:** Vertices in  $\mathcal{N} = 4$  sYM in addition to the vertices in figure 2.1. Fermions, gluons and scalars are represented by solid, curly and dashed lines, respectively. The fermion flow is indicated by the arrows. Note that there are four fermion and six scalar flavours in the theory.

are massless and transform in the adjoint representation of  $SU(N_c)$ . This theory is in the following abbreviated as  $\mathcal{N} = 4$  sYM. The Lagrangian of the theory reads

$$\begin{aligned} \mathcal{L}_{\mathcal{N}=4} = \text{Tr} \left[ -\frac{1}{2} F_{\mu\nu} F^{\mu\nu} + 2i \bar{\lambda}_{\dot{\alpha}A} \sigma_{\mu}^{\dot{\alpha}\beta} D^{\mu} \lambda_{\beta}^A - (D_{\mu} \phi^I)(D^{\mu} \phi^I) + \frac{1}{2} g_{\text{YM}} [\phi^I, \phi^J] [\phi^I, \phi^J] \right. \\ \left. - g_{\text{YM}} \bar{\Sigma}_{AB}^I \lambda^{\alpha A} [\phi^I, \lambda_{\alpha}^B] + g_{\text{YM}} \Sigma^{IAB} \bar{\lambda}_{\dot{\alpha}A} [\phi^I, \bar{\lambda}_{\dot{B}}^{\alpha}] \right], \end{aligned} \quad (2.106)$$

where  $\Sigma^I$  and  $\bar{\Sigma}^I$  are Yukawa matrices,  $\sigma^{\mu} = (\mathbb{1}, \vec{\sigma})$  and  $\vec{\sigma}$  are Pauli matrices. The trace is in color space and the covariant derivative is in the adjoint representation  $D^{\mu} \Phi = \partial^{\mu} \Phi - i g_{\text{YM}} [A^{\mu}, \Phi]$ , where  $\Phi$  is some field of the supermultiplet. We omitted the gauge fixing term and the terms involving ghosts, as they are identical to QCD. The Lagrangian in eq. (2.106) can be derived from a  $\mathcal{N} = 1$  Yang-Mills theory in ten space-time dimension by means of dimensional reduction, see e.g. [145]. Therefore the Yukawa matrices  $\Sigma^I$  and  $\bar{\Sigma}^I$  are related to Dirac matrices in six-dimensional (Euclidean) space and satisfy  $\Sigma^I \bar{\Sigma}^J + \Sigma^J \bar{\Sigma}^I = -2\delta^{IJ}$ . In figure 2.12 we show the interaction vertices, which are present in addition to the QCD vertices shown in figure 2.1. Note that the Feynman rules for Majorana fermions are more subtle than those for Dirac fermions due to the fermion flow. This is relevant for the two distinct scalar-fermion vertices, cf. figure 2.12. For further information on the Feynman rules of Majorana fermions we refer to [146].

Although  $\mathcal{N} = 4$  sYM has no direct phenomenological applications, it has many interesting properties. This makes it particularly useful as a testing ground for developing new ideas and techniques for analytic multi-loop calculations. In the remainder of this section we focus on the properties that are relevant for chapter 4. First we discuss the most prominent feature of  $\mathcal{N} = 4$  sYM: it is a four-dimensional interacting conformal QFT.

### 2.5.2 Conformal symmetry

Conformal transformations leave the metric invariant up to a local scaling factor

$$dx^2 \rightarrow \Omega(x) dx^2. \quad (2.107)$$

This means that a conformal transformation locally preserves angles. Obviously, the Poincaré group is a subgroup ( $\Omega(x) \equiv 1$ ) of the conformal group. The additional generators of the conformal group read

$$D = -ix_\mu \partial^\mu, \quad K^\mu = i(2x^\mu x_\nu \partial^\nu - x^2 \partial^\mu), \quad (2.108)$$

where the former generates dilatations (scale transformations) and the latter special conformal boosts. A finite special conformal boost is given by

$$x^\mu \rightarrow \frac{x^\mu - a^\mu x^2}{1 - 2a \cdot x + a^2 x^2}, \quad (2.109)$$

where  $a^\mu$  is the parameter of the boost. This transformation can also be obtained from an inversion  $x^\mu \rightarrow x^\mu/x^2$ , then a translation with  $-a^\mu$  and finally again an inversion.

We already argued that QCD is not conformal, due to the non-vanishing beta function (and the quark masses).  $\mathcal{N} = 4$  sYM on the other hand is a conformal theory, even at the quantum level. This means that the beta function vanishes to all orders in perturbation theory. Hence amplitudes are UV finite and can only have IR divergences. The vanishing of the beta function was first observed in perturbation theory up to three loops [147–152] and later shown to be an all order statement [153–155]. However, this does not mean that there are no UV divergences in  $\mathcal{N} = 4$  sYM. Operators like for instance a cusped Wilson loop or the Konishi operator  $O_K = \text{Tr}[\phi^I \phi^I]$  [156] still give rise to UV divergences and have to be renormalized.

### 2.5.3 Dual conformal symmetry

There are only two free parameters in  $\mathcal{N} = 4$  sYM: the Yang-Mills coupling  $g_{\text{YM}}$  and the number of colors  $N_c$  of the gauge group  $SU(N_c)$ . One often studies the limit  $N_c \rightarrow \infty$  and  $g_{\text{YM}} \rightarrow 0$  such that  $g^2 = g_{\text{YM}}^2 N_c / (16\pi^2)$  remains finite. In this limit only planar Feynman diagrams contribute to scattering amplitudes or correlation functions [157]. One particularly interesting feature is that maximally helicity violating (MHV) scattering amplitudes have a hidden symmetry in this planar limit. The symmetry is called dual conformal symmetry<sup>7</sup> [158–162]. It is an exact symmetry at tree level, which is broken at loop level.

Let us consider the one loop box integral shown in figure 2.13 as an simple example to illustrate the dual conformal symmetry. The box integral in momentum space is given by

$$I_{\text{box}} = \int \frac{d^d k}{i\pi^{d/2}} \frac{(p_1 + p_2)^2 (p_2 + p_3)^2}{[-k^2][-(k + p_1)^2][-(k + p_1 + p_2)^2][-(k + p_1 + p_2 + p_3)^2]}, \quad (2.110)$$

with  $p_i^2 = 0$ . This integral is UV finite, but suffers from IR divergences.

---

<sup>7</sup>Dual conformal symmetry is a dynamical symmetry and it is not realized on the level of the Lagrangian.



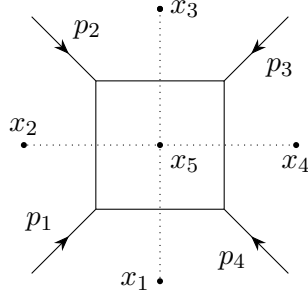


**Figure 2.13:** Box integral defined in eq. (2.110). The internal propagators and the external momenta  $p_i$  are massless. The dual coordinates  $x_i$  are indicated by dots and connected by dotted lines.

Next we introduce dual coordinates (or region momenta)  $x_i$  defined by

$$x_{ij} = x_i - x_j, \quad k = x_{51}, \quad p_1 = x_{12}, \quad p_2 = x_{23}, \quad p_3 = x_{34}, \quad p_4 = x_{41}. \quad (2.111)$$

They also have a graphical representation, see figure 2.13. After the change of variables the box integral takes the form

$$I_{\text{box}} = \int \frac{d^d x_5}{i\pi^{d/2}} \frac{x_{12}^2 x_{23}^2}{x_{15}^2 x_{25}^2 x_{35}^2 x_{45}^2}. \quad (2.112)$$

Assuming the integral would be free of any IR divergences and we could compute it directly in  $d = 4$  dimensions, this integral would be invariant under (dual) conformal transformation. The only non-trivial transformation to check are special conformal boosts. As argued above, we equivalently check for translation and inversion invariance. Translation invariance is trivial due to the differences  $x_{ij}$ . Under inversion it is straightforward to show that  $x_{ij} \rightarrow x_{ij}/(x_i^2 x_j^2)$  while the integration measure transforms as  $d^4 x_5 \rightarrow d^4 x_5/(x_5^2)^d$ . Thus we conclude that the box integral is naively dual conformal invariant in  $d = 4$  dimensions.

The box integral is however IR divergent and dimensional regularization breaks the dual conformal symmetry. Still, in [158] it was observed that up to three loops all integrals contributing to the four-gluon amplitude are naively dual conformal. At one-loop only the box integral in eq. (2.110) contributes. This can be utilised in the computation of the integrand of an amplitude, since (naive) dual conformal symmetry strongly restricts the allowed loop integrals, see e.g. [163–165]. The breaking of the dual conformal symmetry can be expressed in terms of anomalous Ward identities involving the generators for dilatations  $D$  and special conformal boosts  $K^\mu$  [161, 162]. These Ward identities have unique solutions for four and five point scattering amplitudes. The solutions agree with the Bernd-Dixon-Smirnov ansatz [166]. For scattering amplitudes with higher multiplicity the Ward identities allow for an a priori arbitrary functional dependence on dual conformal cross-ratios [161, 162]. Note that the Ward identities were derived from a

duality between polygonal light-like Wilson loops and MHV scattering amplitudes. For more information on this duality we refer to the original works [160, 161, 167] and the reviews [168, 169].

In chapter 4 we consider massive amplitudes in  $\mathcal{N} = 4$  sYM [72], where the masses are generated by the Higgs mechanism. The masses regulates the IR divergences of the amplitudes in a natural way. Hence these amplitudes are finite and we do not need dimensional regularization. Dual conformal symmetry is an exact symmetry of these scattering amplitudes. We use this in chapter 4 for a dual conformal partial wave analysis, allowing us to find suitable variables to describe the Regge limit of the massive scattering amplitudes.

Note that dual conformal transformations are very distinct from conformal transformations. The former act on dual coordinates, while the latter act on space-time coordinates and thus also on field operators. Dual conformal symmetry is a dynamical symmetry, hence it is not realized on the level of the Lagrangian. In fact it can be viewed as the generalization of the hidden Laplace-Runge-Lenz symmetry of the hydrogen atom [170]. The preservation of the Laplace-Runge-Lenz vector extends the  $SO(3)$  rational symmetry of the hydrogen atom to a  $SO(4)$  symmetry.

#### 2.5.4 Maldacena Wilson line operator

We close this section with a brief discussion on supersymmetric Wilson lines. In section 2.3 we showed that the interactions of an infinitely heavy quark moving along a path  $C$  are described by a phase factor given by a Wilson line  $W[C]$ , c.f. eqs. (2.63) and (2.65). In  $\mathcal{N} = 4$  sYM all particles are massless due to supersymmetry. One can however introduce massive  $W$ -bosons via a Higgs mechanism. In complete analogy to HQET, the corresponding phase factor for the  $W$ -bosons is then given by the Maldacena Wilson line [171]

$$W_{\mathcal{N}=4}[C] = \text{P exp} \left[ ig_{\text{YM}} \int_C ds \left\{ \dot{x}_\mu A^\mu(x(s)) + |\dot{x}| n_I(s) \phi^I(x(s)) \right\} \right], \quad (2.113)$$

with  $n^2(s) = 1$ . For a detailed derivation see e.g. [172]. Here we are only interested in time-like contours ( $|\dot{x}| = \sqrt{\dot{x}^2}$ ). For a light-like contour ( $|\dot{x}| = 0$ ) the Maldacena Wilson line reduces to the ordinary Wilson line.

At first, the appearance of the scalars  $\phi_I$  in eq. (2.113) seems surprising. However, this can be understood from the ten-dimensional reduction of the  $\mathcal{N} = 1$  sYM Lagrangian to the four-dimensional  $\mathcal{N} = 4$  sYM Lagrangian, as we show below. We start with the ten-dimensional Wilson line

$$W[C] = \text{P exp} \left[ ig_{\text{YM}} \int_C dX_m A^m(X) \right]. \quad (2.114)$$

## 2.5 Maximally supersymmetric Yang Mills theory

In the dimensional reduction we assume that the gluons  $A^m$  and the other fields only depend on the first four components  $x^\mu$  of the ten-dimensional space-time coordinate  $X^m$ . Furthermore, the ten-dimensional gluons are decomposed as follows  $A^m = (A^\mu, \phi^I)$ , where  $A^\mu$  and  $\phi^I$  will eventually be the gluons and scalars of  $\mathcal{N} = 4$  sYM. By considering a light-like contour with the parametrization  $\dot{X}^m = (\dot{x}^\mu, i|\dot{x}|n^I)$ , we get the Maldacena Wilson line in eq. (2.113).

The amount of supersymmetries preserved by the Maldacena Wilson line depends on the specific contour. For instance the straight Wilson line and the circular Wilson loop are 1/2 BPS (Bogomol'nyi-Prasad-Sommerfield) operators, i.e. their expectation values preserve half of the supersymmetries. There are also contours leading to fewer supersymmetries, see e.g. [173–176].



---

## Multiloop techniques

---

In this appendix we explain the various steps of a (multi-)loop computation. As a simple example we consider in most parts the angle-dependent cusp anomalous dimension at one loop. Note that we also comment on features and issues which appear in more involved computations. The computationally most expensive and involved parts of a loop calculation of a scattering amplitude or correlation function are the computation of the integrand and the master integrals. After this is done one obtains the bare result of the scattering amplitude or correlation function. The next step is then the renormalization of the bare result. Renormalization, however, is well understood and straightforward in theories where multi-loop results are desired, like e.g. QCD,  $\mathcal{N} = 4$  sYM and at leading order in HQET and SCET. Here we do not address phase space integration, which is eventually needed to compute a cross section or decay rate from a scattering amplitude.

We start this chapter with an overview of the general computational workflow of a loop calculation, where the main steps are summarized. The following sections then address in more detail the required multi-loop techniques and methods appearing in the different steps of the calculation. This includes IBP reductions of Feynman integrals, Feynman integral representations, dimensional recurrence relations and the differential equation method for computing master integrals. Furthermore, we review harmonic polylogarithms, a class of functions which frequently appear in multi-loop computations.

### 3.1 Workflow of a loop calculation

The aim of this section is to explain the workflow of a loop calculation on the example of the one-loop angle-dependent cusp anomalous dimension  $\Gamma_{\text{cusp}}(\phi)$ . We compute  $\Gamma_{\text{cusp}}(\phi)$  in momentum space using the HQET formalism. In sections 2.3 the physical background of  $\Gamma_{\text{cusp}}(\phi)$  and its connection to HQET is explained. In order to compute it we only need the one particle irreducible vertex function  $V(\phi)$  in HQET. Loosely speaking  $V(\phi)$



**Figure 3.1:** On the left the only one-loop diagram contributing to the vertex function  $V(\phi)$  is shown. On the right the graphical representation of the integral family defined in eq. (3.1) is shown. Gluon, eikonal and quadratic propagators are denoted by curly, double and solid lines, respectively.

loop order	gluonic	with fermion loop(s)	total
1	1	0	1
2	10	1	11
3	158	33	191
4	3184	1047	4231

**Table 3.1:** Number of Feynman diagrams contributing to the vertex function  $V(\phi)$  up four loops.

can be interpreted as a scattering amplitude of an infinitely heavy quark which moves with velocity  $v_1$ , then scatters at an external (classical) gauge field to instantaneously change its velocity to  $v_2$ . We have  $v_1^2 = v_2^2 = 1$  and the Euclidean cusp angle is given by  $\cos(\phi) = v_1 \cdot v_2$ . See also the one-loop diagram in figure 3.1. Below we go step by step through the different stages of the calculation. This section is intended to be an overview and summary and we explain some of the subjects presented here in more detail in the following sections.

### 3.1.1 Feynman diagrams

In a perturbative calculation which relies on an expansion in Feynman diagrams, the first step is to identify all the needed Feynman diagrams at a given loop order. At tree level or one-loop the Feynman diagrams for scattering amplitudes or correlation functions with few external legs can be found manually. The number of Feynman diagrams, however, increases rapidly with the number of loops and legs of a scattering amplitude or a correlation function. In table 3.1 we show the number of Feynman diagrams contributing to  $V(\phi)$  up to including and four loops. At one-loop only one Feynman diagram contributes to  $V(\phi)$ . It is presented in figure 3.1.

We want to remind the reader that Feynman diagrams are graphical representations of Wick contractions. Hence finding all relevant Feynman diagrams is essentially a combinatorial problem, which can be automatized. For the research projects in this thesis

```

*--#[ D1 :

* vertices :
  cV(3,Hv,hv,gl,1*3+1,1*3+2,1*3+3,k1-q1,q1,-k1) *
  cV(3,Hw,hw,gl,2*3+1,2*3+2,2*3+3,-q2,-k1+q2,k1) *
  cV(3,Hw,hv,ph,3*3+1,3*3+2,3*3+3,k1-q2,-k1+q1,-q3) *

* propagators :
  cP(gl,gl,1*3+3,2*3+3,-k1) *
  cP(hv,Hv,3*3+2,1*3+1,-k1+q1) *
  cP(hw,Hw,2*3+2,3*3+1,-k1+q2) *

* legs :
  cI(hv,1,1*3+2,q1) *
  cO(hw,2*3+1,2,q2) *
  cO(ph,3*3+3,3,q3) *

* diagram factor :
  (+1);

*--#[ D1 :

```

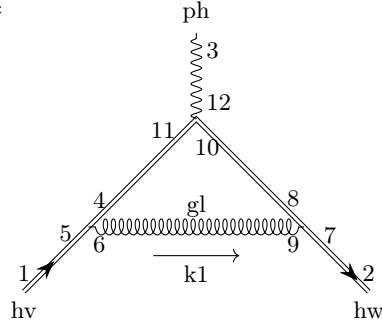


**Figure 3.2:** Sample output from **qgraf** [177] and the corresponding Feynman diagram.

The output style of **qgraf** can be customized to a very high degree to suit the problem at hand. Here **cV**, **cP**, **cI** and **cO** are heads for the vertices, propagators, incoming particles and outgoing particles, respectively. The diagram factor is the product of the symmetry factor and factors of  $(-1)$  from closed fermion and ghost loops as well as from interchanged fermion legs. We denote in the output file gluons, photons and the HQET fields  $h_{v_1}$  and  $h_{v_2}$  with **ph**, **gl**, **hv** and **hw**, respectively. Additionally we have  $H_v = \bar{h}_{v_1}$  and  $H_w = \bar{h}_{v_2}$ . The photon is only introduced as an ancillary particle to have a cusp, i.e. a vertex with  $\bar{h}_{v_2}$  and  $h_{v_1}$ . Furthermore,  $q_1$ ,  $q_2$  and  $q_3$  are the external momenta assigned by **qgraf**. In this problem we can set them to zero. The loop momentum is denoted by  $k_1$ . The vertices, propagators and legs have unique indices which specify how the propagators and legs are attached to the vertices. See also the Feynman diagram where the indices are shown. These indices are computed from internal counters of **qgraf**, hence they have for instance the form  $1*3+1$  instead of simply 4.

we use the computer program **qgraf** [177] to generate the Feynman diagrams. A sample **qgraf** output of the diagram in figure 3.1 is shown in figure 3.2.

### 3.1.2 Integral families

The next step is to find enough integral families, such that each Feynman diagram can be mapped to at least one of these families. In our example we only need one integral family given by

$$G(a_1, a_2, a_3) = e^{\epsilon\gamma_E} \int \frac{d^d k}{i\pi^{d/2}} \frac{1}{D_1^{a_1} D_2^{a_2} D_3^{a_3}}, \quad a_i \in \mathbb{Z}, \quad (3.1)$$

where we have the following factors in the denominator

$$D_1 = -2v_1 \cdot k + 1, \quad D_2 = -2v_2 \cdot k + 1, \quad D_3 = -k^2. \quad (3.2)$$

For the kinematics we have  $v_1^2 = v_2^2 = 1$  and  $v_1 \cdot v_2 = \cos(\phi)$ . Furthermore, we introduce the variable  $x = e^{i\phi}$ . It turns out that  $x$  is the natural variable for computing the necessary Feynman integrals. The Feynman diagram generated by **qgraf** in figure 3.2 is mapped with the momentum shift  $k \rightarrow -k$  to the integral family above. To search for a mapping of a Feynman diagram to an integral family we only need to consider the denominator of the diagram, i.e. only the propagator structure of the diagram is relevant. In this way we can associate with each Feynman diagram a scalar integral. The mapping of an integral to an integral family is described in more detail in section 3.2.

Finding the integral families can be done manually by looking at the Feynman diagrams. A good starting point are the planar Feynman diagrams. Using dual coordinates (see section 2.5) it is possible to construct one planar integral family which covers all planar Feynman diagrams. Empirically this planar family also covers a big fraction of the non-planar diagrams. Then we add successively non-planar integral families until all Feynman diagrams are covered. The process of finding all the necessary integral families can be automatized, as it is for example implemented in the Mathematica package **TopoID** [178, 179]. Note that **TopoID** does not support eikonal propagators.

Due to the IBP reduction in the later stages of the calculation we only consider complete integral families<sup>1</sup>. At this stage of the calculation the integral families can also have linearly dependent propagators. Such integral families are needed in calculations with HQET or massive propagators, because these calculations can involve Feynman diagrams with linear dependent propagators.

---

<sup>1</sup>For the meaning of complete in this context see section 3.2



### 3.1.3 Feynman rules

We proceed by substituting the specific Feynman rules for the vertices, propagators and external legs in the Feynman diagrams. Using the HQET Feynman rules we get for the diagram in figure 3.1

$$\frac{\text{Tr}[T_R^a T_R^a]}{N_c} \int \frac{d^d k}{(2\pi)^d} \frac{-2i}{[-2v_2 \cdot k + 1]} \frac{-2i}{[-2v_1 \cdot k + 1]} (ig_{\text{YM}} v_2^\mu) (ig_{\text{YM}} v_1^\nu) \frac{i}{[-k^2]} \left( g_{\mu\nu} + \xi^b \frac{k_\mu k_\nu}{[-k^2]} \right). \quad (3.3)$$

We work in covariant gauge, where  $\xi^b = 0$  corresponds to Feynman and  $\xi^b = 1$  to Landau gauge. Here we have, for readability, already taken care of the color part of the diagram.

### 3.1.4 Lorentz, color and Dirac algebra

After substituting the Feynman rules, the next step is to perform the Lorentz, Dirac and color algebra. Then every diagram is expressed as a linear combination of scalar integrals of the integral families found in the beginning of the calculation. In our example we get for the one-loop diagram

$$\mathcal{N} \frac{\alpha_s^b}{4\pi} C_R \left\{ \xi^b [G(0, 1, 2) + G(1, 0, 2) - G(1, 1, 2) - G(0, 0, 2)] - 2 \frac{1+x^2}{x} G(1, 1, 1) \right\}, \quad (3.4)$$

where  $x = e^{i\phi}$  and  $\phi$  is the Euclidean cusp angle. The factor  $\mathcal{N} = (4\pi)^\epsilon e^{-\epsilon\gamma_E}$  follows from the definition of the integrals and the generic loop factor  $1/(2\pi)^d$ . It is not important and will eventually be absorbed in the renormalization scale, since we employ the  $\overline{\text{MS}}$  scheme.

Performing the Lorentz, Dirac and color algebra and rewriting the diagrams in terms of scalar integrals can be computational expensive at higher loop order or if the problem has many legs. However, this step is easy to parallelize. In principle each diagram can be computed on a different CPU core.

### 3.1.5 Partial fraction decomposition

It is possible that Feynman diagrams can have linearly dependent propagators, which consequently lead to integrals with the same property. This is for example the case in the computation of the cusp anomalous dimension and the quark jet function starting at two loops. The publicly available IBP reduction programs like **FIRE** [180, 181], **Reduze** [182, 183], **KIRA** [184, 185] and **LiteRed** [186, 187] only support out of the box integrals with linear independent propagators. For this reason we perform a multivariate partial fraction decomposition of the integrals with linear dependent propagators before the IBP

reduction using the algorithm introduced in [188]. The algorithm constructs for a given integral family a set of replacement rules. Then the partial fraction decomposition of any integral of the family is achieved by recursively applying these rules to the integral. The use of a Gröbner basis when constructing the replacement rules ensures that the recursion terminates. After the partial fraction decomposition an integral with linear dependent propagators is expressed in a linear combination of integrals with linear independent propagators.

### 3.1.6 Integration-by-parts reduction

After expressing all diagrams in terms of scalar Feynman integrals, we perform the IBP reduction of these integrals. With the help of the IBP reduction we can express any integral of a given integral family in terms of a finite number of basis integrals of the same integral family. These basis integrals are also called master integrals. Note that the choice of master integrals is not unique, but there is some degree of freedom to choose master integrals. The number of master integrals is typically much smaller than the number of Feynman integrals appearing in the diagrams, which means we only have to compute a relatively small number of integrals. Therefore the IBP reduction simplifies a problem tremendously and is the key ingredient of Feynman diagram based perturbative calculations. The IBP reduction, however, is typically also the computationally most expensive part of a (multi-)loop calculation.

Applied to our example problem we find that there two master integrals, which we choose to be  $G(0, 1, 1)$  and  $G(1, 1, 1)$ . Expressing the one-loop diagram in terms of these master integrals we get

$$\mathcal{N} \frac{\alpha_s^b}{4\pi} C_R \left\{ 2\xi^b(d-3)G(0, 1, 1) - \left[ \xi^b(d-4)\frac{(1+x)^2}{2x} + 2\frac{1+x^2}{x} \right] G(1, 1, 1) \right\}. \quad (3.5)$$

Note that the simplification due to the IBP reduction of  $V(\phi)$  at one-loop is not so big, because we only have one diagram. For the IBP reduction in this example as well as for the projects in this thesis we use **FIRE5** [180] in combination with **LiteRed** [186, 187].

If we need several integral families to accommodate all the Feynman diagrams, then the IBP reduction has to be performed for each family separately and for each family we get a set of master integrals. In general these sets are not pairwise disjoint. Some master integrals can appear in several or even all integral families, albeit they can have different momentum space representations in each integral family. The next step after the IBP reduction is to find a minimal set of independent master integrals of all integral families. For this we search for mappings between the master integrals of all the integral families. Note that if a gauge invariant object is expressed in terms of independent master integrals, then the gauge parameter has to drop out. This can be utilized as a powerful crosscheck of the calculation even before computing the master integrals.

### 3.1.7 Computing the master integrals

To obtain the bare result the only task left is to compute the master integrals. In section 3.3 we compute the eikonal bubble integral  $G(0, 1, 1)$  using Feynman parameters. The triangle integral  $G(1, 1, 1)$  is computed in section 3.5 using the differential equation method. Substituting their respective analytic results in eq. (3.5) we get

$$\mathcal{N}C_R\frac{\alpha_s^b}{4\pi\epsilon}\left[2\frac{1+x^2}{1-x^2}\log(x)-\xi^b\right]+\mathcal{O}(\epsilon^0). \quad (3.6)$$

### 3.1.8 Renormalization

The last step is the renormalization. Since we take the HQET propagators to be off-shell, the expression in eq. (3.6) is IR finite. All the divergences are of UV origin. To uncover the UV divergences from the cusp point, we first have to take care of the UV divergences from the operators in the QCD Lagrangian. This is conveniently achieved by substituting the bare strong coupling constant and the bare gauge parameter (if present) by their renormalized counterparts using  $\alpha_s^b = \mu^{2\epsilon}Z_\alpha\alpha_s(\mu)$  and  $1 - \xi^b = Z_A(1 - \xi(\mu))$  in eq. (3.6). Since the renormalization factors have the form  $Z = 1 + \mathcal{O}(\alpha_s(\mu))$ , these substitutions do not affect the structure of the one-loop result. Next we absorb the normalization factor  $\mathcal{N}$  into the renormalization scale  $\mu$  and compute

$$\log V(\phi) - \log V(0) = \frac{\alpha_s(\mu)}{\pi} \left[ \frac{C_R}{2\epsilon} \left( \frac{1+x^2}{1-x^2} \log(x) + 1 \right) + \mathcal{O}(\epsilon^0) \right] + \mathcal{O}(\alpha_s^2(\mu)), \quad (3.7)$$

with  $x = e^{i\phi}$ . At this point the only divergences left are those from the cusp point. Since the cusp anomalous dimension is gauge invariant, the gauge parameter has to drop out in the divergent terms, as we can observe in the one-loop result above. Following along the lines of section 2.2 we finally get for the cusp anomalous dimension

$$\begin{aligned} \Gamma_{\text{cusp}}(\phi, \alpha_s) &= -\frac{\alpha_s(\mu)}{\pi} C_R \left( \frac{1+x^2}{1-x^2} \log(x) + 1 \right) + \mathcal{O}(\alpha_s^2(\mu)) \\ &= \frac{\alpha_s(\mu)}{\pi} C_R (\phi \cot \phi - 1) + \mathcal{O}(\alpha_s^2(\mu)). \end{aligned} \quad (3.8)$$

### 3.1.9 Implementation

Several of the steps explained above are implemented as custom **Mathematica** code written by the author. The code was extensively used in all three projects of the thesis. First the code reads in the **qgraf** output and then finds the momentum shifts of the loop momenta that map the Feynman diagrams to user-defined integral families. Next we use the code to perform the Lorentz, color and Dirac algebra and express every diagram in

terms of scalar integrals. In the code the algorithm of [188] is implemented for the partial fraction decomposition of integrals with linearly dependent propagators. For the IBP reduction we use the publicly available programs `FIRE5` in combination with `LiteRed`. To find the minimal set of master integrals we again use the custom code. Furthermore, the code includes several functions to compute the differential equation for the master integrals (see section 3.5).

With this code we automatized the computation of Feynman diagrams to a very high degree. The last missing piece for a complete automatization is the process of finding all the required integral families. Although the code is written in `Mathematica`, for all the projects in this thesis the performance was sufficient. A significant performance boost can most likely be achieved by implementing the computationally most expensive parts of the code in `FORM` [189–191].

## 3.2 Integration-by-parts reductions of Feynman integrals

Integration-by-parts (IBP) reduction of Feynman integrals [192, 193] is a crucial tool in modern multi-loop computations. It allows to express any Feynman integral in a given problem in terms of a finite set of so-called master integrals. Therefore only these master integrals have to be calculated. The number of master integrals is typically several orders of magnitude smaller than the number of Feynman integrals appearing in all the required Feynman diagrams, especially at higher loop order. Furthermore, IBP reductions are a key ingredient in the differential equation method to compute master integrals [194–200]. Before we explain the IBP reduction itself we introduce some terminology used in this context.

### 3.2.1 Integral family

In eq. (3.1) we introduced the integral family needed for the computation of the cusp anomalous dimension  $\Gamma_{\text{cusp}}(\phi, \alpha_s)$  at one loop. The family has three factors  $\{D_i\}$  given in eq. (3.2). We allow these factors to be raised to some integer powers  $\{a_i\}$ . In general an  $L$ -loop integral family has the form

$$e^{L\gamma_L\epsilon} \int \frac{d^d k_1}{i\pi^{d/2}} \cdots \int \frac{d^d k_L}{i\pi^{d/2}} \frac{1}{D_1^{a_1} \cdots D_n^{a_n}}, \quad (3.9)$$

where the factors  $\{D_i\}$  depend on the loop momenta, the external momenta and internal masses. The factors can be quadratic or eikonal. For the IBP reduction, which we explain in the following subsections, it is important that the integral family is complete in the sense that every scalar product involving loop momenta can be expressed in terms of the factors  $\{D_i\}$ . Furthermore, linearly independent factors are preferable.

In most cases the integral families are deduced from Feynman diagrams. Then the propagators of the Feynman diagram, i.e. the factors in the denominator, define all or a subset of the factors  $\{D_i\}$ . For this reason we call factors of the form  $1/D_i$  also simply propagators. Often additional factors which are not needed to match the propagators in a Feynman diagram have to be introduced to render an integral family complete. These additional factors can then only appear in the numerator of an integral of the family. They can be directly written in the form of quadratic propagators or as scalar products, i.e. as eikonal propagators.

A sector of an integral family is the set of all integrals with the same propagators, i.e. we allow the propagators to be raised to different powers and we allow for factors in the numerator. The corner integral of a sector is the integral with no numerators and where all propagators have power one. There is an important observation which states that if the corner integral of a sector is zero, then all integrals of the sector also vanish. The top level sector of an integral family is the sector, where all allowed propagators are present. It is possible that an integral family has equivalent sectors. Two sectors are called equivalent when their corner integrals can be mapped onto each other.

Let us consider the integral family in eq. (3.1) as an example. The following integrals  $G(0, 1, 1)$ ,  $G(0, 2, 1)$  and  $G(-1, 1, 2)$  belong to the same sector, where the first integral is the corner integral. In the following we use the corner integral as a representative of the sector. The integral family (3.1) has in total seven sectors represented by  $G(0, 0, 1)$ ,  $G(0, 1, 0)$ ,  $G(1, 0, 0)$ ,  $G(1, 1, 0)$ ,  $G(0, 1, 1)$ ,  $G(1, 0, 1)$  and  $G(1, 1, 1)$ . The first four corner integrals are scaleless and therefore zero in dimensional regularization. Hence only the last three sectors have non-vanishing integrals. The sectors  $G(0, 1, 1)$  and  $G(1, 0, 1)$  are equivalent. We have the relation  $G(a_1, a_2, a_3) = G(a_2, a_1, a_3)$ , when  $a_2$  is a negative integer. The last integral  $G(1, 1, 1)$  represents the top level sector. Mappings between sectors of the same integral family as well as the knowledge on sectors with only vanishing integrals provide valuable information for the IBP reduction and can increase its performance significantly.

The natural starting point to establish if two sectors are equivalent or if an integral belongs to an integral family are shifts of the loop momenta. For example the two tadpole integrals

$$\int \frac{d^d k}{i\pi^{d/2}} \frac{1}{-(k+p)^2 + m^2}, \quad \int \frac{d^d k}{i\pi^{d/2}} \frac{1}{-k^2 + m^2} \quad (3.10)$$

have different propagators, but with the shift  $k \rightarrow k - p$  in the first integral we see that both integrals are identical. In this trivial example we can read off the momentum shift. When we have a more involved problem we can simply try a huge set of momentum shifts to establish an identity. This is a brute force method, but it works sufficiently fast for problems with either few external momenta or if the number of loops is small enough. Sometimes two integrals are identical, but there exist no momentum shift that relates both integrals. This is the case for example for the integrals  $G(1, 0, 1)$  and  $G(0, 1, 1)$ .

However, using the algorithm introduced in [188] we directly see the identity. The algorithm uses the  $\mathcal{U}$  and  $\mathcal{F}$  polynomials of Feynman integrals (see section 3.3) to test whether these integrals are identical. We want to remark that the algorithm of [188] is considerably faster than the trial and error method and it works also at a high loop order as well as with several external momenta. It is implemented in the IBP programs **LiteRed** [186,187] and **Kira** [184,185] for finding the mappings between the sectors of an integral family. Note that with the algorithm we can only prove that two integrals are either identical or not. In the former case the algorithm does not provide the momentum shift, even if there exists one.

### 3.2.2 IBP identities

The underlying principle behind IBP reductions are IBP identities [192, 193] between integrals of the same family. For instance for the integral family defined in eq. (3.1) we have the following IBP identity

$$\begin{aligned} 0 &= e^{\epsilon\gamma_E} \int \frac{d^d k}{i\pi^{d/2}} \frac{\partial}{\partial k^\mu} \frac{k^\mu}{D_1^{a_1} D_2^{a_2} D_3^{a_3}} \\ &= (d - a_1 - a_2 - 2a_3) G(a_1, a_2, a_3) + a_1 G(a_1 + 1, a_2, a_3) + a_2 G(a_1, a_2 + 1, a_3) . \end{aligned} \quad (3.11)$$

In the first step we used Gauß's theorem to relate the volume integral over the divergence of a vector field to a surface integral, where the surface lies at infinity. The surface integral evaluates to zero, because either the integrand falls off sufficiently fast at infinity or the integral is scaleless. In the second step we rewrite the numerator resulting from computing the divergence in terms of the factors  $D_1$ ,  $D_2$  and  $D_3$ . Then we express the result in terms of scalar integrals of the integral family. At this stage we see that it is important for the IBP identities that the integral family is complete. If the integral family is not complete, then it is possible that we encounter in the second step some numerator which cannot be expressed in the factors  $\{D_i\}$ . Completely analogous we can derive two more IBP identities

$$\begin{aligned} 0 &= 2a_1 G(a_1 + 1, a_2, a_3) - a_3 G(a_1 - 1, a_2, a_3 + 1) + a_3 G(a_1, a_2, a_3 + 1) \\ &\quad + 2a_2 \cos(\phi) G(a_1, a_2 + 1, a_3) , \end{aligned} \quad (3.12)$$

$$\begin{aligned} 0 &= 2a_2 G(a_1, a_2 + 1, a_3) - a_3 G(a_1, a_2 - 1, a_3 + 1) + a_3 G(a_1, a_2, a_3 + 1) \\ &\quad + 2a_1 \cos(\phi) G(a_1 + 1, a_2, a_3) , \end{aligned} \quad (3.13)$$

where we used the differential operators  $v_1^\mu \partial / \partial k^\mu$  and  $v_2^\mu \partial / \partial k^\mu$ , respectively. We see that the IBP identities relate integrals  $G(a_1, a_2, a_3)$  with different indices  $a_1$ ,  $a_2$  and  $a_3$  to each other. In the next subsection we briefly discuss two strategies how this can be utilized to express any integral of an integral family in terms of a finite set of basis integrals.

Note that there exists also identities relating integrals with different indices which are derived from the Lorentz invariance of the integrals [198]. These Lorentz invariance

identities are however not linearly independent from the IBP identities [201] and therefore do not provide any new information. Still, in practical applications it can be useful to include them.

### 3.2.3 IBP reductions with recursion relations

The idea behind the first strategy is to use the IBP identities to derive recursion relations, which express more complicated integrals in terms of simpler ones. In order to do so we first need a measure of what is simple. Considering the sector represented by  $G(0, 1, 1)$  the answer is easy: the smaller the sum  $a_2 + a_3$ , the simpler the integral  $G(0, a_2, a_3)$ . With this measure we see that the corner integral is the simplest integral of the sector.

Using the IBP identities (3.11) and (3.13) with  $a_3 \equiv 0$  we can find two simple recursion relations satisfying the criteria above

$$G(0, a_2 + 1, a_3) = \frac{(a_2 + 2a_3 - d)}{a_2} G(0, a_2, a_3) , \quad (3.14)$$

$$G(0, a_2, a_3 + 1) = \frac{2(d - a_2 - 2a_3)(a_2 + 2a_3 - d + 1)}{a_3(2a_3 - d + 2)} G(0, a_2, a_3) . \quad (3.15)$$

Provided the conditions  $G(0, 0, a_3) = 0$  and  $G(0, a_2, 0) = 0$  it is clear that with the help of both equations we can relate any integral  $G(0, a_2, a_3)$  to the corner integral  $G(0, 1, 1)$ . For this reason we refer to  $G(0, 1, 1)$  as the master integral of the sector. Note that the choice of master integrals is not unique. We can equally well choose  $G(0, 2, 1)$  as the master integral, although it is more complicated than  $G(0, 1, 1)$ . The IBP reduction does not provide any further information on the master integrals. They have to be calculated by other means.

The strategy of IBP reduction using recursion relations is implemented in the **Mathematica** program **LiteRed** [186, 187]. The program tries to derive such recursion relations in a heuristic fashion. It is however not guaranteed that the program is always successful.

### 3.2.4 IBP reductions with Laporta's algorithm

Most commonly Laporta's algorithm [202] or a derivative thereof is used for the IBP reduction. Public available IBP reduction programs are **FIRE** [180, 181], **Reduze** [182, 183] and **KIRA** [184, 185]. Compared to the previous method Laporta's algorithm has the advantage that it can in principle solve any IBP problem. Practically, however, it is limited by the available computational resources. The basic idea behind the algorithm is to generate a linear system of equations by substituting integers for the indices  $a_i$  in the IBP identities. The integrals are treated as the unknowns and are assigned a weight. We then solve the linear system by expressing the higher weight integrals in terms of lower

weight integrals. Since the linear system does not have full rank, not all integrals are determined by it. The remaining unknown integrals are the master integrals.

As an example we again work with the sector  $G(0, 1, 1)$ . We generate the relevant system with the IBP identities (3.11) and (3.13) and consider  $a_3 \equiv 0$  and  $a_2, a_3 \in \{1, 2\}$  as seeds

$$\begin{pmatrix} d-3 & 0 & 0 & 1 & 0 & 0 & 0 & 0 \\ 0 & 1 & 0 & 2 & 0 & 0 & 0 & 0 \\ 0 & d-5 & 0 & 0 & 1 & 0 & 0 & 0 \\ 0 & 0 & 2 & 0 & 2 & 0 & 0 & 0 \\ 0 & 0 & 0 & d-4 & 0 & 0 & 2 & 0 \\ 0 & -1 & 0 & 0 & 1 & 0 & 4 & 0 \\ 0 & 0 & 0 & 0 & d-6 & 0 & 0 & 2 \\ 0 & 0 & -2 & 0 & 0 & 2 & 0 & 4 \end{pmatrix} \cdot \begin{pmatrix} G(0, 1, 1) \\ G(0, 1, 2) \\ G(0, 1, 3) \\ G(0, 2, 1) \\ G(0, 2, 2) \\ G(0, 2, 3) \\ G(0, 3, 1) \\ G(0, 3, 2) \end{pmatrix} = \vec{0}. \quad (3.16)$$

Here we already used that the sectors  $G(0, 0, 1)$  and  $G(0, 1, 0)$  have only vanishing integrals. The matrix in eq. (3.16) has rank seven and it has eight rows. Hence all integrals in eq. (3.16) can be expressed through one master integral. Using the sum of the indices  $a_2 + a_3$  as weight, the master integral is  $G(0, 1, 1)$ .

Above we considered only one sector of the integral family in eq. (3.1). As discussed before, the integral family only has three non-vanishing sectors and two of them are equivalent. Using IBP reductions we find for each unique sector one master integral. We choose the master integrals to be the corner integrals of the sectors, i.e. we have  $G(0, 1, 1), G(1, 1, 1)$  as master integrals.

In general a non-vanishing sector can also have zero or more than one master integral. Which integrals are chosen as master integrals in Laporta's algorithm depends on the definition for the weight of an integral. A general definition can be found in [202], where Laporta's algorithm was introduced or in [203]. These definitions coincide with the natural understanding of when we call an integral simple. Integrals with fewer propagators have smaller weight. Furthermore, integrals with smaller propagator powers and with fewer factors in the numerator have smaller weight. Assuming a sector has several master integrals, then the corner integral is always chosen as master integral by this criteria. For the additional master integrals we then have to decide if we prefer integrals with raised propagator powers or with factors in the numerator.

In more complicated IBP reductions the linear system can become large and in general the matrix of the system depends rationally on the space time dimension  $d$ , the kinematic invariants and internal masses. For this reason the IBP reductions can be computationally involved. During the generation of the linear system the information on the vanishing sectors and mappings between sectors should always be taken into account, because they reduce the size of the linear system and therefore improve the performance.



### 3.3 Feynman parameter integrals

Only in very simple Feynman integrals, like for instance the massive tadpole integral, the integration over the  $d$  dimensional loop momentum can directly be performed. It is however possible at the cost of introducing parameter integrals to rewrite the integrand of a generic Feynman integral into a form, where the loop integration can be performed. Therefore one trades the  $d$  dimensional loop integrations for a finite set of parameter integrations. The dependence on the kinematic invariants in the parameter integral representation becomes manifest, unlike in the integral in momentum space. Here we discuss Feynman parameter integrals. They are extremely useful to compute single scale integrals. In a single scale integral the dependence on the scale factorizes and is fixed by dimensional analysis, hence the only non-trivial information is the  $d$  dependent function multiplying the scale dependence. A multi-scale integral is harder to compute analytically, because then the parameter integrals depend non-trivially on the scales. The Feynman parameter integral representation is also the starting point for numerical integration using sector decomposition [204–209] and Mellin-Barnes techniques (see e.g. [210,211]). Furthermore, it can be used to establish dimensional recurrence relations [212] allowing to express a  $d - 2$  dimensional integral through  $d$  dimensional integrals.

In the following we first introduce the Feynman parameter integral representation and present two examples. Then we derive the representation and discuss with its help dimensional recurrence relations. We conclude this section with a strategy to efficiently compute loop integrals using the Feynman parameters.

#### 3.3.1 Definition and notation

We consider a generic  $L$  loop integral with  $n$  denominators  $D_i$  raised to some power  $a_i \in \mathbb{C} \setminus \{-1, -2, -3, \dots\}$

$$I(a_1, \dots, a_n) = \int \frac{d^d k_1}{i\pi^{d/2}} \cdots \int \frac{d^d k_L}{i\pi^{d/2}} \frac{1}{D_1^{a_1} \cdots D_n^{a_n}}. \quad (3.17)$$

The denominators can be massless, massive or eikonal, i.e. they have the general form  $D_i = -q_i^2 + m_i^2$  or  $D_i = v_i \cdot q_i + \delta_i$ . Here  $q_i$  is a linear combination of the loop momenta  $(k_1, \dots, k_L)$  and the external momenta,  $m_i$  is the mass of the propagator,  $v_i$  the direction of the eikonal propagator and  $\delta_i$  its off-shellness. The Feynman parameter integral representation of (3.17) is then given by [78, 213, 214]

$$I = \frac{\Gamma(a - Ld/2)}{\prod_{k=1}^n \Gamma(a_k)} \int_0^\infty dx_1 \cdots \int_0^\infty dx_n \delta\left(1 - \sum_{k \in I} x_k\right) \prod_{k=1}^n x_k^{a_k-1} \frac{\mathcal{U}^{a-(L+1)d/2}}{\mathcal{F}^{a-Ld/2}}, \quad (3.18)$$

with  $a = \sum_{k=1}^n a_k$  and  $I$  is a non empty subset of  $\{1, 2, \dots, n\}$ . The freedom of choice for  $I$  is known as Cheng-Wu theorem [215].  $\mathcal{U}$  is the first and  $\mathcal{F}$  the second Symanzik



**Figure 3.3:** The massless bubble integral (left) and the eikonal bubble integral (right) with arbitrary propagator powers  $a_1$  and  $a_2$ . Quadratic and eikonal propagators are represented by solid and double lines, respectively.

polynomial. They depend on the parameters  $\{x_i\}$ , the masses and the kinematic invariants. Both  $\mathcal{U}$  and  $\mathcal{F}$  are homogeneous polynomials in  $\{x_i\}$  with degree  $L$  and  $L + 1$ , respectively. We compute them from the denominators in (3.17) via

$$\sum_{k=1}^n x_k D_k = - \sum_{i,j=1}^n k_i^\mu M_{ij} g_{\mu\nu} k_j^\nu + 2 \sum_{j=1}^n k_j^\mu Q_{j,\mu} + J, \quad (3.19)$$

where  $M$  is a  $L \times L$  matrix,  $Q$  an  $L$ -dimensional vector and  $J$  a scalar in the  $(k_1, \dots, k_n)$  space<sup>2</sup>. Then we have

$$\mathcal{U} = \det(M), \quad \mathcal{F} = \det(M)(Q_\mu^T M^{-1} Q^\mu + J). \quad (3.20)$$

It is also possible to read off both polynomials from the graph of the integral [210, 216]. For a review on the properties of Feynman parameter integrals see for instance [216].

### 3.3.2 Examples

Before we proceed with the derivation of eq. (3.18) we present two examples:

- The massless bubble integral appears frequently in one-loop and in multi-loop calculations as a subintegral, because it corresponds to the simplest graph one encounters in problems with massless particles. We show in the following that the bubble integral evaluates to Gamma functions times a propagator raised to some power, which is dictated by power counting. Here we consider the most general case

$$I_{\text{bub}}(a_1, a_2) = \int \frac{d^d k}{i\pi^{d/2}} \frac{1}{[-k^2]^{a_1} [-(k+p)^2]^{a_2}}, \quad p^2 \neq 0. \quad (3.21)$$

In figure 3.3 the graphical representation of the integral is shown. From

$$x_1 D_1 + x_2 D_2 = -(x_1 + x_2)k^2 - 2k \cdot p x_2 - p^2 x_2 \quad (3.22)$$

<sup>2</sup>The components of  $Q$  are Lorentz vectors, hence the notation  $Q_{k,\mu}$  in eq. (3.19).

we can read of  $M$ ,  $Q$  and  $J$  and compute the Symanzik polynomials to wit

$$\mathcal{U} = x_1 + x_2 \quad \mathcal{F} = [-p^2]x_1x_2. \quad (3.23)$$

As the condition in the  $\delta$ -distribution we choose  $1 = x_1 + x_2$ , such that the  $\mathcal{U}$  Polynomial equals one. Putting all pieces together and performing the trivial  $x_2$  integration in eq. (3.18) we are left with an integral which can be expressed through Gamma-functions:

$$\begin{aligned} I_{\text{bub}} &= \frac{1}{[-p^2]^{a-d/2}} \frac{\Gamma(a_1 + a_2 - d/2)}{\Gamma(a_1)\Gamma(a_1)} \int_0^1 dx_1 (1-x_1)^{d/2-a_1-1} x_1^{d/2-a_2-1} \\ &= \frac{\Gamma(a_1 + a_2 - d/2)\Gamma(d/2 - a_1)\Gamma(d/2 - a_2)}{\Gamma(a_1)\Gamma(a_1)\Gamma(d - a_1 - a_2)} \frac{1}{[-p^2]^{a_1+a_2-d/2}}. \end{aligned} \quad (3.24)$$

- The eikonal bubble integral appears in HQET or Wilson line computations. Its graphical representation is shown in figure 3.3. Again we consider the most general case

$$I_{\text{eik}}(a_1, a_2) = \int \frac{d^d k}{i\pi^{d/2}} \frac{1}{[-2v \cdot (k+p) + \delta]^{a_1} [-k^2]^{a_2}}, \quad v^2 = 1, \quad (3.25)$$

where  $p$  is some external momentum,  $v$  is the direction of the eikonal propagator and  $\delta$  its off-shellness. Proceeding along the same way as in the massless bubble integral we find for the Symanzik polynomials

$$\mathcal{U} = x_2, \quad \mathcal{F} = x_1^2 + x_1x_2[-2v \cdot p + \delta]. \quad (3.26)$$

Here we choose the  $\delta$ -distribution such that we can set  $x_1 = 1$  and integrate  $x_2$  from zero to infinity. We obtain

$$\begin{aligned} I_{\text{eik}} &= \frac{\Gamma(a_1 + a_2 - d/2)}{\Gamma(a_1)\Gamma(a_1)} \int_0^\infty dx_2 x_2^{a_1+2a_2-d-1} (1 + [-2v \cdot p + \delta]x_2)^{-a_1-a_2+d/2} \\ &= \frac{\Gamma(d/2 - a_2)\Gamma(a_1 + 2a_2 - d)}{\Gamma(a_1)\Gamma(a_1)} \frac{1}{[-2v \cdot p + \delta]^{a_1+2a_2-d}}. \end{aligned} \quad (3.27)$$

In the second step we used a suitable variable transformation to factor out the dependence on the kinematics. Then the remaining integral evaluates to Gamma functions. The eikonal bubble integral shares the same feature as the massless bubble integral. It evaluates to Gamma functions times a eikonal propagator raised to some power, which is dictated by power counting.

### 3.3.3 Derivation of the Feynman parameter integral representation

In the following we briefly sketch the derivation of the Feynman parameter integral representation, following in most parts along the lines of [210]. The first step is to rewrite the integral into a form, where the integration over loop momenta can be performed easily. For this we introduce the Schwinger parametrization

$$\frac{1}{A^n} = \frac{1}{\Gamma(n)} \int_0^\infty dy y^{n-1} e^{-Ay}. \quad (3.28)$$

To show this identify we substitute  $y' = Ay$  in the integral. Then the dependence on  $A$  factors out of the integral and the remaining integral is exactly the integral representation of  $\Gamma(n)$ , hence this establishes the identity.

Using the Schwinger parametrization on every denominator in eq. (3.17) we obtain a Gaußian integral <sup>3</sup>, where the argument of the exponential has the form of eq. (3.19)

$$I = \int_0^\infty \frac{dx_1}{\Gamma(a_1)} \cdots \int_0^\infty \frac{dx_n}{\Gamma(a_n)} \prod_{j=1}^n x_j^{a_j-1} \times \int \frac{d^d k_1}{i\pi^{d/2}} \cdots \int \frac{d^d k_L}{i\pi^{d/2}} \exp \left( \sum_{i,j=1}^n k_i^\mu M_{ij} g_{\mu\nu} k_j^\nu - 2 \sum_{j=1}^n k_j^\mu Q_{j,\mu} - J \right). \quad (3.29)$$

Computing the  $(d \times L)$ -dimensional Gaußian integral we obtain

$$I = \int_0^\infty \frac{dx_1}{\Gamma(a_1)} \cdots \int_0^\infty \frac{dx_n}{\Gamma(a_n)} \prod_{j=1}^n x_j^{a_j-1} \frac{1}{[\det(M)]^{d/2}} \exp(-Q_\mu^T M^{-1} Q^\mu - J). \quad (3.30)$$

Two remarks are in order: First, we compute the Gaußian integral in Minkowski space, hence for each loop integral we get an additional factor of  $i$  compared to Euclidean space. This factor cancels with the  $1/i$  in the integration measure of the loop momenta. Second, due to the Minkowski metric in the matrix  $M_{ij} g_{\mu\nu}$  we get  $d$  factors of  $[\det(M)]^{1/2}$ .

Next we perform the variable transformation  $(y_1, \dots, y_n) \mapsto (\xi, x_2, x_3, \dots, x_n)$  with  $\xi = \sum_{j \in I} y_j$  and  $x_j = y_j/\xi$ , where  $I$  is a non-empty subset of  $\{1, 2, \dots, n\}$  with  $1 \in I$ . Without loss of generality we replace here the parameter  $y_1$ . We can equally well replace any other parameter as long as it appears in  $\xi$ . The Jacobian of this transformation reads  $\xi^{n-1}$ . Note that by construction  $M$ ,  $Q$  and  $J$  are linear in  $\xi$ . To restore the integration over the variable  $x_1$  we introduce a factor of one in the form of

$$1 = \int_0^\infty dx_1 \delta \left( 1 - \sum_{k \in I} x_k \right). \quad (3.31)$$

Finally we integrate over  $\xi$  from zero to infinity to get eq. (3.18).

<sup>3</sup>To have a Gaußian integral it is important that each loop momentum appears in at least one quadratic propagator.

### 3.3.4 Dimensional recurrence relations

In this subsection we discuss dimensional recurrence relations, which relate Feynman integrals in different space time dimensions to each other. The lowering and raising dimensional recurrence relation allow to express a  $d$  dimensional integral in terms of  $d-2$  and  $d+2$  dimensional integrals, respectively [212,217]. In the following we focus on the raising dimensional recurrence relation and derive it following along the lines of [212], where this equation was first introduced.

The raising dimensional recurrence relation for a generic  $L$  loop Feynman integral as in eq. (3.17) reads

$$I^{(d-2)}(a_1, \dots, a_n) = (-1)^L \mathcal{U}(\{\hat{A}_i\}) I^{(d)}(a_1, \dots, a_n), \quad (3.32)$$

where  $\mathcal{U}$  is the first Symanzik polynomial of the integral and the raising operator  $\hat{A}_i$  acts as follows

$$\hat{A}_i I^{(d)}(a_1, \dots, a_i, \dots, a_n) = a_i I^{(d)}(a_1, \dots, a_i + 1, \dots, a_n). \quad (3.33)$$

Note that lowering and raising dimensional recurrence relations are conveniently implemented in `LiteRed`. This implementation is based on the Baikov representation [217,218].

To derive the raising dimensional recurrence relation in eq. (3.32) we assume that the integral  $I$  in eq. (3.17) only has massive quadratic propagators  $D_i = -q_i^2 + m_i^2$  with distinct masses  $m_i$ . After eq. (3.32) is established we can safely set the masses to any value. The extension of the derivation to include eikonal propagators is trivial. We only exclude them to shorten the intermediate expression below and the final result in eq. (3.32) is also valid for integrals with eikonal propagators. The basic idea of the derivation is to trade the raising operators  $\hat{A}_i$  in eq. (3.32) for derivatives w.r.t. the masses

$$\hat{A}_i I^{(d)}(a_1, \dots, a_n) = \frac{\partial}{\partial m_i^2} I^{(d)}(a_1, \dots, a_n). \quad (3.34)$$

Then we compute the right-hand side of eq. (3.32) using the parameter representation in eq. (3.30). With the internal masses we see that  $J$  has the following form

$$J = \sum_{i=1}^n x_i m_i^2 + (\text{terms independent of } \{m_i^2\}). \quad (3.35)$$

Hence we have

$$\mathcal{U}\left(\left\{\frac{\partial}{\partial m_i^2}\right\}\right) \exp(-J) = (-1)^L \mathcal{U}(\{x_i\}) \exp(-J), \quad (3.36)$$

where we used that the first Symanzik polynomial  $\mathcal{U}$  is homogeneous with degree  $L$ . Assembling all pieces we find eq. (3.30).

Often one is interested in the dimensional recurrence relation of several integrals of an integral family. In this case it is convenient to directly work with the master integrals  $\vec{f} = (f_1, \dots, f_m)$  of the integral family. Applying the raising dimensional recurrence relation to the master integrals and then performing an IBP reduction we get

$$\vec{f}^{(d-2)} = T \vec{f}^{(d)}, \quad (3.37)$$

where  $T$  is an invertible  $m \times m$  matrix. It depends rationally on  $d$ , the kinematic invariants and the internal masses. The advantage of this approach is that we only have to compute the dimensional recurrence relation once and all the necessary information is saved in  $T$ . If we now want to express a  $d$  dimensional integral in terms of the  $d - 2$  dimensional master integrals we IBP reduce it and then use eq. (3.37).

### 3.3.5 Strategy for computing Feynman parameter integrals

We conclude this section with a brief discussion on a strategy that allows to efficiently compute Feynman integrals using the Feynman parameters. The strategy is similar to the one presented in [219–221]. The Feynman integral representation becomes especially powerful in combination with the `Maple` package `HyperInt` [222]. This is a dedicated package for computing parameter integrals. A restriction however is that the parameter integral has to be finite, i.e. the only source for a divergence in the dimensional regularization parameter  $\epsilon$  can be the Gamma function multiplying the parameter integral in eq. (3.18). The restriction is due to IBP and dimensional recurrence relations not as severe as it first seems. Both type of relations allow to express divergent integrals through finite integrals, where the finite integrals can have different dimensions, other powers for the propagators or even additional propagators. This strategy was employed in the computation of the cusp anomalous dimension and the quark jet function in the chapters 6 and 5.

To illustrate this strategy in more detail we consider the eikonal bubble integral  $I_{\text{eik}}(1, 1)$  defined in eq. (3.25) and compute it in two dimension. Although in this example we can compute the integral with full dependence on  $d$ , in general we only need the Laurant series expansion of the integral in the dimensional regularization parameter  $\epsilon$  up to a certain order. This can be used to simplify the calculation of the integral. If the Feynman parameter integral is finite in the limit  $\epsilon \rightarrow 0$ , one can expand the integrand before integration to the required order. The dependence on  $\epsilon$  of the resulting parameter integrals then factorizes. In the case of a divergent parameter integral in the limit  $\epsilon \rightarrow 0$ , some subtleties arise and one needs sector decomposition to handle these integrals. This is beyond the scope of this discussion and we focus on the finite case.

The eikonal bubble integral  $I_{\text{eik}}(1, 1)$  in two dimension is IR divergent, but UV finite, which can be seen from the IR and UV analysis presented in section 2.1.3. The only way to improve the IR behavior of the integral is to compute it in higher dimensions, at the cost of worsening the UV behavior. The integral  $I_{\text{eik}}(a_1, 1)$  with  $a_1 \geq 1$  is in four

dimension IR finite. By choosing  $a_1 \geq 3$  we can also render the integral UV finite and in particular we see that then the parameter integral in eq. (3.27) is also finite in the limit  $\epsilon \rightarrow 0$ . Therefore we use dimensional recurrence and IBP relations to relate  $I_{\text{eik}}(3, 1)$  in four dimensions to  $I_{\text{eik}}(1, 1)$  in two dimension. We start with the dimensional recurrence relation  $I_{\text{eik}}^{(2-2\epsilon)}(1, 1) = -I_{\text{eik}}^{(4-2\epsilon)}(1, 2)$ . With the IBP identities (3.14) and (3.15) we finally get

$$I_{\text{eik}}^{(2-2\epsilon)}(1, 1) = -\frac{2}{\epsilon}[-2v \cdot p + \delta]I_{\text{eik}}^{(4-2\epsilon)}(3, 1). \quad (3.38)$$

Note that this equation is in perfect agreement with the general result of the eikonal bubble integral in eq. (3.27). If the general result would not be available, the final step is then to compute  $I_{\text{eik}}^{(4-2\epsilon)}(3, 1)$  as described above. First we expand the integrand of the Feynman parameter integral in  $\epsilon$  and then compute the parameter integrals using `HyperInt`.

## 3.4 Harmonic polylogarithms

Harmonic polylogarithms (HPLs) often appear in multi-loop computations with one non-trivial variable. They were first introduced in [223]. In this appendix we summarize important properties of HPLs, where we closely follow in most parts [223, 224], except for the asymptotic expansion of HPLs. Here we use the method of [225].

### 3.4.1 Definition

The HPLs can be defined recursively on the interval  $x \in (0, 1)$  by the differential equation

$$\frac{d}{dx}H_{n,\vec{m}}(x) = f_n(x)H_{\vec{m}}(x), \quad (3.39)$$

where the integration kernels are given by

$$f_0(x) = \frac{1}{x}, \quad f_1(x) = \frac{1}{1-x}, \quad f_{-1}(x) = \frac{1}{1+x}. \quad (3.40)$$

The boundary condition of the differential equation reads

$$H_{\vec{m}}(0) = 0, \quad \text{if } \vec{m} \neq \vec{0}, \quad H_{\underbrace{0, \dots, 0}_{n \text{ times}}}(x) = \frac{1}{n!} \log^n(x). \quad (3.41)$$

From this definition it is easy to see that the HPLs can be represented as iterated integrals

$$H_{n,\vec{m}}(x) = \int_0^x dt f_n(t) H_{\vec{m}}(t), \quad \text{if } \vec{m} \neq \vec{0}. \quad (3.42)$$

Often a shorthand notation for the indices is used, where the number of consecutive 0 in front of a 1 is added to it and in the case of a  $-1$  is subtracted from it. For example we have  $H_{0,1,0,0,-1}(x) = H_{2,-3}(x)$ .

The transcendental weight or simply weight of an HPL is given by the number of integrations. There are three weight one HPLs given  $H_0(x) = \log(x)$ ,  $H_1(x) = -\log(1-x)$  and  $H_{-1}(x) = \log(1+x)$ . We also assign weight to numerical constants such as  $\pi$  and  $\zeta_n$ , where  $\pi$  has weight one and  $\zeta_n$  has weight  $n$ . Rational functions like eg.  $(1+x)$  and  $x/(1-x^2)$  have weight zero. A linear combination of HPLs with coefficients given by rational functions has uniform weight, if all the HPLs have the same weight. For instance the function

$$(1+x)H_{0,0}(x) + \frac{x}{1-x^2}H_{-1,0}(x) \quad (3.43)$$

has uniform weight two. If we further restrict the coefficients to be rational, then we have a pure function. The function

$$3H_{0,0}(x) + \frac{4}{9}H_{-1,0}(x) \quad (3.44)$$

is a pure weight two function. A pure function of weight  $w$  has the property that its derivative is a uniform weight function of weight  $w-1$ . Note that the notion of weight naturally extends also to iterated integral with different integration kernels than in eq. (3.40). Both, uniform weight and pure functions play an important role in the differential equation method for computing master integrals presented in section 3.5.

By considering the interval  $x \in (0, 1)$  we avoid potential logarithmic divergences and branch cuts. On this interval the HPLs are manifestly real and analytic. In the following subsection we lift this restriction and discuss the analytic continuation to other intervals and the asymptotic expansion near singular points.

### 3.4.2 Shuffle algebra and analytic continuation

The HPLs satisfy a shuffle algebra. The product of two HPLs of weight  $w_n$  and  $w_m$  can be rewritten as the sum over HPLs of weight  $w_m + w_n$

$$H_{\vec{m}}(x)H_{\vec{n}}(x) = \sum_{\vec{k}=\vec{m} \sqcup \vec{n}} H_{\vec{k}}(x), \quad (3.45)$$

where the sums run over all shuffles of  $\vec{m}$  and  $\vec{n}$ . These are all combinations of elements of  $\vec{m}$  and  $\vec{n}$  which preserve the internal ordering of  $\vec{m}$  and  $\vec{n}$ . The shuffle algebra is a direct consequence of the representation of the HPLs as iterated integrals. Let us consider a simple example

$$H_1(x)H_{0,-1}(x) = H_{1,0,-1}(x) + H_{0,1,-1}(x) + H_{0,-1,1}(x). \quad (3.46)$$



The shuffle algebra relates HPLs with the same argument. There are also relations between HPLs with different arguments. Two trivial relations of this kind are for example  $H_{0,0}(x^2) = 2^2 H_{0,0}(x)$  and  $H_1(1-x) = -H_0(x)$ . See for instance [223, 224].

With the help of the shuffle algebra the logarithmic behavior of HPLs near singular points can be made manifest. An HPL has a potential logarithmic divergence at  $x = 1$  if it has leading ones in the indices and at  $x = 0$  if it has trailing zeros in the indices. We focus on the point  $x = 0$  and consider  $H_{-1,1,0,0}(x)$  as an example. Using the shuffle algebra we extract the trailing zeros or equivalently powers of  $\log(x)$  and get

$$\begin{aligned} H_{-1,1,0,0}(x) = & \frac{1}{2} H_{-1,1}(x) \log^2(x) - [H_{-2,1}(x) + H_{-1,2}(x)] \log(x) \\ & + H_{-3,1}(x) + H_{-2,2}(x) + H_{-1,3}(x). \end{aligned} \quad (3.47)$$

The remaining HPLs are analytic near  $x = 0$  and vanish at this point. Expanding these HPLs in a Taylor series we therefore obtain the asymptotic expansion of  $H_{-1,1,0,0}(x)$  near  $x = 0$ .

Before we explain the asymptotic expansion in more detail we discuss the analytic continuation of the HPLs to other intervals than  $(0, 1)$ . HPLs can have branch cuts on the intervals  $(-1, 0)$ ,  $(1, \infty)$  and  $(-\infty, -1)$  due to the kernels  $f_0$ ,  $f_1$  and  $f_{-1}$ , respectively. We focus on the analytic continuation to  $(-1, 0)$ . Trailing zeros in the indices of an HPL give rise to a branch cut on this interval, while HPLs without trailing zeros are analytic on the interval  $(-1, 1)$ . As described before we extract trailing zeros with the shuffle algebra and make the dependence on  $\log(x)$  manifest. The analytic continuation is then achieved by using  $\log(-x \pm i\epsilon) = \log(x) \pm i\pi$ , where  $x > 0$  and  $\epsilon$  is infinitesimally small. Considering the example in eq. (3.47) we get for  $x \in (-1, 0)$

$$H_{-1,1,0,0}(-x + i\epsilon) = -\frac{\pi^2}{2} H_{1,-1}(-x) + H_{1,-1,0,0}(-x) + i\pi H_{1,-1,0}(-x), \quad (3.48)$$

where we again used the shuffle algebra to rewrite products of HPLs with  $\log(-x)$  as sums of HPLs. Note that for  $x \in (-1, 0)$  all HPLs in the above equation are manifestly real.

### 3.4.3 Asymptotic expansion

There are several ways to obtain the asymptotic expansion of HPLs around singular points [223, 224]. Here we derive a differential equation for the HPLs and solve it in an asymptotic expansion as explained in [225] and summarized in appendix 4.8 We illustrate our approach on a simple example and compute the (asymptotic) expansion of  $H_{0,1}(x)$  around  $x = 0$ . Note that the calculation straightforwardly generalize to arbitrary HPLs and expansion points.

The first step is to compute a linear and homogeneous differential equation of the form

$$x\vec{H}'(x) = A(x)\vec{H}(x), \quad (3.49)$$

where  $\vec{H}(x)$  is a vector of HPLs including  $H_{1,0}(x)$ . The differential equation has to be homogeneous. This is achieved by adding the lower weight HPL  $H_0(x)$  and the constant function  $x \mapsto 1$  to the vector of HPLs:  $\vec{H}(x) = (1, H_0(x), H_{1,0}(x))$ . From the definition of the HPLs it follows that the alphabet of the differential equation is given by the kernels (3.40) and that the matrix  $A(x)$  is a strictly lower triangular matrix if the HPLs in  $\vec{H}(x)$  are sorted w.r.t. increasing weight. In addition the matrix  $A(x)$  is holomorphic around  $x = 0$  due to the explicit factor of  $x$  on the left-hand side of eq. (3.49). Hence the method of [225] can be used to solve the differential equation. It is straightforward to compute the matrix in the differential equation

$$A(x) = \begin{pmatrix} 0 & 0 & 0 \\ 1 & 0 & 0 \\ 0 & \frac{x}{1-x} & 0 \end{pmatrix}. \quad (3.50)$$

In order to obtain the asymptotic expansion of  $\vec{H}(x)$  we need the Taylor series expansion of the matrix  $A(x) = \sum_{k \geq 0} x^k A_k$ . The general solution of eq. (3.49) then has the form

$$\vec{H}(x) = P(x)e^{\log(x)A_0}\vec{H}_0, \quad (3.51)$$

where the matrix  $P(x) = \mathbb{1} + \sum_{k \geq 1} x^k P_k$  can be computed recursively from the  $A_k$  as outlined in appendix 4.8. The matrix exponential

$$e^{\log(x)A_0} = \begin{pmatrix} 1 & 0 & 0 \\ \log(x) & 1 & 0 \\ 0 & 0 & 1 \end{pmatrix} \quad (3.52)$$

generates the logarithmic terms in the asymptotic expansion. Note that it can easily be computed with the `MatrixExp` command of `Mathematica`.

The next step is to compute the boundary value  $\vec{H}_0$ . For this we solve eq. (3.51) for  $\vec{H}_0$  and take the limit  $x \rightarrow 0$ . The result is  $\vec{H}_0 = (1, 0, 0)$ . Since by construction  $P(0) = \mathbb{1}$  we do not need its higher order terms to compute the boundary value. The only subtlety before taking the limit  $x \rightarrow 0$  is to make the cancellation of the logarithmically divergent terms manifest. This is achieved by using the shuffle algebra on  $\vec{H}(x)$ .

Assembling all pieces we finally have

$$H_{1,0}(x) = x(\log(x) - 1) + x^2 \left( \frac{\log(x)}{2} - \frac{1}{4} \right) + x^3 \left( \frac{\log(x)}{3} - \frac{1}{9} \right) + \mathcal{O}(x^4). \quad (3.53)$$

### 3.5 Differential equation method

The differential equation method [194–199] is a very powerful technique for computing loop integrals in dimensional regularization and has been successfully applied to many problems. It was for instance employed in the calculation of the two-loop master integrals for three-jet production [59–63]. The basic idea is to derive a differential equation for an integral basis of an integral family and then solve it with the appropriate boundary condition to obtain the analytic expression for the master integrals. The derivation of the differential equation heavily relies on IBP reductions. One of the most crucial steps is to find an integral basis where the differential equation is particularly simple. An integral basis with uniform transcendental weight fulfills this criterion [199]. Then the dependence on  $\epsilon$  in the differential equation is completely factorized and the dependence on the variables is in Fuchsian form. This allows us to solve the differential equation order by order in  $\epsilon$  in terms of Chen iterated integrals [226], provided a boundary condition. In general the boundary conditions can be obtained from kinematic limits, where the master integrals become simpler and can be computed by other means. Often the boundary conditions (or at least a subset thereof) can also be deduced from the singularity structure of the differential equation. For a pedagogical introduction into the differential equation method see for instance [200].

#### 3.5.1 Deriving the differential equation

In the following we discuss the differential equation method on the master integrals needed for the one-loop cusp anomalous dimension. The integral family is defined in eq. (3.1) and shown in figure 3.1. We have two master integrals, which can be chosen to be  $\vec{f} = (G(0, 1, 1), G(1, 1, 1))$ . The aim is to compute a linear first order differential equation of the form [194–197]

$$\frac{d}{dx} \vec{f}(x, \epsilon) = A(x, \epsilon) \vec{f}(x, \epsilon), \quad (3.54)$$

where  $A(x, \epsilon)$  is a rational  $2 \times 2$  matrix depending on  $x$  and the dimensional regularization parameter  $\epsilon$ . Since the first master integral is a (HQET) propagator type integral, it does not depend on the cusp angle and its derivative w.r.t.  $x$  has to vanish. Still it has to be included into the system, because the second master integral is coupled to it by the off diagonal elements of  $A(x, \epsilon)$ .

The integrals in the loop momentum representation only implicitly depend on  $x$  through the vectors  $v_1$  and  $v_2$ . Therefore the first step in deriving the differential equation is to express the differential operator  $d/dx$  through derivatives w.r.t.  $v_1$  and  $v_2$ . The most general ansatz reads

$$\frac{d}{dx} = \sum_{i,j=1}^2 v_i^\mu M_{ij} \frac{\partial}{\partial v_j^\mu}, \quad (3.55)$$

where the  $2 \times 2$  matrix  $M$  is restricted by the kinematics. Here we have the conditions

$$\frac{d}{dx}v_1^2 = 0, \quad \frac{d}{dx}v_2^2 = 0, \quad \frac{d}{dx}v_1 \cdot v_2 = \frac{1}{2} \left(1 - \frac{1}{x^2}\right), \quad (3.56)$$

which follow from  $v_1^2 = v_2^2 = 1$  and  $v_1 \cdot v_2 = (x + 1/x)/2$ . With these conditions we can only fix three of the four components of  $M$ . Keeping the undetermined component as an open parameter it has to drop out in the final differential equation (3.54). This can be either used as a cross check or one can set the parameter to a value which simplifies the differential operator.

Often the ansatz for a differential operator can be more restrictive. It is even possible to choose an ansatz with fewer parameters than conditions, as long as these conditions are satisfied. In our example we can for instance use

$$\frac{d}{dx} = \frac{1}{1-x^2} \left( -\frac{1+x^2}{x} v_1^\mu + 2v_2^\mu \right) \frac{\partial}{\partial v_1^\mu}. \quad (3.57)$$

A simpler differential operator has the advantage that the computational effort to obtain the differential equation is smaller. This is especially important for complex Feynman integrals with many loops and/or scales.

Applying the differential operator (3.57) to the master integrals  $\vec{f}$  we obtain integrals with raised powers of propagators and numerators of the form  $v_1 \cdot k$  and  $v_2 \cdot k$ . Since the integral family is complete, we can rewrite the numerators in terms of the factors in eq. (3.2). Therefore  $d\vec{f}/dx$  can be expressed as a linear combination of integrals of the same integral family. Using IBP identities we then relate these integrals to the master integrals and get the matrix in the differential equation

$$A(x, \epsilon) = \begin{pmatrix} 0 & 0 \\ \left(\frac{2}{x-1} - \frac{2}{x+1}\right)\epsilon - \frac{1}{x-1} + \frac{1}{x+1} & \left(\frac{2}{x+1} - \frac{1}{x}\right)\epsilon - \frac{1}{x-1} + \frac{1}{x} - \frac{1}{x+1} \end{pmatrix}. \quad (3.58)$$

The matrix is rational in  $x$  and  $\epsilon$  and has a triangular structure. Next we discuss how a better choice of basis integrals leads to a considerably simpler differential equation [199].

### 3.5.2 Differential equation in UT form

In our example the following basis of integrals

$$\vec{g}(x, \epsilon) = \epsilon \left( G(0, 1, 2), \epsilon \frac{1-x^2}{x} G(1, 1, 1) \right) \quad (3.59)$$

simplifies the differential equation such that solving it in an expansion in  $\epsilon$  is almost trivial. We have

$$\frac{d}{dx}\vec{g}(x, \epsilon) = \epsilon \tilde{A}_x(x) \vec{g}(x, \epsilon), \quad \tilde{A}_x(x) = \begin{pmatrix} 0 & 0 \\ -\frac{2}{x} & \frac{2}{x+1} - \frac{1}{x} \end{pmatrix}. \quad (3.60)$$

The dependence on  $\epsilon$  is completely factorized and the differential equation is in Fuchsian form, i.e. it only has simple poles in  $x$ , which can give rise to logarithmic divergences. An integral basis satisfying such a differential equation has uniform transcendental weight (UT), if  $\epsilon$  is assigned weight  $-1$  [199]. For this reason we call such an integral basis UT basis and we refer to the differential equation (3.60) to be in UT form. The set of denominators  $\{x, 1+x\}$  describes the divergences of the differential equation. It is called alphabet and its elements are called letters, because they determine the class of function to which the UT integrals can evaluate. Here the UT basis evaluates to HPLs.

The uniform weight property of the integral basis in eq. (3.59) becomes apparent when solving the differential equation in an expansion in  $\epsilon$ . The overall normalization of the basis was chosen such that its expansion in  $\epsilon$  starts at  $\mathcal{O}(\epsilon^0)$ . We substitute

$$\vec{g}(x, \epsilon) = \sum_{k \geq 0} \epsilon^k \vec{g}^{(k)}(x) \quad (3.61)$$

in the differential equation and obtain by comparing coefficients

$$\frac{d}{dx} \vec{g}^{(0)}(x) = 0 \quad (3.62)$$

$$\frac{d}{dx} \vec{g}^{(k)}(x) = \tilde{A}_x(x) \vec{g}^{(k-1)}(x), \quad k > 1. \quad (3.63)$$

We see that we can solve the differential equation iteratively order by order in  $\epsilon$ , provided a boundary condition.

For the boundary condition of the integral  $g_2(x, \epsilon)$  we consider the limit  $x \rightarrow 1$ , where we have a straight Wilson line. The integral  $G(1, 1, 1)$  is regular in this limit and due to the prefactor  $(1 - x^2)/x$  we have  $g_2(1, \epsilon) = 0$ . The differential equation cannot be used to compute the eikonal bubble integral  $g_1(x, \epsilon)$ . However, we computed it in section 3.3 using Feynman parameters:

$$g_1(x, \epsilon) = e^{\epsilon \gamma_E} \Gamma(1 + 2\epsilon) \Gamma(1 - \epsilon) = -1 - \frac{5\pi^2}{12} \epsilon^2 + \mathcal{O}(\epsilon^3). \quad (3.64)$$

From the alphabet  $\{x, 1+x\}$  and the iterative structure of the differential equation above it is clear that  $g_2(x, \epsilon)$  evaluates to HPLs (see section 3.4). We simply integrate eq. (3.63) w.r.t.  $x$  and fix the integration constant with the help of the boundary condition to obtain

$$g_2(x, \epsilon) = -\epsilon H_0(x) + \epsilon^2 \left( H_{0,0}(x) - 2H_{-1,0}(x) - \frac{\pi^2}{6} \right) + \mathcal{O}(\epsilon^3). \quad (3.65)$$

The analytic result for  $\vec{g}(x, \epsilon)$  has uniform weight zero, where the coefficient function  $\vec{g}^{(k)}(x)$  multiplying  $\epsilon^k$  is a pure function of weight  $k$ . This directly follows from the form of differential equation. We start with  $\vec{g}^{(0)}(x) = (-1, 0)$ , which is a pure function of weight zero. By integrating eq. (3.63) w.r.t.  $x$  we then successively increase the weight by one in each iteration step, due to the Fuchsian form of  $\tilde{A}_x(x)$ . We see that solving the differential equation, especially in the univariate case, is straightforward. The actual challenge is to find a UT basis. This will be discussed in subsection 3.5.4.

### 3.5.3 Beyond one variable and one loop

So far we only considered a univariate one-loop problem. Below we comment on the new features appearing beyond one variable and one loop.

In a multivariate problem we get for each kinematic invariant and internal mass a differential equation

$$\partial_i \vec{f} = A_i(\vec{x}, \epsilon) \vec{f}, \quad (3.66)$$

with  $\partial_i = \partial/\partial x_i$ . Here  $\vec{f}$  is the vector of master integrals and  $\vec{x}$  is the vector of the kinematic invariants and masses. The integrability condition  $\partial_i \partial_j \vec{f} = \partial_j \partial_i \vec{f}$  translates to the following condition on the matrices

$$[A_j, A_i] + \partial_i A_j - \partial_j A_i = 0. \quad (3.67)$$

These integrability conditions offer a simple cross check for the matrices  $A_j$ . Beyond one loop a sector in an integral family can have more than one master integral. For this reason the matrices  $A_i$  in general do not have a triangular, but a block triangular structure, if the master integrals are ordered with increasing number of propagators and the master integrals of the same sectors are grouped. The size of a diagonal block equals the number of master integrals in the corresponding sector.

If we can find a UT basis  $\vec{g}(\vec{x}, \epsilon)$ , then we can write the differential equations in the following compact form [199, 200]

$$d\vec{g} = \epsilon d\tilde{A}(\vec{x}) \vec{g}, \quad (3.68)$$

where we only need one matrix  $\tilde{A}(\vec{x})$ <sup>4</sup>. Furthermore, the matrix is given as a linear combination of logarithms, i.e. it has the form

$$\tilde{A}(\vec{x}) = \sum_{k=1}^n \tilde{a}_k \log(\alpha_k(\vec{x})), \quad (3.69)$$

where  $\tilde{a}_k$  are rational matrices independent of the kinematics and the letters  $\alpha_k(\vec{x})$  are algebraic functions of the kinematic invariants and masses. The set  $\{\alpha_1, \dots, \alpha_n\}$  forms the alphabet of the differential equation and has to be linearly independent. It determines the class of functions to which the UT integrals evaluate. We can write the formal solution to eq. (3.68) as Chen iterated integrals [226]

$$\vec{g}(\vec{x}, \epsilon) = P \exp \left( \epsilon \int_{C[\vec{x}, \vec{x}_0]} d\tilde{A}(\vec{x}) \right) \vec{g}(\vec{x}_0, \epsilon), \quad (3.70)$$

---

<sup>4</sup>In the example in eq. (3.60) we get  $\tilde{A}(x)$  by integrating  $\tilde{A}_x(x)$  w.r.t.  $x$ .

where the path  $C[\vec{x}, \vec{x}_0]$  starts at  $\vec{x}_0$  and ends at  $\vec{x}$ . Note the similarity to Wilson lines, where also a path ordered exponential appears. Different choices of the path  $C[\vec{x}, \vec{x}_0]$  lead to different representations of the solution.

As already indicated it is not guaranteed that a UT basis exists for a given integral family. The easiest counterexample is the sunrise integral with three massive propagators. This integral evaluates to elliptic functions [227–232], which are not within the class of generalized polylogarithms [233]. See also [54, 55, 57, 58, 234–237] for other examples of integrals which do not evaluate to generalized polylogarithms.

### 3.5.4 Finding a UT basis

We saw that the differential equation becomes particularly simple when we consider a UT basis, that is an integral basis with uniform transcendental weight. Therefore one of the major challenges is to find such a basis. In the following we give a brief overview of some of the available methods and algorithms to systematically construct a UT basis. In particular we derive the UT basis in eq. (3.59).

#### Integrals with constant leading singularities

The normalization factor  $(1 - x^2)/x$  of the integral  $g_2(x, \epsilon)$  in the UT basis in eq. (3.59) can be found by studying the integrand of  $G(1, 1, 1)$ . In [199, 238] it was conjectured that integrals with constant leading singularities [238] are natural candidates for a UT basis. We compute the leading singularities by replacing the integration over the real axis by contour integrals around the poles of the integrand. The contour integrals are finite, hence we can work in  $d = 4$  dimensions. Furthermore, the contour integrals essentially amount to taking residues of the integrand at the poles. Therefore we only have to study the integrand which is in general much easier than computing the integral. If we can write the integrand as a logarithmic differential form, then taking the residues is trivial and we can read off the leading singularity. Such a representation of the integrand is called d log-form [239].

For Wilson line integrals it turns out that the position space representation is better suited for this analysis than the momentum space representation. In section 2.2 we have already studied Wilson line integrals in position space. Let us neglect the IR regulator for a moment and work in  $d = 4$  dimensions. Then we can read off the position space integrand of  $G(1, 1, 1)$  from eq. (2.41) and write it as a differential form<sup>5</sup> [41, 200]

$$\frac{ds_1 \wedge ds_2}{s_1^2 + s_2^2 + (x + 1/x)s_1 s_2} = \frac{x}{1 - x^2} d \log(s_1 x + s_2) \wedge d \log(s_1 + s_2 x). \quad (3.71)$$

In the d log-form we see that the leading singularity of  $G(1, 1, 1)$  is given by  $x/(1 - x^2)$ .

<sup>5</sup>Note that the integrand in eq. (2.41) corresponds to  $(v_1 \cdot v_2) G(1, 1, 1)$ .

We can perform the same analysis with the IR regulator and find the same leading singularity. With the differential equation (3.60) we prove that  $g_2(x, \epsilon) = \epsilon^2(1 - x^2)/x \times G(1, 1, 1)$  has uniform weight and therefore our result is in perfect agreement with the conjecture of [199]. For a more detailed analysis of the leading singularities of Wilson line integrals involving an IR regulator see [41].

The eikonal bubble integral  $G(0, 1, 2)$  in our UT basis in eq. (3.59) cannot be written as a d log-form. However, in two dimension the integral  $G(0, 1, 1)$  has a d log-form with leading singularity one. Using dimensional recurrence relations we have  $G^{(4-2\epsilon)}(0, 1, 2) = -G^{(2-2\epsilon)}(0, 1, 1)$ , which explains why we included the integral in our UT basis. We can also read off the UT property directly from the general result for the eikonal bubble integral in eq. (3.27). In general it can be worthwhile to study the leading singularities not only in four, but also shifted space dimension. With the help of the dimensional recurrence relation the information can then be transported back to four dimensions.

For Wilson line integrals it turns out that the position space representation, where we have to compute parameter integrals, is a natural starting point for this analysis. This feature is somewhat unique to Wilson line integrals and in general an algorithm that uses the momentum space representation as a starting point is desired. Using directly the components of the loop momenta<sup>6</sup> as integration variables leads however to problems due to the quadratic nature of the propagators. Often it turns out that spinor helicity variables provide a suitable parametrization for computing d log-forms [240]. In the spinor helicity parametrization the propagators are linear in each new integration variable. Note that in intermediate steps in the computation large expressions can arise, which are non-trivial to handle. We briefly discuss in the next point a dedicated algorithm to compute leading singularities.

### Wasser's algorithm for computing leading singularities

The algorithm by Wasser [240] computes the leading singularities of an a priori arbitrary integrand. In order for the algorithm to successfully run through a suitable parametrization for the integration variables is often crucial. As previously mentioned in the case of loop integrals spinor helicity variables often work<sup>7</sup>. Wasser's algorithm was for instance used for a four-loop form factor calculation [241] as well as for the computation of the two-loop five point master integrals [62, 63]. This shows that the algorithm not only can deal with high loop orders but also with many scales<sup>8</sup>.

The method of computing leading singularities is powerful, but also often computationally challenging and requires dedicated computer code. Next we discuss a graphical way of finding UT integrals.

<sup>6</sup>We want to remind the reader that we compute d log-forms in  $d = 4$  dimensions.

<sup>7</sup>The computer implementation of the algorithm conveniently provides a function for the transformation from loop momenta to spinor helicity variables.

<sup>8</sup>The massless five point kinematic has five independent invariants.



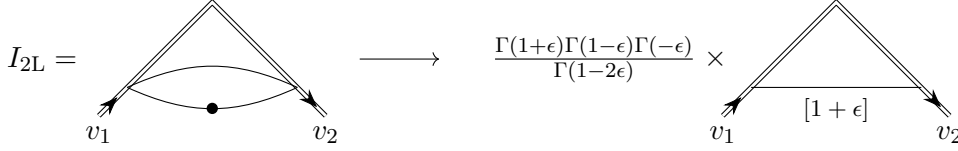


**Figure 3.4:** The integral  $I_{2L}$  is needed for the two-loop cusp anomalous dimension  $\Gamma_{\text{cusp}}(\phi, \alpha_s)$ . On the right side we have integrated out the bubble integral. A dot on a propagator means that this propagator is squared. The quadratic propagator of the right integral is raised to power  $1 + \epsilon$ .

### Using building blocks

In this approach we use building blocks to "construct" UT integrals and recycle in this way lower loop results. This is a more heuristic than algorithmic way in finding UT integrals. The UT integrals are conveniently constructed with the help of the diagram of the integral, i.e. its graphical representation.

Let us consider the two-loop integral  $I_{2L}$  on the left side of figure 3.4 as an example. It has the massless bubble integral  $I_{\text{bub}}(1, 2)$  defined in eq. (3.21) as a subintegral. Integrating out the bubble integral we get

$$I_{2L} = \frac{\Gamma(1 + \epsilon)\Gamma(1 - \epsilon)\Gamma(-\epsilon)}{\Gamma(1 - 2\epsilon)} \times G(1, 1, 1 + \epsilon), \quad (3.72)$$

see also figure 3.4. The prefactor built from Gamma functions has uniform transcendental weight, hence we only need to study the integral  $G(1, 1, 1 + \epsilon)$ . The power of the third propagator of the integral is not exactly one, but slightly shifted due to the  $d = 4 - 2\epsilon$  dimensional bubble integral. In many cases this shift does not spoil the uniform weight property of the integral. Note that this is a heuristic observation. For this reason we can simply proceed by investigating the integral  $G(1, 1, 1)$  instead. We already computed its normalization factor. It is given by  $x/(1 - x^2)$ . Therefore we conclude that  $(1 - x^2)/x \times I_{2L}$  should have uniform weight. In [41] it was proven by computing the differential equation that this is indeed the case. Here it was crucial to use a bubble integral with one dot to get a uniform weight prefactor and the correct power for the third propagator. Furthermore, we could recycle our knowledge on  $G(1, 1, 1)$  as well as on the bubble integral. From this example we see that the bubble integral with a dot is a suitable building block for "constructing" uniform weight integrals. Completely analogous to the bubble integral there are also building blocks made from triangle and box integrals (see e.g. [240]).

The methods presented so far can be used to search for UT integrals before even computing the differential equation. However, there are also methods and algorithms for finding UT integrals with the help of the differential equation of a non-UT basis. We discuss some of them in the following.

### Integrating out $\mathcal{O}(\epsilon^0)$ terms in the differential equation

Often the differential equation or at least a part of it is already in Fuchsian form, but is not yet proportional to  $\epsilon$ . We consider the matrix  $A(x, \epsilon)$  in eq. (3.58) as an example. Here the  $\mathcal{O}(\epsilon^0)$  terms are removed by multiplying the integral  $G(1, 1, 1)$  with the normalization factor  $(1 - x^2)/x$ , c.f. eq. (3.59). This factor can directly be computed from the matrix  $A(x, \epsilon)$  as shown presently.

We consider a basis change from  $\vec{f}$  to a new basis  $\vec{h}$ . Using IBP reductions it can be written as  $\vec{h} = T\vec{f}$ , where  $T$  is an invertible matrix. Then the matrix  $B$  of the new differential equation is related to the old one via

$$B = TAT^{-1} + \frac{dT}{dx}T^{-1}. \quad (3.73)$$

The aim is to find a transformation matrix  $T$ , such that  $B$  is in UT-form [200]. Here we focus on the triangle integral  $G(1, 1, 1)$ . The diagonal element  $A_{2,2}$  associated with this integral is already close to the desired form and we only need to find a transformation which removes the  $\mathcal{O}(\epsilon^0)$  term. We make the ansatz  $T = \text{diag}(1, \mathcal{N}(x))$  and get the differential equation

$$\frac{1}{\mathcal{N}} \frac{d\mathcal{N}}{dx} + A_{2,2}|_{\epsilon=0} = 0 \quad (3.74)$$

from the condition that the  $\mathcal{O}(\epsilon^0)$  term in eq. (3.73) vanishes. We solve the differential equation by separating the variables and get  $\mathcal{N} = (1 - x^2)/x$ .

This is a general and powerful method to find the normalization factor of an integral. It can be used when the diagonal element is in Fuchsian form and has terms proportional to  $\epsilon^0$  and  $\epsilon$ , which is frequently the case. After the normalization the corresponding diagonal element is in UT form and the non-diagonal elements are often also in or close to UT form.

Note that the  $\mathcal{O}(\epsilon^0)$  term of non-diagonal elements can be removed in a similar manner. For this one can use the ansatz  $T = \mathbb{1} + \tilde{T}$  for the transformation matrix in eq. (3.73) and then solve the resulting differential equation for  $\tilde{T}$ .

### Lee's algorithm

In case of a single variable problem an algorithm for finding a UT basis was introduced by Lee [242] and publicly available computer implementations of the algorithm were presented in [243, 244]. The algorithm takes the differential equation matrix  $A(x, \epsilon)$  of an arbitrary integral basis as an input and then calculates a matrix  $T$  that transforms the differential equation in UT form (see eq. (3.73) for the transformation between two

integral bases). The transformation matrix  $T$  is computed in three consecutive steps. First the differential equation matrix is brought into Fuchsian form

$$A(x, \epsilon) \rightarrow B(x, \epsilon) = \sum_{k=1}^n \frac{B_k(\epsilon)}{x - x_k}, \quad (3.75)$$

where  $\{x_k\}$  are the singular points of the differential equation. Next the eigenvalues of the matrices  $B_k(\epsilon)$  are normalized, such that they are proportional to  $\epsilon$ . The last step is to find a constant transformation that completely factorizes  $\epsilon$ . The algorithm is restricted to a transformation that is rational in  $x$  and  $\epsilon$ , hence it will not find a solution if square roots are involved.

### Meyer's algorithm

A different algorithm was introduced by Meyer [245–247]. A computer implementation is publicly available in [247]. The algorithm of Meyer can deal with a multivariate problem. Similar to Lee's algorithm, it takes the differential equation matrices  $A_i(\vec{x}, \epsilon)$  of some integral basis as an input. Instead of computing the transformation matrix  $T$  directly from the matrices  $A_i(\vec{x}, \epsilon)$ , the algorithm uses an ansatz for  $T$ . The ansatz is rational in  $\vec{x}$  and  $\epsilon$  and is based on the singular structure of the matrices. Then the unknown coefficients in the ansatz are fixed by the requirement that the transformed differential equation matrices are in UT-form. Even when a UT basis exists, it is possible that the algorithm cannot find a transformation matrix  $T$ , because the chosen ansatz was too restrictive.

### Comments on the choice of variables

For the differential equation method it is not only important to have a good integral basis, but also suitable variables. In the example with the cusp anomalous dimension we use for instance  $x = e^{i\phi}$  instead of just  $\phi$  or  $\cos \phi$ .

A different example is the triangle integral  $I_{\text{tri}}$  with three off-shell legs shown in figure 3.5. It has the leading singularity  $1/R$  with

$$R = \sqrt{(p_1 \cdot p_2)^2 - p_1^2 p_2^2}, \quad (3.76)$$

where  $p_1$  and  $p_2$  are incoming momenta with  $p_1^2, p_2^2 \neq 0$ . Therefore we conclude that the integral  $R \times I_{\text{tri}}$  has uniform transcendental weight, which can easily be proven by deriving its differential equation. With the variable transformation

$$(p_1 \cdot p_2, p_1^2, p_2^2) \mapsto (p_2^2(u^2 + v^2), 2p_2^2 uv, p_2^2) \quad (3.77)$$

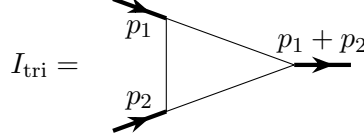


**Figure 3.5:** Triangle integral with off-shell legs, i.e. we have for the incoming momenta  $p_1^2, p_2^2 \neq 0$ . Massless quadratic propagators and off-shell legs are represented by thin and thick lines, respectively.

the square root can be rationalized:  $R = p_2^2(u^2 - v^2)$ . Hence the variables  $(u, v, p_2^2)$  are better suited to describe the problem.

Note that the algorithms of Lee and Meyer are restricted to rational transformations, hence for these algorithms it is crucial to find a rational parametrization for possible square roots. With Wasser's algorithm we can compute the leading singularity of  $I_{\text{tri}}$  in the variables  $p_1^2, p_2^2$  and  $p_1 \cdot p_2$ , but in more complicated cases square roots are also problematic and should be avoided. In [248] an algorithm for finding rational parametrizations of square roots was presented.

### 3.5.5 Summary and final comments

In this section we presented the differential equation method, a powerful technique to compute loop integrals. One of the major challenges is to find an integral basis leading to a simple differential equation. We saw that a UT basis has a particular simple differential equation, which in the univariate case is almost trivial to solve.

We discussed several methods and algorithms to find a UT basis. In practice one can combine these methods and algorithms. For example one can use the heuristic approach with building blocks to find UT integrals for the sectors with few propagators and use Wasser's algorithm to study the remaining sectors. Sometimes the heuristic approach does not give UT integrals, but integrals where the differential equation is close to UT-form. Then the final transformation to a UT basis can be obtained with the algorithms of Lee or Mayer.

Finally we discuss how the differential equation itself can provide valuable information on the boundary condition of the integrals. The differential equations for the integrals needed for the two and three-loop cusp anomalous dimension  $\Gamma_{\text{cusp}}(\phi, \alpha_s)$  have the full HPL alphabet  $\{x, 1+x, 1-x\}$ , where  $x = e^{i\phi}$ . The last letter can give rise to logarithmic divergences at  $x = 1$ . In the straight line limit, where  $x \rightarrow 1$ , the integrals are however regular. Therefore the integration constants when solving the differential equation have to be chosen such that the logarithmic divergences at  $x = 1$  are absent. This leads to conditions on the integration constants which allow to compute a subset of them. The observation that the singular structure of the differential equation provides information

on the boundary conditions is not restricted to Wilson line integrals, but a rather general observation. This was for example used in chapter 4 and in [249].



---

## Subleading Regge limit from a soft anomalous dimension

---

This chapter is published in [75] under the creative commons license CC-BY 4.0 (<http://creativecommons.org/licenses/by/4.0/>). We performed minor modifications to the text, the notation and the formatting.

### Abstract

Wilson lines capture important features of scattering amplitudes, for example soft effects relevant for infrared divergences, and the Regge limit. Beyond the leading power approximation, corrections to the eikonal picture have to be taken into account. In this chapter, we study such corrections in a model of massive scattering amplitudes in  $\mathcal{N} = 4$  super Yang-Mills, in the planar limit, where the mass is generated through a Higgs mechanism. Using known three-loop analytic expressions for the scattering amplitude, we find that the first power suppressed term has a very simple form, equal to a single power law. We propose that its exponent is governed by the anomalous dimension of a Wilson loop with a scalar inserted at the cusp, and we provide perturbative evidence for this proposal. We also analyze other limits of the amplitude and conjecture an exact formula for a total cross section at high energies.

### 4.1 Introduction

Future physics analyses at the LHC will require conceptional advances in the theoretical understanding of scattering processes. One new frontier will be higher-loop processes depending on many mass and kinematic scales, e.g. when considering mixed QCD and electroweak processes. While in some cases a numerical approach may be feasible and

adequate, it seems clear that conceptual breakthroughs will be driven by new analytic ideas.

When dealing with processes depending on many scales, an important question is to understand in which situations systematic expansions can be applicable, and how the latter can be obtained systematically. One particularly interesting and important limit is the eikonal limit, which describes emission of soft radiation. At leading power, the physics is described by correlation functions of Wilson lines. Many recent papers are dedicated to studying power corrections to the eikonal limit [42–44].

It is often extremely helpful to have a toy model at hand for developing new ideas. Among various Yang-Mills theories, the  $\mathcal{N} = 4$  super Yang-Mills theory stands out as a particularly nice model. It is often dubbed the hydrogen atom of quantum field theory, due to a hidden symmetry that is the generalization of the Laplace-Runge-Lenz symmetry of the hydrogen atom. In order to be able to study massive scattering amplitudes, we give a vacuum expectation value to some of the scalar fields in the model. In this way, we can consider four-particle amplitudes depending on two Mandelstam variables and a mass. The amplitudes are UV and IR finite, so that they can be evaluated directly in four dimensions.

One of many examples where this model brought about conceptual advances for generic quantum field theories is in understanding the structure of Feynman integrals [238], which is closely related to their analytic evaluation [199]. The three-loop planar Feynman integrals needed for the amplitude mentioned above were computed in ref. [250], using a version of the differential equations method with improvements for integrals finite in four dimensions. These formulas provide a fully analytic result for a three-loop four-point amplitude depending on three scales.

One exciting feature of the amplitude is that many of its physically interesting limits are either exactly known, or governed by integrability. This is the case for the Regge limit, which at leading power is controlled by the anomalous dimension of a cusped Wilson loop, a problem that is known to be integrable [251, 252]. The amplitude is exactly known in the high-energy limit, and equal to the Bern-Dixon-Smirnov (BDS) ansatz [72, 162, 166]. Moreover, the low-energy limit is described by an effective action, and in the forward limit the amplitude can be interpreted as a total cross section of producing massive  $W$ -bosons and other particles; an exact formula for that cross section at high energies will be conjectured below. Finally, it is possible to study threshold effects that are related to bound states of a hydrogen-like system [170].

In this chapter, we study in detail the various physical limits mentioned above, focusing in particular on the Regge limit. It is well-known that in the planar limit it is described by a single power law, involving the gluon Regge trajectory, which is a nontrivial function of the internal masses and momentum transfer. Surprisingly, we will observe from the explicit three-loop amplitude that the first subleading power is also controlled by a single power law. This is rather remarkable in light of the current understanding of



subleading powers in the Regge limit, where, for example, quark loops typically produce double logarithmic corrections (see [253, 254]). In contrast, in this theory we find only a single power of logarithm per loop order.

In order to better understand this phenomenon and hopefully initiate a systematic expansion in the Regge limit, we will make use of a special property of this model, wherein the Regge limit can be mapped to a limit of a massless internal leg. This was used before to give an alternative definition of the Regge trajectory as the anomalous dimension of a cusped Wilson loop with a finite angle. This kind of soft limit is at the moment under better theoretical control since it is conceptually closer to the limit of soft external momenta studied in [42–44]. We will make a proposal for an independent definition of the first subleading exponent, namely as the anomalous dimension of a Wilson loop with a scalar inserted at the cusp. We test this proposal by explicitly computing this anomalous dimension up to two loops.

The chapter is organized as follows. In section 4.2, we define the model and amplitudes under consideration. We discuss in detail the various physical limits and point out the all-loop structure expected in some of them, using the one-loop result as a pedagogical example. Section 4.3 summarizes our observations about the Regge limit at next-to-leading power, up to three loops. Then, in section 4.4 we compute the anomalous dimension of a cusped Wilson loop with a scalar insertion, and test our proposal that its anomalous dimension is equal to the second Regge trajectory appearing at subleading power. We present our conclusions in section 4.5. The chapter contains several appendices with technical details. Appendix 4.6 collects our results for a total cross section, and evidence for its conjectured high-energy limit. Appendix 4.7 explains the use of dual conformal symmetry to conveniently parametrize the Regge expansion. Appendix 4.8 contains a detailed account of the analytic continuation and differential equation technology needed to derive the various expansions of the three-loop scattering amplitude. In appendix 4.9 we discuss the calculation of the Feynman integrals for the two-loop Wilson line calculation.

## 4.2 Massive scattering amplitudes in $\mathcal{N} = 4$ super Yang-Mills

### 4.2.1 Setup and four-particle amplitudes

We consider  $\mathcal{N} = 4$  sYM in the planar limit. We spontaneously break the  $SU(N_c)$  gauge group to  $SU(N_c - 4) \times SU(4) \times U(1)$ . In this way, in addition to the “gluons” of the unbroken  $SU(N_c - 4)$  part of the gauge group, we have massless bosons from the unbroken  $SU(4)$  subgroup, a  $U(1)$  photon, and massive  $W$ -bosons from the off-diagonal part. In what follows we will take  $N_c$  large and discuss the leading term of the amplitudes.

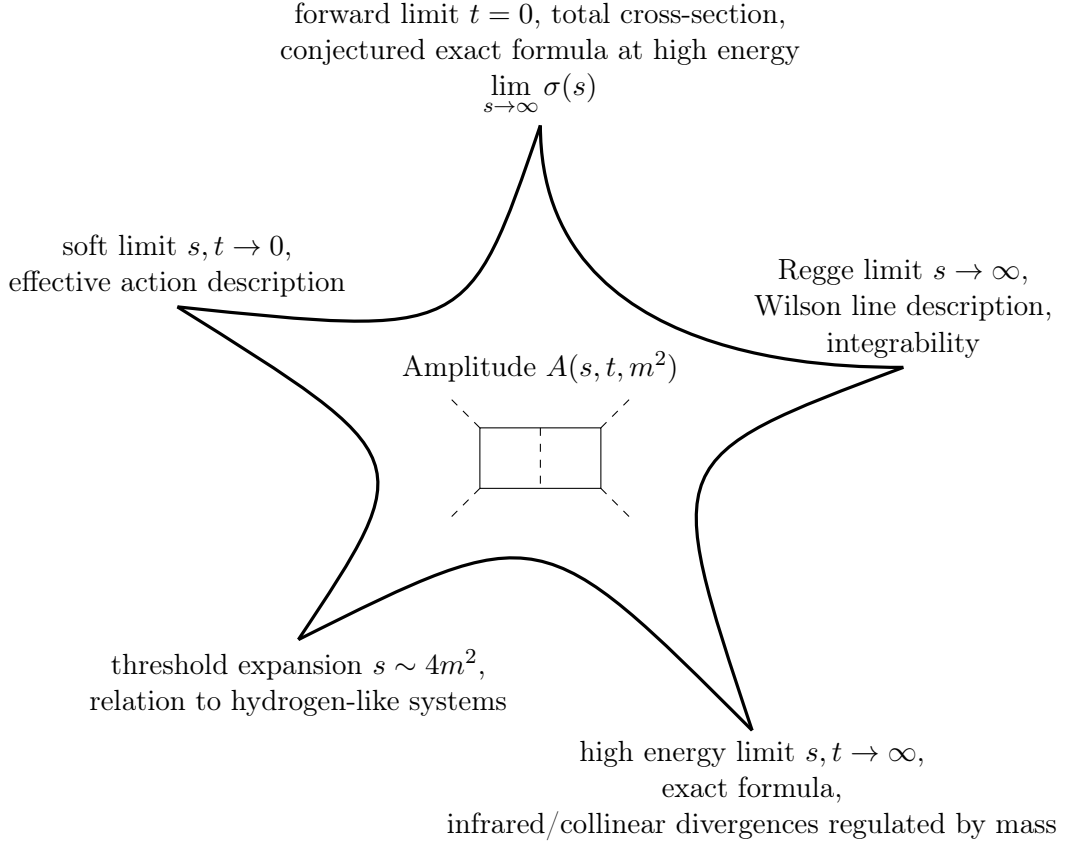


**Figure 4.1:** The scattering amplitude  $A(s, t, m^2)$  has various physically interesting and overlapping limits. In many of the latter, exact results are known or conjectured (e.g. high-energy limit), while other limits are known to be governed by integrability.

As discussed in ref. [72], this allows us to consider color-ordered amplitudes  $Y\bar{Y} \rightarrow Y\bar{Y}$ .<sup>1</sup> For further papers discussing various aspects of massive amplitudes on the Coulomb branch of  $\mathcal{N} = 4$  super Yang-Mills, see [73, 74, 256–265]. Here the particle  $Y$  is one of the off-diagonal generators of the unbroken  $SU(4)$  subgroup, lying above the diagonal;  $\bar{Y}$  is then the Hermitian conjugate. We choose  $Y$  to be a complex scalar within the  $\mathcal{N} = 4$  supermultiplet, but since the setup preserves supersymmetry any other helicity choice would give an equivalent result. An important motivation for considering such amplitudes is that they are natural from the AdS/CFT viewpoint [159], and that they have a dual conformal symmetry [72].

At tree-level, the result for the scattering amplitude is the same as in the unbroken theory,

$$A_{Y\bar{Y} \rightarrow Y\bar{Y}}^{\text{tree}} = -2g_{\text{YM}}^2 \frac{s}{t}. \quad (4.1)$$

<sup>1</sup>One can also consider scattering of the  $U(1)$  photons, as was done in ref. [255].

Amplitudes with other external states, such as gluons, are related to this one by supersymmetry. At loop level, at leading order in  $N_c$ , the interactions are mediated by massive  $W$ -bosons, whose mass provides a natural IR regularization. We define

$$A_{Y\bar{Y} \rightarrow Y\bar{Y}} = A_{Y\bar{Y} \rightarrow Y\bar{Y}}^{\text{tree}} M \left( \frac{4m^2}{-s}, \frac{4m^2}{-t} \right). \quad (4.2)$$

The amplitude  $M$  can be expanded perturbatively in the coupling  $g^2 \equiv g_{\text{YM}}^2 N_c / (16\pi^2)$ , as

$$M = 1 + g^2 M^{(1)} + g^4 M^{(2)} + g^6 M^{(3)} + \mathcal{O}(g^8). \quad (4.3)$$

The expression for the loop integrand of  $M$  up to four loops was derived using unitarity cuts [266]. The loop integrals up to three loops were evaluated analytically in ref. [250]. The main focus of this chapter is to investigate the various limits discussed above, and to understand surprising structures appearing in them. We use the technology of ref. [250] to derive the expansions.

In this section, we use the one-loop expressions as a pedagogical example, and point out the all-loop structure, whenever the latter is known. The one-loop term  $M^{(1)}$  of eq. (4.3) is given by a massive one-loop box integral, which evaluates to (the form below is due to [267])

$$\begin{aligned} M^{(1)} = & -\frac{2}{\beta_{uv}} \left\{ 2 \log^2 \left( \frac{\beta_{uv} + \beta_u}{\beta_{uv} + \beta_v} \right) + \log \left( \frac{\beta_{uv} - \beta_u}{\beta_{uv} + \beta_u} \right) \log \left( \frac{\beta_{uv} - \beta_v}{\beta_{uv} + \beta_v} \right) - \frac{\pi^2}{2} \right. \\ & \left. + \sum_{i=u,v} \left[ 2 \text{Li}_2 \left( \frac{\beta_i - 1}{\beta_{uv} + \beta_i} \right) - 2 \text{Li}_2 \left( -\frac{\beta_{uv} - \beta_i}{\beta_i + 1} \right) - \log^2 \left( \frac{\beta_i + 1}{\beta_{uv} + \beta_i} \right) \right] \right\}. \end{aligned} \quad (4.4)$$

Here we introduced dimensionless variables

$$u = \frac{4m^2}{-s}, \quad v = \frac{4m^2}{-t}, \quad (4.5)$$

and the following abbreviations,

$$\beta_u = \sqrt{1+u}, \quad \beta_v = \sqrt{1+v}, \quad \beta_{uv} = \sqrt{1+u+v}. \quad (4.6)$$

The functions appearing in eq. (4.4) are examples of polylogarithms, with the dilogarithm defined as  $\text{Li}_2(x) = -\int_0^x \log(1-y)/y \, dy$ . The above formulas are valid in the Euclidean region  $u, v > 0$ . In order to continue to other regions, a small imaginary part has to be added to  $s$  and  $t$ , according to the Feynman prescription.

As already mentioned in the introduction of this chapter, the amplitude has several physically interesting limits, that we discuss presently, as summarized in figure 4.1.

### 4.2.2 Soft limit

When  $|s|, |t| \ll m^2$  (keeping  $s/t$  fixed), the massive  $W$ -bosons can be integrated out, leading to a local effective action. At tree-level, the massive  $W$ -bosons do not appear when scattering the light  $SU(4)$  particles, so that the scattering amplitude is the same as in the unbroken theory. On the other hand, at loop level (and in the large  $N_c$  limit), the light particles do not interact directly among themselves, but through a loop of massive  $W$ -bosons. We have

$$\frac{1}{st} M\left(\frac{4m^2}{-s}, \frac{4m^2}{-t}\right) = \frac{1}{st} - \frac{g^2}{6m^4} + \mathcal{O}(1/m^6). \quad (4.7)$$

In this formula, the  $g^2/(6m^4)$  term is one-loop exact, as predicted from non-renormalization theorems (see ref. [268] and references therein).

### 4.2.3 Forward limit and total cross section

In the forward limit  $t = 0$ , the optical theorem relates the imaginary part of the scattering amplitude of massless scalars  $Y\bar{Y} \rightarrow Y\bar{Y}$  to the total cross section of  $Y, \bar{Y}$  producing a pair of massive  $W$ -bosons, plus other particles. We have [80]

$$\sigma_{Y\bar{Y} \rightarrow X} = \frac{1}{2E_{\text{cm}} p_{\text{cm}}} \lim_{t \rightarrow 0} \text{Im}(A) = \frac{1}{s} \lim_{t \rightarrow 0} \text{Im}(A_{Y\bar{Y} \rightarrow Y\bar{Y}}), \quad (4.8)$$

where  $E_{\text{cm}} = \sqrt{s}$  is the center of mass energy and  $p_{\text{cm}} = \sqrt{s}/2$  is the center of mass momentum of one particle. We have

$$\lim_{t \rightarrow 0} A_{Y\bar{Y} \rightarrow Y\bar{Y}} = -2g_Y^2 M \lim_{t \rightarrow 0} \frac{s}{t} M\left(\frac{4m^2}{-s}, \frac{4m^2}{-t}\right). \quad (4.9)$$

In the Euclidean region  $-s > 0$  we find

$$\lim_{t \rightarrow 0} \frac{-m^2}{t} M^{(1)} = \beta_u \log\left(\frac{\beta_u - 1}{\beta_u + 1}\right) + 2. \quad (4.10)$$

Analytically continuing to  $s > 4m^2$  (taking into account the Feynman  $i0$  prescription), and taking the imaginary part of eq. (4.10), and using formula (4.8), we arrive at

$$\sigma_{Y\bar{Y} \rightarrow X} = \frac{2\pi g_{YM}^2}{m^2} \beta_u + \mathcal{O}(g^4) = \frac{32\pi^3 g^2}{N_c m^2} \beta_u + \mathcal{O}(g^4). \quad (4.11)$$

In appendix 4.6, we compute this cross section to the three-loop order, and observe a simple pattern, which we argue allows us to propose an exact formula of its high energy limit:

$$\lim_{s \rightarrow \infty} \sigma_{Y\bar{Y} \rightarrow X} = \frac{2\pi g_{YM}^2}{m^2} B(g^2). \quad (4.12)$$

Here  $B(g^2)$  is the Bremsstrahlung function, given below in eq. (4.21) as an *exact* function of the coupling. It is striking, in particular, that the total cross section for massless scalars or photons remains finite as  $s \rightarrow \infty$ . This is likely a consequence of working at the leading order in the large  $N_c$  limit (which neglects, in particular, the interactions within the unbroken  $SU(4)$  subgroup).

It is instructive to recall Pomeranchuk's theorem [269], which states that if the cross section grows with energy, the cross section for a particle and its antiparticle will be asymptotically equal. The hypothesis of the theorem is not satisfied: here the cross section does not grow with energy. Interestingly, the conclusion is also maximally violated: the amplitude for the antiparticle process vanishes at this order:  $\sigma_{YY \rightarrow X} = O(1/N_c^2)$ .

#### 4.2.4 Threshold expansion

Let us consider the amplitude close to the threshold  $s = 4m^2$  for producing a pair of  $W$ -bosons. We expect the perturbative series to break down in the regime when the velocity  $\beta_u \sim g^2$ , for the following reason. The produced  $W$ -bosons interact by exchanging massless gauge fields and scalars (and fermions), from the unbroken part of the gauge group, which lead to an attractive  $1/r$  potential. This causes the  $W$ -bosons to form non-relativistic Hydrogen-like bound states, which are exactly stable in the large  $N_c$  limit. Their binding energies are of order  $\Delta E \sim mg^4$  at weak coupling. While one cannot see these bound states in our fixed-order calculation, one should still be expected to see the perturbative series diverge when the kinetic energy becomes of this order. Recalling that  $\beta_u = \sqrt{1 - 4m^2/s}$ , this indeed translates to  $\beta_u \sim g^2$ .

Physically, the leading terms should originate from a nonrelativistic hydrogen-like system with the Hamiltonian in the center-of-mass frame<sup>2</sup>

$$H = \frac{p^2}{m} - \frac{\lambda}{4\pi r}. \quad (4.13)$$

The contribution of this system can in fact be computed analytically as a function of  $g^2/\beta_u$  (see ref. [270], eq. (4.55)):

$$\lim_{\beta_u \rightarrow 0^+} \frac{m^2 \text{Im} M(u, \frac{-4m^2}{t})}{-\pi g^2 t} = \frac{4\pi^2 g^2}{1 - e^{-\frac{4\pi^2 g^2}{\beta_u}}} + \mathcal{O}(\beta_u^2, g^2 \beta_u, \dots). \quad (4.14)$$

To all orders in  $g^2$  this predicts the most singular term as the velocity  $\beta_u \rightarrow 0$ . This resummation accounts for certain ladder graphs; these are the same graphs which govern the Regge limit. There is in fact a very close connection between these two limits, as discussed in ref. [170]. Higher order corrections to eq. (4.14) should be interpreted as relativistic and many-body corrections to the Coulomb Hamiltonian.

---

<sup>2</sup>The potential is twice that coming from gauge boson exchange, due to the scalar exchange.

### 4.2.5 High energy limit

We can take  $s, t$  to be much larger than the mass,  $m^2/s \rightarrow 0, m^2/t \rightarrow 0$ , with  $s/t$  fixed. In this case, the mass serves as an infrared and collinear regulator, leading to double logarithms of the small mass. Expanding eq. (4.4) in this limit, we obtain

$$M\left(\frac{4m^2}{-s}, \frac{4m^2}{-t}\right) = 1 + g^2 \left[ -2 \log\left(\frac{m^2}{-s}\right) \log\left(\frac{m^2}{-t}\right) + \pi^2 \right] + \mathcal{O}(g^4). \quad (4.15)$$

It was argued [72], based on anomalous dual conformal Ward identities originally derived for Wilson loops [162], that the four-point amplitude should have the following exact form,

$$\begin{aligned} \log M\left(\frac{4m^2}{-s}, \frac{4m^2}{-t}\right) &= \frac{K(g)}{8} \left[ -2 \log\left(\frac{m^2}{-s}\right) \log\left(\frac{m^2}{-t}\right) + \pi^2 \right] \\ &\quad + \tilde{\mathcal{G}}_0(g) \left[ \log\left(\frac{m^2}{-s}\right) + \log\left(\frac{m^2}{-t}\right) \right] + \tilde{c}(g) + \mathcal{O}(m^2), \end{aligned} \quad (4.16)$$

where  $K(g)$  is the light-like cusp anomalous dimension [26, 271],  $\tilde{\mathcal{G}}_0$  is a collinear anomalous dimension, and  $\tilde{c}$  a coupling-dependent constant. Eq. (4.16) can be viewed as a mass-regulated version of the BDS ansatz [166], which was originally formulated within dimensional regularization.

The small mass limit and eq. (4.16) were studied previously using Mellin-Barnes techniques in refs. [73, 74]. In the preceding sections, we derived analytic formulas for  $M$  up to three loops. As a check, we reproduced eq. (4.16) to that order by taking the small mass limit of our formulas. For reference the coefficients are  $K(g^2) = 8g^2 - 16\zeta_2 g^4 + 176\zeta_4 g^6$ ;  $\tilde{\mathcal{G}}_0 = -4\zeta_3 g^4 + g^6(36\zeta_5 - 8\zeta_2\zeta_3)$ ;  $\tilde{c}(g^2) = 3g^4\zeta_4 - g^6(50\zeta_6 + 16\zeta_3^2)$ .

The fact that the logarithm of the amplitude does not grow faster than  $\log(s)$  is consistent with the behaviour expected in the Regge limit  $s \gg m^2, t$ , that will be discussed presently. The fact that eq. (4.16) contains only a single logarithm (and no further  $s$  dependence) means that  $M$  is Regge exact (in the small mass limit).<sup>3</sup>

### 4.2.6 Regge limit

The leading term in the Regge limit  $s \gg m^2, t$ , up to power corrections, has been discussed in refs. [73, 74]. It is given by a single power law,

$$\lim_{s \rightarrow \infty} M\left(\frac{4m^2}{-s}, \frac{4m^2}{-t}\right) = \tilde{r}_0(t) \left(\frac{-s}{m^2}\right)^{j_0(t)+1} + \mathcal{O}(1/s). \quad (4.17)$$

<sup>3</sup>The property of Regge-exactness was observed in the dimensionally-regularized massless case in refs. [160, 272].

The leading terms are given by

$$j_0 = -1 + 2g^2\phi \tan \frac{\phi}{2} + \mathcal{O}(g^4), \quad \tilde{r}_0 = 1 + \mathcal{O}(g^2), \quad (4.18)$$

where

$$t = 4m^2 \sin^2 \frac{\phi}{2}. \quad (4.19)$$

We note that in planar  $\mathcal{N} = 4$  super Yang-Mills, the Regge trajectory is equal to the angle-dependent cusp anomalous dimension [73],

$$j_0(t) + 1 = -\Gamma_{\text{cusp}}(\phi). \quad (4.20)$$

The angle-dependent cusp anomalous dimension is an extremely interesting quantity in its own right. In QCD the full angle dependence is known up to three loops [41], while in  $\mathcal{N} = 4$  sYM theory it was computed up to three loops in [264] and in the planar limit up to four loops in [273]. Furthermore, it is controlled by integrability [251, 252] in  $\mathcal{N} = 4$  sYM theory. In particular the method of ref. [274] can be used to evaluate  $j_0$  numerically at any value of the coupling. We refer the interested reader to [41, 264] for a discussion of its various properties. Here we wish to point out that its small angle limit is known exactly [275],

$$\Gamma_{\text{cusp}}(\phi) = -\phi^2 B(g^2), \quad B(g^2) = \frac{1}{4\pi^2} \frac{\sqrt{\lambda} I_2(\sqrt{\lambda})}{I_1(\sqrt{\lambda})} \approx g^2 - \frac{2}{3}\pi^2 g^4 + \frac{2}{3}\pi^4 g^6 + \dots \quad (4.21)$$

Here  $\lambda = g_{\text{YM}}^2 N_c$ , and  $I_1$  and  $I_2$  are Bessel functions. The  $\phi^4$ -term in the small angle expansion of  $\Gamma_{\text{cusp}}(\phi)$  is also known analytically [274].

Computing the three-loop Regge limit (4.17) of the amplitude, as described in appendix 4.8, we computed  $j_0(t)$ , and hence  $\Gamma_{\text{cusp}}(\phi)$ , to the three-loop order. In this way, we reproduced the result of ref. [264]. For the explicit expressions we refer to that reference.

#### 4.2.7 Discussion

In summary, we studied a scattering amplitude of four complex scalars in  $\mathcal{N} = 4$  sYM theory with a spontaneously broken gauge group, which is known as an analytic function of the variables  $u = 4m^2/(-s)$  and  $v = 4m^2/(-t)$  up to three loops [250]. We studied several kinematic limits. To obtain these limits we used techniques for differential equation and calculated the amplitude in an (asymptotic) expansion, in principle to any order in the expansion parameter. For convenience of the reader, we provide our results as computer-readable supplementary material in the publication [75] on which this chapter is based on. Interestingly, we find that the leading terms of most of the above limits are in principle known to all loop orders, or are controlled by an integrable model.

In the case of massless amplitudes, a systematic expansion around the collinear limit could be found and described via integrability [276,277]. The above observations nurture the hope that something similar can be done for massive amplitudes, at least in one of the above limits. Focusing on the first subleading term in the Regge limit, we will find a remarkably simple structure. In the remainder of this chapter, we discuss these findings in detail.

### 4.3 Regge expansion using dual conformal partial waves

The Regge limit is a likely candidate around which one can hope to build a systematic expansion. When discussing power-suppressed terms, however, the choice of variable used to express the leading term (4.17) becomes important. In this section we will use symmetries to derive a good parametrization of the limit, and we will find that the first power-correction is then controlled by a single independent power.

#### 4.3.1 Dual conformal partial wave analysis

A simple improvement over expanding in inverse powers of  $1/s$  in the Regge limit at fixed  $t$  is to use instead the partial wave expansion, where each power gets upgraded to a Regge pole. Each Regge pole contributes proportional to a Legendre function, producing an asymptotic expansion of the amplitude in the form (see eq. (A.12) of [278] or (2.9.6) of [279]):

$$A(s, t) \simeq \sum_{j_n(t)} \tilde{c}_n(t) Q_{-j_n(t)-1}(\cos \theta_3), \quad \text{with} \quad \cos \theta_3 = 1 + \frac{2s}{t}, \quad (4.22)$$

where  $j_n(t)$  denote the Regge trajectories and  $Q_{-j-1}$  are associated Legendre functions. In the Regge limit these tend to<sup>4</sup>

$$\lim_{s \rightarrow \infty} Q_{-j-1}(\cos \theta_3) \propto \left(\frac{2s}{t}\right)^j + j \left(\frac{2s}{t}\right)^{j-1} + \frac{j(j-1)^2}{2j-1} \left(\frac{2s}{t}\right)^{j-2} + \dots \quad (4.23)$$

This highlights how each Regge pole resums an infinite tower of inverse powers of  $s$ . The Legendre functions which control each tower originate physically from the  $\text{SO}(2,1)$  Lorentz subgroup which preserves the spacelike momentum exchanged in the  $t$ -channel. For this reason, the expansion (4.22) generally contains fewer independent coefficients than the straightforward  $1/s$  expansion. This is analogous to how conformal blocks are used to resum descendant operators in conformal field theories.

---

<sup>4</sup>The right-hand side shows the expansion of:  $\frac{-\tan(\pi j)\Gamma(j+1)}{\sqrt{\pi}2^j\Gamma(j+\frac{1}{2})}Q_{-j-1}(z) = z^j {}_2F_1(-\frac{j}{2}, \frac{1-j}{2}, \frac{1}{2} - j, 1/z^2)$ .



### 4.3 Regge expansion using dual conformal partial waves

The  $\mathcal{N} = 4$  sYM amplitude that we consider benefits from a larger  $\text{SO}(4)$  or  $\text{SO}(3,1)$  dual conformal symmetry. It was identified in [170] as a relativistic version of the Laplace-Runge-Lenz symmetry of the hydrogen-like bound states which appear in intermediate states of the amplitude. This symmetry implies further relations among the Regge trajectories.

Using the embedding formalism to work out the action of the dual conformal symmetry on the kinematical invariants, and the detailed form of  $\text{SO}(4)$  Legendre functions, a symmetry-improved expansion around the Regge limit is derived in appendix 4.7:

$$\lim_{Y \rightarrow 0} \frac{1+Y}{1-Y} M = \sum_{n=0}^{\infty} r_n(t) Y^{-j_n(t)-1}, \quad (4.24)$$

where the variable, which vanishes in the Regge limit  $s \rightarrow \infty$ , is (recall eq. (4.6) for our notations)

$$Y = \frac{\beta_{uv} - \beta_v}{\beta_{uv} + \beta_v} \equiv e^{i\theta} \quad \text{where} \quad \cos \theta = 1 + \frac{2s}{t} - \frac{s}{2m^2}. \quad (4.25)$$

Again each term behaves in the Regge limit like a power of  $s$ :  $Y^{-j-1} \propto s^{j+1}$ , however an intricate tower of subleading powers, similar to but distinct from eq. (4.23), is associated with each  $\text{SO}(4)$  Regge trajectory  $j_n(t)$ .

The angle (4.25) is distinct from the usual scattering angle between the two external massless photons (see eq. (4.22)), due to the  $-s/(2m^2)$  term. This makes the angle real in the physical region of  $t$ -channel scattering when  $0 < t < 4m^2$  and  $-t < s < 0$ . It is hyperbolic above the massive continuum  $t > 4m^2$ , or whenever  $|s|$  is sufficiently large, as is assumed in the Regge limit formula (4.24).

As an application of this formula, we have subtracted from the three-loop amplitude described in the preceding section its leading behavior:  $r_0(t)Y^{-j_0(t)-1}$ , which is known to exponentiate to a single power law (with exponent previously given in ref. [264, 274]). Amazingly, looking at the remainder, we find that the first subleading power also exponentiates! That is, we find to three loops that the logarithm of the remainder is linear in  $\log Y$ . We can thus write

$$\lim_{Y \rightarrow 0} \frac{1+Y}{1-Y} M = r_0(t)Y^{-j_0(t)-1} + r_1(t)Y^{-j_1(t)-1} + \mathcal{O}(Y^2), \quad (4.26)$$

where  $j_0 \approx -1$  and  $j_1 \approx -2$ . This is rather remarkable: in principle the first subleading term could have been a sum of multiple power laws. In fact, had we used the straightforward  $1/s$  expansion, or the usual  $\text{SO}(3)$  Regge pole expansion, we would have (artificially) found at subleading order two distinct power laws, with one exponent mysteriously equal to the leading exponent minus one, thus hinting at the presence of a hidden symmetry.

Since we have only one single subleading power, taking the limit of the three-loop amplitude of ref. [250] using the method detailed in appendix 4.8, allows us to extract

its exponent to three loops. Defining

$$x = \frac{\beta_v - 1}{\beta_v + 1}, \quad \xi = \frac{1}{\beta_v} = \frac{1 - x}{1 + x}, \quad (4.27)$$

our result for the Regge trajectory is:

$$\begin{aligned} j_1 = & -2 - 4g^2 + g^4 \left[ -\frac{1}{\xi} \left( 4\zeta_2 H_1 + \frac{H_1^3}{6} \right) - 8\xi H_1 + 2H_1^2 + 16(\zeta_2 + 1) \right] \\ & g^6 \left[ 32H_{1,2} - 16(4\zeta_2 - 6\zeta_3 + 15\zeta_4 + 8) - 12(2\zeta_2 + 1)H_1^2 - \frac{5H_1^4}{6} + \frac{8H_1^3}{3} \right. \\ & + \xi \left( 48(\zeta_2 + 2)H_1 + \frac{14H_1^3}{3} - 16H_1^2 - 64H_2 \right) - 8\xi^2 H_1^2 \\ & \left. + \frac{1}{\xi} \left( -8H_{1,1,2} + \frac{2}{3}(4\zeta_2 + 1)H_1^3 + 8(2\zeta_2 - 3\zeta_3 + 11\zeta_4)H_1 + \frac{H_1^5}{20} - \frac{H_1^4}{6} \right) \right], \end{aligned} \quad (4.28)$$

where  $H$  are HPLs [223, 224] with argument  $1 - x^2$ . The residue starts as  $r_1 = 2 + 8g^2(2H_{-1}(x) + 2H_1(x) - 1) + \mathcal{O}(g^4)$ .

We also looked at the next powers in the expansion. We find that there is never any double logarithm, that is, never more than one power of logarithm per loop order. To leading logarithm order, the sub-sub-leading term in the amplitude is given as

$$\begin{aligned} \frac{1+Y}{1-Y} M(u, Y) \Big|_{Y^2} = & Y^2 \left[ 2 + 8g^2 \log(Y) \frac{\xi^2 - 1}{\xi^2} - 8g^4 \log^2(Y) \frac{(2\xi^4 - 6\xi^2 + 5)}{\xi^2(1 - \xi^2)} \right. \\ & \left. - 64g^6 \log^3(Y) \frac{\xi^4 - 4\xi^2 + 5}{3\xi^2(1 - \xi^2)} \right]. \end{aligned} \quad (4.29)$$

One can show that this not the exponential of a single power.

For convenience, the full three-loop expansions of  $j_0$ ,  $j_1$ ,  $r_0$ ,  $r_1$  and sub-subleading amplitudes are recorded in the supplementary material attached to the arXiv submission of [75].

### 4.3.2 From the Regge limit to Wilson lines with a cusp

While we currently lack a systematic effective field theory framework to characterize the subleading powers (4.26) in the Regge limit, to make progress we will use a map to an equivalent problem involving a cusped Wilson line, following [73, 170, 264]. The idea is to generalize the Higgs symmetry breaking pattern by further breaking  $SU(4)$  down to  $U(1)^4$ , thus allowing a distinct mass  $m_i$  for the  $W$ -bosons. The amplitude still

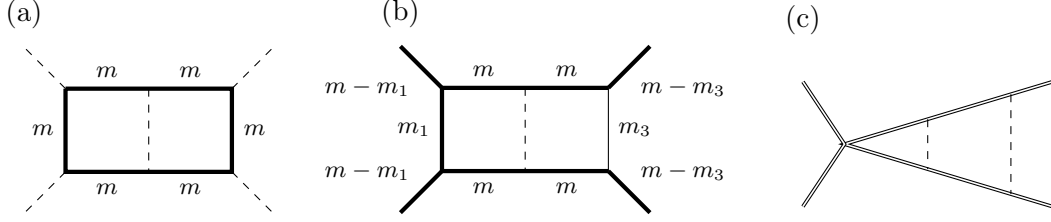


**Figure 4.2:** The amplitude on the left, with four massive  $W$ -bosons (thick lines) running outside the loop, is equivalent, through eq. (4.30), to an amplitude with unequal-mass bosons. In a limit equivalent to the Regge limit, one of the masses go to zero, revealing IR divergences within the associated cusp.

depends only on six-dimensional dot products of the vectors (4.65), which give rise to two independent cross-ratios, now equal to [280, 281]:

$$u = \frac{4m_1m_3}{-s + (m_1 - m_3)^2}, \quad v = \frac{4m_2m_4}{-t + (m_2 - m_4)^2}. \quad (4.30)$$

These reduce, in the equal-mass case, to our previous definitions, e.g.  $u = \frac{4m^2}{-s}$ , see figure 4.2 (a). That the amplitude  $M$  depends only on these two cross-ratios has an implication which is familiar in the non-relativistic limit: the cross-ratios then depend only on the kinetic energy divided by the reduced mass. Most important for us, will be the fact that the Regge limit  $s \rightarrow \infty$  of this amplitude, is equivalent to the massless limit  $m_3 \rightarrow 0$ . See figure 4.2 (b), where we also set  $m_2 = m_4 = m$  for simplicity.

Logarithms in such a massless limit are naturally associated with soft quanta coupled to Wilson lines with a cusp geometry, see figure 4.2 (c). This was used in [264] to obtain the 3-loop cusp anomalous dimension from the leading power in the Regge limit of the amplitude. It was used in the other direction in [170], to obtain the bound state spectrum of hydrogen-like states from the latter (and further analyzed at strong coupling [282]). Using the same map for the first subleading power, the subleading Regge trajectory  $j_1$  (see eq. (4.26)) can thus be used to predict that a Wilson line with a cusp has an excitation with scaling dimension:

$$\Gamma_{\text{cusp},\Phi}(\phi) \equiv -j_1 - 1 = 1 + 4g^2 + \mathcal{O}(g^4), \quad (4.31)$$

where  $j_1$  is given to three loops by eq. (4.28). The variable  $x$  used in that expression can be expressed in terms of the cusp angle  $\phi$  between  $v_1$  and  $v_2$  shown in figure 4.3 as

$$x = e^{i\phi}, \quad i\xi = \tan \frac{\phi}{2}. \quad (4.32)$$

In summary, the fact that the first power correction in the Regge limit exponentiates is remarkable and strongly suggests the existence of a systematic expansion with a nice structure. In the next section, we make a proposal for how to determine  $j_1(t)$ , or equivalently the scaling dimension  $\Gamma_{\text{cusp},\Phi}(\phi)$ , in terms of an effective field theory calculation.

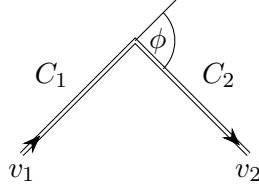


**Figure 4.3:** Wilson line with two straight line segments forming a cusp.

## 4.4 Renormalization of Wilson lines with operator insertions

In this section we show perturbatively up to two loops that the exponent  $j_1$  in the power suppressed term in the Regge limit can be identified as the scaling dimension of a cusped Wilson loop with a scalar inserted at the cusp point.

### 4.4.1 Cusped Wilson line

We recall that we found for the exponent  $j_0$  of the leading term in the Regge limit the relation  $j_0 + 1 = -\Gamma_{\text{cusp}}$ , where  $\Gamma_{\text{cusp}}$  is the anomalous dimension of a Wilson loop operator  $W_{\text{cusp}}$  with a cusp; see eq. (4.20). To define  $W_{\text{cusp}}$  properly, we consider the Maldacena-Wilson line operator [171]

$$W[C] = \text{P exp} \left[ ig_{\text{YM}} \int_C ds \left\{ \dot{x}_\mu A^\mu(x(s)) + |\dot{x}| \Phi(x(s)) \right\} \right], \quad (4.33)$$

where  $\Phi$  is one of the six scalars. The fields are taken to be in the adjoint representation of the gauge group<sup>5</sup>. In the following, we will work in the large  $N_c$  limit. The contour consists of two straight line segments  $C_1 = \{\tau v_1^\mu | \tau \in [-\infty, 0]\}$  and  $C_2 = \{\tau v_2^\mu | \tau \in [0, \infty]\}$ , which form a cusp at the origin. Note that the directions are chosen such that  $v_1$  is incoming and  $v_2$  is outgoing; see figure 4.3. The cusp angle is defined as

$$\cos(\phi) = v_1 \cdot v_2 = \frac{1}{2} \left( x + \frac{1}{x} \right), \quad v_1^2 = v_2^2 = 1. \quad (4.34)$$

The Wilson loop operator we are interested in is then simply given by

$$W_{\text{cusp}} = W[C_1] W[C_2]. \quad (4.35)$$

It is invariant under the interchange  $v_1 \leftrightarrow -v_2$ , which follows from the definition of the contours.

The operator (4.35) renormalizes multiplicatively:  $W_{\text{cusp}}^{\text{r}} = Z_{\text{cusp}}^{-1} W_{\text{cusp}}^{\text{b}}$ , where the left-hand side is finite [23–25, 110, 111, 283, 284]. In a conformal field theory, such as

<sup>5</sup>Note that there is no trace in the definition, as the Wilson lines extend to infinity.

#### 4.4 Renormalization of Wilson lines with operator insertions

$\mathcal{N} = 4$  sYM, the renormalization factor  $Z_{\text{cusp}}$  has the following form in  $D = 4 - 2\epsilon$  dimensions, see e.g. [285],

$$\log Z_{\text{cusp}} = - \sum_{L \geq 1} \frac{(g^2)^L}{2L\epsilon} \Gamma_{\text{cusp}}^{(L)}, \quad (4.36)$$

where  $\Gamma_{\text{cusp}}(\phi) = \sum_{L \geq 1} (g^2)^L \Gamma_{\text{cusp}}^{(L)}$  is the (angle-dependent) cusp anomalous dimension.

To motivate which subleading power operators to consider, let us discuss schematically what might be anticipated from a systematic analysis of the massless limit  $m_3 \rightarrow 0$  of the preceding subsection, in the framework of HQET. One would start by integrating out the heavy (internal)  $W$ -bosons, which should reduce the  $2 \rightarrow 2$  amplitude at leading power to a matrix element of local operators which creates a pair of heavy (scalar) quarks:

$$\bar{h}_{v_2} h_{v_1}. \quad (4.37)$$

Taking the matrix element in a state with two heavy particles, the propagator for the HQET fields  $q$  simply produce Maldacena-Wilson lines, thus recovering  $W_{\text{cusp}}$ . Schematically, two kinds of power corrections are then expected: either from higher-dimensional operators in the HQET Lagrangian, or from higher-dimensional corrections to the local operator. The former adds operator insertions along the Wilson lines, whereas the latter adds fields or derivatives strictly at the cusps. For the present analysis, we shall assume that the leading power corrections come entirely from cusp insertions, and ignore the corrections to the Wilson lines.

##### 4.4.2 Operator mixing and renormalization

For the first power correction, we are led to consider local HQET operators with mass dimension one higher than (4.37), for example  $\bar{h}_{v_2} \Phi h_{v_1}$ . As we ignore corrections to the HQET Lagrangian, the heavy quark fields become again simply Maldacena-Wilson lines, and we can treat this as a scalar insertion in  $W_{\text{cusp}}$ . Since the small mass  $m_3$  is controlled by the Higgs mechanism, it should be better viewed as a property of the state rather than of the operator, and in the free theory the scalar  $\Phi$  simply becomes its expectation value  $m_3$ . The considered operator can in principle mix with any other which has the same mass dimension and Lorentz indices. The only gauge invariant operator built from  $\mathcal{N} = 4$  sYM fields fulfilling these criteria involve derivatives within the plane of the cusp (and therefore total derivatives). We are thus led to consider the two sYM operators:

$$\partial W_{\text{cusp}} = \frac{i}{g_{\text{YM}}} (v_2 - v_1)_\mu \partial^\mu W_{\text{cusp}}, \quad (4.38)$$

$$W_{\text{cusp}, \Phi} = W[C_1] \Phi(x) W[C_2]. \quad (4.39)$$

The relative sign in (4.38) comes from the symmetry under  $v_1 \leftrightarrow -v_2$ .

In the case where the scalars which couple to the Wilson line are orthogonal to the scalars inserted at the cusp, the anomalous dimension is known from integrability [274], see also [286] for related work using localization techniques. Here, however, these scalars are the same. This setup was considered by Alday and Maldacena in [287], where they computed the anomalous dimension at one loop for the straight line case. We extend the calculation to two loops with a dependence on the cusp angle.

In general both operators can mix at loop level. In order to resolve this mixing, we will consider suitable correlation functions of these operators. Since  $\langle 0 | W_{\text{cusp}, \Phi} | 0 \rangle$  has no tree-level contribution, we find it more convenient to consider the correlation function with an additional scalar  $\Phi(p_3)$ . We take the latter to be on-shell,  $p_3^2 = 0$ , so that the correlation functions are gauge independent.

At tree-level, we find

$$\langle 0 | \partial W_{\text{cusp}} | \Phi(p_3) \rangle = \frac{[(v_1 - v_2) \cdot p_3]^2}{(v_1 \cdot p_3)(v_2 \cdot p_3)} + \mathcal{O}(g^2) = \frac{(s_1 + s_2)^2}{s_1 s_2} + \mathcal{O}(g^2), \quad (4.40)$$

$$\langle 0 | W_{\text{cusp}, \Phi} | \Phi(p_3) \rangle = 1 + \mathcal{O}(g^2). \quad (4.41)$$

These correlation functions depend on the cusp angle  $\phi$ , as well as on the two invariants  $s_1 = -2v_1 \cdot p_3$  and  $s_2 = +2v_2 \cdot p_3$ . In the following, the different momentum-dependence of the correlation functions, together with the fact that the (UV) renormalization matrix must be independent of the external momentum  $p_3$ , will allow us to resolve the operator mixing.

Moreover, since  $\partial W_{\text{cusp}}$  is a derivative of the lower dimensional operator  $W_{\text{cusp}}$ , it renormalizes multiplicatively with the same renormalization factor, and we thus expect the mixing matrix to be triangular. Taking also into account that operator mixing only appears at the loop level, we have the following structure of the renormalization matrix for  $\vec{W} = (\partial W_{\text{cusp}}, W_{\text{cusp}, \Phi})$ ,

$$\mathbf{Z} = \begin{pmatrix} Z_{\text{cusp}} & 0 \\ Z_{\text{mix}} & Z_{\text{cusp}, \Phi} \end{pmatrix}, \quad (4.42)$$

with

$$Z_{\text{mix}} = g^2 \frac{Z_{\text{mix}}^{(1)}}{\epsilon} + \mathcal{O}(g^4), \quad Z_{\text{cusp}, \Phi} = 1 + g^2 \frac{Z_{\text{cusp}, \Phi}^{(1)}}{\epsilon} + \mathcal{O}(g^4). \quad (4.43)$$

In the following, we show up to two loops that  $\mathbf{Z}$  is diagonal, i.e. that  $W_{\text{cusp}, \Phi}$  renormalizes multiplicatively up to that loop order. This accidental vanishing of  $Z_{\text{mix}}$  might be related to the enhanced (dual conformal) symmetry of our setup, which we are not exploiting in the present calculation.

The correlation functions not only have UV divergences coming from the cusp and the operator insertion, but also soft and collinear divergences from the on-shell scalars.

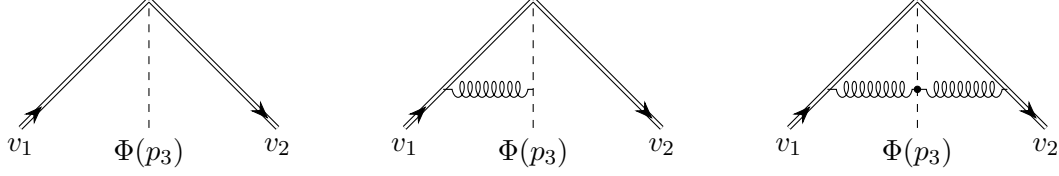


**Figure 4.4:** Sample diagrams for the correlation function  $\langle 0 | W_{\text{cusp}, \Phi} | \Phi(p_3) \rangle$ . Double, curly and dashed lines represent Wilson lines, gluons and scalars, respectively

The latter can be renormalized with a common IR Z-factor

$$\log(Z_{\text{IR}}^{-1}) = \sum_{L \geq 1} (g^2)^L \left( \frac{K^{(L)}}{8} \frac{1}{(\epsilon L)^2} \left( 1 - \epsilon L \log \left( \frac{s_1 s_2}{\mu^2} \right) \right) - \frac{\gamma_{HgH}^{(L)}}{2\epsilon L} \right), \quad (4.44)$$

where  $\mu$  is the renormalization scale, and  $K^{(L)}$  is the coefficient of  $(g^2)^L$  in the cusp anomalous dimension defined below (4.16);  $\gamma_{HgH}$ , discussed below, is interpreted physically as the SCET collinear anomalous dimension of one massless field, plus that of two heavy fields. This Z-factor simultaneously renormalizes the IR divergences of both correlation functions, because the structure of the IR divergences arises only from the configuration of the external lines and not from the cusp point. Likewise UV divergences only come from the cusp and the operator insertion and not from the external scalar. The renormalization condition is then given by

$$Z_{\text{IR}}^{-1} \mathbf{Z}^{-1} \langle 0 | \vec{W} | \Phi(p_3) \rangle = \mathcal{O}(\epsilon^0). \quad (4.45)$$

Given the known cusp anomalous dimension (4.36), this equation allows us to determine the IR Z-factor and then the missing pieces in  $\mathbf{Z}^{-1}$ .

#### 4.4.3 One-loop calculation

Let us now discuss in some detail the one-loop calculation. In figure 4.4 and 4.5 some sample Feynman diagrams are shown. We find the following result for the correlation functions,

$$\begin{aligned} \langle 0 | \partial W_{\text{cusp}} | \Phi(p_3) \rangle &= \frac{(s_1 + s_2)}{2g_{\text{YM}}} \langle 0 | W_{\text{cusp}} | \Phi(p_3) \rangle \\ &= \frac{(s_1 + s_2)^2}{s_1 s_2} \left\{ 1 + g^2 \left( -\frac{1}{\epsilon^2} + \frac{1}{\epsilon} \left[ \log \left( \frac{s_1 s_2}{\mu^2} \right) + \xi \log(x) \right] + \mathcal{O}(\epsilon^0) \right) \right\} + \mathcal{O}(g^4), \end{aligned} \quad (4.46)$$

$$\langle 0 | W_{\text{cusp}, \Phi} | \Phi(p_3) \rangle = 1 + g^2 \left( -\frac{1}{\epsilon^2} + \frac{1}{\epsilon} \left[ \log \left( \frac{s_1 s_2}{\mu^2} \right) - 2 \right] + \mathcal{O}(\epsilon^0) \right) + \mathcal{O}(g^4). \quad (4.47)$$

The IR Z-factor (4.44) is determined by the first component of (4.45), with the result

$$K^{(1)} = 8, \quad \gamma_{HgH}^{(1)} = 0. \quad (4.48)$$

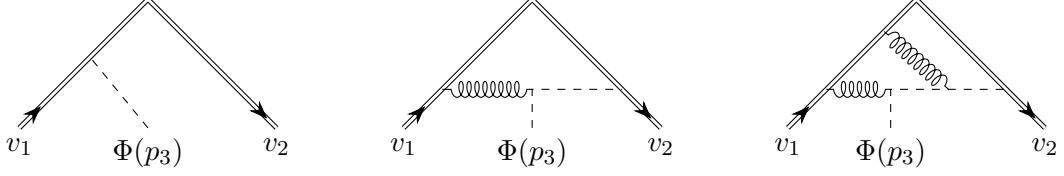


**Figure 4.5:** Sample diagrams for the correlation function  $\langle 0 | \partial W_{\text{cusp}} | \Phi(p_3) \rangle$ . Double, curly and dashed lines represent Wilson lines, gluons and scalars, respectively

The first matches the expansion of the cusp anomalous dimension  $K(g^2) = 8g^2 - 16g^4\zeta_2 + \mathcal{O}(g^6)$  stated earlier.

The second component of (4.45) then allows us to calculate the remaining pieces of  $\mathbf{Z}^{-1}$  (or, equivalently  $\mathbf{Z}$ ). We can deduce that at the one-loop level, the lower off-diagonal element in  $\mathbf{Z}^{-1}$  has to vanish. This is seen as follows. The tree level contribution of (4.46) to the second component in (4.45) has the form  $[g^2 Z_{\text{mix}}^{(1)}(s_1 + s_2)^2] / [\epsilon s_1 s_2]$ . However, there is no one-loop contribution from (4.47) of this form and  $Z_{\text{mix}}^{(1)}$  can not depend on  $s_1$  and  $s_2$ , hence we have  $Z_{\text{mix}}^{(1)} = 0$ . For the diagonal element we find  $Z_{\text{cusp}, \Phi}^{(1)} = -2$ .

For the general case of a renormalization matrix, the corresponding anomalous dimension matrix  $\mathbf{\Gamma}$  is given by

$$\mathbf{\Gamma} = \mathbf{Z}^{-1} \frac{d\mathbf{Z}}{d \log(\mu)}, \quad \text{with} \quad \frac{dg^2}{d \log(\mu)} = -2\epsilon g^2. \quad (4.49)$$

Here we used that the beta-function vanishes in  $\mathcal{N} = 4$  sYM theory. In our case the renormalization matrix is diagonal, and therefore the matrix inversion is trivial. In this way, adding the engineering dimension of the scalar insertion, we obtain

$$\Gamma_{\text{cusp}, \Phi} = 1 + 4g^2 + \mathcal{O}(g^4). \quad (4.50)$$

This is in agreement with our conjectured relation (4.31) (and also with the computation of the same anomalous dimension in [287]).

#### 4.4.4 Extension to two loops and discussion

We proceeded to perform the calculation to two loops. Some details of this calculation, and in particular the computation of the necessary Feynman integrals, can be found in appendix 4.9. Proceeding as in the one-loop case and subtracting the known UV divergences of  $W_{\text{cusp}}$ , we find for the IR renormalization coefficients

$$K^{(2)} = -16\zeta_2, \quad \gamma_{HgH}^{(2)} = -2\zeta_3. \quad (4.51)$$

The cusp anomalous dimension matches the expected result, but it is also instructive to compare the value of the second, single-logarithmic IR divergence. According to ref. [38],



it should be the sum of a collinear anomalous dimension for massless particles, plus the IR anomalous dimensions for the two massive fundamental Wilson lines (or equivalently heavy particles):

$$\gamma_{HgH} = \gamma_g + 2\gamma_{H,\text{fund}}. \quad (4.52)$$

The known two-loop collinear anomalous dimension for any parton in this theory is  $\gamma_g = 2g^4\zeta_3$ , which matches with the maximal transcendental part of the QCD result for either a gluon or an adjoint quark (see [288]). The massive case  $\gamma_{H,\text{fund}}$  was not calculated, to our knowledge, however we can take the maximal transcendental part of the result for an adjoint QCD quark as given in [38]:  $\gamma_{H,\text{adjoint}} = -4g^4\zeta_3 \equiv 2\gamma_{H,\text{fund}}$ . These indeed sum up to the value (4.51), which we conclude is consistent with the principle of maximal transcendentality and the known QCD values.

Proceeding to the UV renormalization, we find that up to two loops,  $\mathbf{Z}^{-1}$  remains diagonal, and gives the anomalous dimension

$$\Gamma_{\text{cusp},\Phi} = 1 + 4g^2 + g^4 \left[ -\frac{1}{\xi} \left( 4\zeta_2 H_1 + \frac{H_1^3}{6} \right) - 8\xi H_1 + 2H_1^2 + 16(\zeta_2 + 1) \right] + \mathcal{O}(g^6), \quad (4.53)$$

where  $H$  are HPLs with argument  $1 - x^2$ . This is in perfect agreement with the conjectured relation (4.31) with the Regge trajectory given in eq. (4.28).

This two-loop calculation provides non-trivial evidence in favor of our proposed relation (4.31), which identifies the subleading Regge trajectory  $j_1$  with the scaling dimension  $\Gamma_{\text{cusp},\Phi}$  of a Wilson loop operator. We note that the Regge trajectory  $j_1$  is known (from the scattering amplitude calculation) to one more order, three-loops. It would be interesting to verify that eq. (4.31) also holds at that order, perhaps using integrability or other methods.

## 4.5 Conclusion and outlook

In this chapter we studied a massive four-particle scattering amplitude in  $\mathcal{N} = 4$  super Yang-Mills. Starting from the three-loop result obtained in [250], we initiated a systematic analysis of this amplitude as a function of all kinematic invariants. While the full amplitude involves complicated multiple polylogarithms that depend on two variables  $s/m^2$  and  $t/m^2$ , it simplifies considerably in various physically interesting limits. In appendix 4.8, we explain in detail how we obtained expansions from the differential equations of [250], and we provide the detailed three-loop formulas for the asymptotic expansions described in section 4.2 as supplementary material (see [75]).

With the results of the asymptotic expansions at hand, we focused on the Regge limit. Using the fact that the amplitude is governed by a hidden symmetry, dual conformal symmetry, we derived a partial wave expansion which incorporates this additional information. It was known that the leading term in the Regge limit exponentiates, with

the exponent given by the anomalous dimension of a Wilson loop with a cusp. In this chapter, we explored subleading, power-suppressed terms. Surprisingly, we found that, in this expansion, the first power suppressed term also exponentiates! We computed the Regge exponent  $j_1$  to three loops, cf. eq. (4.28).

Moreover, by using the symmetry to map the Regge kinematics to a soft expansion, cf. section 4.3.2, we argued that the relevant operator controlling the subleading Regge limit should be a cusped Wilson loop with a scalar insertion at the cusp. We verified this proposal to two loops in perturbation theory. In order to do so, we performed a soft current calculation for massive quarks, to two loops, and found a perfect match. The details of the calculation of the Feynman integrals are presented in appendix 4.9.

While we found that all integrals needed to compute the divergent part of the two-loop correlation functions required only multiple polylogarithms. It is interesting to mention that some of the finite integrals involve elliptic polylogarithms.

We briefly discuss some interesting questions for future work. Our asymptotic expansions provide a wealth of data to explore higher order terms in the power expansion. At sub-subleading power in the Regge limit ( $1/s^2$ ), we compared the expansion (4.29) with an ansatz with two power laws. We find that such an ansatz is inconsistent with angle-independent one-loop exponents, a property which would be expected in the perturbative expansion. However, it is possible to write a consistent ansatz with three exponents. Such an ansatz could be tested once higher-loop results for the scattering amplitude become available.

It would be interesting to derive a systematic expansion using HQET as sketched around eq. (4.37), exploiting the setup of section 4.3.2 where the problem is mapped to a massless limit  $m_3 \rightarrow 0$ . The leading order terms correspond to the cusped Wilson loop, while we proposed that at first order one needs to consider a scalar insertion into the Wilson loop. However, in general, the Lagrangian of this effective theory contains an infinite series of irrelevant operators suppressed by the heavy mass, giving corrections to the Wilson lines, analogous to those considered in [42, 43, 289, 290]. At higher orders in the power expansion, these may cause triangular mixing between the operator (4.37) and higher-dimensional ones. This could prevent the amplitude from being a sum of pure power laws. It would thus be very interesting to elucidate the structure at higher powers, and ultimately to translate these findings to the usual null Wilson lines approach to the Regge limit.

Once the operators are identified, a separate question consists in computing their anomalous dimensions. The cusp anomalous  $\Gamma_{\text{cusp}}$  is known to be governed by an integrable system [251, 252], which was simplified in [291]. It would thus be interesting to see if the first subleading trajectory, given to three loops in eq. (4.28), can be reproduced quantitatively by extending the methods used in [274]. We also wish to point out that though the AdS/CFT correspondence, it may be possible to study the anomalous dimensions at strong coupling [172].

## 4.6 Appendix I: The total cross section to three loops

Here we discuss the total cross section  $\sigma_{\text{tot}} = \sigma_{Y\bar{Y} \rightarrow X}$ , see eq. (4.8), up to three-loop order, using the results of [250]. We will observe an interesting property about its high-energy behavior that motivates the all-loop prediction (4.12).

In [250] the integrals contributing to the three-loop amplitude were computed. They fulfill a differential equation with trivial boundary conditions at  $s = t = 0$ . To study the forward limit  $t = 0$  we thus only need to integrate with respect to  $s$ , or equivalently  $u = \frac{4m^2}{-s}$ . The differential equations have logarithmic-type singularities at  $u = 0, -1$ , and a square-root type singularity at  $u = -1$ . Upon switching to the variable  $x = \frac{\beta_u - 1}{\beta_u + 1}$ , the alphabet becomes  $\{x, 1+x, 1-x\}$ . From this it follows that the limit of  $M$  can be written in terms of harmonic polylogarithms [223, 224] with argument  $x$ . Our result takes the form

$$\lim_{t \rightarrow 0} \frac{m^2}{-t} M^{(1)} = 2 + \frac{1+x}{1-x} \log(x), \quad (4.54)$$

$$\begin{aligned} \lim_{t \rightarrow 0} \frac{m^2}{-t} M^{(2)} = & -24\text{Li}_3(-x) + 16\log(x)\text{Li}_2(-x) + 4\log^2(x)\log(1+x) \\ & -18\zeta_3 - 4\zeta_2\log(x). \end{aligned} \quad (4.55)$$

The two-loop result originates solely from the horizontal ladder,  $s^2 t G_{1,1,1,0,1,0,1,1,1}$ , because the other integral is explicitly proportional to  $st^2$ . For the same reason, at three-loops only two integrals from [250] contribute to the forward limit.

$$\begin{aligned} \lim_{t \rightarrow 0} \frac{m^2}{-t} M^{(3)} = & \frac{1-x}{1+x} \left[ -96H_{0,-1,-1,0,0}(x) - 32H_{0,-1,0,-1,0} + 80H_{0,-1,0,0,0} \right. \\ & + 32H_{0,-1,1,0,0} + 128H_{0,0,-1,-1,0} - 16H_{0,0,1,0,0} + 32H_{0,1,-1,0,0} \\ & + 96H_{0,1,0,-1,0} - 64H_{0,1,0,0,0} + \zeta_3(120H_{0,1} - 8H_{0,-1}) \\ & + \zeta_2(-16H_{0,-1,0} + 64H_{0,0,-1} + 48H_{0,1,0} + 24\zeta_3) + 28\zeta_4 H_0 + 70\zeta_5 \Big] \\ & - 64H_{0,0,-1,0,0} + 64H_{0,-1,0,0,0} - 48H_{0,1,0,0,0} + 48H_{0,0,1,0,0} \\ & + 32\zeta_4 H_0 + 120\zeta_5. \end{aligned} \quad (4.56)$$

The first term originates from the ladder while the last line originates from the tennis court diagram. Here  $H$  are HPLs of argument  $x$ , which we omitted for brevity. Note that all formulas above are symmetric under  $x \rightarrow 1/x$ , as may be verified by using identities between the HPLs for different arguments [223, 224].

The physical region above the threshold  $s > 4m^2$ , where the inelastic cross section (4.8) is nonzero, correspond to  $-1 < x < 0$ . This region can be reached by analytic continuation. In total we can identify three regions relevant for the analytic continuation: the Euclidean region, below the threshold and above the threshold. In the Euclidean region and below the threshold the amplitude is real. Above the threshold, however,

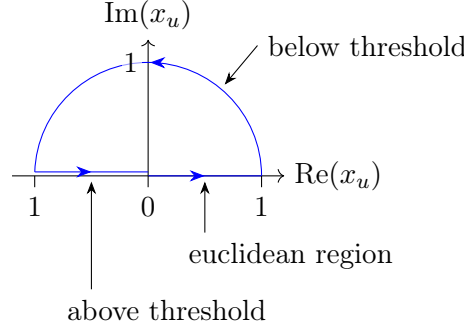


**Figure 4.6:** Analytic continuation in the forward limit regime, from  $s < 0$  (Euclidean region), to  $0 < s < 4m^2$  (below threshold), to  $s > 4m^2$  (above threshold).

the amplitude has a branch cut and following Feynman's  $i0$  prescription we have to evaluate the HPLs slightly above the real axis. The analytic continuation is illustrated in figure 4.6. By calculating the imaginary part of the amplitude we find for the total cross section

$$\sigma_{Y\bar{Y} \rightarrow X} = \frac{2\pi g_{\text{YM}}^2}{m^2} [g^2 X_1 + g^4 X_2 + g^6 X_3 + \mathcal{O}(g^8)] , \quad (4.57)$$

where

$$X_1 = \frac{1+x}{1-x} , \quad (4.58)$$

$$X_2 = 16\text{Li}_2(-x) + 8\log(-x)\log(x+1) - \frac{2\pi^2}{3} , \quad (4.59)$$

$$\begin{aligned} X_3 = & -48H_{-3,0}(-x) + 64H_{3,0}(-x) + 48H_{-2,0,0}(-x) - 64H_{2,0,0}(-x) \\ & - 48\zeta_2 H_{-2}(-x) + 64\zeta_2 H_2(-x) + 32\zeta_4 \\ & + \frac{1-x}{1+x} \left[ 16H_{-3,0}(-x) + 96H_{-2,2}(-x) - 32H_{2,2}(-x) + 128H_{3,1}(-x) \right. \\ & + 64H_{-2,0,0}(-x) + 32H_{-2,1,0}(-x) + 32H_{2,-1,0}(-x) - 80H_{2,0,0}(-x) \\ & \left. - 96H_{2,1,0}(-x) - 112\zeta_2 H_{-2}(-x) + 96\zeta_2 H_2(-x) + 28\zeta_4 \right] . \end{aligned} \quad (4.60)$$

Here we have chosen a form that is manifestly real-valued for  $-1 < x < 0$ .

The cross section (4.57) can be seen to approach a constant in the high-energy limit  $x \rightarrow 0$ :

$$X_1 \rightarrow 1 , \quad X_2 \rightarrow -\frac{2\pi^2}{3} , \quad X_3 \rightarrow \frac{2\pi^4}{3} . \quad (4.61)$$

Remarkably, this agrees precisely with the perturbative expansion of the Bremsstrahlung function (4.21)! This is not a coincidence. To see this, we use the leading Regge behavior

of the amplitude at large  $s$  and fixed  $t$

$$\lim_{s \rightarrow \infty} M\left(\frac{4m^2}{-s}, \frac{4m^2}{-s}\right) = \tilde{r}_0(t)(-s - i0)^{1+j_0(t)} + \mathcal{O}(1/s), \quad (4.62)$$

where  $\tilde{r}_0$  and  $j_0 + 1$  are given in (4.18). Because of the mass gap of the  $W$ -bosons, loop corrections to the *amplitude*  $A \propto Ms/t$  must be real and analytic around  $t = 0$ , which implies that the coefficient of  $1/t$  is tree-level exact. Thus the loop corrections to these parameters must vanish at the origin:  $\tilde{r}_0(0) = 1$  and  $j_0(0) = -1$ . Furthermore, the coefficient  $\tilde{r}_0$  is real, so the imaginary part originates from the trajectory. Thus

$$\lim_{t \rightarrow 0} \lim_{s \rightarrow \infty} \frac{1}{-t} \text{Im } M(s, t) = \pi \frac{d}{dt} j_0(t) \Big|_{t=0}. \quad (4.63)$$

Eq. (4.63) is a bit unusual since the cross section involves the slope of the Regge trajectory at  $t = 0$  rather than the intercept, as is more usual. This happens here because the intercept precisely vanishes. Using the relation (4.21) expressing the slope at  $t = 0$  in terms of the (exactly known) Bremsstrahlung function gives the prediction (4.12) for the total cross section, generalizing (4.61) to all orders.

## 4.7 Appendix II: Regge expansion using dual conformal partial waves

As discussed in section 4.3, the enhanced symmetry of the amplitude we look at makes it possible to efficiently organize the Regge limit. In this section we derive this improved expansion which exploits dual conformal symmetry.

It will be helpful to use the embedding formalism, which realizes Minkowski space as the null cone in  $\mathbb{R}^{4,2}$ . The region momenta associated to each (planar) loop are represented as a (projective) 6-vector

$$X^A = (\vec{x}, \frac{x^2}{2\mu} - \frac{\mu}{2} \mid x^0, \frac{x^2}{2\mu} + \frac{\mu}{2}), \quad (4.64)$$

where the first four components (before the vertical line) are spacelike and the last two are timelike. Here  $\mu$  is an arbitrary scale and  $x^2 = \vec{x}^2 - (x^0)^2$ . In the presence of internal masses we also need to consider timelike dual coordinates for the external regions (see figure 4.7), satisfying  $Y_i^2 = -m^2$ :

$$Y_i^A = (\vec{y}, \frac{y^2+m^2}{2\mu} - \frac{\mu}{2} \mid y^0, \frac{y^2+m^2}{2\mu} + \frac{\mu}{2}). \quad (4.65)$$

These definitions ensure that six-dimensional dot products give massless and massive momentum space propagators:

$$-2X_i \cdot X_j = (x_i - x_j)^2, \quad -2X_i \cdot Y_j = (x_i - y_j)^2 + m^2. \quad (4.66)$$

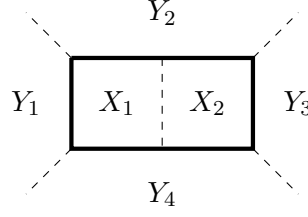


**Figure 4.7:** Visualization of the dual coordinates defined in (4.66)-(4.67). Solid and dashed lines represent massive and massless particles, respectively

This notation is helpful because the dual conformal symmetry  $SO(4,2)$  acts linearly as rotations of these 6-vectors. The external momenta of our planar four-particle scattering problem are encoded in the differences between the above points  $Y_i^A$  as:  $y_{i+1}^\mu - y_i^\mu = p_i^\mu$ . For definiteness let us begin by assuming kinematics with a timelike  $t$ -channel, with  $0 < t < 4m^2$  where  $t = -(p_2 + p_3)^2$ . We can use Lorentz invariance to go to the rest frame of  $p_2 + p_3$  and use translation invariance in  $y$ -space to set  $\vec{y}_2 = \vec{y}_4 = 0$ . Furthermore, the energies of  $p_1, p_2$  must be equal and opposite, which allows to set  $y_1^0 = y_3^0 = 0$ . In this frame the dual coordinates reduce to

$$Y_1 = \begin{pmatrix} -\vec{p}_1 \\ \frac{t}{2\alpha} \\ 0 \\ \frac{2m^2}{\alpha} \end{pmatrix}, \quad Y_2 = \begin{pmatrix} \vec{0} \\ 0 \\ \frac{1}{2}\sqrt{t} \\ \frac{\alpha}{2} \end{pmatrix}, \quad Y_3 = \begin{pmatrix} \vec{p}_2 \\ \frac{t}{2\alpha} \\ 0 \\ \frac{2m^2}{\alpha} \end{pmatrix}, \quad Y_4 = \begin{pmatrix} \vec{0} \\ 0 \\ -\frac{1}{2}\sqrt{t} \\ \frac{\alpha}{2} \end{pmatrix}, \quad (4.67)$$

where  $\alpha = \sqrt{4m^2 - t}$  and in addition we have chosen  $\mu = \frac{\alpha}{2}$  in order to set to zero the last spacelike component of  $Y_2$  and  $Y_4$ .

The  $SO(4)$  symmetry is apparent in this frame: these are simply the rotations of the first four components, which preserve the two dual coordinates  $Y_2$  and  $Y_4$  bounding the  $t$ -channel. This contains the usual  $SO(3)$  rotations of a pair of particles in its rest frame, with three additional generators which are related, in the nonrelativistic limit, to the flow generated by the Laplace-Runge-Lenz vector of the hydrogen atom [170].

From eq. (4.67) we see that the dependence on the Mandelstam variable  $s = -(p_1 + p_2)^2$  is encoded in the  $SO(4)$ -invariant angle between the first four components of  $Y_1$  and those of  $Y_3$ . From a short computation:

$$\cos \theta \equiv \frac{-\vec{p}_1 \cdot \vec{p}_2 + \frac{t^2}{4\alpha^2}}{p_1^2 + \frac{t^2}{4\alpha^2}} = 1 + \frac{2s}{t} - \frac{s}{2m^2}, \quad (4.68)$$

where we have simplified using that  $\vec{p}_1^2 = \vec{p}_2^2 = \frac{t}{4}$  and  $-\vec{p}_1 \cdot \vec{p}_2 = \frac{t}{4} + \frac{s}{2}$ . As noted in the text, this angle differs from the usual scattering angle between the two external massless photons (see eq. (4.22)) by the  $-s/(2m^2)$  term. It is real, for example, in the  $t$ -channel region where  $0 < t < 4m^2$  and  $-t < s < 0$ .

We now derive the corresponding partial wave expansion, starting from the case where the angle is real and then analytically continuing. The idea is to express the dependence on  $s$  in terms of  $\text{SO}(4)$  spherical harmonics; for each  $\text{SO}(4)$  spin  $j$  these sum up to a Chebyshev polynomial (the  $\text{SO}(4)$  analog of the Legendre polynomials):

$$A = \sum_{j=0}^{\infty} c_j(t) P'_j(\cos \theta), \quad P'_j(\cos \theta) = \frac{\sin((j+1)\theta)}{(j+1)\sin(\theta)}. \quad (4.69)$$

Using the relation similar to (4.2) between the  $Y\bar{Y} \rightarrow \bar{Y}Y$  amplitude and the stripped matrix element  $M$ ,

$$A = \frac{t}{s} M(s, t) = \frac{1 - t/4m^2}{\sin^2(\theta/2)} M(s, t) \quad (4.70)$$

and absorbing  $s$ -independent factors into the coefficients  $c_j(t)$ , we can rewrite this as an expansion for  $M$ :

$$\frac{1+Y}{1-Y} M(s, t) = \sum_{j=0}^{\infty} c'_j(t) (Y^{j+1} - Y^{-j-1}), \quad Y \equiv e^{i\theta} = \frac{\beta_{uv} - \beta_v}{\beta_{uv} + \beta_v}. \quad (4.71)$$

We note that, as a mathematical statement about bases of functions, one could equally well apply this decomposition to  $M$  itself (or to  $M$  times any function of the cross-ratios  $u, v$ ). The amplitude  $A$  is singled out physically since its  $t$ -channel cuts have a Hilbert space interpretation in terms of intermediate states acted upon by  $\text{SO}(4)$ .<sup>6</sup>

We now have an expansion valid for real angles. To reach the Regge limit  $Y \rightarrow 0$  where the angle is imaginary, we follow the standard procedure and rewrite the sum as an integral using the Watson-Sommerfeld trick [278, 279]:

$$\frac{1+Y}{1-Y} M(s, t) = \int_{-\epsilon - i\infty}^{-\epsilon + i\infty} \frac{i dj}{2 \sin(\pi j)} c_j(t) (e^{-i\pi j} Y^{j+1} - e^{i\pi j} Y^{-j-1}), \quad (4.72)$$

where we have assumed that  $0 < \theta < \pi$  and the phases have been chosen such that the integrand vanishes at large imaginary  $j$  (assuming that  $c_j(t)$  is bounded). The idea is that, deforming the contour to the right and picking up the residues of  $\sin(\pi j)$ , this reproduces the sum (4.71). But taking the Regge limit  $Y \rightarrow 0$ , a different contour deformation becomes appropriate. The contour can still be closed to the right in the first term, but now to the left in the second term.

Two types of singularities arise: poles from the inverse sine factor, which add up to:

$$c_{-1}(t) + \sum_{k \geq 0} Y^{k+1} (c_k(t) + c_{-2-k}(t)). \quad (4.73)$$

<sup>6</sup>This can be checked from the numerators of the various contributions to  $M$ , for example the  $L$ -loop  $t$ -channel ladder. The  $s$ -dependence of its coefficient  $st^L$ , which is non-factorized since it couples directly the two endpoints  $Y_1, Y_3$  of the ladder, cancels in the amplitude we use.

These however neatly cancel out, because for *integer* spin  $j$  the coefficients  $c_j$  are odd under  $j \rightarrow -j - 2$ . Such a cancellation of kinematic poles can be proved from the Froissard-Gribov inversion formula and occurs generally for any  $\text{SO}(D)$  expansion; a detailed discussion in the  $\text{SO}(3)$  case can be found in refs. [278, 279]. All that remain are the Regge poles of  $c_k(t)$  from the second term, which add up to the asymptotic expansion:

$$\lim_{Y \rightarrow 0} \frac{1+Y}{1-Y} M = \sum_{n=0}^{\infty} r_n(t) Y^{-j_n(t)-1}, \quad (4.74)$$

where we have defined the residues  $r_n(t) = \frac{\pi e^{i\pi j_n(t)}}{\sin(\pi j_n(t))} \text{Res}_{j=j_n(t)} c_j(t)$ . This formula is used in the main text to efficiently organize the Regge expansion  $Y \sim \frac{1}{s} \rightarrow 0$ .

## 4.8 Appendix III: Method for expanding the three-loop amplitude

Here we explain how to express the amplitude in various limits, which in general can contain logarithmic divergences. In principle, we could use the analytic expressions for the master integrals derived in ref. [250], and expand them using properties of the iterated integrals they were expressed in. We find it more convenient to obtain such expansions directly from differential equation for the master integrals that were derived in ref. [250].

In order to do so, we use a well-known procedure for solving differential equations in a limit, following closely the textbook [225]. Let  $x$  be parameter that parametrizes the expansion around  $x = 0$ , and let  $\vec{f}$  be the vector of master integrals. As we will see, the solution for  $\vec{f}$  takes the general form  $P(x)x^{A_0}\vec{f}_0$ , where  $P(x)$  is a (matrix) polynomial in  $x$ ; the matrix exponential  $x^{A_0}$  contains possible logarithmic divergences, and  $\vec{f}_0$  is the finite boundary value at  $x = 0$ . Given possible powers of logarithms  $\log(x)$ , one may also call  $\vec{f}_0$  the ‘regularized’ boundary value.

A technical point is related to obtaining such boundary values for all expansions that we are interested in. The boundary value considered in ref. [250] is taken at  $s, t \rightarrow 0$ , see figure 4.8. In order to obtain appropriate boundary values for other expansions, we first transport this value to other regions, along appropriate paths. By ‘transporting’ we mean solving the differential equation along a given path. In principle one could choose any convenient path. However, some choices are preferable over others. In particular, one can often find paths for which the one-parameter solution is expressible in terms of a relatively simple class of functions, the HPLs. This is the case for the paths shown in figure 4.8.

As we will discuss in more detail in the following, special care is required when singular boundaries are approached (corresponding to singularities of the differential equation). When several of such boundaries intersect, it is important to clarify how the singular



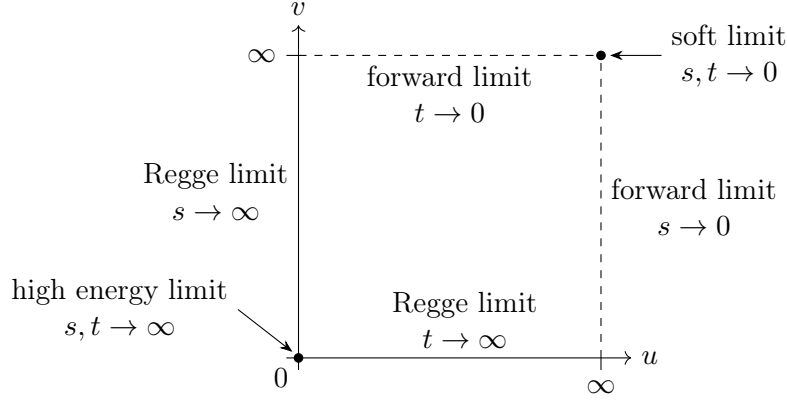


**Figure 4.8:** Different limits we consider in the  $u - v$  plane. To derive expansions, first the boundary value for each limit is obtained. Initially known in the soft limit, the boundary value is transported along the edge of the diagram.

boundary is approached. In mathematical language, one can perform a ‘blowup’ that resolves singular intersections of boundaries.

As a non-trivial verification of our analytic continuation procedure, we verified that, upon returning to the original point  $s, t \rightarrow 0$  after going around the whole square in the positive quadrant shown in figure 4.8, we recover the correct boundary value.

#### 4.8.1 Solving the differential equation in an expansion

In this section we follow [225] closely. Given a square  $n$ -th order matrix  $\bar{A}(x)$ , which is holomorphic on a connected open set  $R \subset \mathbb{C}$ , the differential equation  $\vec{f}'(x) = \bar{A}(x)\vec{f}(x)$  has a unique solution on  $R$ , provided a boundary condition  $\vec{f}(a) = \vec{f}_{BV}$ ,  $a \in R$ . Furthermore, this solution is holomorphic on  $R$ . We are interested in the more special case where the matrix  $\bar{A}(x)$  has a regular singular point  $x_p \notin R$ . Without loss of generality we choose  $x_p = 0$ . Then the differential equation can be rewritten as

$$x\vec{f}'(x) = A(x)\vec{f}(x). \quad (4.75)$$

As a first step in solving (4.75) we perform a transformation  $\vec{f}(x) = P(x)\vec{g}(x)$  with a non-singular holomorphic matrix  $P(x)$  to get

$$x\vec{g}'(x) = B(x)\vec{g}(x). \quad (4.76)$$

The new matrix  $B(x)$  is determined by  $P(x)$  and  $A(x)$ . Our aim is now to find a  $P(x)$  such that  $B(x)$  becomes as simple as possible, in order to solve (4.76). As we will see, in practice, we can choose  $B(x)$  and then calculate  $P(x)$  using

$$xP'(x) = A(x)P(x) - P(x)B(x).$$

Inserting the respective power series for  $A(x) = \sum_{k \in \mathbb{N}_0} A_k x^k$  as well as for  $B(x)$  and  $P(x)$  in the differential equation above, we obtain, after equating the coefficients, the following recursion relation

$$A_0 P_0 - P_0 B_0 = 0, \quad (4.77)$$

$$(A_0 - k\mathbb{1})P_k - P_k B_0 = - \sum_{j=0}^{k-1} (A_{k-j} P_j - P_j B_{k-j}), \quad k > 0. \quad (4.78)$$

At this point a subtleness arises: We are of course interested in an unique solution of the problem, but the matrix equation  $AX - XB = 0$  for given square matrices  $A$  and  $B$  can in principle has a non-trivial solution for the matrix  $X$ . One can show that the equation  $AX - XB = 0$  has such a non-trivial solution  $X \neq 0$  if and only if  $A$  and  $B$  have at least one common eigenvalue.

Equipped with this knowledge, we now choose a certain matrix  $B(x)$ . If  $A$  in (4.75) is a constant matrix, then we do not need to simplify the problem any further. Therefore we choose as our starting point  $B_0 = A_0$  and  $P_0 = \mathbb{1}$ .

From the previous argument we know that if no pair of eigenvalues of the matrix  $A_0$  differs by a positive integer, the  $P_k$  are determined by (4.78). In our case the matrix appearing in the differential equation for the master integrals is a lower triangular matrix with vanishing diagonal elements, hence all eigenvalues are zero and the former condition is trivially fulfilled. We choose  $B_k = 0$  for  $k > 0$  in order to obtain a simple differential equation after the transformation. With the choice  $B(x) = A_0$  the solution of (4.76) is given by  $x^{A_0}$ . Returning to the original problem, we find the asymptotic expansion of the solution of (4.75)

$$\vec{f}(x) = P(x) x^{A_0} \vec{f}_0 = P(x) \exp[A_0 \log(x)] \vec{f}_0, \quad (4.79)$$

where  $P(x)$  is calculated recursively from (4.78) using  $P_0 = \mathbb{1}$ ,  $B_0 = A_0$  and  $B_k = 0$  for  $k > 0$ .

We wish to make the following comments.

- As was already mentioned earlier, the solution may have logarithmic divergences in the limit  $x \rightarrow 0$ . If present, these are described by the matrix exponential  $\exp[A_0 \log(x)]$ . We call  $\vec{f}_0$  the boundary value at  $x = 0$ , even in such singular cases.
- One can interpret the matrix  $F(x) = P(x) x^{A_0} = P(x) \exp[A_0 \log(x)]$  as the fundamental system of solutions of the matrix differential equation  $x F'(x) = A(x) F(x)$ .

In the following subsections, we describe in more detail the procedure of obtaining the boundary values for the different expansions, and on the choice of variables for the latter.

### 4.8.2 Soft expansion

The soft or low energy limit describes the region where  $|s|, |t| \ll 4m^2$ . We perform the calculation in the Euclidean region  $s, t < 0$ , but the result is valid in the entire region  $|s|, |t| \ll 4m^2$ , since the result is simply a polynomial in  $s$  and  $t$ .

In order to derive the soft expansion, we can use our starting boundary value at  $m \rightarrow \infty$  with  $\vec{g}_{\text{start}} = (1, 0, \dots, 0)$ . For solving the differential equation we introduce the transformation

$$s = -\frac{4m^2(1+R)}{R}x^2, \quad t = -4m^2(1+R)x^2 \quad \left( \Leftrightarrow u+v = \frac{1}{x^2}, \quad R = \frac{u}{v} \right), \quad (4.80)$$

with the ratio  $R = u/v = t/s$  fixed. The differential equation is then solved for small  $x$ , as explained above.

Applying this to the amplitude, we find, up to three loops,

$$\begin{aligned} \frac{M-1}{st} \approx & -\frac{g^2}{6m^4} - \frac{s+t}{m^6} \left( \frac{g^2}{60} + \frac{g^4}{12} - \frac{g^6}{3} \right) \\ & - \frac{st}{m^8} \left( \frac{g^2}{840} + \frac{g^4}{180} \right) - \frac{s^2+t^2}{m^8} \left( \frac{g^2}{420} + \frac{g^4}{45} - \frac{g^6}{24} \right). \end{aligned} \quad (4.81)$$

As mentioned earlier, the  $1/m^4$  term is one-loop exact. In the perturbative expansion this feature is evident already pre-integration: all higher-loop integrals appearing in the perturbative expansion are explicitly proportional to at least  $s^2t$  or  $st^2$ , e.g. see figure 7 of [163] for the five loop integrand.

It is noteworthy that all coefficients are rational multiples of  $g^2 = g_{YM}^2 N / (16\pi^2)$ ; no transcendental numbers such as  $\zeta$  values appear. Technically this can be traced to the fact that in ref. [250] a uniform weight basis could be found in which all but one integral vanish in the low-energy limit. It would be interesting to see if this remains the case at higher loop orders.

### 4.8.3 Regge expansion

Switching from the kinematic invariants  $s$  and  $t$  to the variables  $u$  and  $v$ , the Regge limit is described by  $v \gg u$ . In our calculation we consider the limit  $u \rightarrow 0$  with  $v > 0$ . To transport the boundary value from our starting point at  $(u, v) = (\infty, \infty)$  (this is the limit  $m \rightarrow \infty$  in the Euclidean region) to our end point, we split the path in two straight line segments  $\gamma_1$  and  $\gamma_2$ . The first path  $\gamma_1 = \{(u, v) = (-t, \infty) | t \in (-\infty, 0]\}$  is parallel to the  $u$ -axis and ends on the  $v$ -axis, while the second path  $\gamma_2 = \{(u, v) = (0, -t) | t \in (-\infty, -\tilde{v}]\}$  is on the  $v$ -axis and ends at some  $\tilde{v} > 0$ .

For the first segment  $\gamma_1$  we take the limit  $v \rightarrow \infty$  and substitute the variable  $u$ :

$$u = \frac{4x_u}{(1-x_u)^2} \quad \Leftrightarrow \quad x_u = \frac{\beta_u - 1}{\beta_u + 1} \quad \text{with } u \in [0, \infty), x_u \in [0, 1). \quad (4.82)$$

This leads to a differential equation for the master integrals  $\vec{g}$  on the path  $\gamma_1$  with the alphabet  $\{x_u, 1-x_u, 1+x_u\}$ ,

$$\frac{d\vec{g}^{\gamma_1}}{dx_u} = A^{\gamma_1}(x_u)\vec{g}^{\gamma_1} = \left[ \lim_{v \rightarrow \infty} \frac{\partial A(x_u, v)}{\partial x_u} \right] \vec{g}^{\gamma_1}. \quad (4.83)$$

Since  $A^{\gamma_1}$  is a lower triangular matrix we obtain the solution recursively. It can be expressed in terms of HPLs and constants, which are determined by the boundary value at  $x_u = 1$ . For the path  $\gamma_2$  we need the boundary value at  $x_u = 0$ . Unlike at  $x_u = 1$  the master integrals exhibit logarithmic divergences at  $x_u = 0$ . To extract the (regularized) boundary value, we use the asymptotic expansion of the differential equation.

The calculation for the second path  $\gamma_2$  is identical to the previous one. In the limit  $u \rightarrow 0$  and with the variable transformation (4.82) for the variable  $v$  the differential equation can be solved on the path  $\gamma_2$  in terms of HPLs. With the previous calculated boundary value at  $x_u = 0$  the integration constants are fixed. With the solution  $\vec{g}^{\gamma_2}(x_v)$  on the second path as our boundary value we finally solve the differential equation in an asymptotic expansion with arbitrary  $v > 0$  in  $x_u$  near  $x_u = 0$  to obtain the master integrals in the Regge limit.

#### 4.8.4 High energy expansion

In the high energy limit we have  $|s|, |t| \gg 4m^2$ . We will work in the Euclidean region. Obtaining the appropriate boundary value at  $(u, v) = (0, 0)$  requires some care, as we discuss presently. The subtlety originates from the singularity structure of the differential equation in the limit  $u, v \rightarrow 0$ . This can be immediately understood by inspecting the alphabet of the differential equation [250], which contains the letters  $\{u, v, u+v, u^2-4v, v^2-4u\}$ . It is sufficient to study these “simple” letters, because the other letters do not add more singularities in the vicinity of  $(u, v) = (0, 0)$ . The corresponding singular lines are shown in figure 4.9(a). The fact that the latter intersect at  $(u, v) = (0, 0)$  implies that one has to specify how exactly this point is approached. The problem of a potential ambiguity can be avoided by switching to appropriate variables that resolve the way the singularity is approached.

The variable transformations can also be understood as choosing more sophisticated paths near the origin to connect the boundary values, which we obtain by approaching the origin  $(u, v) = (0, 0)$  on the  $u$ -axis or  $v$ -axis. These two boundary values are denoted by  $\vec{g}_{BV}^u$  and  $\vec{g}_{BV}^v$ . In figure 4.9 these paths are shown. The first transformation or path

$$\gamma_\delta(t) = (u, v) = (\delta(1-t), \delta t), \quad t \in [0, 1], \quad \delta > 0 \quad (4.84)$$

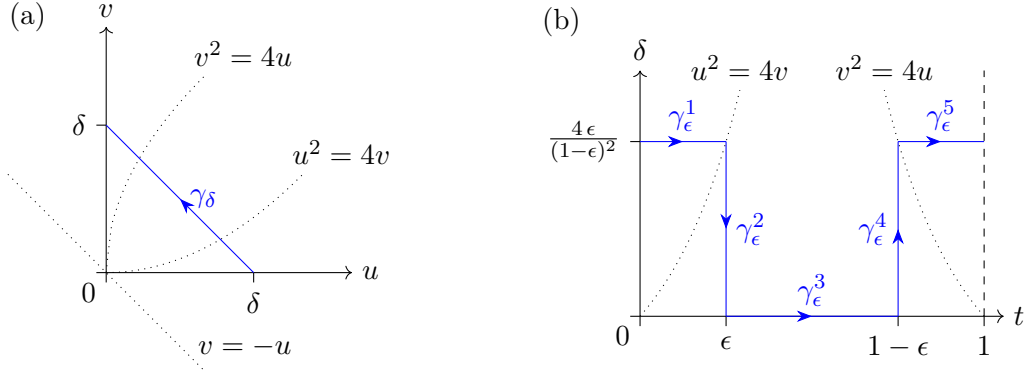


**Figure 4.9:** Left: Choice of path in the  $u$ - $v$ -plane. Right: Choice of path in the  $t$ - $\delta$ -plane.

resolves the ambiguity of the first three considered letters

$$\{u, v, u + v\} \longrightarrow \{\delta, t, 1 - t\}.$$

This transformation is sufficient at one- and two-loops, but not at three-loops, where the new letters  $\{\log(u^2 - 4v), \log(v^2 - 4u)\}$  first appear. Therefore we introduce a further transformation. The corresponding path  $\gamma_\epsilon$  in the  $\delta$ - $t$ -plane is shown in figure 4.9(b) and it is divided into five straight sections  $\gamma_\epsilon^i$ ,  $i = 1, 2, \dots, 5$ . The crucial point is now that after the transformation the ambiguities are resolved and we can take the limit  $\epsilon \rightarrow 0$  on the separate sections. Then we solve the differential equation in this limit. For example, the first segment can be parameterized by

$$\gamma_\epsilon^1(\tau) = (\delta, t) = \left( \frac{4\epsilon}{(1-\epsilon)^2}, \epsilon\tau \right), \quad \tau \in [0, 1] \quad \epsilon > 0.$$

In the limit  $\epsilon \rightarrow 0$  the alphabet becomes  $\{\tau, 1 - \tau, 1 + \tau\}$  and therefore the solution of the differential equation is given in terms of HPLs. However, a new subtleness arises, which we so far have not encountered. The solution exhibit logarithmic divergences at  $\tau = 0$  and  $\tau = 1$ . This means we have to fix the integration constants using the asymptotic expansion at  $\tau = 0$ . The boundary value at  $\tau = 0$  in the limit  $\epsilon \rightarrow 0$  is  $\tilde{g}_{BV}^u$  from before. The differential equation on the other sections can also be solved in terms of HPLs in the same way. After extracting the boundary value at the end point of the last section  $\gamma_\epsilon^5$  we precisely get  $\tilde{g}_{BV}^v$ , which is a strong crosscheck for our calculations. Additionally the solution on the third section  $\gamma_\epsilon^3|_{\epsilon \rightarrow 0} = (\delta, t) = (0, \tau)$ ,  $\tau \in [0, 1]$  is our desired boundary value for the high energy expansion. The boundary value depends only on the ratio  $R = u/v$  via  $\tau = t = 1/(1 + R)$ . With the known identities between HPLs the boundary value can be rewritten such that only HPLs with argument  $R$  appear.

Now we are finally in a position to calculate the high energy expansion. For this we transform from  $(u, v)$  to  $(\epsilon, R)$  using

$$\frac{4\epsilon}{(1-\epsilon)^2} = u + v, \quad R = \frac{u}{v}$$

and solve the differential equation in an asymptotic expansion in  $\epsilon$ . The final result is then rewritten in  $\rho = \epsilon/(1 - \epsilon)^2 = (u + v)/4$ .

#### 4.8.5 Threshold expansion

We now consider the threshold expansion of the amplitude. For this we solve the differential equation in an asymptotic expansion in  $\beta_u = \sqrt{1 + u}$  around  $\beta_u = 0$  in the physical region  $-s < t < 0$ . As in the previous limits the transportation of boundary value is the most complicated part of the calculation. However, we can use the results from the forward limit, where the master integrals were calculated in the limit  $v \rightarrow \infty$  for arbitrary  $4m^2 < s$ . As the next step we extract the boundary value at the threshold  $\beta_u = 0$ . So far we only have considered the case  $v \rightarrow \infty$  or equivalently  $t \rightarrow 0^-$ , but we are interested in an expansion in  $\beta_u$  for arbitrary  $-s < t < 0$  or equivalently  $1 < v < \infty$ . Therefore we solve the differential equation at the threshold in the new variable

$$v = \frac{4(1 - y)^2}{(1 - (1 - y)^2)^2}, \quad \text{with } y \in (0, 2 - \sqrt{2}), \quad (4.85)$$

in terms of iterated integrals. This variable transformation is chosen such that the alphabet does not contain any square roots; it is polynomial, with the highest degree being four. For brevity we do not write it down here. The integration constants of the solution of the differential equation are fixed by the previously extracted boundary value. Note that the solution does not have any divergences at  $y = 0$  or equivalently  $v = \infty$ . Finally we use this solution as the new boundary value for the asymptotic expansion of the master integrals in  $\beta_u$  around  $\beta_u = 0$ . We are only interested in the imaginary part of the amplitude, which simplifies the result significantly. The imaginary part of the amplitude depends only polynomially on  $t$ , whereas the real part contains iterated integrals.

### 4.9 Appendix IV: Soft current computation

For the one- and two-loop calculation we used the Feynman diagrammatic approach and evaluated the correlation functions in momentum space. The diagrams were generated with **qgraf** [177] and the output further processed with a custom **Mathematica** code which expresses the result in terms of a number of scalar loop integrals. To treat the Majorana fermions we used the techniques described in [146]. The IBP reduction to a set of master integrals was done with **FIRE5** [180, 292, 293] in combination with **LiteRed** [186, 187]. As a non trivial cross-check the calculation was done in covariant gauge. The gauge parameter drops out after the IBP reduction to master integrals. In addition our **Mathematica** code was tested by reproducing the two-loop cusp anomalous dimension [41, 264, 273] and the two-loop jet function in soft-collinear effective theory [140].

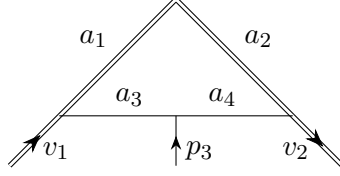


**Figure 4.10:** One-loop soft current integral topology

In this appendix we discuss the calculation of the one- and two-loop master integrals with the differential equation method [194–200]. We explain the one-loop case in detail. As a cross-check we compared the analytic results for the master integrals on several kinematic points in the Euclidean region with the numerical results obtained from FIESTA4 [294]. We found perfect agreement within the error bars.

### 4.9.1 One-loop master integrals

Let us briefly recall the kinematics of our problem. With the two directions of the Wilson lines  $v_1$  and  $v_2$ , and the on-shell momentum  $p_3$  of the external scalar, we can build three invariants

$$\cos(\phi) = v_1 \cdot v_2 = \frac{1}{2} \left( x + \frac{1}{x} \right), \quad s_1 = -2v_1 \cdot p_3 \quad s_2 = +2v_2 \cdot p_3, \quad (4.86)$$

where we used  $v_1^2 = v_2^2 = 1$  and  $p_3^2 = 0$ . In the following, the variable  $x = e^{i\phi}$  turns out to be most useful. At this point it is also worthwhile to introduce the Gram determinant  $G(q_1, q_2, q_3) = \det(q_i \cdot q_j)$  formed by the three vectors. It is given by

$$G(v_1, v_2, p_3) = -\frac{1}{4x} (s_1 x + s_2)(s_2 x + s_1). \quad (4.87)$$

If all the vectors lie in the same plane the Gram determinant vanishes. This hypersurface will turn out to be useful later when determining boundary values for the differential equations.

The one-loop integral family is defined as

$$G_{a_1, a_2, a_3, a_4} = e^{\epsilon \gamma_E} \int \frac{d^D k}{i\pi^{D/2}} \frac{1}{D_1^{a_1} D_2^{a_2} D_3^{a_3} D_4^{a_4}}, \quad (4.88)$$

where  $a_k \in \mathbb{Z}$  and the propagators are given by

$$\begin{aligned} D_1 &= -2(k + p_3) \cdot v_1, & D_3 &= -(k + p_3)^2, \\ D_2 &= -2k \cdot v_2, & D_4 &= -k^2. \end{aligned} \quad (4.89)$$

See figure 4.10. The integral family has five master integrals. In the one-loop case it is possible to find a basis, where all master integrals have uniform transcendental weight.

Such a basis is called UT or canonical basis. The master integrals  $\vec{g}$  of an UT basis fulfill a particular nice differential equation [199]

$$d\vec{g}(x, s_1, s_2) = \epsilon d\tilde{A}(x, s_1, s_2) \vec{g}(x, s_1, s_2), \quad (4.90)$$

where the  $\epsilon$  dependence is completely factorized and the matrix  $\tilde{A}$  is a linear combination of logarithms with coefficients given by rational matrices. The set of all different logarithm appearing in  $\tilde{A}$  is called alphabet of the differential equation. A possible choice of a UT basis is given by <sup>7</sup>

$$\begin{aligned} \tilde{g}_1 &= \frac{1}{2}\epsilon s_2 G_{0,1,2,0}, & \tilde{g}_2 &= -\frac{1}{2}\epsilon s_1 G_{1,0,0,2}, & \tilde{g}_3 &= \epsilon^2 \frac{1-x^2}{x} G_{1,1,0,1}, \\ \tilde{g}_4 &= \epsilon^2 \frac{1-x^2}{x} G_{1,1,1,0}, & \tilde{g}_5 &= -\frac{1}{4}\epsilon^2 s_1 s_2 G_{1,1,1,1}. \end{aligned} \quad (4.91)$$

The alphabet consists of seven letters  $\{1+x, x, 1-x, s_1, s_2, s_1x+s_2, s_2x+s_1\}$ . We remark that the last two letters appear as factors in the Gram determinant (4.87).

We solve the differential equation in the variable  $x$  for arbitrary  $s_1$  and  $s_2$  in an  $\epsilon$ -expansion  $\vec{g} = \sum_{k=1} \epsilon^k \vec{g}^{(k)}$  using iterated integrals. Then the integration constants are functions of  $s_1$  and  $s_2$ . It turns out that they are determined by the analytic properties of the integrals in certain limits of  $x$ , and in terms of the two (trivial) bubble integrals

$$\begin{aligned} \tilde{g}_1 &= -\frac{1}{2}e^{\epsilon\gamma_E}\Gamma(1+2\epsilon)\Gamma(1-\epsilon)(s_2)^{-2\epsilon}, \\ \tilde{g}_2 &= \frac{1}{2}e^{\epsilon\gamma_E}\Gamma(1+2\epsilon)\Gamma(1-\epsilon)(s_1)^{-2\epsilon}. \end{aligned} \quad (4.92)$$

In this way we get the full solution of the differential equation. The feature that boundary values can be obtained trivially from the differential equations and physical considerations appears to be rather general, and has been observed in many calculations, see e.g. [249].

In order to understand how to obtain the boundary values, we only need to consider two limits, as will be described presently. First we consider the limit of a straight Wilson line ( $v_1 = v_2$ ), where we have  $x = 1$ . Physically we do not expect any divergent behavior near  $x = 1$ , but the letter  $(1-x)$  can in principle give rise to logarithmic divergences. Such divergences can be extracted from the iterated integrals using the shuffle algebra they fulfill. The condition that there are no such divergences then yields a linear system of equations. The second limit is approached when all external vectors lie in the same plane. Then the Gram determinant (4.87) vanishes, hence one factor  $(s_1x+s_2)$  or  $(s_2x+s_1)$  must vanish. We expect the integrals to remain finite in this limit. Assuming  $s_2 > s_1 > 0$ , it is sufficient to consider the limit  $x \rightarrow -s_1/s_2$ . The calculation is then identical to the first limit, except that we leave the Euclidean region to analytically continue the iterated integrals. For this we extract the logarithms  $\log(x)$  from the iterated integrals using the shuffle algebra and use  $\log(-x+i0^+) = \log(x) + i\pi$ .

<sup>7</sup>We mark the one-loop master integrals with a tilde to distinguish them from the two-loop master integrals.



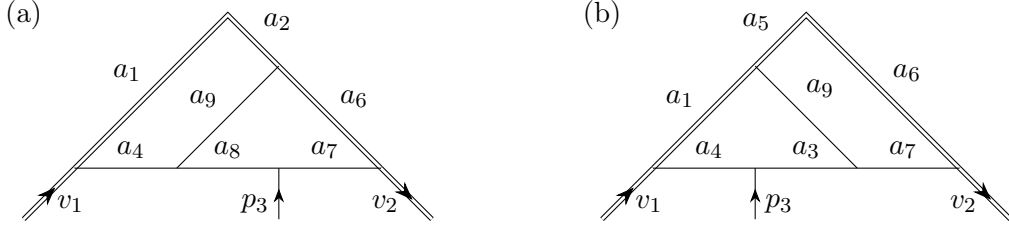


**Figure 4.11:** Two-loop soft current integral topologies.

We need the one-loop master integrals to order  $\mathcal{O}(\epsilon^3)$  for the two-loop renormalization. To this order all master integrals can be expressed in terms of HPLs with the arguments  $x$ ,  $s_1/s_2$ ,  $xs_1/s_2$  and  $xs_2/s_1$ .

### 4.9.2 Two-loop master integrals

We can express all planar Feynman diagrams needed in our calculation as subdiagrams of a single integral family. This is particularly straightforward to see when using dual coordinates. We define the integral family as

$$G_{a_1, \dots, a_9} = e^{2\epsilon \gamma_E} \int \frac{d^D k_1}{i\pi^{D/2}} \int \frac{d^D k_2}{i\pi^{D/2}} \prod_{k=1}^9 \frac{1}{D_k^{a_k}}, \quad (4.93)$$

where  $a_k \in \mathbb{Z}$  and the propagators are given by

$$\begin{aligned} D_1 &= -2k_1 \cdot v_1, & D_4 &= -k_1^2, & D_7 &= -k_2^2, \\ D_2 &= -2(k_1 - p_3) \cdot v_2, & D_5 &= -2(k_2 + p_3) \cdot v_1, & D_8 &= -(k_2 + p_3)^2, \\ D_3 &= -(k_1 - p_3)^2, & D_6 &= -2k_2 \cdot v_2, & D_9 &= -(k_1 - k_2 - p_3)^2. \end{aligned} \quad (4.94)$$

The subtopologies we need for the calculation of the master integrals appearing in the correlation functions are defined by  $G_{a_1, a_2, b_3, a_4, b_5, a_6, a_7, a_8, a_9}$  and  $G_{a_1, a_2, a_3, b_4, a_5, b_6, a_7, a_8, a_9}$ , where  $a_k$  is an arbitrary integer and  $b_k$  is zero or a positive integer. They are related to each other through interchanging  $v_2 \leftrightarrow -v_1$ . In figure 4.11 both subtopologies are shown. Note that in the Feynman diagrams more subtopologies appear, but after IBP reduction all master integrals can be mapped onto these two. For these subtopologies we have in total 47 master integrals.

As in the one-loop case, we derived differential equations for all of them. Fixing the boundary values is analogous to the one-loop case. In order to fix all boundary values we computed the following integrals

$$g_1 = \frac{1}{2} \epsilon^2 s_2 G_{0,0,0,2,0,1,0,0,2} = \frac{1}{2} e^{2\epsilon \gamma_E} \Gamma^2(1 - \epsilon) \Gamma(1 + 4\epsilon) (s_2)^{-4\epsilon}, \quad (4.95)$$

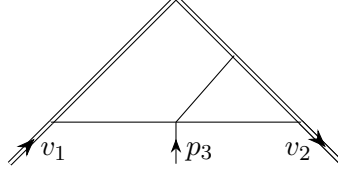


Figure 4.12: Elliptic sector

$$g_6 = \frac{1}{4} \epsilon^2 s_2^2 G_{0,1,0,2,0,1,0,2,0} = \frac{1}{4} e^{2\epsilon \gamma_E} \Gamma^2(1-\epsilon) \Gamma^2(1+2\epsilon) (s_2)^{-4\epsilon},$$

$$g_{16} = \frac{1}{2} \epsilon^3 s_2 G_{0,2,0,1,0,1,1,0,1} = \left[ -\frac{\pi^2 \epsilon^2}{48} + \frac{9\epsilon^3 \zeta_3}{8} + \mathcal{O}(\epsilon^4) \right] (s_2)^{-4\epsilon}.$$

and their symmetric counterparts with  $v_2 \rightarrow -v_1$ . The last integral was calculated with Mellin-Barnes techniques using the `Mathematica` package `MB.m` [295].

An interesting new feature of this calculation is that there is a sector of the differential equations that leads to elliptic polylogarithms. The relevant integral sector is shown in figure 4.12. The elliptic nature of the integral can be seen by considering the projection of the differential equations onto that sector, as we describe below. The latter contains two master integrals.

Our expectation was that the elliptic sector should be irrelevant for the computation of the divergent part of the correlation function (4.46). Given this expectation, we made a choice of master integrals that have good IR and UV properties, namely  $g_{38} = \epsilon^4 G_{1,1,0,1,0,1,1,0,1}$  and  $g_{39} = \epsilon^4 G_{1,1,-1,1,0,1,1,0,1}$ . Indeed, with this choice it turns out that the elliptic sector decouples from the integrals needed for our correlation function, to the order in  $\epsilon$  that was required. The remaining 37 master integrals with fewer propagators than the elliptic sector are in UT form (4.90), with the same alphabet as the one-loop master integrals. As in the one-loop case, up to the order in  $\epsilon$  that is needed for the renormalization of the correlation functions (4.45), all master integrals at two loops can be expressed in terms of HPLs.

For this reason a further analysis of the elliptic sector was not needed here. However, we do wish to make a few observations that may be of interest for future studies. The differential equation w.r.t.  $x$ , projected onto the elliptic sector, i.e. neglecting contribution from the lower sectors, is given by

$$\frac{\partial}{\partial x} \begin{pmatrix} g_{38} \\ g_{39} \end{pmatrix}_{\text{max cut}} = A_{\text{elliptic}} \begin{pmatrix} g_{38} \\ g_{39} \end{pmatrix}_{\text{max cut}}, \quad (4.96)$$

with

$$A_{\text{elliptic}} = \begin{pmatrix} \frac{(6\epsilon-1)s_1 s_2 (x-1)(x+1)}{4x(xs_1+s_2)(s_1+xs_2)} & \frac{-(6\epsilon-1)(x-1)(x+1)(s_2 x^2 + 2s_1 x + s_2)}{4x^2 s_2 (xs_1+s_2)(s_1+xs_2)} \\ \frac{(2\epsilon-1)s_1^2 s_2 (s_2 x^2 + 2s_1 x + s_2)}{4(x-1)(x+1)(xs_1+s_2)(s_1+xs_2)} & \frac{(2\epsilon-1)[8x(x^2+1)(s_1^2+s_2^2) + (7x^4+18x^2+7)s_2 s_1]}{4x(x-1)(x+1)(xs_1+s_2)(s_1+xs_2)} \end{pmatrix}. \quad (4.97)$$

Note that the matrix is affine in  $\epsilon$ . One could simplify it further, but this will not be discussed here. See ref. [200] and references therein for a general discussion.

In order to bring this differential equation into canonical form, one needs to solve the differential equation at  $\epsilon = 0$ . It is sufficient to find the solution for one of the two solutions, as the other one can be obtained via the coupled equations. Here we focus on the integral  $g_{38}$ . This integral is both UV and IR finite.

The desired solution at  $\epsilon = 0$  can be found from the maximal cut of the integral [234, 296], which is the natural generalization of the leading singularities [199] to the elliptic case. Using the Baikov representation [218] and a loop-by-loop approach for calculating the maximal cut [297, 298], we get the homogeneous solutions

$$\frac{1}{\sqrt{a_2}} K\left(\frac{a_1}{a_2}\right), \quad \frac{1}{\sqrt{a_2}} K\left(1 - \frac{a_1}{a_2}\right), \quad (4.98)$$

where  $K$  is the complete elliptic integral of the first kind and we have

$$a_{1/2} = \frac{s_2}{2} \left[ s_1 \left( x + \frac{1}{x} \right) + 2s_2 \mp 2\sqrt{\frac{1}{x} (s_1 x + s_2) (s_2 x + s_1)} \right]. \quad (4.99)$$



# Massless quark jet function

---

This chapter is published in [76] under the creative commons license CC-BY 4.0 (<http://creativecommons.org/licenses/by/4.0/>). We performed minor modifications to the text, the notation and the formatting.

### Abstract

We calculate the massless quark jet function to three-loop order. The quark jet function is a universal ingredient in SCET factorization for many collider and decay processes with quark initiated final state jets. Our three-loop result contributes to the resummation for observables probing the invariant mass of final state quark jets at  $N^3LL'$ . It represents the first complete three-loop result for a factorization ingredient describing collinear radiation. Furthermore it constitutes a major component of the  $N$ -jettiness subtraction/slicing method at  $N^3LO$ , which eventually may enable the calculation of fully-differential cross sections with a colorful final state at this order.

## 5.1 Introduction

In QCD processes involving highly energetic partons factorization plays a crucial role. Most importantly it provides a mean to disentangle perturbative physics from nonperturbative physics. Ideally the nonperturbative effects can thus be absorbed into universal (process-independent) functions as e.g. the parton distribution functions. More generally, whenever there is a strong hierarchy of scales one can hope to establish a factorization formula at leading order in the small scale ratio(s) that separates the physics happening at the different scales. Besides a considerable simplification this usually allows to resum large logarithms of the small scale ratio(s) to all orders in perturbation theory via RGEs

for the individual factorization ingredients. Such factorization formulae are conveniently derived in soft-collinear effective theory (SCET) [14–19].

In the following we will consider decay or scattering processes with final state jets and a large scale hierarchy between the jet invariant masses ( $\sim \tau$ ) and the total center of mass energy ( $\sim Q$ ). The cross section differential in a generic observable  $\tau$  that constrains the jet invariant mass then schematically takes the factorized form

$$\frac{d\sigma}{d\tau} = H(Q) \times [B_a \otimes B_b \otimes J_{i_1} \otimes \dots \otimes J_{i_N} \otimes S](\tau) \quad (5.1)$$

at leading order in  $\tau/Q$  and all orders in  $\alpha_s$ . The  $\otimes$  symbol denotes a convolution of the type

$$A(\tau) \otimes B(\tau) \equiv \int d\tau' A^i(\tau - \tau') B(\tau'). \quad (5.2)$$

For concreteness we assume here a process with two incoming ( $a, b$ ) and  $N$  outgoing partons involved in the hard interaction, which is described by the hard function  $H(Q)$ , as e.g. observed in proton-proton collisions at the LHC. For  $\tau \ll Q$  the initial state radiation is then collimated along the two incoming beam directions and the final state radiation is collimated along  $N$  different jet directions. Wide-angle soft emissions are taken into account by the soft function  $S(\tau)$ . The beam functions  $B_i(\tau)$  and the jet functions  $J_i(\tau)$  describe the effects of collinear radiation in the beam and final state jets, respectively. The functions  $S$ ,  $B_i$ , and  $J_i$  are universal in the sense that they are independent of the details of the hard process (e.g. the colorless final state). The collinear functions  $B_i$  and  $J_i$  are furthermore equal for any observable that in the collinear limit effectively reduces to a measurement of the jet invariant mass ( $\tau \rightarrow \sqrt{s}$ ). A prime example for such an observable obeying factorization<sup>1</sup> as in eq. (5.1) is the  $N$ -jettiness event shape [304] including the special cases beam thrust [305] (0-jettiness) and thrust [121] ( $\sim 2$ -jettiness in lepton collisions).

In this chapter we focus on the jet function  $J(s)$  for the case that the corresponding hard parton initiating the jet is a massless (anti-)quark. The SCET (quark) jet function was introduced in ref. [17]. It can be defined in terms of standard QCD fields as [140]

$$J(s) = \frac{1}{\pi N_c} \text{Im} \left[ \frac{i}{\bar{n} \cdot p} \int d^d x e^{-ip \cdot x} \langle 0 | T \text{Tr} \left[ \frac{\not{\bar{n}}}{4} W^\dagger(0) \psi(0) \bar{\psi}(x) W(x) \right] | 0 \rangle \right], \quad (5.3)$$

where  $T$  is the time-ordering operator,  $n^\mu$  is the lightlike jet direction ( $\bar{n} \cdot n = 2, n^2 = \bar{n}^2 = 0$ ),  $p^\mu$  is the jet momentum ( $s \equiv p^2$ ), the trace is over color ( $N_c = 3$ ) and spinor indices, and

$$W(x) = \text{P exp} \left[ i g \int_{-\infty}^0 ds \bar{n} \cdot A(x + s\bar{n}) \right] \quad (5.4)$$

---

<sup>1</sup>Neglecting potential factorization breaking effects due to Glauber modes [299–302] in hadron collisions, which are however absent up to three loops in fixed-order perturbation theory [303].

denotes a ( $n$ -collinear) Wilson line. This definition implies that we can use standard QCD Feynman rules in the calculation of the jet function as soft radiation has already been decoupled from the (leading order) collinear SCET Lagrangian by means of a field redefinition [17]. At one-loop the quark jet function was computed in refs. [138, 139] and the gluon jet function in ref. [135]. The two-loop results for the quark and gluon jet function were obtained in ref. [140] and ref. [136], respectively.

The two-loop quark jet function contributes to a number of important cross section predictions with resummation beyond NNLL accuracy, e.g. in DIS [124], for thrust [20, 21, 123], C-parameter [22, 125], and heavy jet mass [126]. To improve their precision to full N<sup>3</sup>LL' level <sup>2</sup> (in the peak region) the three-loop correction to the quark jet function is required. This is particularly desirable for the latter three observables as they are used for precise determinations of  $\alpha_s$  from  $e^+e^-$  data. Another good motivation to calculate  $J(s)$  at three loops is the perspective to extend the  $N$ -jettiness (infrared) subtraction/slicing method [303, 307], which has been applied successfully to several NNLO processes with final state jets [307–311], to N<sup>3</sup>LO.

## 5.2 Calculation

We work in general covariant gauge with gauge parameter  $\xi$ , where  $\xi = 0$  corresponds to Feynman gauge, and use dimensional regularization ( $d = 4 - 2\epsilon$ ). We generate the three-loop Feynman diagrams for  $J(s)$  with **qgraf** [177]. The output is then further processed using a custom code that does the color, Lorentz, and Dirac algebra. Our code also performs partial fractioning of products of the eikonal Wilson line propagators following the strategy outlined in ref. [188], and finally maps the resulting terms onto (scalar) integral topologies with twelve linearly independent propagators/numerators.

For the integrals in each topology we then perform an IBP reduction to master integrals with the public computer program **FIRE5** [180] in combination with **LiteRed** [186, 187]. Next, we identify master integrals that are related across the different topologies by shifts of the loop momenta. In this way we find 34 master integrals in five topologies. This set of master integrals however turns out to be redundant. Four extra (one-to-one) IBP relations among the master integrals are revealed by the following tricks:

The first is to search for identities between integrals based on their Feynman parameter representation using the algorithm of ref. [188], which is implemented in the **FindRules** command of **FIRE5**. In practice we apply **FindRules** to a large list of (test) integrals. The output are a number of equalities among these integrals, which must hold

---

<sup>2</sup>For thrust, C-parameter, and heavy jet mass at N<sup>3</sup>LL' also the respective soft function correction is currently missing. In the primed counting scheme the N<sup>x</sup>LO boundary terms of the functions in the factorization formula are included for N<sup>x</sup>LL' accuracy. For details and advantages of this scheme see, e.g., ref. [306].

after IBP reduction. In our case this required two more independent relations among the 34 master integral candidates.

Even more relations are found via dimensional recurrence [212, 217, 312]. Compact formulae that relate a generic  $d$ -dimensional integral to a linear combination of either  $(d+2)$ -dimensional or  $(d-2)$ -dimensional integrals with the same kind (but different powers) of propagators have been derived using Baikov's representation [218] of Feynman integrals in refs. [217, 312]. They are implemented in the **RaisingDDR** and **LoweringDDR** commands of **LiteRed**, respectively. By applying **RaisingDDR** we can thus directly express the 34  $d$ -dimensional master integral candidates as linear combinations of integrals in  $d+2$  dimensions. We then IBP reduce the output, and lower the dimension of the resulting integrals back to  $d$  using the **LoweringDDR** command. Comparing the result to the original integrals after another IBP reduction yields four equalities among the 34 master integrals, including the two relations found with the **FindRules** trick.

We have checked all four extra relations analytically to the required order in  $\epsilon$ . We are thus left with 30 master integrals, which have maximally eight quadratic and two linear (Wilson line) propagators. Expressing the full three-loop amplitude of the quark jet function in terms of these master integrals the dependence on the gauge parameter  $\xi$  manifestly vanishes as expected. This provides a first cross-check of our setup.

The next step is to compute the master integrals to high enough order in  $\epsilon$ . For this we adopt a strategy similar to the one described in refs. [219–221]. First, we note that the dependence of the master integrals on the two external scalar products  $s = p^2$  and  $\bar{n} \cdot p$  is completely fixed by scaling properties. From reparametrization invariance [313, 314] and dimensional counting in eq. (5.3) we even know that the full three-loop contribution equals  $[(-s - i0)^{-1-3\epsilon} \times \text{const.}]$  before taking the imaginary part. In order to determine the constant we can therefore safely set  $s = -1$  and  $\bar{n} \cdot p = 1$  in the evaluation of the master integrals for convenience.

We then switch to a new basis of master integrals that are quasi-finite [220] in some integer dimension, in our case  $d = 4$  or  $d = 6$ . By ‘quasi-finite’ we mean integrals that are either convergent or their divergence can be factored out in a simple way. We allow e.g. divergences ( $\propto 1/\epsilon^n$ ) contained in the prefactor of the corresponding Feynman parameter representation of the integral or generated as an overall prefactor by integrating over the Feynman parameters associated with the linear propagators. The latter integrations are always straightforward to carry out. We are thus left with up to eight convergent Feynman parameter integrals to be done.

A quasi-finite basis can be constructed as follows. The basic idea is to increase the dimension of a given IR divergent integral to  $d = n - 2\epsilon$  ( $n \in \mathbb{Z}$ ,  $n > 4$ ) in order to render it IR (quasi-)finite. For our master integrals  $n = 6$  turned out to be sufficient. One can then carefully increase the power of some propagators (by one) to decrease the degree of UV divergence without generating new IR singularities.<sup>3</sup> Once a quasi-finite integral

---

<sup>3</sup>Bubble-type subintegrals can of course be conveniently integrated out in  $d$  dimensions beforehand.



is found in this way it can be related to the original master integral plus integrals with less propagators in  $d = 4 - 2\epsilon$  dimensions by dimensional recurrence and another IBP reduction. In some (exceptional) cases the quasi-finite integral does not reduce to the original master integral and one has to try another quasi-finite candidate. An algorithm that for a given integral automatically determines a desired number of proper quasi-finite integrals in shifted spacetime dimensions is implemented in the public program **Reduze** [183].

To perform the remaining convergent Feynman parameter integrals of the quasi-finite master integrals we first expand the integrands to sufficiently high order in  $\epsilon$ . After that we integrate them using the **HyperInt** package [222]. This code automatically evaluates linearly reducible convergent (Feynman) integrals in terms of multiple polylogarithms. With the outlined procedure we were able to compute all 30 master integrals analytically to the required order in  $\epsilon$ . We have checked all master integral results numerically using the sector decomposition programs **FIESTA** [294] and **pySecDec** [315]. For many of the master integrals we also have obtained analytic results with the Mellin Barnes technique [316,317] employing the **MB** package [295,318] as well as the PSLQ algorithm [319]. We found perfect agreement in all cases.

To complete the calculation of the bare three-loop contribution to  $J(s)$  we have to take the imaginary part according to eq. (5.3) and consistently expand in  $\epsilon$ . To this end we use

$$\text{Im}\left[(-s - i0)^{-1-a\epsilon}\right] = -\sin(\pi a\epsilon) \theta(s) s^{-1-a\epsilon} \quad (5.5)$$

and

$$\mu^{2a\epsilon} \theta(s) s^{-1-a\epsilon} = -\frac{\delta(s)}{a\epsilon} + \sum_{n=0}^{\infty} \frac{(-a\epsilon)^n}{n!} \frac{1}{\mu^2} \mathcal{L}_n\left(\frac{s}{\mu^2}\right) \quad (5.6)$$

with the usual plus distributions defined as

$$\mathcal{L}_n(x) = \left[ \frac{\theta(x) \ln^n x}{x} \right]_+ = \lim_{\epsilon \rightarrow 0} \frac{d}{dx} \left[ \theta(x - \epsilon) \frac{\ln^{n+1} x}{n+1} \right]. \quad (5.7)$$

Convolutions among the  $\mathcal{L}_n(s)$  take the form

$$(\mathcal{L}_m \otimes \mathcal{L}_n)(s) = V_{-1}^{mn} \delta(s) + \sum_{k=0}^{m+n+1} V_k^{mn} \mathcal{L}_k(s). \quad (5.8)$$

A generic expression for  $V_k^{mn}$  is given in ref. [320].

### 5.3 Result

The bare and renormalized jet functions are related by

$$J^b(s) = Z_J(s, \mu) \otimes J(s, \mu). \quad (5.9)$$

Throughout this work we employ the  $\overline{\text{MS}}$  renormalization scheme. The RGE of the jet function reads

$$\frac{d}{d \log \mu} J(s, \mu) = \gamma_J(s, \mu) \otimes J(s, \mu), \quad (5.10)$$

with the anomalous dimension

$$\gamma_J(s, \mu) = -(Z_J)^{-1}(s, \mu) \otimes \frac{d}{d \log \mu} Z_J(s, \mu) \quad (5.11)$$

$$= -2K(\alpha_s) \frac{1}{\mu^2} \mathcal{L}_0\left(\frac{s}{\mu^2}\right) + \gamma_J(\alpha_s) \delta(s). \quad (5.12)$$

The collinear jet anomalous dimension  $\gamma_J(\alpha_s)$  is equal to the one of the (virtuality-dependent) beam function [321]. In the following we use the expansions

$$\begin{aligned} K(\alpha_s) &= \sum_{n \geq 1} \left(\frac{\alpha_s}{\pi}\right)^n K^{(n)}, & \gamma_J(\alpha_s) &= \sum_{n \geq 1} \left(\frac{\alpha_s}{\pi}\right)^n \gamma^{(n)}, \\ J(s, \mu) &= \sum_{n \geq 0} \left(\frac{\alpha_s(\mu)}{\pi}\right)^n J^{(n)}(s, \mu), & \beta(\alpha_s) &= - \sum_{k \geq 0} \left(\frac{\alpha_s}{4\pi}\right)^{k+1} \beta_k. \end{aligned} \quad (5.13)$$

The coefficients of the light-like cusp anomalous dimension  $K^{(n)}$  [25, 107] and the collinear jet anomalous dimension  $\gamma^{(n)}$  [124] for  $n = 1, 2, 3$  are e.g. listed in ref. [321]. For the light-like cusp anomalous dimension see also appendix 6.8. The jet function coefficients have the form

$$J_i^{(m)}(s, \mu) = J_{i,-1}^{(m)} \delta(s) + \sum_{n=0}^{2m-1} J_{i,n}^{(m)} \frac{1}{\mu^2} \mathcal{L}_n\left(\frac{s}{\mu^2}\right). \quad (5.14)$$

The coefficients of the  $\mu$ -dependent plus distributions in eq. (5.14) can be expressed in terms of lower-loop coefficients and anomalous dimensions by iteratively solving the RGE in eq. (5.10). Up to three loops we find<sup>4</sup>

$$\begin{aligned} J_0^{(1)} &= -\frac{\gamma^{(1)}}{2}, \\ J_1^{(1)} &= K^{(1)}, \\ J_0^{(2)} &= J_{-1}^{(1)} \left( -\frac{\beta_0}{16} - \frac{\gamma^{(1)}}{8} \right) + \frac{1}{12} \pi^2 \gamma^{(1)} K^{(1)} - \frac{\gamma^{(2)}}{2} + \left[ K^{(1)} \right]^2 \zeta_3, \end{aligned}$$

---

<sup>4</sup>The presence of zeta-values  $\zeta_n$  in the solution is due to the convolutions among the plus distributions.

$$\begin{aligned}
J_1^{(2)} &= \frac{1}{4} K^{(1)} J_{-1}^{(1)} + \frac{\beta_0 \gamma^{(1)}}{8} + \frac{[\gamma^{(1)}]^2}{4} - \frac{1}{6} \pi^2 [K^{(1)}]^2 + K^{(2)}, \\
J_2^{(2)} &= K^{(1)} \left( -\frac{\beta_0}{8} - \frac{3\gamma^{(1)}}{4} \right), \\
J_3^{(2)} &= \frac{[K^{(1)}]^2}{2}, \\
J_0^{(3)} &= J_{-1}^{(1)} \left( K^{(1)} \left( \frac{\pi^2 \beta_0}{96} + \frac{\pi^2 \gamma^{(1)}}{48} \right) - \frac{\beta_1}{64} - \frac{\gamma^{(2)}}{8} + \frac{1}{4} [K^{(1)}]^2 \zeta_3 \right) \\
&\quad + J_{-1}^{(2)} \left( -\frac{\beta_0}{32} - \frac{\gamma^{(1)}}{32} \right) + K^{(1)} \left( \frac{1}{8} \beta_0 \gamma^{(1)} \zeta_3 + \frac{1}{4} [\gamma^{(1)}]^2 \zeta_3 + \frac{\pi^2 \gamma^{(2)}}{12} + 2K^{(2)} \zeta_3 \right) \\
&\quad + [K^{(1)}]^2 \left( \frac{\pi^4 \beta_0}{360} + \frac{\pi^4 \gamma^{(1)}}{360} \right) + \frac{1}{12} \pi^2 \gamma^{(1)} K^{(2)} - \frac{\gamma^{(3)}}{2} + [K^{(1)}]^3 \left( 3\zeta_5 - \frac{\pi^2 \zeta_3}{3} \right), \\
J_1^{(3)} &= J_{-1}^{(1)} \left( \frac{3\beta_0 \gamma^{(1)}}{32} + \frac{\beta_0^2}{32} + \frac{[\gamma^{(1)}]^2}{16} - \frac{1}{24} \pi^2 [K^{(1)}]^2 + \frac{K^{(2)}}{4} \right) + \gamma^{(1)} \left( \frac{\beta_1}{32} + \frac{\gamma^{(2)}}{2} \right) \\
&\quad + \frac{1}{16} K^{(1)} J_{-1}^{(2)} + [K^{(1)}]^2 \left( -\frac{3}{4} \beta_0 \zeta_3 - 2\gamma^{(1)} \zeta_3 \right) + \frac{\beta_0 \gamma^{(2)}}{4} - \frac{1}{180} \pi^4 [K^{(1)}]^3 \\
&\quad + K^{(1)} \left( -\frac{1}{16} \pi^2 \beta_0 \gamma^{(1)} - \frac{1}{12} \pi^2 [\gamma^{(1)}]^2 - \frac{\pi^2 K^{(2)}}{3} \right) + K^{(3)}, \\
J_2^{(3)} &= K^{(1)} J_{-1}^{(1)} \left( -\frac{\beta_0}{8} - \frac{3\gamma^{(1)}}{16} \right) + [K^{(1)}]^2 \left( \frac{\pi^2 \beta_0}{16} + \frac{\pi^2 \gamma^{(1)}}{4} \right) + K^{(1)} \left( -\frac{\beta_1}{32} - \frac{3\gamma^{(2)}}{4} \right) \\
&\quad + K^{(2)} \left( -\frac{\beta_0}{4} - \frac{3\gamma^{(1)}}{4} \right) - \frac{3}{32} \beta_0 [\gamma^{(1)}]^2 - \frac{1}{32} \beta_0^2 \gamma^{(1)} - \frac{[\gamma^{(1)}]^3}{16} + \frac{5}{2} [K^{(1)}]^3 \zeta_3, \\
J_3^{(3)} &= \frac{1}{8} [K^{(1)}]^2 J(1, -1) + K^{(1)} \left( \frac{5\beta_0 \gamma^{(1)}}{24} + \frac{\beta_0^2}{48} + \frac{[\gamma^{(1)}]^2}{4} + K^{(2)} \right) - \frac{1}{6} \pi^2 [K^{(1)}]^3, \\
J_4^{(3)} &= [K^{(1)}]^2 \left( -\frac{5\beta_0}{48} - \frac{5\gamma^{(1)}}{16} \right), \\
J_5^{(3)} &= \frac{[K^{(1)}]^3}{8}. \tag{5.15}
\end{aligned}$$

where  $\beta_0 = \frac{11}{3} C_A - \frac{4}{3} T_F n_f$  and  $\beta_1 = \frac{34}{3} C_A^2 - (\frac{20}{3} C_A + 4C_F) T_F n_f$  with  $n_f$  the number of active flavors. Our result for the three-loop quark jet function perfectly reproduces eq. (5.15). This provides another strong cross-check and at the same time represents the first direct calculation of  $\gamma^{(3)}$ , which up to now has been inferred from RG consistency [124] using the three-loop results of refs. [107, 322]. For  $m = 1, 2, 3$  the constants  $J_{-1}^{(m)}$  are e.g. collected in ref. [303], albeit with a slightly different conventions. The new

result of our work is

$$\begin{aligned}
 J_{-1}^{(3)} = & C_F^3 \left( -\frac{25\zeta_3^2}{12} + \frac{11\pi^2\zeta_3}{96} + \frac{137\zeta_3}{32} - \frac{11\zeta_5}{8} - \frac{9871\pi^6}{544320} + \frac{311\pi^4}{1440} - \frac{3505\pi^2}{4608} + \frac{1173}{512} \right) \\
 & + C_A C_F^2 \left( \frac{53\zeta_3^2}{24} + \frac{275\pi^2\zeta_3}{216} - \frac{28241\zeta_3}{1728} + \frac{35\zeta_5}{36} + \frac{1547\pi^6}{311040} + \frac{18703\pi^4}{77760} \right. \\
 & \quad \left. - \frac{17585\pi^2}{4608} + \frac{206197}{20736} \right) \\
 & + C_A^2 C_F \left( \frac{191\zeta_3^2}{72} + \frac{197\pi^2\zeta_3}{288} - \frac{187951\zeta_3}{15552} - \frac{95\zeta_5}{144} + \frac{221\pi^6}{326592} + \frac{1009\pi^4}{103680} \right. \\
 & \quad \left. - \frac{464665\pi^2}{279936} + \frac{50602039}{3359232} \right) \\
 & + n_f T_F C_A C_F \left( -\frac{1}{9}\pi^2\zeta_3 + \frac{3707\zeta_3}{1296} + \frac{\zeta_5}{6} - \frac{209\pi^4}{12960} + \frac{17081\pi^2}{17496} - \frac{2942843}{419904} \right) \\
 & + n_f T_F C_F^2 \left( -\frac{17}{108}\pi^2\zeta_3 + \frac{701\zeta_3}{162} + \frac{5\zeta_5}{6} - \frac{1469\pi^4}{19440} + \frac{4853\pi^2}{3456} - \frac{261587}{31104} \right) \\
 & + (n_f T_F)^2 C_F \left( \frac{47\zeta_3}{486} + \frac{\pi^4}{360} - \frac{233\pi^2}{1944} + \frac{124903}{209952} \right). \tag{5.16}
 \end{aligned}$$

It is often convenient to work with the Laplace transform

$$\tilde{J}(\nu, \mu) = \int_0^\infty ds e^{-\nu s} J(s), \tag{5.17}$$

because the convolutions of eq. (5.2) type turn in to simple products in Laplace space. The Laplace space equivalents to our eqs. (5.14) and (5.15) can be read off from ref. [20]. The new three-loop constant related to eq. (5.16) in their notation is

$$\begin{aligned}
 c_3^J = & 25.06777873 C_F^3 + 32.81169125 C_A C_F^2 - 0.7795843561 C_A^2 C_F \\
 & - 31.65196210 C_A C_F n_f T_F - 61.78995095 C_F^2 n_f T_F + 28.49157341 C_F n_f^2 T_F^2, \tag{5.18}
 \end{aligned}$$

where for the sake of brevity we have evaluated the exact analytical result to ten valid digits for each color factor. The constant  $c_3^J$  equals the position space coefficient  $j_3$  affecting the  $\alpha_s$  determinations in refs. [21, 22, 123], where until now  $j_3 = 0 \pm 3000$  has been assumed. Evaluating eq. (5.18) for  $N_c = 3$ ,  $T_F = 1/2$  and  $n_f = 5$  we have  $j_3 = -128.6512525$ .

In ref. [323] the N<sup>3</sup>LO non-logarithmic constant of the (normalized) thrust cumulant cross section in the singular limit was obtained from a fit to fixed-order data produced by the Monte Carlo program EERAD3 [324], albeit with large numerical errors. With our new three-loop jet function constant in eq. (5.16) and the known three-loop hard function [21] at hand we can use this result to extract a rough estimate for the unknown thrust ( $q\bar{q}$

channel) soft function constant at three loops. In Laplace (position) space and adopting the notation of ref. [20] ( $c_3^S$ ) and ref. [21] ( $s_3$ ) we find ( $N_c = 3$ ,  $T_F = 1/2$ ,  $n_f = 5$ )

$$c_3^S = 2s_3 + 691 = -19988 \pm 1440 \text{ (stat.)} \pm 4000 \text{ (syst.)}. \quad (5.19)$$

## 5.4 Summary

In this chapter we have presented our calculation of the quark jet function  $J(s)$  at three loops. The main result is the three-loop contribution to the  $\delta(s)$  coefficient and given in eq. (5.16). All other terms at this order can be derived from RG consistency conditions in terms of previous results, see eq. (5.15). The new contribution is a necessary ingredient to many N<sup>3</sup>LL' resummed processes with final state jets. It has e.g. a direct impact on existing  $\alpha_s$  determinations from  $e^+e^-$  event shapes. Our calculation also represents the first step toward possible applications of the  $N$ -jettiness IR slicing (or subtraction) method at N<sup>3</sup>LO.



# Matter dependence of the four-loop QCD cusp anomalous dimension

---

This chapter is published in [77] under the creative commons license CC-BY 4.0 (<http://creativecommons.org/licenses/by/4.0/>). We performed minor modifications to the text, the notation and the formatting.

### Abstract

We compute the fermionic contributions to the cusp anomalous dimension in QCD at four loops as an expansion for small cusp angle. As a byproduct we also obtain the respective terms of the four-loop HQET wave function anomalous dimension. Our new results at small angles provide stringent tests of a recent conjecture for the exact angle dependence of the matter terms in the four-loop cusp anomalous dimension. We find that the conjecture does not hold for two of the seven fermionic color structures, but passes all tests for the remaining terms. This provides strong support for the validity of the corresponding conjectured expressions with full angle dependence. Taking the limit of large Minkowskian angle, we extract novel analytic results for certain terms of the light-like cusp anomalous dimension. They agree with the known numerical results. Finally, we study the anti-parallel lines limit of the cusp anomalous dimension. In a conformal theory, the latter is proportional to the static quark-antiquark potential. We use the new four-loop results to determine parts of the conformal anomaly term.

## 6.1 Introduction

The cusp anomalous dimension is a universal and ubiquitous quantity in QCD and the effective field theories describing its IR behavior as e.g. HQET and SCET. It governs

the IR singularity structure of QCD scattering amplitudes [27, 29–32]. In the presence of massive partons the IR divergences are controlled by the angle-dependent cusp anomalous dimension  $\Gamma_{\text{cusp}}(\phi, \alpha_s)$ . It can be determined from the UV divergences of a time-like Wilson loop with a cusp of (Euclidean) angle  $\phi$  [27]. The light-like cusp anomalous dimension  $K(\alpha_s)$  relevant for scattering of massless partons emerges as the  $\phi \rightarrow i\infty$  limit of  $\Gamma_{\text{cusp}}(\phi, \alpha_s)$  [27, 28]. It is the key ingredient to Sudakov resummation for scattering processes at high-energy colliders.

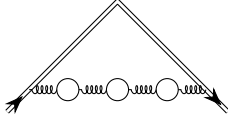
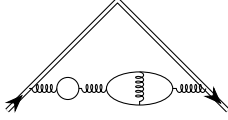
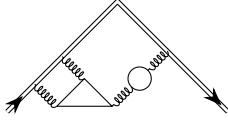
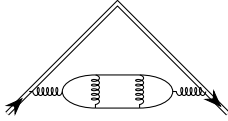
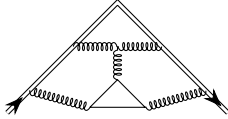
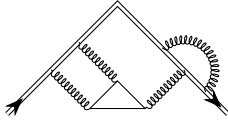
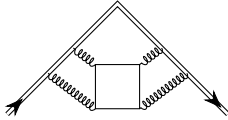
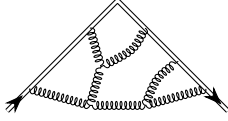
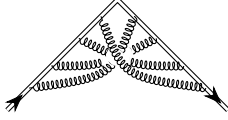
In addition to the light-like limit, there are two more interesting limits, the anti-parallel lines and the small angle limit. In the anti-parallel lines limit the cusp anomalous dimension is in one-to-one correspondence with the static quark-antiquark potential up to terms that are due to the conformal anomaly of (massless) QCD [41, 275, 339]. At small cusp angle the cusp anomalous dimension is given by a regular expansion  $\Gamma_{\text{cusp}}(\phi, \alpha_s) = -\phi^2 B(\alpha_s) + \mathcal{O}(\phi^4)$  in  $\phi^2$  and corresponds to the Bremsstrahlung function. The Bremsstrahlung function describes the radiation loss of a slowly moving heavy quark in an external gauge field. Furthermore, the cusp anomalous dimension determines the renormalization group (RG) running of the Isgur-Wise function, a universal function in HQET [9, 10]. At small cusp angles it is used for the extraction of the CKM matrix element  $V_{cb}$  from semileptonic  $B \rightarrow D^{(*)}$  decays, see e.g. [39].

The QCD cusp anomalous dimension  $\Gamma_{\text{cusp}}(\phi, \alpha_s)$  is known up to three loops [40, 41] in perturbation theory for arbitrary  $\phi$ . At four loops partial results are available and summarized in table 6.1. At four loops in  $\mathcal{N} = 4$  super Yang Mills (sYM) theory the light-like limit of the cusp anomalous dimension has been computed numerically [340, 341] and the full angle dependence is known analytically in the planar limit [273]. In addition, the Bremsstrahlung coefficient  $B(\alpha_s)$  is known exactly (to all loop orders, and including the full color dependence) in  $\mathcal{N} = 4$  sYM [275].

In [40, 41] it was observed that, up to three loops, the cusp anomalous dimension has a universal structure. Namely, expanding  $\Gamma_{\text{cusp}}(\phi)$  in  $K(\alpha_s)$  instead of  $\alpha_s$ , the coefficients of  $K^n(\alpha_s)$  are universal. In particular, they are equal in QCD, pure Yang-Mills, and  $\mathcal{N} = 4$  sYM. Based on their observation the authors of [40, 41] conjectured that this universality holds to all orders in perturbation theory. The conjecture allows to predict the fermionic contributions to  $\Gamma_{\text{cusp}}(\phi)$  in QCD at a given loop order (up to a normalization factor) using only lower loop results as an input. By ‘fermionic’ contributions we refer to terms that depend on  $n_f$ , the number of active fermion flavors.

A major goal of this chapter is to check the validity of these predictions at four loops. The idea is to predict the fermionic four-loop terms with full angle dependence and verify the conjectured expressions against analytic results for  $\Gamma_{\text{cusp}}(\phi)$  calculated in the small angle expansion. This analysis was initiated in [335] by investigating the  $n_f$  term proportional to the quartic Casimir color factor. It was found that the conjecture does not hold for that particular color structure. This may be connected to the special nature of the quartic Casimir contributions, which appear at four loops for the first time



color structure	sample diagram	$\Gamma_{\text{cusp}}(\phi)$	$\phi \ll 1$	light-like	$\gamma_h$
$(T_F n_f)^3 C_R$		[115]	[115]	[325, 326]	[327]
$(T_F n_f)^2 C_R C_F$		[41, 328]	[41, 328]	[41, 328, 329]	[41, 328]
$(T_F n_f)^2 C_R C_A$		[ $\times$ ]	[ $\times$ ]	[329–331]	[332] [ $\times$ ]
$(T_F n_f) C_R C_F^2$		[333]	[333]	[333]	[333]
$(T_F n_f) C_R C_F C_A$		[ $\times$ ]	[ $\times$ ]	[334]* [ $\times$ ]	[332]* [ $\times$ ]
$(T_F n_f) C_R C_A^2$			[ $\times$ ]	[334]* [ $\times$ ]	[332]* [ $\times$ ]
$n_f \frac{d_R d_F}{N_R}$			[335] [ $\times$ ]	[334, 336]* [241, 337]	[335]
$n_f^1, N_c \rightarrow \infty$			[ $\times$ ]	[330, 334]	[ $\times$ ]
$C_R C_A^3$				[334, 336]*	[332]*
$\frac{d_R d_A}{N_R}$				[334, 336]*	[332]*
$n_f^0, N_c \rightarrow \infty$				[334, 338]	

**Table 6.1:** Four-loop contributions to  $\Gamma_{\text{cusp}}(\phi)$  and its limits in QCD as well as the HQET field anomalous dimension  $\gamma_h$ . The \* marks numerical results. The results [ $\times$ ] are obtained in this work.

in the perturbative expansion and are the reason for Casimir scaling violation. It is therefore interesting to ask whether the conjecture possibly holds for the other four-loop color structures. For the terms proportional to  $(n_f T_F)^3 C_R$ ,  $(n_f T_F)^2 C_R C_F$  and  $(n_f T_F) C_R C_F^2$ , in the following called ‘Abelian’ color structures (as they are independent of  $C_A$ ), a quick answer can be given: these contributions are known with full angle dependence, cf. table 6.1, and exactly comply with the conjecture.

This encouraged us to extend the analysis also to the other four-loop  $n_f$  contributions, where no explicit all-angle result is available to date. In this chapter we therefore compute the corresponding terms up to  $\mathcal{O}(\phi^4)$  and partly  $\mathcal{O}(\phi^6)$  in the small angle expansion and use them to test the conjecture. From the  $\mathcal{O}(\phi^0)$  term of our Wilson loop calculation we obtain analytical expressions for the four-loop heavy quark field anomalous dimension in HQET. Our approach closely follows the lines of [335]. In addition, we study the anti-parallel lines limit of the cusp anomalous dimension. Given our findings regarding the validity of the conjecture at four loops we derive new terms in its relation to the static quark-antiquark potential.

The remainder of this chapter is organized as follows. In section 6.2 we present the setup and in section 6.3 details of our calculation. Section 6.4 contains our four-loop results for the small angle expansion of the cusp anomalous dimension as well as the HQET field anomalous dimension. In section 6.5 we review the conjecture of [40, 41], test it against our results for the small angle expansion and discuss the outcome. Section 6.6 elaborates on the consequences for the relation between the cusp anomalous dimension and the static potential. We conclude in section 6.7. In appendix 6.8 we collect all conjectured expressions for the four-loop cusp anomalous dimension with full angle dependence.

## 6.2 Definitions and ultraviolet properties of Wilson line operators

We start with the definition of the cusp anomalous dimension in QCD. To this end we consider a closed Wilson loop with a time-like integration contour  $C$

$$W = \frac{1}{N_R} \text{Tr}_R \langle 0 | T P \exp \left( i g_{\text{YM}} \int_C dx^\mu A_\mu(x) \right) | 0 \rangle = 1 + \mathcal{O}(g^2) . \quad (6.1)$$

Here  $A_\mu = A_\mu^a T_R^a$  is the gluon field,  $T$  and  $P$  are the time- and path-ordering operators, the trace is over (color) indices in the representation  $R$  of the gauge group  $SU(N_c)$  and  $\alpha_s = g^2/(4\pi)$ . A cusp in the integration contour gives rise to UV divergences, which are renormalized multiplicatively [24, 25]. The associated anomalous dimension depends on the cusp angle  $\phi$  and is correspondingly called cusp anomalous dimension  $\Gamma_{\text{cusp}}(\phi, \alpha_s)$ . To compute it we conveniently consider a contour consisting of two straight line segments

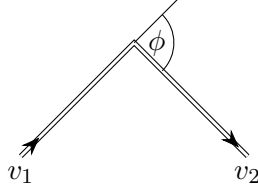


**Figure 6.1:** Wilson line with two straight line segments forming a cusp with Euclidean cusp angle  $\phi$ .

along directions  $v_1^\mu$  and  $v_2^\mu$  ( $v_1^2 = v_2^2 = 1$ ), which form a cusp in the origin and extend to infinity where the contour is closed, see figure 6.1. The Euclidean cusp angle is defined by  $\cos \phi = v_1 \cdot v_2$ . In Minkowskian spacetime and for real  $v_1$  and  $v_2$  the Euclidean cusp angle is purely imaginary leading to the definition of the Minkowskian cusp angle  $\cosh \varphi = v_1 \cdot v_2$ , such that  $\phi = i\varphi$ . The full angle-dependent cusp anomalous dimension was computed up to three loops in [23, 25, 40, 41, 264] and we use the same setup as in [41] to calculate it in the small angle expansion at four loops.

The cusp anomalous dimension appears also in the context of HQET, see e. g. [39, 114, 115]. In the HQET picture the Wilson line configuration depicted above corresponds to a heavy quark moving with four-velocity  $v_1^\mu$ , then scattering at an external (electromagnetic) source to instantaneously change its velocity to  $v_2^\mu$ . This allows us to compute the cusp anomalous dimension using HQET momentum space Feynman rules for the heavy quark propagator and the heavy-quark–gluon vertex

$$\begin{aligned} \text{Heavy quark propagator: } \frac{v}{\overline{p}} &= \frac{i}{v \cdot p + \delta}, & \text{Heavy quark-gluon vertex: } \text{double line with wavy line} &= ig_{\text{YM}} v^\mu T_R^a. \end{aligned} \quad (6.2)$$

The double line represents a heavy quark (or Wilson) line with  $v^2 = 1$  in the  $SU(N_c)$  representation  $R$ . We take the heavy quark to be slightly off-shell  $\delta \neq 0$  in order to regulate IR divergences in eq. (6.1), since we are only interested in the UV divergences arising from loops involving the cusp. The off-shellness  $\delta$  can be interpreted as the residual energy of the heavy quark. Without loss of generality we choose  $\delta = -1/2$  in our calculation.

We distinguish two types of Feynman diagrams contributing to the Wilson loop in eq. (6.1). The first are HQET self-energy diagrams, which are  $\phi$ -independent. The second are (one-particle-irreducible) vertex corrections depending on the cusp angle. The sum of the former is related to the sum of the latter at zero cusp angle by a HQET Ward identity. Denoting the sum of the vertex diagrams as  $V(\phi)$ , we thus have [25]

$$\log W = \log V(\phi) - \log V(0) + \mathcal{O}(\epsilon^0) = \log Z_{\text{cusp}} + \mathcal{O}(\epsilon^0), \quad (6.3)$$

where we have introduced the  $\overline{\text{MS}}$  cusp renormalization constant  $Z_{\text{cusp}}$ . Here we use

dimensional regularization with  $d = 4 - 2\epsilon$  and we expand as

$$\Gamma_{\text{cusp}}(\phi, \alpha_s) = \sum_{k \geq 1} \left( \frac{\alpha_s}{\pi} \right)^k \Gamma_{\text{cusp}}^{(k)}(\phi). \quad (6.4)$$

The cusp anomalous dimension is defined by the RGE

$$\Gamma_{\text{cusp}}(\phi, \alpha_s) = \frac{d \log Z_{\text{cusp}}}{d \log \mu}, \quad (6.5)$$

where  $\mu$  is the renormalization scale. Iteratively solving this equation yields

$$\begin{aligned} \log Z_{\text{cusp}} = & -\frac{\alpha_s}{\pi} \frac{\Gamma_{\text{cusp}}^{(1)}}{2\epsilon} + \left( \frac{\alpha_s}{\pi} \right)^2 \left[ \frac{\beta_0 \Gamma_{\text{cusp}}^{(1)}}{16\epsilon^2} - \frac{\Gamma_{\text{cusp}}^{(2)}}{4\epsilon} \right] \\ & + \left( \frac{\alpha_s}{\pi} \right)^3 \left[ -\frac{\beta_0^2 \Gamma_{\text{cusp}}^{(1)}}{96\epsilon^3} + \frac{\beta_1 \Gamma_{\text{cusp}}^{(1)} + 4\beta_0 \Gamma_{\text{cusp}}^{(2)}}{96\epsilon^2} - \frac{\Gamma_{\text{cusp}}^{(3)}}{6\epsilon} \right] \\ & + \left( \frac{\alpha_s}{\pi} \right)^4 \left[ +\frac{\beta_0^3 \Gamma_{\text{cusp}}^{(1)}}{512\epsilon^4} - \frac{\beta_0 (\beta_1 \Gamma_{\text{cusp}}^{(1)} + 2\beta_0 \Gamma_{\text{cusp}}^{(2)})}{256\epsilon^3} \right. \\ & \left. + \frac{\beta_2 \Gamma_{\text{cusp}}^{(1)} + 4\beta_1 \Gamma_{\text{cusp}}^{(2)} + 16\beta_0 \Gamma_{\text{cusp}}^{(3)}}{512\epsilon^2} - \frac{\Gamma_{\text{cusp}}^{(4)}}{8\epsilon} \right] + \mathcal{O}(\alpha_s^5). \end{aligned} \quad (6.6)$$

From this expression we see that, at a given order in perturbation theory, the poles higher than  $1/\epsilon$  are determined by lower order results of the cusp anomalous dimension and the  $\beta$ -function of QCD. The only new information at each loop enters through the  $1/\epsilon$  term. For the  $\beta$ -function we use

$$\frac{d \log \alpha_s}{d \log \mu} = -2\epsilon + 2\beta(\alpha_s), \quad \beta(\alpha_s) = -\sum_{k \geq 0} \left( \frac{\alpha_s}{4\pi} \right)^{k+1} \beta_k, \quad (6.7)$$

with  $\beta_0 = \frac{11}{3} C_A - \frac{4}{3} T_F n_f$ . The relevant higher order coefficients can e.g. be found in [97, 342]. The parameter  $n_f$  denotes the number of active fermion flavors.

So far we considered the angle-dependent cusp anomalous dimension  $\Gamma_{\text{cusp}}(\phi, \alpha_s)$ , originating from the UV divergences of a cusped Wilson loop with a time-like integration contour. For a light-like integration contour the corresponding light-like cusp anomalous dimension is denoted by  $K(\alpha_s)$ . The light-like limit is reached for  $\phi \rightarrow i\infty$  or equivalently for  $\varphi \rightarrow \infty$  and we have [27, 28]

$$\Gamma_{\text{cusp}}(\phi, \alpha_s) = -i\phi K(\alpha_s) \quad \text{for } \phi \rightarrow i\infty. \quad (6.8)$$

As mentioned in the introduction the cusp anomalous dimension and especially its light-like limit are universal and appear in many physical quantities. The recent four-loop results of  $K(\alpha_s)$  are for instance obtained from the computation of the quark (and a

### 6.3 Four-loop calculation of matter-dependent terms at small angle

scalar) form factor [241, 330, 337, 338] and splitting functions [329, 331, 334, 336]. In the form factor the light-like cusp anomalous dimension appears in the  $1/\epsilon^2$  IR divergences [27, 29–32]. The splitting functions  $P_{ij}(x)$  govern the evolution of the parton distribution functions [343–345]. In this context the light-like cusp anomalous dimension is relevant for the threshold limit  $x \rightarrow 1$  [346].

Finally we briefly discuss the heavy quark field renormalization in HQET. The corresponding  $\overline{\text{MS}}$  renormalization constant  $Z_h$  can be obtained from the derivative of the HQET self energy  $\Sigma_h(\delta)$  w.r.t. the residual energy  $\delta$  of the heavy quark using

$$\log \left( 1 - \frac{d\Sigma_h}{d\delta} \right) = -\log Z_h + \mathcal{O}(\epsilon^0). \quad (6.9)$$

Note that the  $L$ -loop term of  $\Sigma_h(\delta)$  is proportional to  $\delta^{1-2L\epsilon}$  according to dimensional analysis. Using the HQET Ward identity

$$V(0) = 1 - \frac{d\Sigma_h}{d\delta}, \quad (6.10)$$

we can relate the renormalization constant to the vertex function at zero cusp angle

$$\log V(0) = -\log Z_h + \mathcal{O}(\epsilon^0). \quad (6.11)$$

This quantity is not gauge invariant (and not observable). The corresponding HQET heavy quark field anomalous dimension therefore also depends not only on the strong coupling  $\alpha_s$ , but also on the gauge. Choosing generalized covariant gauge a dependence on the gauge parameter  $\xi$  remains:

$$\gamma_h(\alpha_s, \xi) = \frac{d \log Z_h}{d \log \mu}. \quad (6.12)$$

This RGE can be solved analogously to eq. (6.6) in a perturbative fashion. This time, however, we have to take the dependence on the gauge parameter  $\xi(\mu)$  into account, which itself is renormalization scale dependent. The relevant terms of the corresponding anomalous dimension can e.g. be found in [97].

## 6.3 Four-loop calculation of matter-dependent terms at small angle

In this section we describe the computation of the cusp anomalous dimension at four loops in the small angle expansion. We begin with the discussion of the color structures. Then we describe the general computational workflow, including the calculation of the Feynman diagrams, partial fraction decomposition, IBP reduction and the computation of the master integrals. Here we follow in the most parts [335]. Finally we point out a subtlety in the renormalization procedure of the off-shell and therefore gauge-dependent Wilson loop in order to obtain eq. (6.6).

### 6.3.1 Color dependence of $\Gamma_{\text{cusp}}$ to four loops

The structure of the QCD cusp anomalous dimension in terms of color factors is determined by non-Abelian exponentiation [347–349]. Up to three loops we have

$$\begin{aligned} \Gamma_{\text{cusp}} = & \frac{\alpha_s}{\pi} C_R \Gamma_{\text{cusp}}^R + \left( \frac{\alpha_s}{\pi} \right)^2 C_R \left[ \Gamma_{\text{cusp}}^{RA} + n_f T_F \Gamma_{\text{cusp}}^{fR} \right] + \left( \frac{\alpha_s}{\pi} \right)^3 C_R \left[ C_A^2 \Gamma_{\text{cusp}}^{RAA} \right. \\ & \left. + (n_f T_F)^2 \Gamma_{\text{cusp}}^{ffR} + n_f T_F \left( C_F \Gamma_{\text{cusp}}^{fRF} + C_A \Gamma_{\text{cusp}}^{fRA} \right) \right] + \mathcal{O}(\alpha_s^4). \end{aligned} \quad (6.13)$$

The quadratic Casimir operators  $C_R$ ,  $C_A$ ,  $C_F$  are defined according to  $T_R^a T_R^a = C_R \mathbb{1}_R$ , where  $T_R^a$  is the generator of the  $SU(N_c)$  representation  $R$  with  $\text{Tr}[T_R^a T_R^b] = T_R \delta^{ab}$  and  $\text{Tr}[\mathbb{1}_R] = N_R$ . In QCD the two relevant representations are the adjoint ( $R = A$ ) and the fundamental representation ( $R = F$ ) with  $T_F = 1/2$ . Up to three loops the cusp anomalous dimension obeys Casimir scaling, i.e. it depends linearly on  $C_R$ , where  $R$  is the representation of the Wilson loop. Starting at four loops, however, Casimir scaling is violated by terms proportional to quartic Casimir operators. There are two types of such color factors at this order, which we denote by  $d_R d_A / N_R$  and  $n_f d_R d_F / N_R$ . Like the color factor  $C_R C_A^3$  the former belongs to the purely gluonic part of the cusp anomalous dimension. The quartic Casimir operators are defined by symmetrized traces<sup>1</sup> of four generators [82]

$$\frac{d_R d_{R'}}{N_R} \equiv \frac{d_R^{abcd} d_{R'}^{abcd}}{N_R}, \quad d_R^{abcd} = \text{STr} \left[ T_R^a T_R^b T_R^c T_R^d \right]. \quad (6.14)$$

At four loops  $\Gamma_{\text{cusp}}$  then takes the form

$$\begin{aligned} \Gamma_{\text{cusp}}^{(4)} = & C_R C_A^3 \Gamma_{\text{cusp}}^{RAAA} + \frac{d_R d_A}{N_R} \Gamma_{\text{cusp}}^{dRA} \\ & + (n_f T_F)^3 C_R \Gamma_{\text{cusp}}^{fffr} + (n_f T_F)^2 \left( C_R C_F \Gamma_{\text{cusp}}^{fRF} + C_R C_A \Gamma_{\text{cusp}}^{fRA} \right) \\ & + n_f T_F \left( C_R C_F^2 \Gamma_{\text{cusp}}^{fRFF} + C_R C_F C_A \Gamma_{\text{cusp}}^{fRFA} + C_R C_A^2 \Gamma_{\text{cusp}}^{fRAA} \right) + n_f \frac{d_R d_F}{N_R} \Gamma_{\text{cusp}}^{fdRF}. \end{aligned} \quad (6.15)$$

In table 6.1 we show for each of the four-loop color structures an example of a contributing Feynman diagram. We will employ the analogous notation regarding the coefficients of the different color factors in eqs. (6.13) and (6.15) also for the light-like cusp anomalous dimension  $K$  and the HQET field anomalous dimension  $\gamma_h$ .

The fermionic quartic Casimir operator  $n_f d_R d_F / N_R$  only appears in 18 Feynman diagrams at four loops. Those are the diagrams with a fermion box subdiagram, where the four gluons are directly attached to the Wilson lines as shown in the (planar) sample diagram in table 6.1. The gluonic quartic Casimir operator does not only appear in the

<sup>1</sup> The symmetrized trace is defined by  $\text{STr}[T^{a_1} \dots T^{a_n}] = \frac{1}{n!} \sum_{\sigma \in S_n} \text{Tr}[T^{a_{\sigma(1)}} \dots T^{a_{\sigma(n)}}]$ , where the sum runs over all permutations of indices.

corresponding diagrams with a gluon or ghost box, but for instance also in diagrams like the example diagram for  $d_R d_A / N_R$  shown in table 6.1. That diagram has the color factor

$$\begin{aligned} \frac{1}{N_R} \text{Tr} \left[ T_R^a T_R^b T_R^c T_R^d T_R^a T_R^b T_R^c T_R^d \right] &= \frac{1}{N_R} \text{Tr} \left[ T_R^a T_R^b T_R^c T_R^d \right] \text{Tr} \left[ T_A^a T_A^b T_A^c T_A^d \right] + \dots \quad (6.16) \\ &= \frac{d_R d_A}{N_R} + \dots, \end{aligned}$$

where the ellipses denote terms involving only quadratic Casimir operators and in the second step we repeatedly used the Lie algebra  $[T_R^a, T_R^b] = i f^{abc} T_R^c$  and  $(T_A^b)_{ac} = i f^{abc}$ . In a similar way also diagrams with three gluon vertices give rise to  $d_R d_A / N_R$  terms. This illustrates that the gluonic quartic Casimir operator appears in a much larger set of Feynman diagrams than  $n_f d_R d_F / N_R$ .

### 6.3.2 Calculation of Feynman diagrams

Next we outline our calculation of the four-loop cusp anomalous dimension expanded in small cusp angle  $\phi$ . More details on the calculation, especially on the analytic evaluation of the master integrals, can be found in [335], where the quartic Casimir  $n_f d_R d_F / N_R$  contribution was studied. Since we are dealing with many more Feynman diagrams than [335], we automatize the calculation to a higher degree. The Feynman diagrams are generated with **qgraf** [177], then mapped to integral topologies and after this the color, Dirac and Lorentz algebra is performed using a dedicated **Mathematica** code.

The integrals appearing in the Feynman diagrams are regular at  $\phi = 0$ . To obtain their small angle expansion we can therefore simply expand their integrand in a Taylor series. In this way we get a power series in  $\phi$ , where the coefficients are given by linear combinations of tensor integrals. We perform a tensor reduction to relate the tensor integrals to scalar integrals. After that only even powers of  $\phi$  survive upon integration, since the original integrals before expansion are functions of  $\cos \phi$ . We end up with expressions for each diagram in terms of scalar four-loop integrals of (Wilson line) propagator-type.

Depending on the Feynman diagram, it may contain integrals with linearly dependent HQET-type propagators. For example the sample diagrams for the color structures  $d_R d_A / N_R$  and  $n_f T_F C_R C_A^2$  in table 6.1 give rise to such integrals in the small angle expansion. In order to prepare them for straightforward integration-by-part (IBP) reduction, we remove the linear dependences between propagators beforehand. This is achieved by applying the multivariate partial fraction decomposition algorithm outlined in [188]. With the help of a Gröbner basis, the algorithm constructs for a given integral topology with linearly dependent propagators a set of replacement rules. For any integral belonging to that topology we then obtain an appropriate partial fraction decomposition by simply applying these rules recursively. The use of a Gröbner basis ensures that the recursion terminates. The result is a sum of integrands with linearly independent propagators.

### 6.3.3 Integral topologies and master integrals

For the IBP reduction we use **FIRE5** [180] in combination with **LiteRed** [186, 187]. After the IBP reduction we are left with 46 master integrals, belonging to five integral topologies shown in figure 6.2. The integral families associated with the first three topologies reduce to 43 master integrals, which are already known [335]. We refer the interested reader to the latter reference for the definition of these topologies. The remaining three master integrals are new and belong to the topologies 4 and 5. One of these three master integrals is a particular case of an integral calculated in [350, 351].

Conveniently we introduce one large set of propagators  $\{D_k\}$  to represent the integrals of both two new topologies 4 and 5 and then restrict the exponents of the propagators accordingly. We define

$$G(a_1, \dots, a_{16}) = e^{4\epsilon\gamma_E} \int \frac{d^d k_1}{i\pi^{d/2}} \int \frac{d^d k_2}{i\pi^{d/2}} \int \frac{d^d k_3}{i\pi^{d/2}} \int \frac{d^d k_4}{i\pi^{d/2}} \prod_{k=1}^{16} D_k^{-a_k}, \quad (6.17)$$

with the denominators

$$\begin{aligned} D_1 &= -2v \cdot k_1 + 1, & D_2 &= -2v \cdot k_2 + 1, & D_3 &= -2v \cdot k_3 + 1, & (6.18) \\ D_4 &= -2v \cdot k_4 + 1, & D_5 &= -k_1^2, & D_6 &= -k_2^2, \\ D_7 &= -k_3^2, & D_8 &= -k_4^2, & D_9 &= -(k_1 - k_2)^2, \\ D_{10} &= -(k_1 - k_3)^2, & D_{11} &= -(k_1 - k_4)^2, & D_{12} &= -(k_2 - k_3)^2, \\ D_{13} &= -(k_2 - k_4)^2, & D_{14} &= -(k_3 - k_4)^2, & D_{15} &= -2v \cdot (k_1 - k_2) + 1, \\ D_{16} &= -2v \cdot (k_1 - k_3) + 1, \end{aligned}$$

and  $v^2 = 1$ . Note that an integral at four loops with our kinematics can have at most 14 linear independent propagators. The restrictions on the (integer) exponents for the two topologies are given by

$$\text{topology 4: } a_{15}, a_{16} = 0 \text{ and } a_{10}, a_{11}, a_{12} \geq 0, \quad (6.19)$$

$$\text{topology 5: } a_1, a_3 = 0 \text{ and } a_4, a_5, a_{10}, a_{11} \geq 0. \quad (6.20)$$

The exponents that are not listed are not restricted.

To compute the three new master integrals we proceed exactly as in [335]. Let us briefly summarize the method here. By raising the power of the (IR-regulated) Wilson line propagators we choose a basis of integrals that are finite up to a factorizable overall UV divergence (and trivial divergent factors from bubble-type subdiagrams that we integrate out). To factor out the overall divergence we conveniently work in position space. Using Feynman parameters we are then left with finite parameter integrals, which we expand to the required order in  $\epsilon$ . The individual terms in the  $\epsilon$  expansion are evaluated with the **HyperInt** package [222]. We checked our analytic results for the master integrals numerically with **FIESTA4** [294]. The analytic results for the master integrals are presented in the appendix 6.9.



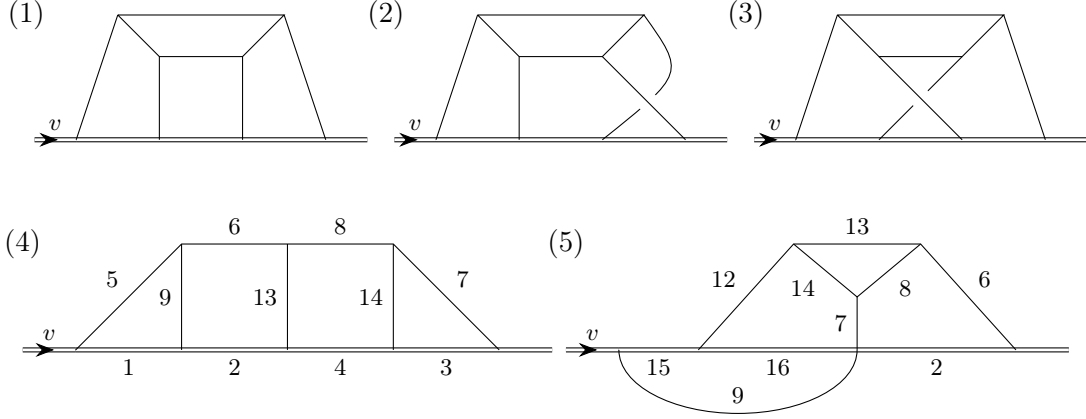


**Figure 6.2:** Integral topologies of the master integrals of all  $n_f$  dependent color structures of the cusp anomalous dimension in the small angle expansion.

### 6.3.4 Renormalization

Putting all pieces together we get the bare expression for the one-particle-irreducible vertex function  $V(\phi)$  and from eq. (6.3) the bare expression of  $\log W$  up to  $\mathcal{O}(\alpha_s^4)$ . In order to extract  $\Gamma_{\text{cusp}}^{(4)}$  using eq. (6.6) we first need to express the bare  $\log W$  in terms of renormalized quantities. All present  $1/\epsilon^n$  divergences are of UV origin, because we introduced an off-shellness  $\delta = -1/2$  in the HQET propagator to regulate the IR divergences. This IR regulator breaks gauge invariance, which becomes evident when computing the off-shell Wilson loop in covariant gauge, i.e. using the gluon propagator

$$\frac{\text{gluon propagator}}{p} = \frac{-i}{p^2 + i0^+} \left( g^{\mu\nu} + \xi \frac{p^\mu p^\nu}{p^2 + i0^+} \right). \quad (6.21)$$

In fact, not only the finite part, but also some divergent terms of  $\log W$  depend on  $\xi$ . The latter are related to the interplay of finite and divergent pieces of lower-loop subdiagrams. Therefore it is crucial to renormalize the gauge parameter  $\xi$ . We emphasize that the corresponding renormalization of the gauge fixing part of the Lagrangian is necessary even when using Feynman gauge ( $\xi = 0$ ) from the start. In our convention the gauge parameter renormalizes according to  $1 - \xi^b = Z_3(1 - \xi(\mu))$ , where  $Z_3$  is the renormalization factor of the gauge field  $A_\mu^b = \sqrt{Z_3} A_\mu^r$ . The required renormalization constants are e.g. given in [97]. After expressing  $\alpha_s^b$  and  $\xi^b$  through the respective renormalized quantities the only divergences left in  $\log W$  are those associated with the Wilson loop cusp and match eq. (6.6). As the cusp anomalous dimension is of UV origin and thus insensitive to the off-shellness, it is gauge invariant. Hence,  $Z_{\text{cusp}}$  must be  $\xi$  independent. This serves as a strong check of our calculation. Note that the finite part of  $\log W$  does depend on the gauge parameter as well as on the off-shellness. The determination of the HQET field anomalous dimension  $\gamma_h$  from  $V(0)$  follows the same lines. Unlike for  $\Gamma_{\text{cusp}}$  in this case, however, a dependence on  $\xi$  persists.

### 6.3.5 Checks of the calculation

We performed several checks of our calculation. Using our computational setup we reproduce the known lower loop results of  $\Gamma_{\text{cusp}}(\phi, \alpha_s)$  [25, 41] and  $\gamma_h(\alpha_s)$  [118–120]. In the case of  $\gamma_h(\alpha_s)$  our findings at four loops are in agreement with the known analytical and numerical results [332]. Regarding the cusp anomalous dimension, our result for the  $n_f C_R C_F^2$  term agrees with [333]. Furthermore, RG consistency and gauge invariance provide stringent tests. Due to the RGE, the higher  $1/\epsilon^n$  poles of  $\log W$  in eq. (6.3) are completely determined by the  $\beta$ -function and lower loop results of the cusp anomalous dimension, see eq. (6.6). The same applies to the HQET field anomalous dimension. We use this as a direct check of our four-loop computation. As argued before all divergent terms in  $\log W$  are gauge invariant. We explicitly verify gauge invariance by computing  $\log W$  in covariant gauge up to four loops and observe that the dependence on the gauge parameter  $\xi$  drops out in the divergent terms. For  $\gamma_h$  this check is not possible, since it is gauge dependent.

## 6.4 Results

In this section we collect our results for the fermionic contributions to the four-loop cusp anomalous dimension  $\Gamma_{\text{cusp}}^{(4)}(\phi)$  in the small angle expansion to  $\mathcal{O}(\phi^4)$  or higher. We also give the corresponding contributions to the HQET heavy quark field anomalous dimension  $\gamma_h^{(4)}(\alpha_s)$ .

### 6.4.1 HQET field anomalous dimension

We determine  $\gamma_h^{(4)}$  from our calculation of the vertex function at zero cusp angle,  $V(0)$ . According to eqs. (6.11) and (6.12) we obtain

$$\gamma_h^{ffRA} = \left( -\frac{35\zeta_3}{24} + \frac{\pi^4}{120} - \frac{4157}{31104} \right) + \xi \left( -\frac{\zeta_3}{24} + \frac{269}{7776} \right), \quad (6.22)$$

$$\gamma_h^{fRFA} = \left( -\frac{15\zeta_5}{8} - \frac{105\zeta_3}{32} + \frac{23\pi^4}{960} + \frac{36503}{13824} \right) + \xi \left( -\frac{11\zeta_3}{32} - \frac{\pi^4}{960} + \frac{767}{1536} \right), \quad (6.23)$$

$$\begin{aligned} \gamma_h^{fRAA} = & \left( -\frac{2299\zeta_5}{1152} - \frac{3\zeta_3^2}{8} + \frac{37\pi^2\zeta_3}{864} + \frac{1751\zeta_3}{256} - \frac{1529\pi^4}{69120} - \frac{\pi^2}{48} + \frac{690965}{497664} \right) \\ & + \xi \left( -\frac{\zeta_5}{576} + \frac{\pi^2\zeta_3}{432} + \frac{65\zeta_3}{192} - \frac{7\pi^4}{23040} + \frac{49729}{497664} \right) \\ & + \xi^2 \left( -\frac{7\zeta_3}{768} + \frac{\pi^4}{46080} - \frac{109}{9216} \right), \end{aligned} \quad (6.24)$$

where we used the notation of eq. (6.15). The result for  $\gamma_h^{ffRA}$  agrees with the analytic expression obtained in [332]. The other two results for  $\gamma_h^{fRFA}$  and  $\gamma_h^{fRAA}$  agree with the numerical results of [332]. Note that the remaining terms can also be found in that reference.

### 6.4.2 Cusp anomalous dimension

Regarding  $\Gamma_{\text{cusp}}^{(4)}(\phi)$ , the results for the three ‘Abelian’ color structures  $(n_f T_F)^3 C_R$  [115],  $(n_f T_F)^2 C_R C_F$  [41, 328] and  $(n_f T_F) C_R C_F^2$  [333] are known with full angle dependence and given in eq. (6.49) in appendix 6.8. The  $\phi^2$  and  $\phi^4$  terms of the  $n_f d_R d_A / N_R$  contribution were computed in [335]. Here we extend its small angle expansion to include the  $\phi^6$  term, see also [352]:

$$\begin{aligned} \Gamma_{\text{cusp}}^{fdRF} = & \phi^2 \left( -\frac{4\pi^2 \zeta_3}{9} + \frac{5\pi^2}{54} + \frac{5\pi^4}{108} \right) \\ & + \phi^4 \left( \frac{71\zeta_3}{225} - \frac{16\pi^2 \zeta_3}{675} - \frac{4\zeta_5}{9} - \frac{23}{900} - \frac{157\pi^2}{8100} + \frac{49\pi^4}{8100} \right) \\ & + \phi^6 \left( \frac{983\zeta_3}{33075} - \frac{32\pi^2 \zeta_3}{11025} - \frac{64\zeta_5}{1323} + \frac{797}{264600} - \frac{1333\pi^2}{595350} + \frac{421\pi^4}{595350} \right) + \mathcal{O}(\phi^8). \end{aligned} \quad (6.25)$$

Using the notation of eq. (6.15) we find for the remaining  $n_f$  dependent color structures in the small angle expansion

$$\begin{aligned} \Gamma_{\text{cusp}}^{ffRA} = & \phi^2 \left( -\frac{35\zeta_3}{81} + \frac{7\pi^4}{3240} + \frac{19\pi^2}{1458} - \frac{1835}{15552} \right) \\ & + \phi^4 \left( -\frac{7\zeta_3}{243} + \frac{7\pi^4}{48600} + \frac{19\pi^2}{21870} - \frac{5201}{699840} \right) \\ & + \phi^6 \left( -\frac{2\zeta_3}{729} + \frac{\pi^4}{72900} + \frac{19\pi^2}{229635} - \frac{25397}{36741600} \right) + \mathcal{O}(\phi^8), \end{aligned} \quad (6.26)$$

$$\begin{aligned} \Gamma_{\text{cusp}}^{fRFA} = & \phi^2 \left( \frac{\pi^2 \zeta_3}{9} - \frac{85\zeta_3}{54} - \frac{5\zeta_5}{12} + \frac{11\pi^4}{2160} - \frac{55\pi^2}{432} + \frac{25943}{15552} \right) \\ & + \phi^4 \left( \frac{\pi^2 \zeta_3}{135} - \frac{41\zeta_3}{405} - \frac{\zeta_5}{36} + \frac{11\pi^4}{32400} - \frac{11\pi^2}{1296} + \frac{24953}{233280} \right) + \mathcal{O}(\phi^6), \end{aligned} \quad (6.27)$$

$$\begin{aligned} \Gamma_{\text{cusp}}^{fRAA} = & \phi^2 \left( -\frac{7}{54} \pi^2 \zeta_3 + \frac{3611\zeta_3}{1296} - \frac{55\zeta_5}{72} + \frac{11\pi^4}{648} - \frac{923\pi^2}{2916} + \frac{48161}{31104} \right) \\ & + \phi^4 \left( -\frac{13\pi^2 \zeta_3}{1350} + \frac{149327\zeta_3}{486000} - \frac{47\zeta_5}{1080} + \frac{293\pi^4}{486000} - \frac{35837\pi^2}{1749600} + \frac{112207}{34992000} \right) + \mathcal{O}(\phi^6). \end{aligned} \quad (6.28)$$

## 6.5 Conjecture on full angle dependence

Before we compare its predictions to our results of the previous section, let us briefly review the conjecture we want to test.

### 6.5.1 Conjecture

In [40, 41] the authors observed an intriguing pattern in the result of the cusp anomalous dimension at the first three loop orders. To see this pattern we expand  $\Gamma_{\text{cusp}}(\phi)$  in an effective coupling  $\lambda = \pi K(\alpha_s)/C_R$  as

$$\Gamma_{\text{cusp}}[\phi, \alpha_s(\lambda)] = \sum_{k \geq 1} \left( \frac{\lambda}{\pi} \right)^k \Omega^{(k)}(\phi). \quad (6.29)$$

In the light-like limit the cusp anomalous dimension equals the lowest order ( $k = 1$ ) term in eq. (6.29) by construction. All higher order  $\lambda$  terms vanish in that limit. Starting at four loops  $\lambda$  depends on the  $SU(N_c)$  representation  $R$  due to the appearance of the quartic Casimir operators. In [40, 41] it was found that the expansion coefficients  $\Omega^{(k)}(\phi)$  for  $k \leq 3$  are independent of the matter content of the theory, i.e. the number of scalars ( $n_s$ ) and fermions ( $n_f$ ), see eqs. (6.46)–(6.48). In particular, they are equal in QCD, pure Yang-Mills, and  $\mathcal{N} = 4$  sYM theory. The parameters  $n_f$  and  $n_s$  enter eq. (6.29) only through the light-like cusp anomalous dimension  $K(\alpha_s)$ , i.e. through  $\lambda$ . Based on this observation, the authors of [40, 41] conjectured that the coefficients  $\Omega^{(k)}(\phi)$  in eq. (6.29) are matter-independent to all orders in the  $\lambda$  expansion.

This conjecture is particularly interesting because of its predictive power. It allows for predictions on the matter-dependent terms in the loop expansion of  $\Gamma_{\text{cusp}}$  based on lower-loop results. This can be understood by re-expanding eq. (6.29) in  $\alpha_s$ :

$$\begin{aligned} \Gamma_{\text{cusp}}(\phi, \alpha_s) &= \frac{\alpha_s}{\pi} \Omega^{(1)}(\phi) + \left( \frac{\alpha_s}{\pi} \right)^2 \left[ \Omega^{(2)}(\phi) + \frac{1}{C_R} K^{(2)} \Omega^{(1)}(\phi) \right] \\ &+ \left( \frac{\alpha_s}{\pi} \right)^3 \left[ \Omega^{(3)}(\phi) + \frac{1}{C_R} \left( K^{(3)} \Omega^{(1)}(\phi) + 2K^{(2)} \Omega^{(2)}(\phi) \right) \right] \\ &+ \left( \frac{\alpha_s}{\pi} \right)^4 \left[ \Omega^{(4)}(\phi) + \frac{1}{C_R} \left( K^{(4)} \Omega^{(1)}(\phi) + 2K^{(3)} \Omega^{(2)}(\phi) + 3K^{(2)} \Omega^{(3)}(\phi) \right) \right. \\ &\quad \left. + \frac{1}{C_R^2} \left( K^{(2)} \right)^2 \Omega^{(2)}(\phi) \right] + \mathcal{O}(\alpha_s^5), \end{aligned} \quad (6.30)$$

where we have already inserted the explicit one-loop expression for the light-like cusp anomalous dimension  $K^{(1)} = C_R$ . To predict for instance the  $n_f$  piece of  $\Gamma_{\text{cusp}}$  at two loops it is sufficient to know  $\Omega^{(1)} = C_R(\phi \tan \phi - 1)$  and the  $n_f$  term of the two-loop light-like cusp anomalous dimension  $K^{fR} = -5n_f T_F C_R / 9$ :

$$\Gamma_{\text{cusp}}^{fR} = n_f T_F \Omega^{(1)} K^{fR} = -n_f T_F C_R \frac{5}{9} (\phi \tan \phi - 1). \quad (6.31)$$

In general, at  $L$  loops the angle dependence of the  $n_f$  contribution to  $\Gamma_{\text{cusp}}$  is completely determined by the lower loop coefficients  $\Omega^{(k)}(\phi)$  with  $k \leq L - 1$ . In addition some  $L$ -loop input, e.g. from the asymptotic behavior of  $\Gamma_{\text{cusp}}^f$  in one of the limits, light-like, small angle or anti-parallel lines, is required to fix the constant  $K^{(L)}$ .

Note that the conjecture does not make any statement on the purely gluonic contributions to the cusp anomalous dimension. In the following we systematically address the question, for which of the fermionic four-loop terms the conjecture can be successfully validated, and if some of the yet unknown contributions to  $\Gamma_{\text{cusp}}^{(4)}(\phi)$  can be predicted reliably. The known  $C_A$ -independent (‘Abelian’) fermionic terms with full angle-dependence are easily confirmed to exactly agree with the conjectured results in eq. (6.49). For the quartic Casimir color structure the check was performed in [335] using the terms in the small angle expansion up to  $\mathcal{O}(\phi^4)$ . Here we extend it to the remaining four-loop  $n_f$  contributions.

### 6.5.2 Test of the conjecture at small angles

In appendix 6.8 we give the expressions for the  $n_f$  terms in  $\Gamma_{\text{cusp}}^{(4)}(\phi)$  as predicted by the conjecture. They are obtained by inserting the known lower order  $\Omega^{(k)}(\phi)$  results [40] in eq. (6.30) and identifying the  $n_f$ -dependence from the  $K^{(i)}$  with  $i = 2, 3, 4$ . Except for the four-loop terms  $K^{fRFA}$  and  $K^{fRAA}$  associated with the color structures  $n_f T_F C_R C_F C_A$  and  $n_f T_F C_R C_A^2$ , respectively [cf. eq. (6.13)], for which only numerical results are available in the literature [334], all relevant terms of the  $K^{(i)}$  are known analytically, cf. table 6.1 and eqs. (6.54) and (6.55). Now we test the conjectured predictions for the (‘non-Abelian’)  $n_f$  contributions, where the full angle dependence is unknown yet, using our results at small angles.

#### Color structures $n_f T_F C_R C_A^2$ and $n_f d_R d_F / N_R$

The contribution with the quartic Casimir factor  $n_f d_R d_F / N_R$  was studied already in [335]. It was found that the conjectured result for that color structure is incorrect. Nevertheless, we repeat here the numerical comparison between conjectured and calculated result in the  $\phi$  expansion including the new  $\phi^6$ :

$$\Gamma^{fdRF} = 0.150721 \phi^2 + 0.00965191 \phi^4 + 0.000925974 \phi^6 + \mathcal{O}(\phi^8), \quad (6.32)$$

$$\Gamma_{\text{conj.}}^{fdRF} = 0.161321 \phi^2 + 0.0107548 \phi^4 + 0.00102426 \phi^6 + \mathcal{O}(\phi^8). \quad (6.33)$$

The first equation is the numerical version of eq. (6.25). The second equation represents the conjectured result, where we have used the recent analytic result for  $K^{fdRF}$  [241, 337] as the four-loop input. Instead, in [335] the overall normalization constant was determined from the anti-parallel lines limit and the quartic Casimir  $n_f$  term in the analytic result for the static potential [353]. In that case the conjectured expression is

numerically even closer to the correct result in eq. (6.32) than is eq. (6.33). Regardless of the overall factor the conjectured  $\phi$  dependence disagrees (at small angles) with the correct result on the analytical level.

Similarly for the color structure  $n_f T_F C_R C_A^2$  the conjecture can be disproved. Using the  $\phi^2$  term of our expanded result in eq. (6.28) we can determine the light-like cusp anomalous dimension term  $K^{fRAA}$  in the conjectured all-angles result, eq. (6.52), analytically. The numerical value  $K^{fRAA} = -3.4375$  is quite close to the known numerical result  $K^{fRAA} = -3.4426 \pm 0.0016$  of [334]. With  $K^{fRAA}$  fixed we obtain an analytical prediction for the  $\phi^4$  term of  $\Gamma^{fRAA}$ . This prediction however contradicts eq. (6.28) despite being numerically close:

$$\Gamma^{fRAA} = 1.09716 \phi^2 + 0.069745 \phi^4 + \mathcal{O}(\phi^6), \quad (6.34)$$

$$\Gamma_{\text{conj.}}^{fRAA} = 1.09716 \phi^2 + 0.069845 \phi^4 + \mathcal{O}(\phi^6). \quad (6.35)$$

### Color structures $(n_f T_F)^2 C_R C_A$ and $n_f T_F C_R C_F C_A$

For the  $(n_f T_F)^2 C_R C_A$  structure the light-like cusp anomalous dimension  $K^{ffRA}$  is known analytically [330, 331], cf. equation eq. (6.55). In the small angle limit we have computed the expansion to  $\mathcal{O}(\phi^6)$ , see eq. (6.26). This allows for three independent test of the conjectured expression in eq. (6.50). We find perfect agreement.

The  $n_f T_F C_R C_F C_A$  structure is more complex and there is less analytical data available. We have obtained the small angle expansion to  $\mathcal{O}(\phi^4)$  in eq. (6.27) and the corresponding light-like limit is only known numerically [334]. These results are still sufficient to allow for one analytical and one numerical check in order to validate the conjecture, i.e. eq. (6.51). Using the  $\phi^2$  term of our result in eq. (6.27) as input we find for the (conjectured) light-like cusp anomalous dimension

$$K_{\text{conj.}}^{fRFA} = -\frac{1}{6}\pi^2 \zeta_3 + \frac{29\zeta_3}{9} + \frac{5\zeta_5}{4} - \frac{11\pi^4}{720} + \frac{55\pi^2}{288} - \frac{17033}{5184} = 0.3031. \quad (6.36)$$

This is in perfect agreement with the known numerical value  $K^{fRFA} = 0.3027 \pm 0.0016$  [334]. In addition, with eq. (6.36) the analytic  $\phi^4$  terms of the conjectured and the computed result match exactly.

### 6.5.3 Summary of results and discussion

For the two color structures  $n_f T_F C_R C_A^2$  and  $n_f d_R d_F / N_R$  the conjecture does not hold. We also checked that a redefinition of the quartic Casimir such that a rational fraction of the  $n_f T_F C_R C_A^2$  coefficient is shifted to the  $n_f d_R d_F / N_R$  coefficient does not change

the conclusion.<sup>2</sup> The  $n_f T_F C_R C_A^2$  and  $n_f d_R d_F / N_R$  terms have in common that, unlike the other fermionic terms, they receive contributions from the diagrams with a one-loop fermion box subdiagram. The latter first appear at four loops, where they represent the most complicated class of Feynman diagrams. It is conceivable that only these particular diagrams are responsible for the disagreement with the conjectured results. This would explain why, at least according to our tests, all fermionic four-loop contributions except for the  $n_f T_F C_R C_A^2$  and  $n_f d_R d_F / N_R$  terms do agree with the conjecture.

Most interestingly, we have shown that the conjectured  $(n_f T_F)^2 C_R C_A$  as well as  $n_f T_F C_R C_F C_A$  contributions to  $\Gamma_{\text{cusp}}(\phi)$ , given in eqs. (6.50) and (6.51), respectively, exactly reproduce both the small  $\phi$  expansion as well as the light-like limit ( $\phi \rightarrow i\infty$ ). We think that these exact predictions of complicated analytical results containing transcendental numbers up to weight five strongly supports the conjecture for both of these color structures. While we were able to perform one such analytical test of the  $n_f T_F C_R C_F C_A$  term, the  $(n_f T_F)^2 C_R C_A$  term even passes three independent analytical tests of that kind. On the other hand, the light-like  $n_f T_F C_R C_F C_A$  prediction is in addition checked numerically at the per-mil level. We remark that unlike for the ‘Abelian’ color structures (without  $C_A$ ), the  $\phi$ -dependence of these terms is not just given by the one-loop coefficient  $\Omega^{(1)}$ , but also involves the more complicated coefficient  $\Omega^{(2)}$  of the  $\lambda$  expansion in eq. (6.29).

Our conjectured result for the  $n_f T_F C_R C_F C_A$  contribution includes the important special case of the light-like cusp anomalous dimension  $K^{fRFA}$ , for which we provide a novel analytic result in eq. (6.36). Based on the evidence found we assume in the following that eq. (6.36) is the correct exact result. As shown in [241], we are thus in the position to determine also the last missing fermionic contribution  $K^{fRAA}$  analytically by combining the other linear  $n_f$  pieces and the known planar  $n_f$  term [330, 334]:

$$K_{\text{conj.}}^{fRAA} = 2K_{\text{planar}, n_f}^{(4)} - \frac{K_{\text{conj.}}^{fRFA}}{2} - \frac{K^{fRFF}}{4} - \frac{K^{fdRF}}{24} \quad (6.37)$$

$$\begin{aligned} &= -\frac{361\zeta_3}{54} + \frac{7\pi^2\zeta_3}{36} + \frac{131\zeta_5}{72} - \frac{24137}{10368} + \frac{635\pi^2}{1944} - \frac{11\pi^4}{2160} \\ &= -3.44271. \end{aligned} \quad (6.38)$$

To obtain eq. (6.37) we have expanded the associated color factors to leading order in  $1/N_c$  in order to match the prefactor of  $K_{\text{planar}, n_f}^{(4)}$ . Again we find perfect agreement of our conjectured result in eq. (6.38) with the numerical result  $K^{fRAA} = -3.4426 \pm 0.0016$  of [334].

---

<sup>2</sup>This includes the particular linear combination obtained in the planar limit ( $N_c \rightarrow \infty$ ) of the linear  $n_f$  contribution to  $\Gamma_{\text{cusp}}(\phi)$ .

## 6.6 Anti-parallel lines limit

In the anti-parallel lines limit the cusp anomalous dimension is closely related to the static quark-antiquark potential, which was first observed at one loop in [339]. The expansion around  $\delta = \pi - \phi \ll 1$  takes the form

$$\Gamma_{\text{cusp}}(\pi - \delta, \alpha_s) = -C_R \alpha_s \frac{V_{\text{cusp}}(\alpha_s)}{\delta} + \mathcal{O}\left(\alpha_s^4 \frac{\log \delta}{\delta}\right), \quad (6.39)$$

where the  $\log \delta$  term at four loops is only present in the  $C_R C_A^3$  color structure [352] and the coefficient  $V_{\text{cusp}}$  is  $\delta$ -independent. The relation to the static quark-antiquark potential can be understood by interpreting  $\delta$  on the right hand side of the equation above as the distance between the static quarks. Indeed, there exists a conformal transformation for  $\delta \ll 1$  that maps the cusp configuration to two anti-parallel Wilson lines separated by the distance  $\delta$ , see e.g. [41, 264]. In momentum space the static quark-antiquark potential is given by [353–355]

$$V(\vec{q}) = -C_R \frac{4\pi\alpha_s(|\vec{q}|)}{\vec{q}^2} V_{Q\bar{Q}}(\alpha_s(|\vec{q}|)), \quad (6.40)$$

where we set the renormalization scale to  $\mu = |\vec{q}|$  in order to avoid logarithms of the form  $\log^n(\mu^2/\vec{q}^2)$ . It is however straightforward to restore the full dependence on the renormalization scale [356]. After Fourier transformation to position space and for equal renormalization scales in the cusp anomalous dimension and the position-space static potential, one directly finds  $V_{\text{cusp}}(\alpha_s) = V_{Q\bar{Q}}(\alpha_s)$  in a conformal theory like  $\mathcal{N} = 4$  sYM, for details we refer to [41].

In QCD, however, conformal invariance is broken by an anomaly, which becomes manifest in the running of the strong coupling  $\alpha_s$ . The relation between  $V_{\text{cusp}}$  and  $V_{Q\bar{Q}}$  must therefore be supplemented by terms proportional to the QCD  $\beta$ -function,  $\beta(\alpha_s) = \mathcal{O}(\alpha_s)$ , see e.g. [357–360],

$$V_{\text{cusp}}(\alpha_s) - V_{Q\bar{Q}}(\alpha_s) = \beta(\alpha_s) C(\alpha_s), \quad C(\alpha_s) = \sum_{k \geq 1} \left(\frac{\alpha_s}{\pi}\right)^k C^{(k)}. \quad (6.41)$$

With the known three-loop cusp anomalous dimension and the two-loop static potential [361–363] we have  $C^{(1)} = (47C_A - 28n_f T_F)/27$  [41]. Note the absence of transcendental terms in this expression.

Since also the three-loop result for the static potential is available analytically [353], we can use the conjecture to extract information on  $C^{(2)}$ . Given that the conjecture does not hold for all color structures at four loops, we decompose the cusp anomalous dimension in two terms. The first term is predicted by the conjecture, while the second term accommodates the correction to the conjecture for the  $n_f T_F C_R C_A^2$  and  $n_f d_R d_F / N_R$



contributions. Assuming the correctness of the conjectured results for all other four-loop color structures we thus write in the anti-parallel lines limit<sup>3</sup>

$$V_{\text{cusp}}(\alpha_s)|_{\text{ferm.}} = V_{\text{conj.}}(\alpha_s) - \left(\frac{\alpha_s}{\pi}\right)^3 n_f \left[ \frac{d_R d_F}{N_R C_R} V_{\text{corr.}}^{fdRF} + T_F C_A^2 V_{\text{corr.}}^{fRAA} \right] + \mathcal{O}(\alpha_s^4). \quad (6.42)$$

According to eq. (6.41) this information from the fermionic contributions is sufficient to fix

$$\begin{aligned} C^{(2)} = & (n_f T_F)^2 \left( \frac{116}{243} + \frac{2\zeta_3}{9} \right) + n_f T_F C_A \left( -\frac{5\zeta_3}{4} - \frac{\pi^4}{24} + \frac{79}{3888} \right) \\ & + n_f T_F C_F \left( \frac{19\zeta_3}{6} + \frac{\pi^4}{60} - \frac{1711}{288} \right) + C_A^2 \left( 3K^{fRAA} - 3V_{\text{corr.}}^{fRAA} - \frac{171\zeta_3^2}{128} - \frac{211\pi^6}{17920} \right. \\ & - \frac{1091\zeta_5}{128} - \frac{55\pi^2\zeta_3}{192} + \frac{203\pi^4}{1152} + \frac{81\zeta_3}{4} - \frac{11821\pi^2}{5184} + \frac{238315}{31104} + \frac{9}{4}\zeta_{-5,-1} \\ & + \frac{21}{32}\pi^2\zeta_3 \log(2) + \frac{3}{2}\pi^2 \text{Li}_4\left(\frac{1}{2}\right) + \frac{1}{16}\pi^2 \log^4(2) - \frac{3}{64}\pi^4 \log^2(2) \\ & \left. + \frac{5}{192}\pi^4 \log(2) + \frac{1}{16}\pi^2 \log(2) \right). \end{aligned} \quad (6.43)$$

The  $(n_f T_F)^2$  and  $n_f T_F C_F$  terms agree with [328] and the absence of the  $C_F^2$  term has also been shown in [333]. The transcendental constants  $\log(2)$ ,  $\text{Li}_4(1/2)$  and  $\zeta_{-5,-1}$  come from the  $\alpha_s^3 n_f T_F C_A^2$  term in the static potential. Also the quartic Casimir  $\alpha_s^3 (n_f d_R d_F)/(N_R C_R)$  term in the static potential contains  $\log(2)$  [353], cf. eq. (6.45) below. This is a rather interesting observation, because only the two color structures that disagree with the conjecture contain transcendental constants other than single zeta values.

We can also quantify the corrections in the anti-parallel lines limit for the quartic Casimir  $n_f d_R d_F/N_R$  color structure. The anomaly term  $\beta(\alpha_s)C(\alpha_s)$  is independent of the quartic Casimir  $n_f d_R d_F/N_R$  at  $\mathcal{O}(\alpha_s^3)$ , thus we have from eqs. (6.41) and (6.42)

$$V_{\text{cusp}}^{fdRF} = K^{fdRF} - V_{\text{corr.}}^{fdRF} = V_{Q\bar{Q}}^{fdRF}. \quad (6.44)$$

With the known value for the light-like cusp anomalous dimension  $K^{fdRF} = -0.484$  [241, 337] and the three-loop static potential [353]

$$\begin{aligned} V_{Q\bar{Q}}^{fdRF} &= \frac{5\pi^6}{192} - \frac{61\pi^2\zeta_3}{24} - \frac{23\pi^4}{48} + \frac{79\pi^2}{72} + \log(2) \left( \frac{21}{4}\pi^2\zeta_3 - \frac{1}{4}\pi^4 \log(2) + \frac{1}{12}\pi^4 + \frac{1}{2}\pi^2 \right) \\ &= -0.444. \end{aligned} \quad (6.45)$$

we see that in the anti-parallel lines limit the correction to the conjecture amounts to  $V_{\text{corr.}}^{fdRF} \approx -10\%$  for the quartic Casimir  $n_f$  contribution.

<sup>3</sup>Note the (traditional) factor of  $1/C_R$  in the definition of the quartic Casimir color structure associated with the  $V^{fdRF}$  potential coefficient. We adopt this convention also in eqs. (6.44) and (6.45).

## 6.7 Conclusion

In this chapter we computed the small angle ( $\phi$ ) expansion of fermionic contributions to the QCD cusp anomalous dimension at four loops. Our results are given in section 6.4. They include terms up to  $\mathcal{O}(\phi^4)$  and for some of the color structures even up to  $\mathcal{O}(\phi^6)$ . From our calculation for zero cusp angle, i.e. at  $\mathcal{O}(\phi^0)$ , we also obtain new analytic results for the HQET field anomalous dimension in generalized covariant ( $\xi$ ) gauge.

We then used our small angle results for  $\Gamma_{\text{cusp}}(\phi)$  to verify the conjecture of [40, 41]. This conjecture allows to predict the full angle dependence of the fermionic part of  $\Gamma_{\text{cusp}}(\phi)$  from lower-loop results. Comparing the predicted four-loop expressions, given in appendix 6.8, to our calculated analytic results at small angle we found strong evidence that the conjectured all-angles expressions are correct for all fermionic contributions except for the  $n_f T_F C_R C_A^2$  and the  $n_f d_R d_F / N_R$  terms. The reason for these exceptions might be connected to four-loop HQET Wilson-line diagrams with a fermion box sub-diagram, which exclusively contribute to the  $n_f T_F C_R C_A^2$  and  $n_f d_R d_F / N_R$  pieces. For further discussion see section 6.5.3.

The conjectured expressions passing our tests include novel results for the color structures  $(n_f T_F)^2 C_R C_A$  and  $n_f T_F C_R C_F C_A$  contributing to  $\Gamma_{\text{cusp}}(\phi)$  with full angle dependence. Using the light-like limit of the conjectured  $n_f T_F C_R C_F C_A$  term together with available results from the literature we determined in addition novel analytic expressions for the  $n_f T_F C_R C_F C_A$  and the  $n_f T_F C_R C_A^2$  contributions to the light-like cusp anomalous dimension. They are in perfect agreement with the known numerical values. This completes the analytic result for the fermionic part of the four-loop light-like cusp anomalous dimension in QCD [241].

Finally, we also studied the anti-parallel lines limit of the cusp anomalous dimension. In this limit  $\Gamma_{\text{cusp}}(\phi)$  is related to the static quark-antiquark potential plus a conformal anomaly term. The latter is proportional to the QCD  $\beta$ -function. In section 6.6, we used our results for  $\Gamma_{\text{cusp}}(\phi)$  in order to explore this relationship. We obtained new contributions to the conformal anomaly term at  $\mathcal{O}(\alpha_s^3)$ .

## 6.8 Appendix I: Lower-loop and conjectured four-loop

### $\Gamma_{\text{cusp}}(\phi)$

In this appendix we list the known and conjectured full angle-dependent results for all fermionic color structures of the cusp anomalous dimension at four loops. The results are expressed in terms of the light-like cusp anomalous dimension  $K(\alpha_s)$  and seven coefficient functions  $A_{1,2,3,4,5}$ , and  $B_{3,5}$ , encoding the angle dependence. For convenience we also present the expansions of the coefficient functions in the small angle and the anti-parallel

lines limits. We start with the expansion coefficients of  $\Gamma_{\text{cusp}}[\phi, \alpha_s(\lambda)]$  in eq. (6.29) as given in [41],

$$\Omega^{(1)}(\phi) = C_R \tilde{A}_1, \quad (6.46)$$

$$\Omega^{(2)}(\phi) = \frac{C_R C_A}{2} \left( \frac{\pi^2 \tilde{A}_1}{6} + \tilde{A}_2 + \tilde{A}_3 \right), \quad (6.47)$$

$$\Omega^{(3)}(\phi) = \frac{C_R C_A^2}{4} \left( -\tilde{A}_2 + \tilde{A}_4 + \tilde{A}_5 + \tilde{B}_3 + \tilde{B}_5 - \frac{\pi^4}{180} \tilde{A}_1 + \frac{\pi^2}{3} (\tilde{A}_2 + \tilde{A}_3) \right), \quad (6.48)$$

where  $\tilde{A}_i = \tilde{A}_i(x)$  and  $\tilde{B}_i = \tilde{B}_i(x)$  with  $x = e^{i\phi}$ . The ‘Abelian’  $n_f$ -dependent contributions to  $\Gamma_{\text{cusp}}(\phi)$  are known. They have the same functional angle dependence as the one-loop result [41, 115, 328, 333]:

$$\Gamma_{\text{cusp}}^{\mathcal{C}} = K^{\mathcal{C}} \tilde{A}_1, \quad \text{with } \mathcal{C} = fffR, fRF, fRFF. \quad (6.49)$$

Here and in the following we use the notation of eqs. (6.13) and (6.15) for the different color structures. Next we give the results for the other fermionic color structures as predicted by the conjecture:

$$\Gamma_{\text{conj.}}^{ffRA} = K^{ffRA} \tilde{A}_1 + \left( \frac{(K^{fR})^2}{2} + K^{ffR} \right) \left( \frac{\pi^2 \tilde{A}_1}{6} + \tilde{A}_2 + \tilde{A}_3 \right), \quad (6.50)$$

$$\Gamma_{\text{conj.}}^{fRFA} = K^{fRFA} \tilde{A}_1 + K^{fRF} \left( \frac{\pi^2 \tilde{A}_1}{6} + \tilde{A}_2 + \tilde{A}_3 \right), \quad (6.51)$$

$$\begin{aligned} \Gamma_{\text{conj.}}^{fRAA} = & K^{fRAA} \tilde{A}_1 + K^{fRA} \left( \frac{\pi^2 \tilde{A}_1}{6} + \tilde{A}_2 + \tilde{A}_3 \right) + K^{fR} \left[ -\frac{\pi^4}{240} \tilde{A}_1 + \frac{\pi^2}{4} (\tilde{A}_2 + \tilde{A}_3) \right. \\ & \left. + \frac{3}{4} (-\tilde{A}_2 + \tilde{A}_4 + \tilde{A}_5 + \tilde{B}_3 + \tilde{B}_5) + K^{RA} \left( \frac{\pi^2 \tilde{A}_1}{6} + \tilde{A}_2 + \tilde{A}_3 \right) \right], \end{aligned} \quad (6.52)$$

$$\Gamma_{\text{conj.}}^{fdRF} = K^{fdRF} \tilde{A}_1. \quad (6.53)$$

Analytical expressions for the light-like cusp anomalous dimension are available up to three loops [25, 107, 108]:

$$\begin{aligned} K = & C_R \frac{\alpha_s}{\pi} + \left( \frac{\alpha_s}{\pi} \right)^2 \left[ -\frac{5}{9} n_f T_F C_R + C_A C_R \left( \frac{67}{36} - \frac{\pi^2}{12} \right) \right] + \left( \frac{\alpha_s}{\pi} \right)^3 \left[ -\frac{1}{27} (n_f T_F)^2 C_R \right. \\ & \left. + n_f T_F C_R C_F \left( \zeta_3 - \frac{55}{48} \right) + n_f T_F C_R C_A \left( -\frac{7\zeta_3}{6} - \frac{209}{216} + \frac{5\pi^2}{54} \right) \right. \\ & \left. + C_R C_A^2 \left( \frac{11\zeta_3}{24} + \frac{245}{96} - \frac{67\pi^2}{216} + \frac{11\pi^4}{720} \right) \right] + \left( \frac{\alpha_s}{\pi} \right)^4 K^{(4)} + \mathcal{O}(\alpha_s^5). \end{aligned} \quad (6.54)$$

Depending on the color factor the contributions at four loops are either known analytically or numerically [241, 326, 330, 331, 334, 336–338]:

$$K^{(4)} = \frac{d_R d_A}{N_R} (-1.9805 \pm 0.0078) + C_R C_A^3 (2.38379 \pm 0.00039)$$

$$\begin{aligned}
 & + (n_f T_F)^3 C_R \left( -\frac{1}{81} + \frac{2\zeta_3}{27} \right) + (n_f T_F)^2 C_R C_A \left( \frac{35\zeta_3}{27} - \frac{7\pi^4}{1080} - \frac{19\pi^2}{972} + \frac{923}{5184} \right) \\
 & + (n_f T_F)^2 C_R C_F \left( -\frac{10\zeta_3}{9} + \frac{\pi^4}{180} + \frac{299}{648} \right) + n_f T_F C_R C_F^2 \left( \frac{37\zeta_3}{24} - \frac{5\zeta_5}{2} + \frac{143}{288} \right) \\
 & + n_f T_F C_R C_F C_A (0.3027 \pm 0.0016) + n_f T_F C_R C_A^2 (-3.4426 \pm 0.0016) \\
 & + n_f \frac{d_R d_F}{N_R} \left( \frac{\pi^2}{6} - \frac{\zeta_3}{3} - \frac{5\zeta_5}{3} \right) .
 \end{aligned} \tag{6.55}$$

The coefficient functions are given by [41]

$$\begin{aligned}
 \tilde{A}_i(x) &= A_i(x) - A_i(x) , \quad \tilde{B}_i(x) = B_i(x) - B_i(x) , \\
 A_1(x) &= \tilde{\xi} \frac{1}{2} H_1(y) , \\
 A_2(x) &= \left[ \frac{\pi^2}{3} + \frac{1}{2} H_{1,1}(y) \right] + \tilde{\xi} \left[ -H_{0,1}(y) - \frac{1}{2} H_{1,1}(y) \right] , \\
 A_3(x) &= \tilde{\xi} \left[ -\frac{\pi^2}{6} H_1(y) - \frac{1}{4} H_{1,1,1}(y) \right] + \tilde{\xi}^2 \left[ \frac{1}{2} H_{1,0,1}(y) + \frac{1}{4} H_{1,1,1}(y) \right] , \\
 A_4(x) &= \left[ -\frac{\pi^2}{6} H_{1,1}(y) - \frac{1}{4} H_{1,1,1,1}(y) \right] + \tilde{\xi} \left[ \frac{\pi^2}{3} H_{0,1}(y) + \frac{\pi^2}{6} H_{1,1}(y) + 2H_{1,1,0,1}(y) \right. \\
 & \quad \left. + \frac{3}{2} H_{0,1,1,1}(y) + \frac{7}{4} H_{1,1,1,1}(y) + 3\zeta_3 H_1(y) \right] + \tilde{\xi}^2 \left[ -2H_{1,0,0,1}(y) - 2H_{0,1,0,1}(y) \right. \\
 & \quad \left. - 2H_{1,1,0,1}(y) - H_{1,0,1,1}(y) - H_{0,1,1,1}(y) - \frac{3}{2} H_{1,1,1,1}(y) \right] , \\
 A_5(x) &= \tilde{\xi} \left[ \frac{\pi^4}{12} H_1(y) + \frac{\pi^2}{4} H_{1,1,1}(y) + \frac{5}{8} H_{1,1,1,1,1}(y) \right] + \tilde{\xi}^2 \left[ -\frac{\pi^2}{6} H_{1,0,1}(y) - \frac{\pi^2}{3} H_{0,1,1}(y) \right. \\
 & \quad \left. - \frac{\pi^2}{4} H_{1,1,1}(y) - H_{1,1,1,0,1}(y) - \frac{3}{4} H_{1,0,1,1,1}(y) - H_{0,1,1,1,1}(y) - \frac{11}{8} H_{1,1,1,1,1}(y) \right. \\
 & \quad \left. - \frac{3}{2} \zeta_3 H_{1,1}(y) \right] + \tilde{\xi}^3 \left[ H_{1,1,0,0,1}(y) + H_{1,0,1,0,1}(y) + H_{1,1,1,0,1}(y) + \frac{1}{2} H_{1,1,0,1,1}(y) \right. \\
 & \quad \left. + \frac{1}{2} H_{1,0,1,1,1}(y) + \frac{3}{4} H_{1,1,1,1,1}(y) \right] , \\
 B_3(x) &= \left[ -H_{1,0,1}(y) + \frac{1}{2} H_{0,1,1}(y) - \frac{1}{4} H_{1,1,1}(y) \right] \\
 & \quad + \tilde{\xi} \left[ 2H_{0,0,1}(y) + H_{1,0,1}(y) + H_{0,1,1}(y) + \frac{1}{4} H_{1,1,1}(y) \right] , \\
 B_5(x) &= \frac{x}{1-x^2} \left[ -\frac{\pi^4}{60} H_{-1}(x) - \frac{\pi^4}{60} H_1(x) - 4H_{-1,0,-1,0,0}(x) + 4H_{-1,0,1,0,0}(x) \right. \\
 & \quad \left. - 4H_{1,0,-1,0,0}(x) + 4H_{1,0,1,0,0}(x) + 4H_{-1,0,0,0,0}(x) + 4H_{1,0,0,0,0}(x) \right. \\
 & \quad \left. + 2\zeta_3 H_{-1,0}(x) + 2\zeta_3 H_{1,0}(x) \right] ,
 \end{aligned} \tag{6.56}$$

with  $\tilde{\xi} = (1 + x^2)/(1 - x^2)$ ,  $y = 1 - x^2$ ,  $x = e^{i\phi}$ . The  $H_{\bar{a}}(y)$  denote HPLs according to [223, 224].

For the small angle expansion of the above coefficient functions around  $\phi = 0$  we find up to  $\mathcal{O}(\phi^6)$ :

$$\begin{aligned}
 A_1(\phi) &= 1 - \frac{1}{3}\phi^2 - \frac{1}{45}\phi^4 - \frac{2}{945}\phi^6 + \mathcal{O}(\phi^8), \\
 A_2(\phi) &= \frac{\pi^2}{3} - 2 - \frac{1}{9}\phi^2 - \frac{14}{675}\phi^4 - \frac{304}{99225}\phi^6 + \mathcal{O}(\phi^8), \\
 A_3(\phi) &= \left(1 - \frac{\pi^2}{3}\right) + \phi^2 \left(\frac{\pi^2}{9} - \frac{7}{18}\right) + \phi^4 \left(\frac{\pi^2}{135} - \frac{2}{225}\right) + \phi^6 \left(\frac{38}{99225} + \frac{2\pi^2}{2835}\right) + \mathcal{O}(\phi^8), \\
 A_4(\phi) &= \left(6\zeta_3 + \frac{2\pi^2}{3} - 6\right) + \phi^2 \left(-2\zeta_3 + \frac{91}{54} + \frac{\pi^2}{27}\right) + \phi^4 \left(-\frac{2\zeta_3}{15} + \frac{1789}{20250} + \frac{14\pi^2}{2025}\right) \\
 &\quad + \phi^6 \left(-\frac{4\zeta_3}{315} + \frac{250121}{20837250} + \frac{304\pi^2}{297675}\right) + \mathcal{O}(\phi^8), \\
 A_5(\phi) &= \left(-3\zeta_3 + \frac{\pi^4}{6} - \frac{2\pi^2}{3} + 2\right) + \phi^2 \left(2\zeta_3 - \frac{65}{54} + \frac{5\pi^2}{27} - \frac{\pi^4}{18}\right) + \phi^4 \left(-\frac{\zeta_3}{5} + \frac{1649}{10125}\right. \\
 &\quad \left. + \frac{41\pi^2}{2025} - \frac{\pi^4}{270}\right) + \phi^6 \left(-\frac{2\zeta_3}{63} + \frac{6401}{1157625} + \frac{349\pi^2}{99225} - \frac{\pi^4}{2835}\right) + \mathcal{O}(\phi^8), \\
 B_3(\phi) &= 4 - \frac{5}{54}\phi^2 - \frac{889}{40500}\phi^4 - \frac{80299}{20837250}\phi^6 + \mathcal{O}(\phi^8), \\
 B_5(\phi) &= \frac{3\zeta_3}{2} + \phi^2 \left(\frac{\zeta_3}{3} + \frac{1}{18}\right) + \phi^4 \left(\frac{11\zeta_3}{225} + \frac{31}{2700}\right) + \phi^6 \left(\frac{202\zeta_3}{33075} + \frac{143}{99225}\right) + \mathcal{O}(\phi^8).
 \end{aligned} \tag{6.57}$$

In the anti-parallel lines limit  $\delta = \pi - \phi \ll 1$  we obtain:

$$\begin{aligned}
 \delta A_1(\pi - \delta) &= -\pi + \mathcal{O}(\delta), \\
 \delta A_2(\pi - \delta) &= 2\pi \log(i\delta) - i\pi^2 + 2\pi \log(2) + \mathcal{O}(\delta), \\
 \delta A_3(\pi - \delta) &= -2\pi \log(i\delta) + i\pi^2 + 2\pi - 2\pi \log(2) + \mathcal{O}(\delta), \\
 \delta A_4(\pi - \delta) &= \frac{\pi^4}{3\delta} + 4\pi \log^2(i\delta) + \left(-4i\pi^2 + \frac{4\pi^3}{3} + 8\pi \log(2)\right) \log(i\delta) \\
 &\quad + 9\pi\zeta_3 - \frac{2i\pi^4}{3} - 2\pi^3 - 8\pi + 4\pi \log^2(2) + \left(\frac{4\pi^3}{3} - 4i\pi^2\right) \log(2) + \mathcal{O}(\delta), \\
 \delta A_5(\pi - \delta) &= -\frac{\pi^4}{3\delta} - 2\pi \log^2(i\delta) + \left(2\pi + 2i\pi^2 - \frac{4\pi^3}{3} - 4\pi \log(2)\right) \log(i\delta) - 9\pi\zeta_3 \\
 &\quad + \frac{2i\pi^4}{3} + \pi^3 - i\pi^2 + 3\pi - 2\pi \log^2(2) + \left(2\pi + 2i\pi^2 - \frac{4\pi^3}{3}\right) \log(2) + \mathcal{O}(\delta), \\
 \delta B_3(\pi - \delta) &= -2\pi \log^2(i\delta) + (-4\pi \log(2) + 2i\pi^2) \log(i\delta) \\
 &\quad - 2\pi \log^2(2) + 2i\pi^2 \log(2) + \mathcal{O}(\delta), \\
 \delta B_5(\pi - \delta) &= \frac{\pi^5}{16} + \mathcal{O}(\delta).
 \end{aligned} \tag{6.58}$$

## 6.9 Appendix II: Master integrals

For the small angle expansion of the fermionic part of the cusp anomalous dimension 46 master integrals are needed; 43 of which are already known [335]. Below we list the three new master integrals, which we compute with the method outlined in section 6.3.3. These integrals are defined by the eqs. (6.17) and (6.18). The first integral is associated with topology 3 and the other two integrals are associated with topology 5 in figure 6.2.

$$\begin{aligned}
G(1, 1, 1, 0, 1, 1, 1, 0, 0, 0, 0, 0, 2, 1, 0, 0) &= \frac{1}{\epsilon^3} \frac{\pi^2}{18} + \frac{1}{\epsilon^2} \left( \frac{2\pi^2}{9} - \frac{7\zeta_3}{3} \right) \\
&+ \frac{1}{\epsilon} \left( -\frac{28\zeta_3}{3} + \frac{181\pi^4}{540} + \frac{2\pi^2}{3} \right) + \left( -\frac{251}{27}\pi^2\zeta_3 - 28\zeta_3 - \frac{250\zeta_5}{3} + \frac{181\pi^4}{135} + \frac{16\pi^2}{9} \right) \\
&+ \epsilon \left( \frac{910\zeta_3^2}{9} - \frac{1004\pi^2\zeta_3}{27} - \frac{224\zeta_3}{3} - \frac{1000\zeta_5}{3} + \frac{1711\pi^6}{1260} + \frac{181\pi^4}{45} + \frac{40\pi^2}{9} \right) \\
&+ \epsilon^2 \left( \frac{3640\zeta_3^2}{9} - \frac{11617\pi^4\zeta_3}{405} - \frac{1004\pi^2\zeta_3}{9} - \frac{560\zeta_3}{3} - \frac{4634\pi^2\zeta_5}{15} - 1000\zeta_5 \right. \\
&\quad \left. - \frac{14729\zeta_7}{6} + \frac{1711\pi^6}{315} + \frac{1448\pi^4}{135} + \frac{32\pi^2}{3} \right) + \mathcal{O}(\epsilon^3),
\end{aligned} \tag{6.59}$$

$$\begin{aligned}
G(0, 1, 0, 0, 0, 1, 1, 0, 1, 0, 0, 0, 1, 2, 1, 2) &= \frac{1}{\epsilon^2} \left( -\frac{\pi^2}{12} \right) + \frac{1}{\epsilon} \left( \frac{9\zeta_3}{4} + \frac{\pi^2}{3} \right) \\
&+ \left( -31\zeta_3 - \frac{277\pi^4}{720} - \pi^2 \right) + \epsilon \left( \frac{487\pi^2\zeta_3}{36} + 27\zeta_3 - \frac{5\zeta_5}{4} + \frac{883\pi^4}{180} + \frac{16\pi^2}{3} \right) \\
&+ \epsilon^2 \left( -\frac{1505\zeta_3^2}{4} - \frac{1753\pi^2\zeta_3}{9} - 408\zeta_3 - 2405\zeta_5 - \frac{703\pi^6}{1680} - \frac{277\pi^4}{60} - \frac{52\pi^2}{3} \right) \\
&+ \epsilon^3 \left( \frac{9085\zeta_3^2}{3} + \frac{98243\pi^4\zeta_3}{1080} + \frac{487\pi^2\zeta_3}{3} + 820\zeta_3 - \frac{23821\pi^2\zeta_5}{60} - 15\zeta_5 \right. \\
&\quad \left. - 4184\zeta_7 + \frac{164417\pi^6}{3780} + \frac{2926\pi^4}{45} + 80\pi^2 \right) + \mathcal{O}(\epsilon^4),
\end{aligned} \tag{6.60}$$

$$\begin{aligned}
G(0, 2, 0, 0, 0, 0, 1, 2, 1, 0, 0, 0, 1, 0, 2, 3) &= \frac{1}{\epsilon} \left( \frac{1}{2} - \frac{\pi^2}{12} \right) \\
&+ \left( 6\zeta_3 - \frac{2\pi^2}{3} + 3 \right) + \epsilon \left( 48\zeta_3 - \frac{167\pi^4}{180} - \frac{5\pi^2}{2} + 14 \right) \\
&+ \epsilon^2 \left( \frac{325\pi^2\zeta_3}{9} + \frac{898\zeta_3}{3} + 372\zeta_5 - \frac{334\pi^4}{45} - \frac{29\pi^2}{3} + 60 \right) \\
&+ \epsilon^3 \left( -584\zeta_3^2 + \frac{2600\pi^2\zeta_3}{9} + 1412\zeta_3 + 2976\zeta_5 - \frac{1733\pi^6}{252} - \frac{4109\pi^4}{90} - 38\pi^2 + 248 \right) \\
&+ \epsilon^4 \left( -4672\zeta_3^2 + \frac{25403\pi^4\zeta_3}{135} + \frac{5494\pi^2\zeta_3}{3} + \frac{18232\zeta_3}{3} + \frac{31891\pi^2\zeta_5}{15} \right. \\
&\quad \left. + \frac{102658\zeta_5}{5} + 20052\zeta_7 - \frac{3466\pi^6}{63} - \frac{1931\pi^4}{9} - \frac{452\pi^2}{3} + 1008 \right) + \mathcal{O}(\epsilon^5).
\end{aligned} \tag{6.61}$$

Using IBP relations, the three master integrals can be exchanged for integrals with uniform transcendental weight:

$$\begin{aligned}
G(1, 1, 1, 0, 2, 1, 1, 0, 0, 0, 0, 2, 1, 0, 0) &= \frac{1}{\epsilon^3(1-2\epsilon)} \left[ \frac{\pi^2}{9} - \epsilon \frac{14\zeta_3}{3} + \epsilon^2 \frac{181\pi^4}{270} \right. \\
&\quad + \epsilon^3 \left( -\frac{502}{27}\pi^2\zeta_3 - \frac{500\zeta_5}{3} \right) + \epsilon^4 \left( \frac{1820\zeta_3^2}{9} + \frac{1711\pi^6}{630} \right) \\
&\quad \left. + \epsilon^5 \left( -\frac{23234}{405}\pi^4\zeta_3 - \frac{9268\pi^2\zeta_5}{15} - \frac{14729\zeta_7}{3} \right) + \mathcal{O}(\epsilon^6) \right], \tag{6.62}
\end{aligned}$$

$$\begin{aligned}
G(0, 1, 0, 0, 0, 0, 1, 2, 2, 0, 0, 0, 2, 0, 1, 2) &= \frac{1}{\epsilon^4} \left[ -\frac{1}{2} - \epsilon^2 \frac{13\pi^2}{6} + \epsilon^3 \frac{110\zeta_3}{3} - \epsilon^4 \frac{63\pi^4}{10} \right. \\
&\quad + \epsilon^5 \left( \frac{1718\pi^2\zeta_3}{9} + \frac{1502\zeta_5}{5} \right) + \epsilon^6 \left( -\frac{22468\zeta_3^2}{9} - \frac{233\pi^6}{15} \right) \\
&\quad \left. + \epsilon^7 \left( \frac{12274\pi^4\zeta_3}{15} + \frac{23366\pi^2\zeta_5}{15} - \frac{74338\zeta_7}{7} \right) + \mathcal{O}(\epsilon^8) \right], \tag{6.63}
\end{aligned}$$

$$\begin{aligned}
G(0, 1, 0, 0, 0, 1, 1, 0, 2, 0, 0, 0, 1, 2, 1, 1) &= \frac{1}{\epsilon^3(1-2\epsilon)} \left[ \frac{\pi^2}{9} - \epsilon \frac{11\zeta_3}{3} + \epsilon^2 \frac{383\pi^4}{540} \right. \\
&\quad + \epsilon^3 \left( -\frac{709}{27}\pi^2\zeta_3 - \frac{335\zeta_5}{3} \right) + \epsilon^4 \left( \frac{4625\zeta_3^2}{9} + \frac{35437\pi^6}{11340} \right) \\
&\quad \left. + \epsilon^5 \left( -\frac{128977}{810}\pi^4\zeta_3 - \frac{7693\pi^2\zeta_5}{15} - \frac{18037\zeta_7}{6} \right) + \mathcal{O}(\epsilon^6) \right]. \tag{6.64}
\end{aligned}$$





---

## Summary

---

In this thesis we performed higher order perturbative calculations with particular focus on Wilson lines. Our results are important for precise theoretical predictions of high-energy collider processes. The first part of the thesis serves as an introduction and review of the necessary theory and technical aspects of multi-loop calculations. In the second part we presented our research results. We studied the cusp anomalous dimension, massive four-particle scattering amplitudes in  $\mathcal{N} = 4$  sYM and the massless quark jet function in SCET. In all three quantities Wilson lines play an important role. The cusp anomalous dimension is defined by the UV divergences due to a cusp in a Wilson line. In the quark jet function Wilson lines ensure gauge invariance and the Regge limit of the massive scattering amplitudes is governed by anomalous dimensions of cusped Wilson line operators. Below we briefly summarize our findings for each quantity.

The most fundamental quantity of these three is the cusp anomalous dimension considered in chapter 6. It is ubiquitous in gauge theories such as QCD. For instance it governs the IR divergences of scattering amplitudes and is a crucial ingredient in the resummation of Sudakov logarithms. It is also relevant for the massive scattering amplitudes in  $\mathcal{N} = 4$  sYM and the quark jet function, which we studied in the chapters 4 and 5, respectively. We computed the matter dependence of the QCD cusp anomalous dimension  $\Gamma_{\text{cusp}}(\phi)$  up to four loops in an expansion for small cusp angles. As a byproduct we obtained the fermionic contributions to the HQET field anomalous dimension at this loop order. The main goal was, however, to test a conjecture about the universal structure of  $\Gamma_{\text{cusp}}(\phi)$ . In particular the conjecture predicts the full angle dependence of the fermionic contributions at four loops using known lower-loop results.

The contributions proportional to  $n_f d_R d_F / N_c$  and  $n_f T_F C_R C_A^2$  predicted by the conjecture deviate from our results from the small angle expansion, whereas the conjectured expressions of the remaining other five fermionic color structures passes several stringent tests. Assuming that the conjecture holds in these cases, we obtained for the first time

results for the full angle dependence of the  $(n_f T_F)^2 C_R C_A$  and  $n_F T_F C_R C_A$  contributions to  $\Gamma_{\text{cusp}}(\phi)$ . Furthermore, we found novel analytic results for the color structures  $n_f T_F C_R C_F C_A$  and  $n_f T_F C_R C_A^2$  of the light-like cusp anomalous dimension.

In chapter 4 we considered massive four particle scattering amplitudes in  $\mathcal{N} = 4$  sYM up to three loops, where the mass is generated by a Higgs mechanism. These amplitudes are IR as well as UV finite and exhibit dual conformal symmetry. They have several interesting kinematic limits, many of which are known exactly or controlled by integrability. In particular we conjectured and verified up to three loops an all order result for the high energy limit of the total cross section. Furthermore, we derived with the available differential equation for the master integrals (asymptotic) expansions in these limits. This allowed us to go beyond the leading contributions and study power corrections. Here we concentrated on the Regge limit, where the leading term is known to follow a single power law with the exponent given by the cusp anomalous dimension. Expressed in suitable variables, which are inspired by a dual conformal partial wave analysis, we showed that also the first power correction exponentiate. We proposed that the exponent is given by the anomalous dimension of a cusped Wilson line with a scalar insertion at the cusp point. With a soft current calculation we provided perturbative evidence for this proposal. We directly computed this anomalous dimension up to two loops and find perfect agreement.

In chapter 5 we computed the massless quark jet function up to three loops. It appears in many SCET factorization formulas for observables with quark initiated final state jets. As such it is for instance crucial for resummed predictions of the event shapes thrust, C-parameter, heavy jet mass as well as for deep inelastic scattering and the  $\bar{B} \rightarrow X_s \gamma$  decay rate in the threshold region. Our result has in particular direct impact on existing precision determinations of the strong coupling constant  $\alpha_s$ .

---

## Overview of publications

---

This thesis is based on the publications listed below. I provide a brief overview of these publications and specify my contribution to the respective research projects<sup>1</sup>.

- R. Brüser, S. Caron-Huot and J. Henn, *Subleading Regge limit from a soft anomalous dimension*, JHEP 1804 (2018) 047 [arXiv:1802.02524 [hep-th]]. Reference [75].

We study massive scattering amplitudes in  $\mathcal{N} = 4$  sYM in various physical interesting kinematic limits up to and including three loops. In particular we show that the Regge limit is governed by anomalous dimensions of Wilson line operators with a cusp. Furthermore, we conjecture an all order expression for the total cross section in the high energy limit.

I computed the (asymptotic) expansions of the scattering amplitude in all the considered kinematic limits. In the Regge limit I cross-checked the dual conformal partial wave expansion and the exponentiation of the leading and subleading contributions. I cross-checked the conjectured all order expressions of the total cross section at high energies and verified this result up to the three loops using the optical theorem and the result for the scattering amplitude in the forward limit. For the soft current computation I derived the integrand of the considered correlation functions as outlined in section 3.1 with my **Mathematica** code. I performed the IBP reduction with **FIRE5** in combination with **LiteRed**. For the computation of the master integrals, which are needed for the soft current computation, I used the differential equation method. I obtained the IR  $Z$ -factor and the anomalous dimensions of the cusped Wilson line operators.

- R. Brüser, Z. L. Liu and M. Stahlhofen, *Three-Loop Quark Jet Function*, Phys. Rev. Lett. 121 (2018) 072003 [arXiv:1804.09722 [hep-ph]]. Reference [76].

In this project we compute the massless quark jet function at three-loop order. It is an important ingredient in SCET factorization for many collider and decay processes.

I computed the integrand of the quark jet function up to three loops as explained in section 3.1. For this I used an improved version of my **Mathematica** code

---

<sup>1</sup>Note that a significant fraction of the computations were performed independently by several people working on the projects. Here I only list my contributions.

written for the  $\mathcal{N} = 4$  sYM project. In particular I implemented the algorithm for multivariate partial fraction decomposition of [188]. I performed the IBP reduction with FIRE5 in combination with LiteRed. With the built in functions of LiteRed I derived the dimensional recurrence relations for the planar master integrals as outlined in section 3.3. I independently renormalized the quark jet function in momentum space and confirmed the results obtained from the renormalization in Laplace space.

- R. Brüser, A. Grozin, M. Stahlhofen and J. Henn, *Matter dependence of the four-loop QCD cusp anomalous dimension: from small angles to all angles*, JHEP 1905 (2019) 186 [arXiv:1902.05076 [hep-ph]]. Reference [77].

We compute the fermionic contributions to the four-loop cusp anomalous dimension in QCD in an expansion in small cusp angle. With these results we test and partially confirm a conjecture predicting the full angle dependence of the fermionic contributions. In this way we obtain novel analytic expressions for the full angle dependence and in particular for the light-like limit of certain color structures of the cusp anomalous dimension at four loops.

I computed the integrand of the vertex function after some improvements with my Mathematica code, which was already used for the other two projects. I implemented routines to handle the color structure with quartic Casimir operators and to efficiently compute the Taylor series expansion at small cusp angle of the integrand of the vertex function. The latter task includes in particular the reduction of tensor integrals to scalar ones. I performed the IBP reduction with FIRE5 in combination with LiteRed. I computed the renormalized results for the cusp anomalous dimension and the HQET field anomalous dimension. For the former quantity I calculated also the conjectured expressions of the fermionic contributions and their expansions in the small angle and anti-parallel lines limit. The study of the anti-parallel lines limit was initiated by fruitful discussions between Gregory Korchemsky and me during my research visit at the IPhT at CEA Saclay.

In addition, I worked also on the following research projects, which however are not included in this thesis.

- R. Brüser, J. Henn, L. Maestri and T. Peraro, *All five-point planar two-loop integrals with one off-shell leg*, in preparation.

We compute the two-loop planar master integrals needed for two-jet plus vector boson and two-jet plus Higgs production with the differential equation method.

- R. Brüser, Z. L. Liu and M. Stahlhofen, *Three-loop soft function for heavy-light scattering and decay processes*, in preparation.

We compute the soft function for heavy-to-light processes up to and including three loops. It is a universal ingredient in SCET factorization formulas for processes with one massive quark and one final state jet initiated by a massless quark. In particular this soft function is relevant for the decay  $\bar{B} \rightarrow X_s \gamma$ .

---

# Bibliography

---

- [1] ATLAS collaboration, *Observation of a new particle in the search for the Standard Model Higgs boson with the ATLAS detector at the LHC*, *Phys. Lett. B* **716** (2012) 1 [1207.7214].
- [2] CMS collaboration, *Observation of a New Boson at a Mass of 125 GeV with the CMS Experiment at the LHC*, *Phys. Lett. B* **716** (2012) 30 [1207.7235].
- [3] D. J. Gross and F. Wilczek, *Ultraviolet Behavior of Nonabelian Gauge Theories*, *Phys. Rev. Lett.* **30** (1973) 1343.
- [4] H. D. Politzer, *Reliable Perturbative Results for Strong Interactions?*, *Phys. Rev. Lett.* **30** (1973) 1346.
- [5] M. A. Shifman and M. B. Voloshin, *On Annihilation of Mesons Built from Heavy and Light Quark and  $\bar{B}_0 \leftrightarrow B_0$  Oscillations*, *Sov. J. Nucl. Phys.* **45** (1987) 292.
- [6] M. A. Shifman and M. B. Voloshin, *On Production of  $d$  and  $D^*$  Mesons in  $B$  Meson Decays*, *Sov. J. Nucl. Phys.* **47** (1988) 511.
- [7] H. D. Politzer and M. B. Wise, *Leading Logarithms of Heavy Quark Masses in Processes with Light and Heavy Quarks*, *Phys. Lett. B* **206** (1988) 681.
- [8] H. D. Politzer and M. B. Wise, *Effective Field Theory Approach to Processes Involving Both Light and Heavy Fields*, *Phys. Lett. B* **208** (1988) 504.
- [9] N. Isgur and M. B. Wise, *Weak decays of heavy mesons in the static quark approximation*, *Phys. Lett. B* **232** (1989) 113.
- [10] N. Isgur and M. B. Wise, *Weak transition form-factors between heavy mesons*, *Phys. Lett. B* **237** (1990) 527.
- [11] B. Grinstein, *The Static Quark Effective Theory*, *Nucl. Phys. B* **339** (1990) 253.
- [12] E. Eichten and B. R. Hill, *An Effective Field Theory for the Calculation of Matrix Elements Involving Heavy Quarks*, *Phys. Lett. B* **234** (1990) 511.

## Bibliography

- [13] H. Georgi, *An Effective Field Theory for Heavy Quarks at Low-energies*, *Phys. Lett.* **B240** (1990) 447.
- [14] C. W. Bauer, S. Fleming and M. E. Luke, *Summing Sudakov logarithms in  $B \rightarrow X_s \gamma$  in effective field theory*, *Phys. Rev. D* **63** (2000) 014006 [[hep-ph/0005275](#)].
- [15] C. W. Bauer, S. Fleming, D. Pirjol and I. W. Stewart, *An Effective field theory for collinear and soft gluons: Heavy to light decays*, *Phys. Rev. D* **63** (2001) 114020 [[hep-ph/0011336](#)].
- [16] C. W. Bauer and I. W. Stewart, *Invariant operators in collinear effective theory*, *Phys. Lett. B* **516** (2001) 134 [[hep-ph/0107001](#)].
- [17] C. W. Bauer, D. Pirjol and I. W. Stewart, *Soft collinear factorization in effective field theory*, *Phys. Rev. D* **65** (2002) 054022 [[hep-ph/0109045](#)].
- [18] C. W. Bauer, S. Fleming, D. Pirjol, I. Z. Rothstein and I. W. Stewart, *Hard scattering factorization from effective field theory*, *Phys. Rev. D* **66** (2002) 014017 [[hep-ph/0202088](#)].
- [19] M. Beneke, A. Chapovsky, M. Diehl and T. Feldmann, *Soft collinear effective theory and heavy to light currents beyond leading power*, *Nucl. Phys.* **B643** (2002) 431 [[hep-ph/0206152](#)].
- [20] T. Becher and M. D. Schwartz, *A precise determination of  $\alpha_s$  from LEP thrust data using effective field theory*, *JHEP* **0807** (2008) 034 [[0803.0342](#)].
- [21] R. Abbate, M. Fickinger, A. H. Hoang, V. Mateu and I. W. Stewart, *Thrust at  $N^3LL$  with Power Corrections and a Precision Global Fit for  $\alpha_s(m_Z)$* , *Phys. Rev. D* **83** (2011) 074021 [[1006.3080](#)].
- [22] A. H. Hoang, D. W. Kolodrubetz, V. Mateu and I. W. Stewart, *Precise determination of  $\alpha_s$  from the  $C$ -parameter distribution*, *Phys. Rev.* **D91** (2015) 094018 [[1501.04111](#)].
- [23] A. M. Polyakov, *Gauge fields as rings of glue*, *Nucl. Phys.* **B164** (1980) 171.
- [24] R. A. Brandt, F. Neri and M.-a. Sato, *Renormalization of loop functions for all loops*, *Phys. Rev.* **D24** (1981) 879.
- [25] G. P. Korchemsky and A. V. Radyushkin, *Renormalization of the Wilson loops beyond the leading order*, *Nucl. Phys.* **B283** (1987) 342.
- [26] I. Korchemskaya and G. Korchemsky, *On lightlike Wilson loops*, *Phys. Lett.* **B287** (1992) 169.

- [27] G. P. Korchemsky and A. V. Radyushkin, *Loop space formalism and renormalization group for the infrared asymptotics of QCD*, *Phys. Lett.* **B171** (1986) 459.
- [28] G. P. Korchemsky and A. V. Radyushkin, *Infrared factorization, Wilson lines and the heavy quark limit*, *Phys. Lett.* **B279** (1992) 359 [[hep-ph/9203222](#)].
- [29] S. V. Ivanov, G. P. Korchemsky and A. V. Radyushkin, *Infrared asymptotics of perturbative QCD: Contour gauges*, *Yad. Fiz.* **44** (1986) 230.
- [30] G. P. Korchemsky and A. V. Radyushkin, *Infrared asymptotics of perturbative QCD: Renormalization properties of the Wilson loops in higher orders of perturbation theory*, *Sov. J. Nucl. Phys.* **44** (1986) 877.
- [31] G. P. Korchemsky and A. V. Radyushkin, *Infrared asymptotics of perturbative QCD. Quark and gluon propagators*, *Sov. J. Nucl. Phys.* **45** (1987) 127.
- [32] G. P. Korchemsky and A. V. Radyushkin, *Infrared asymptotics of perturbative QCD. Vertex functions*, *Sov. J. Nucl. Phys.* **45** (1987) 910.
- [33] S. Catani, *The Singular behavior of QCD amplitudes at two loop order*, *Phys. Lett.* **B427** (1998) 161 [[hep-ph/9802439](#)].
- [34] E. Gardi and L. Magnea, *Factorization constraints for soft anomalous dimensions in QCD scattering amplitudes*, *JHEP* **03** (2009) 079 [[0901.1091](#)].
- [35] T. Becher and M. Neubert, *On the structure of infrared singularities of gauge-theory amplitudes*, *JHEP* **06** (2009) 081 [[0903.1126](#)].
- [36] E. Gardi and L. Magnea, *Infrared singularities in QCD amplitudes*, *Nuovo Cim.* **C32N5-6** (2009) 137 [[0908.3273](#)].
- [37] T. Becher and M. Neubert, *Infrared Singularities of Scattering Amplitudes and  $N^3LL$  Resummation for  $n$ -Jet Processes*, [1908.11379](#).
- [38] T. Becher and M. Neubert, *Infrared singularities of QCD amplitudes with massive partons*, *Phys. Rev.* **D79** (2009) 125004 [[0904.1021](#)].
- [39] M. Neubert, *Heavy quark symmetry*, *Phys. Rept.* **245** (1994) 259 [[hep-ph/9306320](#)].
- [40] A. Grozin, J. M. Henn, G. P. Korchemsky and P. Marquard, *Three loop cusp anomalous dimension in QCD*, *Phys. Rev. Lett.* **114** (2015) 062006 [[1409.0023](#)].
- [41] A. Grozin, J. M. Henn, G. P. Korchemsky and P. Marquard, *The three-loop cusp anomalous dimension in QCD and its supersymmetric extensions*, *JHEP* **01** (2016) 140 [[1510.07803](#)].

- [42] E. Laenen, L. Magnea, G. Stavenga and C. D. White, *Next-to-eikonal corrections to soft gluon radiation: a diagrammatic approach*, *JHEP* **01** (2011) 141 [1010.1860].
- [43] A. Luna, S. Melville, S. G. Naculich and C. D. White, *Next-to-soft corrections to high energy scattering in QCD and gravity*, *JHEP* **01** (2017) 052 [1611.02172].
- [44] I. Moutl, I. W. Stewart and G. Vita, *A subleading operator basis and matching for  $gg$  to  $H$* , *JHEP* **07** (2017) 067 [1703.03408].
- [45] I. Moutl, I. W. Stewart, G. Vita and H. X. Zhu, *First Subleading Power Resummation for Event Shapes*, *JHEP* **08** (2018) 013 [1804.04665].
- [46] M. Beneke, A. Broggio, M. Garry, S. Jaskiewicz, R. Szafron, L. Vernazza et al., *Leading-logarithmic threshold resummation of the Drell-Yan process at next-to-leading power*, *JHEP* **03** (2019) 043 [1809.10631].
- [47] M. A. Ebert, I. Moutl, I. W. Stewart, F. J. Tackmann, G. Vita and H. X. Zhu, *Subleading power rapidity divergences and power corrections for  $q_T$* , *JHEP* **04** (2019) 123 [1812.08189].
- [48] I. Moutl, I. W. Stewart and G. Vita, *Subleading Power Factorization with Radiative Functions*, 1905.07411.
- [49] M. van Beekveld, W. Beenakker, E. Laenen and C. D. White, *Next-to-leading power threshold effects for inclusive and exclusive processes with final state jets*, 1905.08741.
- [50] M. van Beekveld, W. Beenakker, R. Basu, E. Laenen, A. Misra and P. Motylinski, *Next-to-leading power threshold effects for resummed prompt photon production*, *Phys. Rev.* **D100** (2019) 056009 [1905.11771].
- [51] R. Bonciani, S. Di Vita, P. Mastrolia and U. Schubert, *Two-Loop Master Integrals for the mixed EW-QCD virtual corrections to Drell-Yan scattering*, *JHEP* **09** (2016) 091 [1604.08581].
- [52] A. von Manteuffel and R. M. Schabinger, *Numerical Multi-Loop Calculations via Finite Integrals and One-Mass EW-QCD Drell-Yan Master Integrals*, *JHEP* **04** (2017) 129 [1701.06583].
- [53] M. Heller, A. von Manteuffel and R. M. Schabinger, *Multiple polylogarithms with algebraic arguments and the two-loop EW-QCD Drell-Yan master integrals*, 1907.00491.
- [54] L. Adams, E. Chaubey and S. Weinzierl, *Planar Double Box Integral for Top Pair Production with a Closed Top Loop to all orders in the Dimensional Regularization Parameter*, *Phys. Rev. Lett.* **121** (2018) 142001 [1804.11144].



- [55] L. Adams, E. Chaubey and S. Weinzierl, *Analytic results for the planar double box integral relevant to top-pair production with a closed top loop*, *JHEP* **10** (2018) 206 [1806.04981].
- [56] M. Becchetti, R. Bonciani, V. Casconi, A. Ferroglia, S. Lavacca and A. von Manteuffel, *Master Integrals for the two-loop, non-planar QCD corrections to top-quark pair production in the quark-annihilation channel*, *JHEP* **08** (2019) 071 [1904.10834].
- [57] R. Bonciani, V. Del Duca, H. Frellesvig, J. M. Henn, M. Hidding, L. Maestri et al., *Evaluating two-loop non-planar master integrals for Higgs + jet production with full heavy-quark mass dependence*, 1907.13156.
- [58] F. Moriello, *Generalised power series expansions for the elliptic planar families of Higgs + jet production at two loops*, 1907.13234.
- [59] T. Gehrmann, J. M. Henn and N. A. Lo Presti, *Analytic form of the two-loop planar five-gluon all-plus-helicity amplitude in QCD*, *Phys. Rev. Lett.* **116** (2016) 062001 [1511.05409].
- [60] C. G. Papadopoulos, D. Tommasini and C. Wever, *The Pentabox Master Integrals with the Simplified Differential Equations approach*, *JHEP* **04** (2016) 078 [1511.09404].
- [61] T. Gehrmann, J. M. Henn and N. A. Lo Presti, *Pentagon functions for massless planar scattering amplitudes*, *JHEP* **10** (2018) 103 [1807.09812].
- [62] D. Chicherin, T. Gehrmann, J. M. Henn, N. A. Lo Presti, V. Mitev and P. Wasser, *Analytic result for the nonplanar hexa-box integrals*, *JHEP* **03** (2019) 042 [1809.06240].
- [63] D. Chicherin, T. Gehrmann, J. M. Henn, P. Wasser, Y. Zhang and S. Zoia, *All master integrals for three-jet production at NNLO*, 1812.11160.
- [64] S. Abreu, F. Febres Cordero, H. Ita, B. Page and M. Zeng, *Planar Two-Loop Five-Gluon Amplitudes from Numerical Unitarity*, *Phys. Rev.* **D97** (2018) 116014 [1712.03946].
- [65] S. Badger, C. Bronnum-Hansen, H. B. Hartanto and T. Peraro, *First look at two-loop five-gluon scattering in QCD*, *Phys. Rev. Lett.* **120** (2018) 092001 [1712.02229].
- [66] S. Abreu, F. Febres Cordero, H. Ita, B. Page and V. Sotnikov, *Planar Two-Loop Five-Parton Amplitudes from Numerical Unitarity*, *JHEP* **11** (2018) 116 [1809.09067].

- [67] S. Badger, C. Bronnum-Hansen, H. B. Hartanto and T. Peraro, *Analytic helicity amplitudes for two-loop five-gluon scattering: the single-minus case*, *JHEP* **01** (2019) 186 [1811.11699].
- [68] S. Abreu, J. Dormans, F. Febres Cordero, H. Ita and B. Page, *Analytic Form of Planar Two-Loop Five-Gluon Scattering Amplitudes in QCD*, *Phys. Rev. Lett.* **122** (2019) 082002 [1812.04586].
- [69] S. Badger, D. Chicherin, T. Gehrmann, G. Heinrich, J. M. Henn, T. Peraro et al., *Analytic form of the full two-loop five-gluon all-plus helicity amplitude*, *Phys. Rev. Lett.* **123** (2019) 071601 [1905.03733].
- [70] S. Abreu, J. Dormans, F. Febres Cordero, H. Ita, B. Page and V. Sotnikov, *Analytic Form of the Planar Two-Loop Five-Parton Scattering Amplitudes in QCD*, *JHEP* **05** (2019) 084 [1904.00945].
- [71] H. B. Hartanto, S. Badger, C. Bronnum-Hansen and T. Peraro, *A numerical evaluation of planar two-loop helicity amplitudes for a W-boson plus four partons*, *JHEP* **09** (2019) 119 [1906.11862].
- [72] L. F. Alday, J. M. Henn, J. Plefka and T. Schuster, *Scattering into the fifth dimension of  $N=4$  super Yang-Mills*, *JHEP* **1001** (2010) 077 [0908.0684].
- [73] J. M. Henn, S. G. Naculich, H. J. Schnitzer and M. Spradlin, *Higgs-regularized three-loop four-gluon amplitude in  $N=4$  SYM: exponentiation and Regge limits*, *JHEP* **1004** (2010) 038 [1001.1358].
- [74] J. M. Henn, S. G. Naculich, H. J. Schnitzer and M. Spradlin, *More loops and legs in Higgs-regulated  $N=4$  SYM amplitudes*, *JHEP* **1008** (2010) 002 [1004.5381].
- [75] R. Brüser, S. Caron-Huot and J. M. Henn, *Subleading Regge limit from a soft anomalous dimension*, *JHEP* **04** (2018) 047 [1802.02524].
- [76] R. Brüser, Z. L. Liu and M. Stahlhofen, *Three-Loop Quark Jet Function*, *Phys. Rev. Lett.* **121** (2018) 072003 [1804.09722].
- [77] R. Brüser, A. Grozin, J. M. Henn and M. Stahlhofen, *Matter dependence of the four-loop QCD cusp anomalous dimension: from small angles to all angles*, *JHEP* **05** (2019) 186 [1902.05076].
- [78] C. Itzykson and J. B. Zuber, *Quantum Field Theory*, International Series In Pure and Applied Physics. McGraw-Hill, New York, 1980.
- [79] S. Weinberg, *The Quantum theory of fields. Vol. 1: Foundations*. Cambridge University Press, 2005.
- [80] M. E. Peskin and D. V. Schroeder, *An Introduction To Quantum Field Theory*. Avalon Publishing, 1995.

- [81] M. D. Schwartz, *Quantum Field Theory and the Standard Model*. Cambridge University Press, 2014.
- [82] T. van Ritbergen, A. N. Schellekens and J. A. M. Vermaseren, *Group theory factors for Feynman diagrams*, *Int. J. Mod. Phys. A* **14** (1999) 41 [[hep-ph/9802376](#)].
- [83] G. 't Hooft and M. J. G. Veltman, *Regularization and Renormalization of Gauge Fields*, *Nucl. Phys.* **B44** (1972) 189.
- [84] C. G. Bollini and J. J. Giambiagi, *Dimensional Renormalization: The Number of Dimensions as a Regularizing Parameter*, *Nuovo Cim.* **B12** (1972) 20.
- [85] J. C. Collins, *Renormalization*, vol. 26 of *Cambridge Monographs on Mathematical Physics*. Cambridge University Press, Cambridge, 1986, 10.1017/CBO9780511622656.
- [86] F. Jegerlehner, *Facts of life with gamma(5)*, *Eur. Phys. J.* **C18** (2001) 673 [[hep-th/0005255](#)].
- [87] G. 't Hooft, *Renormalization of Massless Yang-Mills Fields*, *Nucl. Phys.* **B33** (1971) 173.
- [88] J. C. Taylor, *Ward Identities and Charge Renormalization of the Yang-Mills Field*, *Nucl. Phys.* **B33** (1971) 436.
- [89] A. A. Slavnov, *Ward Identities in Gauge Theories*, *Theor. Math. Phys.* **10** (1972) 99.
- [90] W. E. Caswell and A. D. Kennedy, *Simple approach to renormalization theory*, *Phys. Rev.* **D25** (1982) 392.
- [91] K. G. Chetyrkin and F. V. Tkachov, *Infrared R-operation and ultraviolet counterterms in the  $\overline{MS}$ -scheme*, *Phys. Lett.* **114B** (1982) 340.
- [92] K. G. Chetyrkin and V. A. Smirnov,  *$R^*$  OPERATION CORRECTED*, *Phys. Lett.* **144B** (1984) 419.
- [93] V. A. Smirnov and K. G. Chetyrkin,  *$R^*$  Operation in the Minimal Subtraction Scheme*, *Theor. Math. Phys.* **63** (1985) 462.
- [94] K. G. Chetyrkin, *Combinatorics of  $\mathbf{R}$ -,  $\mathbf{R}^{-1}$ -, and  $\mathbf{R}^*$ -operations and asymptotic expansions of feynman integrals in the limit of large momenta and masses*, 1701.08627.
- [95] K. G. Chetyrkin, G. Falcioni, F. Herzog and J. A. M. Vermaseren, *The method of global  $R^*$  and its applications*, *PoS RADCOR2017* (2018) 004 [[1801.03024](#)].

## Bibliography

- [96] T. Luthe, A. Maier, P. Marquard and Y. Schroder, *Complete renormalization of QCD at five loops*, *JHEP* **03** (2017) 020 [1701.07068].
- [97] K. G. Chetyrkin, G. Falcioni, F. Herzog and J. A. M. Vermaseren, *Five-loop renormalisation of QCD in covariant gauges*, *JHEP* **10** (2017) 179 [1709.08541].
- [98] G. 't Hooft, *Dimensional regularization and the renormalization group*, *Nucl. Phys.* **B61** (1973) 455.
- [99] W. A. Bardeen, A. Buras, D. Duke and T. Muta, *Deep Inelastic Scattering Beyond the Leading Order in Asymptotically Free Gauge Theories*, *Phys. Rev. D* **18** (1978) 3998.
- [100] P. A. Baikov, K. G. Chetyrkin and J. H. Kühn, *Five-Loop Running of the QCD coupling constant*, *Phys. Rev. Lett.* **118** (2017) 082002 [1606.08659].
- [101] PARTICLE DATA GROUP collaboration, *Review of Particle Physics*, *Phys. Rev.* **D98** (2018) 030001.
- [102] F. Bloch and A. Nordsieck, *Note on the Radiation Field of the electron*, *Phys. Rev.* **52** (1937) 54.
- [103] T. Kinoshita, *Mass singularities of Feynman amplitudes*, *J. Math. Phys.* **3** (1962) 650.
- [104] T. D. Lee and M. Nauenberg, *Degenerate Systems and Mass Singularities*, *Phys. Rev.* **133** (1964) B1549.
- [105] T. Gehrmann, E. W. N. Glover, T. Huber, N. Iqizlerli and C. Studerus, *Calculation of the quark and gluon form factors to three loops in QCD*, *JHEP* **1006** (2010) 094 [1004.3653].
- [106] O. Almelid, C. Duhr and E. Gardi, *Three-loop corrections to the soft anomalous dimension in multileg scattering*, *Phys. Rev. Lett.* **117** (2016) 172002 [1507.00047].
- [107] S. Moch, J. A. M. Vermaseren and A. Vogt, *The three loop splitting functions in QCD: The nonsinglet case*, *Nucl. Phys.* **B688** (2004) 101 [hep-ph/0403192].
- [108] A. Vogt, S. Moch and J. A. M. Vermaseren, *The Three-loop splitting functions in QCD: The Singlet case*, *Nucl. Phys.* **B691** (2004) 129 [hep-ph/0404111].
- [109] E. Eichten and F. L. Feinberg, *Spin Dependent Forces in Heavy Quark Systems*, *Phys. Rev. Lett.* **43** (1979) 1205.
- [110] J.-L. Gervais and A. Neveu, *The Slope of the Leading Regge Trajectory in Quantum Chromodynamics*, *Nucl. Phys.* **B163** (1980) 189.

- [111] I. Ya. Arefeva, *QUANTUM CONTOUR FIELD EQUATIONS*, *Phys. Lett.* **93B** (1980) 347.
- [112] M. Neubert, *Heavy quark effective theory*, *Subnucl. Ser.* **34** (1997) 98 [hep-ph/9610266].
- [113] T. Mannel, W. Roberts and Z. Ryzak, *A Derivation of the heavy quark effective Lagrangian from QCD*, *Nucl. Phys.* **B368** (1992) 204.
- [114] A. V. Manohar and M. B. Wise, *Heavy quark physics*, *Camb. Monogr. Part. Phys. Nucl. Phys. Cosmol.* **10** (2000) 1.
- [115] A. G. Grozin, *Heavy quark effective theory*, *Springer Tracts Mod. Phys.* **201** (2004) 1.
- [116] A. F. Falk, H. Georgi, B. Grinstein and M. B. Wise, *Heavy meson form-factors from QCD*, *Nucl. Phys.* **B343** (1990) 1.
- [117] A. G. Grozin, *Introduction to effective field theories. 3. Bloch–Nordsieck effective theory, HQET*, 1305.4245.
- [118] D. J. Broadhurst and A. G. Grozin, *Two loop renormalization of the effective field theory of a static quark*, *Phys. Lett.* **B267** (1991) 105 [hep-ph/9908362].
- [119] K. Melnikov and T. van Ritbergen, *The three loop on-shell renormalization of QCD and QED*, *Nucl. Phys.* **B591** (2000) 515 [hep-ph/0005131].
- [120] K. G. Chetyrkin and A. G. Grozin, *Three loop anomalous dimension of the heavy–light quark current in HQET*, *Nucl. Phys.* **B666** (2003) 289 [hep-ph/0303113].
- [121] E. Farhi, *A QCD Test for Jets*, *Phys. Rev. Lett.* **39** (1977) 1587.
- [122] T. Becher, *Les Houches Lectures on Soft-Collinear Effective Theory*, in *Les Houches summer school: EFT in Particle Physics and Cosmology Les Houches, Chamonix Valley, France, July 3-28, 2017*, 2018, 1803.04310.
- [123] R. Abbate, M. Fickinger, A. H. Hoang, V. Mateu and I. W. Stewart, *Precision Thrust Cumulant Moments at  $N^3LL$* , *Phys. Rev.* **D86** (2012) 094002 [1204.5746].
- [124] T. Becher, M. Neubert and B. D. Pecjak, *Factorization and Momentum-Space Resummation in Deep-Inelastic Scattering*, *JHEP* **01** (2007) 076 [hep-ph/0607228].
- [125] A. H. Hoang, D. W. Kolodrubetz, V. Mateu and I. W. Stewart, *C-parameter distribution at  $N^3LL'$  including power corrections*, *Phys. Rev.* **D91** (2015) 094017 [1411.6633].

## Bibliography

- [126] Y.-T. Chien and M. D. Schwartz, *Resummation of heavy jet mass and comparison to LEP data*, *JHEP* **08** (2010) 058 [1005.1644].
- [127] T. Becher and M. Neubert, *Analysis of  $Br(\bar{B} \rightarrow X(s)\gamma)$  at NNLO with a cut on photon energy*, *Phys. Rev. Lett.* **98** (2007) 022003 [hep-ph/0610067].
- [128] E. C. Poggio, H. R. Quinn and S. Weinberg, *Smearing the Quark Model*, *Phys. Rev.* **D13** (1976) 1958.
- [129] M. A. Shifman, *Quark hadron duality*, in *At the frontier of particle physics. Handbook of QCD. Vol. 1-3*, (Singapore), pp. 1447–1494, World Scientific, World Scientific, 2001, hep-ph/0009131, DOI.
- [130] M. D. Schwartz, *Resummation and NLO matching of event shapes with effective field theory*, *Phys. Rev.* **D77** (2008) 014026 [0709.2709].
- [131] ALEPH collaboration, *Studies of QCD at  $e^+e^-$  centre-of-mass energies between 91-GeV and 209-GeV*, *Eur. Phys. J.* **C35** (2004) 457.
- [132] T. Becher, A. Broggio and A. Ferroglia, *Introduction to Soft-Collinear Effective Theory*, *Lect. Notes Phys.* **896** (2015) pp.1 [1410.1892].
- [133] I. Stewart, *Lectures on the Soft-Collinear Effective Theory*, <https://ocw.mit.edu/courses/physics/8-851-effective-field-theory-spring-2013/lecture-notes/>.
- [134] M. Beneke and T. Feldmann, *Multipole expanded soft collinear effective theory with nonAbelian gauge symmetry*, *Phys. Lett.* **B553** (2003) 267 [hep-ph/0211358].
- [135] T. Becher and M. D. Schwartz, *Direct photon production with effective field theory*, *JHEP* **02** (2010) 040 [0911.0681].
- [136] T. Becher and G. Bell, *The gluon jet function at two-loop order*, *Phys. Lett.* **B695** (2011) 252 [1008.1936].
- [137] P. Banerjee, P. K. Dhani and V. Ravindran, *Gluon jet function at three loops in QCD*, *Phys. Rev.* **D98** (2018) 094016 [1805.02637].
- [138] C. W. Bauer and A. V. Manohar, *Shape function effects in  $B \rightarrow X(s)\gamma$  and  $B \rightarrow X(u)\ell\bar{\nu}$  decays*, *Phys. Rev.* **D70** (2004) 034024 [hep-ph/0312109].
- [139] S. W. Bosch, B. O. Lange, M. Neubert and G. Paz, *Factorization and shape function effects in inclusive B meson decays*, *Nucl. Phys.* **B699** (2004) 335 [hep-ph/0402094].
- [140] T. Becher and M. Neubert, *Toward a NNLO calculation of the  $\bar{B} \rightarrow X(s)\gamma$  decay rate with a cut on photon energy. II. Two-loop result for the jet function*, *Phys. Lett.* **B637** (2006) 251 [hep-ph/0603140].

- [141] T. Becher and M. Neubert, *Threshold resummation in momentum space from effective field theory*, *Phys. Rev. Lett.* **97** (2006) 082001 [[hep-ph/0605050](#)].
- [142] F. Gliozzi, J. Scherk and D. I. Olive, *Supersymmetry, Supergravity Theories and the Dual Spinor Model*, *Nucl. Phys.* **B122** (1977) 253.
- [143] L. Brink, J. H. Schwarz and J. Scherk, *Supersymmetric Yang-Mills Theories*, *Nucl. Phys.* **B121** (1977) 77.
- [144] M. F. Sohnius, *Introducing Supersymmetry*, *Phys. Rept.* **128** (1985) 39.
- [145] A. V. Belitsky, S. E. Derkachov, G. P. Korchemsky and A. N. Manashov, *Superconformal operators in  $N=4$  superYang-Mills theory*, *Phys. Rev.* **D70** (2004) 045021 [[hep-th/0311104](#)].
- [146] H. K. Dreiner, H. E. Haber and S. P. Martin, *Two-component spinor techniques and Feynman rules for quantum field theory and supersymmetry*, *Phys. Rept.* **494** (2010) 1 [[0812.1594](#)].
- [147] S. Ferrara and B. Zumino, *Supergauge Invariant Yang-Mills Theories*, *Nucl. Phys.* **B79** (1974) 413.
- [148] E. C. Poggio and H. N. Pendleton, *Vanishing of Charge Renormalization and Anomalies in a Supersymmetric Gauge Theory*, *Phys. Lett.* **72B** (1977) 200.
- [149] D. R. T. Jones, *Charge Renormalization in a Supersymmetric Yang-Mills Theory*, *Phys. Lett.* **72B** (1977) 199.
- [150] L. V. Avdeev, O. V. Tarasov and A. A. Vladimirov, *Vanishing of the three-loop charge renormalization function in a supersymmetric gauge theory*, *Phys. Lett.* **96B** (1980) 94.
- [151] M. T. Grisaru, M. Rocek and W. Siegel, *Zero Three Loop beta Function in  $N=4$  Superyang-Mills Theory*, *Phys. Rev. Lett.* **45** (1980) 1063.
- [152] W. E. Caswell and D. Zanon, *Vanishing Three Loop Beta Function in  $N = 4$  Supersymmetric Yang-Mills Theory*, *Phys. Lett.* **100B** (1981) 152.
- [153] M. F. Sohnius and P. C. West, *Conformal Invariance in  $N=4$  Supersymmetric Yang-Mills Theory*, *Phys. Lett.* **100B** (1981) 245.
- [154] S. Mandelstam, *Light Cone Superspace and the Ultraviolet Finiteness of the  $N=4$  Model*, *Nucl.Phys.* **B213** (1983) 149.
- [155] L. Brink, O. Lindgren and B. E. W. Nilsson, *The Ultraviolet Finiteness of the  $N=4$  Yang-Mills Theory*, *Phys. Lett.* **123B** (1983) 323.
- [156] K. Konishi, *Anomalous Supersymmetry Transformation of Some Composite Operators in SQCD*, *Phys. Lett.* **135B** (1984) 439.

- [157] G. 't Hooft, *A Planar Diagram Theory for Strong Interactions*, *Nucl. Phys.* **B72** (1974) 461.
- [158] J. Drummond, J. Henn, V. Smirnov and E. Sokatchev, *Magic identities for conformal four-point integrals*, *JHEP* **0701** (2007) 064 [[hep-th/0607160](#)].
- [159] L. F. Alday and J. M. Maldacena, *Gluon scattering amplitudes at strong coupling*, *JHEP* **0706** (2007) 064 [[0705.0303](#)].
- [160] J. M. Drummond, G. P. Korchemsky and E. Sokatchev, *Conformal properties of four-gluon planar amplitudes and Wilson loops*, *Nucl. Phys.* **B795** (2008) 385 [[0707.0243](#)].
- [161] J. M. Drummond, J. Henn, G. P. Korchemsky and E. Sokatchev, *On planar gluon amplitudes/Wilson loops duality*, *Nucl. Phys.* **B795** (2008) 52 [[0709.2368](#)].
- [162] J. Drummond, J. Henn, G. Korchemsky and E. Sokatchev, *Conformal Ward identities for Wilson loops and a test of the duality with gluon amplitudes*, *Nucl.Phys.* **B826** (2010) 337 [[0712.1223](#)].
- [163] Z. Bern, J. J. M. Carrasco, H. Johansson and D. A. Kosower, *Maximally supersymmetric planar Yang-Mills amplitudes at five loops*, *Phys. Rev.* **D76** (2007) 125020 [[0705.1864](#)].
- [164] Z. Bern, L. J. Dixon, D. A. Kosower, R. Roiban, M. Spradlin, C. Vergu et al., *The Two-Loop Six-Gluon MHV Amplitude in Maximally Supersymmetric Yang-Mills Theory*, *Phys. Rev.* **D78** (2008) 045007 [[0803.1465](#)].
- [165] D. A. Kosower, R. Roiban and C. Vergu, *The Six-Point NMHV amplitude in Maximally Supersymmetric Yang-Mills Theory*, *Phys. Rev.* **D83** (2011) 065018 [[1009.1376](#)].
- [166] Z. Bern, L. J. Dixon and V. A. Smirnov, *Iteration of planar amplitudes in maximally supersymmetric Yang-Mills theory at three loops and beyond*, *Phys.Rev.* **D72** (2005) 085001 [[hep-th/0505205](#)].
- [167] A. Brandhuber, P. Heslop and G. Travaglini, *MHV amplitudes in  $N=4$  super Yang-Mills and Wilson loops*, *Nucl. Phys.* **B794** (2008) 231 [[0707.1153](#)].
- [168] L. F. Alday and R. Roiban, *Scattering Amplitudes, Wilson Loops and the String/Gauge Theory Correspondence*, *Phys. Rept.* **468** (2008) 153 [[0807.1889](#)].
- [169] J. M. Henn, *Duality between Wilson loops and gluon amplitudes*, *Fortsch. Phys.* **57** (2009) 729 [[0903.0522](#)].
- [170] S. Caron-Huot and J. M. Henn, *Solvable Relativistic Hydrogenlike System in Supersymmetric Yang-Mills Theory*, *Phys. Rev. Lett.* **113** (2014) 161601 [[1408.0296](#)].



- [171] J. M. Maldacena, *Wilson loops in large  $N$  field theories*, *Phys. Rev. Lett.* **80** (1998) 4859 [[hep-th/9803002](#)].
- [172] N. Drukker, D. J. Gross and H. Ooguri, *Wilson loops and minimal surfaces*, *Phys. Rev.* **D60** (1999) 125006 [[hep-th/9904191](#)].
- [173] K. Zarembo, *Supersymmetric Wilson loops*, *Nucl. Phys.* **B643** (2002) 157 [[hep-th/0205160](#)].
- [174] N. Drukker, S. Giombi, R. Ricci and D. Trancanelli, *More supersymmetric Wilson loops*, *Phys. Rev.* **D76** (2007) 107703 [[0704.2237](#)].
- [175] A. Dymarsky and V. Pestun, *Supersymmetric Wilson loops in  $N=4$  SYM and pure spinors*, *JHEP* **04** (2010) 115 [[0911.1841](#)].
- [176] V. Cardinali, L. Griguolo and D. Seminara, *Impure Aspects of Supersymmetric Wilson Loops*, *JHEP* **06** (2012) 167 [[1202.6393](#)].
- [177] P. Nogueira, *Automatic Feynman graph generation*, *J. Comput. Phys.* **105** (1993) 279.
- [178] J. Hoff, *The Mathematica package TopoID and its application to the Higgs boson production cross section*, *J. Phys. Conf. Ser.* **762** (2016) 012061 [[1607.04465](#)].
- [179] J. Hoff and A. Pak, *TopoID (unpublished)*,  
<https://github.com/thejensemenn/TopoID/> .
- [180] A. V. Smirnov, *FIRE5: a C++ implementation of Feynman Integral REDuction*, *Comput. Phys. Commun.* **189** (2015) 182 [[1408.2372](#)].
- [181] A. V. Smirnov and F. S. Chuharev, *FIRE6: Feynman Integral REDuction with Modular Arithmetic*, [1901.07808](#).
- [182] C. Studerus, *Reduze-Feynman Integral Reduction in C++*, *Comput. Phys. Commun.* **181** (2010) 1293 [[0912.2546](#)].
- [183] A. von Manteuffel and C. Studerus, *Reduze 2 - Distributed Feynman Integral Reduction*, [1201.4330](#).
- [184] P. Maierhöfer, J. Usovitsch and P. Uwer, *Kira - A Feynman integral reduction program*, *Comput. Phys. Commun.* **230** (2018) 99 [[1705.05610](#)].
- [185] P. Maierhöfer and J. Usovitsch, *Kira 1.2 Release Notes*, [1812.01491](#).
- [186] R. N. Lee, *Presenting LiteRed: a tool for the Loop InTEgrals REDuction*, [1212.2685](#).
- [187] R. N. Lee, *LiteRed 1.4: a powerful tool for reduction of multiloop integrals*, *J. Phys. Conf. Ser.* **523** (2014) 012059 [[1310.1145](#)].

## Bibliography

- [188] A. Pak, *The toolbox of modern multi-loop calculations: novel analytic and semi-analytic techniques*, *J. Phys. Conf. Ser.* **368** (2012) 012049 [1111.0868].
- [189] J. A. M. Vermaseren, *New features of FORM*, [math-ph/0010025](#).
- [190] J. Kuipers, T. Ueda, J. A. M. Vermaseren and J. Vollinga, *FORM version 4.0*, *Comput. Phys. Commun.* **184** (2013) 1453 [1203.6543].
- [191] B. Ruijl, T. Ueda and J. Vermaseren, *FORM version 4.2*, [1707.06453](#).
- [192] F. V. Tkachov, *A Theorem on Analytical Calculability of Four Loop Renormalization Group Functions*, *Phys. Lett.* **100B** (1981) 65.
- [193] K. G. Chetyrkin and F. V. Tkachov, *Integration by parts: The algorithm to calculate  $\beta$  functions in 4 loops*, *Nucl. Phys.* **B192** (1981) 159.
- [194] A. V. Kotikov, *Differential equations method: New technique for massive Feynman diagrams calculation*, *Phys. Lett.* **B254** (1991) 158.
- [195] A. V. Kotikov, *Differential equation method: The Calculation of  $N$  point Feynman diagrams*, *Phys. Lett.* **B267** (1991) 123.
- [196] Z. Bern, L. J. Dixon and D. A. Kosower, *Dimensionally regulated pentagon integrals*, *Nucl. Phys.* **B412** (1994) 751 [[hep-ph/9306240](#)].
- [197] E. Remiddi, *Differential equations for Feynman graph amplitudes*, *Nuovo Cim.* **A110** (1997) 1435 [[hep-th/9711188](#)].
- [198] T. Gehrmann and E. Remiddi, *Differential equations for two-loop four-point functions*, *Nucl. Phys.* **B580** (2000) 485 [[hep-ph/9912329](#)].
- [199] J. M. Henn, *Multiloop integrals in dimensional regularization made simple*, *Phys.Rev.Lett.* **110** (2013) 251601 [[1304.1806](#)].
- [200] J. M. Henn, *Lectures on differential equations for Feynman integrals*, *J. Phys.* **A48** (2015) 153001 [[1412.2296](#)].
- [201] R. N. Lee, *Group structure of the integration-by-part identities and its application to the reduction of multiloop integrals*, *JHEP* **07** (2008) 031 [[0804.3008](#)].
- [202] S. Laporta, *High precision calculation of multiloop Feynman integrals by difference equations*, *Int.J.Mod.Phys.* **A15** (2000) 5087 [[hep-ph/0102033](#)].
- [203] T. Peraro, *FiniteFlow: multivariate functional reconstruction using finite fields and dataflow graphs*, [1905.08019](#).
- [204] T. Binoth and G. Heinrich, *An automatized algorithm to compute infrared divergent multiloop integrals*, *Nucl. Phys.* **B585** (2000) 741 [[hep-ph/0004013](#)].

- [205] T. Binoth and G. Heinrich, *Numerical evaluation of multiloop integrals by sector decomposition*, *Nucl. Phys.* **B680** (2004) 375 [[hep-ph/0305234](#)].
- [206] T. Binoth and G. Heinrich, *Numerical evaluation of phase space integrals by sector decomposition*, *Nucl. Phys.* **B693** (2004) 134 [[hep-ph/0402265](#)].
- [207] G. Heinrich, *Sector Decomposition*, *Int. J. Mod. Phys.* **A23** (2008) 1457 [[0803.4177](#)].
- [208] C. Bogner and S. Weinzierl, *Resolution of singularities for multi-loop integrals*, *Comput. Phys. Commun.* **178** (2008) 596 [[0709.4092](#)].
- [209] C. Bogner and S. Weinzierl, *Blowing up Feynman integrals*, *Nucl. Phys. Proc. Suppl.* **183** (2008) 256 [[0806.4307](#)].
- [210] V. A. Smirnov, *Feynman integral calculus*. 2006.
- [211] J. M. Henn and J. C. Plefka, *Scattering Amplitudes in Gauge Theories*, *Lect. Notes Phys.* **883** (2014) pp.1.
- [212] O. V. Tarasov, *Connection between Feynman integrals having different values of the space-time dimension*, *Phys. Rev.* **D54** (1996) 6479 [[hep-th/9606018](#)].
- [213] M. C. Bergere and Y.-M. P. Lam, *Asymptotic expansion of Feynman amplitudes. Part 1: the convergent case*, *Commun. Math. Phys.* **39** (1974) 1.
- [214] E. R. Speer, *Renormalization and ward identities using complex space-time dimension*, *J. Math. Phys.* **15** (1974) 1.
- [215] H. Cheng and T. T. Wu, *Expanding protons: scattering at high energies*. 1987.
- [216] C. Bogner and S. Weinzierl, *Feynman graph polynomials*, *Int. J. Mod. Phys.* **A25** (2010) 2585 [[1002.3458](#)].
- [217] R. N. Lee, *Calculating multiloop integrals using dimensional recurrence relation and D-analyticity*, *Nucl. Phys. Proc. Suppl.* **205-206** (2010) 135 [[1007.2256](#)].
- [218] P. A. Baikov, *Explicit solutions of the multiloop integral recurrence relations and its application*, *Nucl. Instrum. Meth.* **A389** (1997) 347 [[hep-ph/9611449](#)].
- [219] E. Panzer, *On hyperlogarithms and Feynman integrals with divergences and many scales*, *JHEP* **03** (2014) 071 [[1401.4361](#)].
- [220] A. von Manteuffel, E. Panzer and R. M. Schabinger, *A quasi-finite basis for multi-loop Feynman integrals*, *JHEP* **02** (2015) 120 [[1411.7392](#)].
- [221] A. von Manteuffel, E. Panzer and R. M. Schabinger, *On the Computation of Form Factors in Massless QCD with Finite Master Integrals*, *Phys. Rev.* **D93** (2016) 125014 [[1510.06758](#)].

- [222] E. Panzer, *Algorithms for the symbolic integration of hyperlogarithms with applications to Feynman integrals*, *Comput. Phys. Commun.* **188** (2015) 148 [1403.3385].
- [223] E. Remiddi and J. A. M. Vermaseren, *Harmonic polylogarithms*, *Int. J. Mod. Phys.* **A15** (2000) 725 [hep-ph/9905237].
- [224] D. Maître, *HPL, a mathematica implementation of the harmonic polylogarithms*, *Comput.Phys.Comm.* **174** (2006) 222 [hep-ph/0507152].
- [225] W. Wasow, *Asymptotic expansions for ordinary differential equations. Pure and Applied Mathematics*. Vol. XIV. Interscience Publishers John Wiley & Sons, Inc., New York-London-Sydney, 1965.
- [226] K.-T. Chen, *Iterated path integrals*, *Bull. Am. Math. Soc.* **83** (1977) 831.
- [227] M. Caffo, H. Czyz, S. Laporta and E. Remiddi, *The Master differential equations for the two loop sunrise selfmass amplitudes*, *Nuovo Cim.* **A111** (1998) 365 [hep-th/9805118].
- [228] S. Laporta and E. Remiddi, *Analytic treatment of the two loop equal mass sunrise graph*, *Nucl. Phys.* **B704** (2005) 349 [hep-ph/0406160].
- [229] S. Bloch and P. Vanhove, *The elliptic dilogarithm for the sunset graph*, *J. Number Theor.* **148** (2015) 328 [1309.5865].
- [230] L. Adams, C. Bogner and S. Weinzierl, *The two-loop sunrise graph in two space-time dimensions with arbitrary masses in terms of elliptic dilogarithms*, *J. Math. Phys.* **55** (2014) 102301 [1405.5640].
- [231] L. Adams, C. Bogner and S. Weinzierl, *The two-loop sunrise integral around four space-time dimensions and generalisations of the Clausen and Glaisher functions towards the elliptic case*, *J. Math. Phys.* **56** (2015) 072303 [1504.03255].
- [232] S. Bloch, M. Kerr and P. Vanhove, *Local mirror symmetry and the sunset Feynman integral*, *Adv. Theor. Math. Phys.* **21** (2017) 1373 [1601.08181].
- [233] A. B. Goncharov, *Multiple polylogarithms, cyclotomy and modular complexes*, *Math.Res.Lett.* **5** (1998) 497 [1105.2076].
- [234] R. Bonciani, V. Del Duca, H. Frellesvig, J. M. Henn, F. Moriello and V. A. Smirnov, *Two-loop planar master integrals for  $Higgs \rightarrow 3$  partons with full heavy-quark mass dependence*, *JHEP* **12** (2016) 096 [1609.06685].
- [235] L. Adams, C. Bogner, A. Schweitzer and S. Weinzierl, *The kite integral to all orders in terms of elliptic polylogarithms*, *J. Math. Phys.* **57** (2016) 122302 [1607.01571].

- [236] A. von Manteuffel and L. Tancredi, *A non-planar two-loop three-point function beyond multiple polylogarithms*, *JHEP* **06** (2017) 127 [1701.05905].
- [237] J. L. Bourjaily, A. J. McLeod, M. Spradlin, M. von Hippel and M. Wilhelm, *Elliptic Double-Box Integrals: Massless Scattering Amplitudes beyond Polylogarithms*, *Phys. Rev. Lett.* **120** (2018) 121603 [1712.02785].
- [238] N. Arkani-Hamed, J. L. Bourjaily, F. Cachazo and J. Trnka, *Local Integrals for Planar Scattering Amplitudes*, *JHEP* **1206** (2012) 125 [1012.6032].
- [239] N. Arkani-Hamed, J. L. Bourjaily, F. Cachazo and J. Trnka, *Singularity Structure of Maximally Supersymmetric Scattering Amplitudes*, *Phys. Rev. Lett.* **113** (2014) 261603 [1410.0354].
- [240] P. Wasser, *Analytic properties of Feynman integrals for scattering amplitudes (Master thesis)*, <https://publications.ub.uni-mainz.de/theses/frontdoor.php?source%20opus=100001967> (2018).
- [241] J. M. Henn, T. Peraro, M. Stahlhofen and P. Wasser, *Matter dependence of the four-loop cusp anomalous dimension*, 1901.03693.
- [242] R. N. Lee, *Reducing differential equations for multiloop master integrals*, *JHEP* **04** (2015) 108 [1411.0911].
- [243] M. Prausa, *epsilon: A tool to find a canonical basis of master integrals*, *Comput. Phys. Commun.* **219** (2017) 361 [1701.00725].
- [244] O. Gituliar and V. Magerya, *Fuchsia: a tool for reducing differential equations for Feynman master integrals to epsilon form*, *Comput. Phys. Commun.* **219** (2017) 329 [1701.04269].
- [245] C. Meyer, *Evaluating multi-loop Feynman integrals using differential equations: automatizing the transformation to a canonical basis*, *PoS* **LL2016** (2016) 028.
- [246] C. Meyer, *Transforming differential equations of multi-loop Feynman integrals into canonical form*, *JHEP* **04** (2017) 006 [1611.01087].
- [247] C. Meyer, *Algorithmic transformation of multi-loop master integrals to a canonical basis with CANONICA*, *Comput. Phys. Commun.* **222** (2018) 295 [1705.06252].
- [248] M. Besier, D. Van Straten and S. Weinzierl, *Rationalizing roots: an algorithmic approach*, *Commun. Num. Theor. Phys.* **13** (2019) 253 [1809.10983].
- [249] J. M. Henn, A. V. Smirnov and V. A. Smirnov, *Evaluating single-scale and/or non-planar diagrams by differential equations*, *JHEP* **1403** (2014) 088 [1312.2588].

- [250] S. Caron-Huot and J. M. Henn, *Iterative structure of finite loop integrals*, *JHEP* **06** (2014) 114 [1404.2922].
- [251] D. Correa, J. Maldacena and A. Sever, *The quark anti-quark potential and the cusp anomalous dimension from a TBA equation*, *JHEP* **1208** (2012) 134 [1203.1913].
- [252] N. Drukker, *Integrable Wilson loops*, *JHEP* **1310** (2013) 135 [1203.1617].
- [253] J. Bartels and M. Lublinsky, *Quark anti-quark exchange in  $\gamma^* \gamma^*$  scattering*, *JHEP* **09** (2003) 076 [hep-ph/0308181].
- [254] Y. V. Kovchegov, D. Pitonyak and M. D. Sievert, *Helicity Evolution at Small- $x$* , *JHEP* **01** (2016) 072 [1511.06737].
- [255] M. Bianchi, J. F. Morales and C. Wen, *Instanton corrections to the effective action of  $\mathcal{N} = 4$  SYM*, *JHEP* **11** (2015) 006 [1508.00554].
- [256] R. M. Schabinger, *Scattering on the Moduli Space of  $N=4$  Super Yang-Mills*, 0801.1542.
- [257] A. Gorsky and A. Zhiboedov, *Aspects of the  $N=4$  SYM amplitude: Wilson polygon duality*, *Nucl. Phys.* **B835** (2010) 343 [0911.3626].
- [258] R. H. Boels, *No triangles on the moduli space of maximally supersymmetric gauge theory*, *JHEP* **05** (2010) 046 [1003.2989].
- [259] S. Caron-Huot and D. O’Connell, *Spinor Helicity and Dual Conformal Symmetry in Ten Dimensions*, *JHEP* **08** (2011) 014 [1010.5487].
- [260] T. Dennen and Y.-t. Huang, *Dual Conformal Properties of Six-Dimensional Maximal Super Yang-Mills Amplitudes*, *JHEP* **01** (2011) 140 [1010.5874].
- [261] N. Craig, H. Elvang, M. Kiermaier and T. Slatyer, *Massive amplitudes on the Coulomb branch of  $N=4$  SYM*, *JHEP* **1112** (2011) 097 [1104.2050].
- [262] M. Kiermaier, *The Coulomb-branch  $S$ -matrix from massless amplitudes*, 1105.5385.
- [263] J. M. Henn, S. Moch and S. G. Naculich, *Form factors and scattering amplitudes in  $N=4$  SYM in dimensional and massive regularizations*, *JHEP* **1112** (2011) 024 [1109.5057].
- [264] D. Correa, J. Henn, J. Maldacena and A. Sever, *The cusp anomalous dimension at three loops and beyond*, *JHEP* **05** (2012) 098 [1203.1019].
- [265] J. Plefka, T. Schuster and V. Verschinin, *From Six to Four and More: Massless and Massive Maximal Super Yang-Mills Amplitudes in 6d and 4d and their Hidden Symmetries*, *JHEP* **01** (2015) 098 [1405.7248].

- [266] Z. Bern, J. J. Carrasco, T. Dennen, Y.-t. Huang and H. Ita, *Generalized Unitarity and Six-Dimensional Helicity*, *Phys.Rev.* **D83** (2011) 085022 [1010.0494].
- [267] A. I. Davydychev, *Standard and hypergeometric representations for loop diagrams and the photon-photon scattering*, **hep-ph/9307323**.
- [268] I. Buchbinder, A. Y. Petrov and A. A. Tseytlin, *Two loop  $N=4$  superYang-Mills effective action and interaction between  $D3$ -branes*, *Nucl.Phys.* **B621** (2002) 179 [hep-th/0110173].
- [269] N. Bogoliubov, A. A. Logunov and I. T. Todorov, *Introduction to Axiomatic Quantum Field Theory*. Reading. Mass.: W. A. Benjamin, Advanced Book Program, 1975.
- [270] M. Beneke, Y. Kiyo and K. Schuller, *Third-order correction to top-quark pair production near threshold I. Effective theory set-up and matching coefficients*, **1312.4791**.
- [271] N. Beisert, B. Eden and M. Staudacher, *Transcendentality and Crossing*, *J.Stat.Mech.* **0701** (2007) P01021 [hep-th/0610251].
- [272] S. G. Naculich and H. J. Schnitzer, *Regge behavior of gluon scattering amplitudes in  $N=4$  SYM theory*, *Nucl. Phys.* **B794** (2008) 189 [0708.3069].
- [273] J. M. Henn and T. Huber, *The four-loop cusp anomalous dimension in  $\mathcal{N} = 4$  super Yang-Mills and analytic integration techniques for Wilson line integrals*, *JHEP* **09** (2013) 147 [1304.6418].
- [274] N. Gromov and F. Levkovich-Maslyuk, *Quantum Spectral Curve for a cusped Wilson line in  $\mathcal{N} = 4$  SYM*, *JHEP* **04** (2016) 134 [1510.02098].
- [275] D. Correa, J. Henn, J. Maldacena and A. Sever, *An exact formula for the radiation of a moving quark in  $\mathcal{N} = 4$  super Yang Mills*, *JHEP* **06** (2012) 048 [1202.4455].
- [276] L. F. Alday, D. Gaiotto, J. Maldacena, A. Sever and P. Vieira, *An Operator Product Expansion for Polygonal null Wilson Loops*, *JHEP* **04** (2011) 088 [1006.2788].
- [277] B. Basso, A. Sever and P. Vieira, *Space-time S-matrix and Flux-tube S-matrix at Finite Coupling*, *Phys.Rev.Lett.* **111** (2013) 091602 [1303.1396].
- [278] S. Donnachie, H. G. Dosch, O. Nachtmann and P. Landshoff, *Pomeron physics and QCD*, *Camb. Monogr. Part. Phys. Nucl. Phys. Cosmol.* **19** (2002) 1.
- [279] P. D. B. Collins, *An Introduction to Regge Theory and High-Energy Physics*, Cambridge Monographs on Mathematical Physics. Cambridge Univ. Press, Cambridge, UK, 2009.

- [280] G. C. Wick, *Properties of Bethe-Salpeter Wave Functions*, *Phys. Rev.* **96** (1954) 1124.
- [281] R. E. Cutkosky, *Solutions of a Bethe-Salpeter equations*, *Phys. Rev.* **96** (1954) 1135.
- [282] R. Espinosa and J. A. García, *Cusp Anomalous dimension and rotating open strings in AdS/CFT*, [1607.05305](#).
- [283] V. S. Dotsenko and S. N. Vergeles, *Renormalizability of phase factors in the nonabelian gauge theory*, *Nucl. Phys.* **B169** (1980) 527.
- [284] H. Dorn, *Renormalization of path ordered phase factors and related hadron operators in gauge field theories*, *Fortsch. Phys.* **34** (1986) 11.
- [285] L. J. Dixon, L. Magnea and G. F. Sterman, *Universal structure of subleading infrared poles in gauge theory amplitudes*, *JHEP* **08** (2008) 022 [[0805.3515](#)].
- [286] M. Bonini, L. Griguolo, M. Preti and D. Seminara, *Bremsstrahlung function, leading Lüscher correction at weak coupling and localization*, *JHEP* **02** (2016) 172 [[1511.05016](#)].
- [287] L. F. Alday and J. Maldacena, *Comments on gluon scattering amplitudes via AdS/CFT*, *JHEP* **11** (2007) 068 [[0710.1060](#)].
- [288] L. J. Dixon, *The Principle of Maximal Transcendentality and the Four-Loop Collinear Anomalous Dimension*, *JHEP* **01** (2018) 075 [[1712.07274](#)].
- [289] A. A. Penin and N. Zerf, *Two-loop Bhabha Scattering at High Energy beyond Leading Power Approximation*, *Phys. Lett.* **B760** (2016) 816 [[1606.06344](#)].
- [290] I. Feige, D. W. Kolodrubetz, I. Moulton and I. W. Stewart, *A Complete Basis of Helicity Operators for Subleading Factorization*, *JHEP* **11** (2017) 142 [[1703.03411](#)].
- [291] N. Gromov, V. Kazakov, S. Leurent and D. Volin, *Quantum Spectral Curve for Planar  $\mathcal{N} = 4$  Super-Yang-Mills Theory*, *Phys. Rev. Lett.* **112** (2014) 011602 [[1305.1939](#)].
- [292] A. V. Smirnov, *Algorithm FIRE – Feynman Integral REduction*, *JHEP* **0810** (2008) 107 [[0807.3243](#)].
- [293] A. V. Smirnov and V. A. Smirnov, *FIRE4, LiteRed and accompanying tools to solve integration by parts relations*, [1302.5885](#).
- [294] A. V. Smirnov, *FIESTA4: Optimized Feynman integral calculations with GPU support*, *Comput. Phys. Commun.* **204** (2016) 189 [[1511.03614](#)].



- [295] M. Czakon, *Automatized analytic continuation of Mellin-Barnes integrals*, *Comput. Phys. Commun.* **175** (2006) 559 [[hep-ph/0511200](#)].
- [296] A. Primo and L. Tancredi, *On the maximal cut of Feynman integrals and the solution of their differential equations*, *Nucl. Phys.* **B916** (2017) 94 [[1610.08397](#)].
- [297] H. Frellesvig and C. G. Papadopoulos, *Cuts of Feynman Integrals in Baikov representation*, *JHEP* **04** (2017) 083 [[1701.07356](#)].
- [298] M. Harley, F. Moriello and R. M. Schabinger, *Baikov-Lee Representations Of Cut Feynman Integrals*, *JHEP* **06** (2017) 049 [[1705.03478](#)].
- [299] J. R. Gaunt, *Glauber Gluons and Multiple Parton Interactions*, *JHEP* **1407** (2014) 110 [[1405.2080](#)].
- [300] M. Zeng, *Drell-Yan process with jet vetoes: breaking of generalized factorization*, *JHEP* **10** (2015) 189 [[1507.01652](#)].
- [301] I. Z. Rothstein and I. W. Stewart, *An Effective Field Theory for Forward Scattering and Factorization Violation*, *JHEP* **08** (2016) 025 [[1601.04695](#)].
- [302] M. D. Schwartz, K. Yan and H. X. Zhu, *Factorization Violation and Scale Invariance*, [1801.01138](#).
- [303] J. Gaunt, M. Stahlhofen, F. J. Tackmann and J. R. Walsh, *N-jettiness Subtractions for NNLO QCD Calculations*, *JHEP* **09** (2015) 058 [[1505.04794](#)].
- [304] I. W. Stewart, F. J. Tackmann and W. J. Waalewijn, *N-Jettiness: An Inclusive Event Shape to Veto Jets*, *Phys. Rev. Lett.* **105** (2010) 092002 [[1004.2489](#)].
- [305] I. W. Stewart, F. J. Tackmann and W. J. Waalewijn, *Factorization at the LHC: From PDFs to Initial State Jets*, *Phys. Rev. D* **81** (2010) 094035 [[0910.0467](#)].
- [306] L. G. Almeida, S. D. Ellis, C. Lee, G. Sterman, I. Sung et al., *Comparing and counting logs in direct and effective methods of QCD resummation*, *JHEP* **1404** (2014) 174 [[1401.4460](#)].
- [307] R. Boughezal, C. Focke, X. Liu and F. Petriello, *W-boson production in association with a jet at next-to-next-to-leading order in perturbative QCD*, *Phys. Rev. Lett.* **115** (2015) 062002 [[1504.02131](#)].
- [308] J. Gao, C. S. Li and H. X. Zhu, *Top Quark Decay at Next-to-Next-to Leading Order in QCD*, *Phys. Rev. Lett.* **110** (2013) 042001 [[1210.2808](#)].
- [309] R. Boughezal, C. Focke, W. Giele, X. Liu and F. Petriello, *Higgs boson production in association with a jet at NNLO using jettiness subtraction*, *Phys. Lett.* **B748** (2015) 5 [[1505.03893](#)].

## Bibliography

- [310] R. Boughezal, J. M. Campbell, R. K. Ellis, C. Focke, W. T. Giele, X. Liu et al., *Z-boson production in association with a jet at next-to-next-to-leading order in perturbative QCD*, *Phys. Rev. Lett.* **116** (2016) 152001 [1512.01291].
- [311] E. L. Berger, J. Gao, C. P. Yuan and H. X. Zhu, *NNLO QCD Corrections to t-channel Single Top-Quark Production and Decay*, *Phys. Rev.* **D94** (2016) 071501 [1606.08463].
- [312] R. N. Lee, *Space-time dimensionality  $D$  as complex variable: Calculating loop integrals using dimensional recurrence relation and analytical properties with respect to  $D$* , *Nucl. Phys.* **B830** (2010) 474 [0911.0252].
- [313] J. Chay and C. Kim, *Collinear effective theory at subleading order and its application to heavy - light currents*, *Phys.Rev.* **D65** (2002) 114016 [hep-ph/0201197].
- [314] A. V. Manohar, T. Mehen, D. Pirjol and I. W. Stewart, *Reparameterization invariance for collinear operators*, *Phys.Lett.* **B539** (2002) 59 [hep-ph/0204229].
- [315] S. Borowka, G. Heinrich, S. Jahn, S. P. Jones, M. Kerner, J. Schlenk et al., *pySecDec: a toolbox for the numerical evaluation of multi-scale integrals*, *Comput. Phys. Commun.* **222** (2018) 313 [1703.09692].
- [316] V. A. Smirnov, *Analytical result for dimensionally regularized massless on shell double box*, *Phys.Lett.* **B460** (1999) 397 [hep-ph/9905323].
- [317] J. Tausk, *Nonplanar massless two loop Feynman diagrams with four on-shell legs*, *Phys.Lett.* **B469** (1999) 225 [hep-ph/9909506].
- [318] A. V. Smirnov and V. A. Smirnov, *On the Resolution of Singularities of Multiple Mellin-Barnes Integrals*, *Eur.Phys.J.* **C62** (2009) 445 [0901.0386].
- [319] H. Ferguson, D. Bailey and S. Arno *Math. Comp.* **68** (1999) 351.
- [320] Z. Ligeti, I. W. Stewart and F. J. Tackmann, *Treating the  $b$  quark distribution function with reliable uncertainties*, *Phys. Rev. D* **78** (2008) 114014 [0807.1926].
- [321] I. W. Stewart, F. J. Tackmann and W. J. Waalewijn, *The Quark Beam Function at NNLL*, *JHEP* **1009** (2010) 005 [1002.2213].
- [322] S. Moch, J. Vermaseren and A. Vogt, *The Quark form-factor at higher orders*, *JHEP* **0508** (2005) 049 [hep-ph/0507039].
- [323] P. F. Monni, T. Gehrmann and G. Luisoni, *Two-Loop Soft Corrections and Resummation of the Thrust Distribution in the Dijet Region*, *JHEP* **1108** (2011) 010 [1105.4560].
- [324] A. Gehrmann-De Ridder, T. Gehrmann, E. W. N. Glover and G. Heinrich, *Infrared structure of  $e^+e^- \rightarrow 3$ -jets at NNLO*, *JHEP* **11** (2007) 058 [0710.0346].

- [325] J. A. Gracey, *Anomalous dimension of nonsinglet Wilson operators at  $O(1/N(f))$  in deep inelastic scattering*, *Phys. Lett.* **B322** (1994) 141 [[hep-ph/9401214](#)].
- [326] M. Beneke and V. M. Braun, *Power corrections and renormalons in Drell–Yan production*, *Nucl. Phys.* **B454** (1995) 253 [[hep-ph/9506452](#)].
- [327] D. J. Broadhurst and A. G. Grozin, *Matching QCD and HQET heavy–light currents at two loops and beyond*, *Phys. Rev.* **D52** (1995) 4082 [[hep-ph/9410240](#)].
- [328] A. Grozin, *Leading and next-to-leading large- $n_f$  terms in the cusp anomalous dimension and quark-antiquark potential*, *PoS* **LL2016** (2016) 053 [[1605.03886](#)].
- [329] B. Ruijl, T. Ueda, J. A. M. Vermaseren, J. Davies and A. Vogt, *First Forcer results on deep-inelastic scattering and related quantities*, *PoS* **LL2016** (2016) 071 [[1605.08408](#)].
- [330] J. M. Henn, A. V. Smirnov, V. A. Smirnov and M. Steinhauser, *A planar four-loop form factor and cusp anomalous dimension in QCD*, *JHEP* **05** (2016) 066 [[1604.03126](#)].
- [331] J. Davies, A. Vogt, B. Ruijl, T. Ueda and J. A. M. Vermaseren, *Large- $n_f$  contributions to the four-loop splitting functions in QCD*, *Nucl. Phys.* **B915** (2017) 335 [[1610.07477](#)].
- [332] P. Marquard, A. V. Smirnov, V. A. Smirnov and M. Steinhauser, *Four-loop wave function renormalization in QCD and QED*, *Phys. Rev.* **D97** (2018) 054032 [[1801.08292](#)].
- [333] A. Grozin, *Four-loop cusp anomalous dimension in QED*, *JHEP* **06** (2018) 073 [[1805.05050](#)].
- [334] S. Moch, B. Ruijl, T. Ueda, J. A. M. Vermaseren and A. Vogt, *Four-Loop Non-Singlet Splitting Functions in the Planar Limit and Beyond*, *JHEP* **10** (2017) 041 [[1707.08315](#)].
- [335] A. Grozin, J. Henn and M. Stahlhofen, *On the Casimir scaling violation in the cusp anomalous dimension at small angle*, *JHEP* **10** (2017) 052 [[1708.01221](#)].
- [336] S. Moch, B. Ruijl, T. Ueda, J. A. M. Vermaseren and A. Vogt, *On quartic colour factors in splitting functions and the gluon cusp anomalous dimension*, *Phys. Lett.* **B782** (2018) 627 [[1805.09638](#)].
- [337] R. N. Lee, A. V. Smirnov, V. A. Smirnov and M. Steinhauser, *Four-loop quark form factor with quartic fundamental colour factor*, [1901.02898](#).
- [338] J. Henn, R. N. Lee, A. V. Smirnov, V. A. Smirnov and M. Steinhauser, *Four-loop photon quark form factor and cusp anomalous dimension in the large- $N_c$  limit of QCD*, *JHEP* **03** (2017) 139 [[1612.04389](#)].

## Bibliography

- [339] W. Kilian, T. Mannel and T. Ohl, *Unimagined imaginary parts in heavy quark effective field theory*, *Phys. Lett.* **B304** (1993) 311 [[hep-ph/9303224](#)].
- [340] R. H. Boels, T. Huber and G. Yang, *Four-Loop nonplanar cusp anomalous dimension in  $\mathcal{N} = 4$  supersymmetric Yang–Mills theory*, *Phys. Rev. Lett.* **119** (2017) 201601 [[1705.03444](#)].
- [341] R. H. Boels, T. Huber and G. Yang, *The Sudakov form factor at four loops in maximal super Yang–Mills theory*, *JHEP* **01** (2018) 153 [[1711.08449](#)].
- [342] T. Luthe, A. Maier, P. Marquard and Y. Schroder, *The five-loop Beta function for a general gauge group and anomalous dimensions beyond Feynman gauge*, *JHEP* **10** (2017) 166 [[1709.07718](#)].
- [343] V. N. Gribov and L. N. Lipatov, *Deep inelastic  $e p$  scattering in perturbation theory*, *Sov. J. Nucl. Phys.* **15** (1972) 438.
- [344] G. Altarelli and G. Parisi, *Asymptotic Freedom in Parton Language*, *Nucl. Phys.* **B126** (1977) 298.
- [345] Y. L. Dokshitzer, *Calculation of the Structure Functions for Deep Inelastic Scattering and  $e^+e^-$  Annihilation by Perturbation Theory in Quantum Chromodynamics.*, *Sov. Phys. JETP* **46** (1977) 641.
- [346] G. P. Korchemsky, *Asymptotics of the Altarelli-Parisi-Lipatov Evolution Kernels of Parton Distributions*, *Mod. Phys. Lett.* **A4** (1989) 1257.
- [347] J. G. M. Gatheral, *Exponentiation of eikonal cross-sections in nonabelian gauge theories*, *Phys. Lett.* **133B** (1983) 90.
- [348] J. Frenkel and J. C. Taylor, *Nonabelian eikonal exponentiation*, *Nucl. Phys.* **B246** (1984) 231.
- [349] G. F. Sterman, *Infrared divergences in perturbative QCD*, *AIP Conf. Proc.* **74** (1981) 22.
- [350] A. G. Grozin, *Calculating three loop diagrams in heavy quark effective theory with integration by parts recurrence relations*, *JHEP* **03** (2000) 013 [[hep-ph/0002266](#)].
- [351] A. G. Grozin, *Lectures on multiloop calculations*, *Int. J. Mod. Phys.* **A19** (2004) 473 [[hep-ph/0307297](#)].
- [352] R. Brüser, A. G. Grozin, J. M. Henn and M. Stahlhofen, *Four-loop results for the cusp anomalous dimension*, *PoS* **LL2018** (2018) 018 [[1807.05145](#)].
- [353] R. N. Lee, A. V. Smirnov, V. A. Smirnov and M. Steinhauser, *Analytic three-loop static potential*, *Phys. Rev.* **D94** (2016) 054029 [[1608.02603](#)].

- [354] C. Anzai, Y. Kiyo and Y. Sumino, *Static QCD potential at three-loop order*, *Phys. Rev. Lett.* **104** (2010) 112003 [0911.4335].
- [355] A. V. Smirnov, V. A. Smirnov and M. Steinhauser, *Three-loop static potential*, *Phys. Rev. Lett.* **104** (2010) 112002 [0911.4742].
- [356] A. V. Smirnov, V. A. Smirnov and M. Steinhauser, *Fermionic contributions to the three-loop static potential*, *Phys. Lett.* **B668** (2008) 293 [0809.1927].
- [357] D. J. Broadhurst and A. L. Kataev, *Connections between deep inelastic and annihilation processes at next to next-to-leading order and beyond*, *Phys. Lett.* **B315** (1993) 179 [hep-ph/9308274].
- [358] R. J. Crewther, *Relating inclusive  $e^+e^-$  annihilation to electroproduction sum rules in quantum chromodynamics*, *Phys. Lett.* **B397** (1997) 137 [hep-ph/9701321].
- [359] V. M. Braun, G. P. Korchemsky and D. Mueller, *The Uses of conformal symmetry in QCD*, *Prog. Part. Nucl. Phys.* **51** (2003) 311 [hep-ph/0306057].
- [360] A. V. Garkusha, A. L. Kataev and V. S. Molokoedov, *Renormalization scheme and gauge (in)dependence of the generalized Crewther relation: what are the real grounds of the  $\beta$ -factorization property?*, *JHEP* **02** (2018) 161 [1801.06231].
- [361] M. Peter, *The Static quark–anti-quark potential in QCD to three loops*, *Phys. Rev. Lett.* **78** (1997) 602 [hep-ph/9610209].
- [362] M. Peter, *The static potential in QCD: A full two loop calculation*, *Nucl. Phys.* **B501** (1997) 471 [hep-ph/9702245].
- [363] Y. Schröder, *The static potential in QCD to two loops*, *Phys. Lett.* **B447** (1999) 321 [hep-ph/9812205].



---

# Acknowledgements

---

I want to take this opportunity to express my gratitude to all who supported me during my PhD project in Mainz. Without their help this thesis would not have been possible.

Firstly, I would like to thank my PhD advisor Johannes M. Henn for his continuous support, patience and motivation. He created a stimulating working atmosphere and shared his vast knowledge on QFT with me. Besides my PhD advisor I especially want to thank Maximilian Stahlhofen and Pascal Wasser for many fruitful discussions. I want to thank my co-advisor Stefan Weinzierl for his support. Many thanks to my collaborators Andrey Grozin, Simon Caron-Huot, Ze Long Liu, Leila Maestri, Tiziana Peraro and Maximilian Stahlhofen for the enjoyable work and many interesting discussions on the research projects.

I am grateful to the entire THEP group in Mainz for the nice working atmosphere and many fascinating discussions about physics as well as non-physics related topics. For the hospitality and a wonderful experience during my research visit in France I am grateful to the Institut de Physique Théorique (IPhT) at CEA Saclay. I especially want to thank Gregory Korchemsky for many stimulating discussions during this visit. I also want to thank the theory group at the Max Planck institute for physics in Munich for frequent and pleasant research visits.

For proofreading the manuscript and many helpful suggestions I am thankful to Moritz Breitbach, Dmitry Chicherin, Christoph Dlapa, Andrey Grozin, Lisa Michaels, Maximilian Stahlhofen, Pascal Wasser and Simone Zoia.

I acknowledge support from the DFG Research Training Group Symmetry Breaking in Fundamental Interactions (GRK 1581), the Gutenberg Forschungskolleg (GFK), the two DFG Clusters of Excellence Precision Physics, Fundamental Interactions and Structure of Matter PRISMA (EXC 1098) and PRISMA<sup>+</sup> (EXC 2118) and the Deutsch-Französische Hochschule under the grant number CDFA-02-18, through a PhD exchange program in theoretical physics.

Finally, I am deeply thankful to my family and friends for supporting me for all those years and for always believing in me.





## Colophon

This thesis was typeset with LaTeX2e using the document class `scrbook` of KOMA-Script from Markus Kohm published on <http://www.komascript.de/> under the LaTeX Project Public License, version 1.3c and BibTeX with the bibliography style file from the *Journal of High Energy Physics* published on <https://jhep.sissa.it/jhep/> under the LaTeX Project Public License, version 1.3c. All figures were drawn using the LaTeX package `TikZ` from Till Tantau published on <https://github.com/pgf-tikz/pgf> under the GNU Public License, version 2. For figure 2.8 additionally the LaTeX package `PGFplots` from Christian Feuersänger was used, which is published on <http://pgfplots.sourceforge.net/> under the GNU General Public License, version 3. The curriculum vitae uses the LaTeX document class `Moderncv` from Xavier Danaux published on <https://github.com/xdanaux/moderncv> under the LaTeX Project Public License, version 1.3c.